Title
Investigation of the 230Th(p,2n)229Pa Reaction as a Route to 225Ac

Author
Kmak, Kelly

Publication Date
2021

Peer reviewed|Thesis/dissertation

Investigation of the ^{230}Th(p,2n)^{229}Pa Reaction as a Route to ^{225}Ac

by

Kelly Kmak

A dissertation submitted in partial satisfaction of the

requirements for the degree of

Doctor of Philosophy

in

Engineering – Nuclear Engineering

in the

Graduate Division

of the

University of California, Berkeley

Committee in charge:

Professor Jasmina Vujic, Chair
Dr. Dawn A. Shaughnessy
Professor Rebecca Abergel
Professor John Arnold

Spring 2021

Investigation of the ^{230}Th(p,2n)^{229}Pa Reaction as a Route to ^{225}Ac

Abstract

Investigation of the ^{230}Th(p,2n)^{229}Pa Reaction as a Route to ^{225}Ac

by

Kelly Kmak

Doctor of Philosophy in Engineering – Nuclear Engineering

University of California, Berkeley

Professor Jasmina Vujic, Chair

Actinium-225 has important medical applications as an agent for targeted alpha therapy, but existing supplies of this isotope are limited. The ^{230}Th(p,2n)^{229}Pa reaction has been considered as a route to ^{225}Ac, however, there is no available cross section data for this reaction in the literature. The purpose of this work is to measure the ^{230}Th(p,2n)^{229}Pa reaction cross section in the energy range where this reaction has been calculated to peak to determine the feasibility of using this reaction for ^{225}Ac production.

As there is not a commercial source of ^{230}Th, for this work, thorium, naturally enriched in ^{230}Th, was separated from uranium ore. A novel procedure was developed for this separation consisting of leaching, liquid-liquid extraction, precipitations and ion exchange chromatography. The thorium was fabricated into accelerator targets using electrodeposition. The final targets were deposited onto a thin (10 μm) titanium backing and were highly uniform and stable. Target thicknesses ranged from ∼900 to 1900 μg Th/cm^2, which was sufficient to make the relevant cross section measurements.

Chemical processing of the irradiated targets was necessary to determine the activity of the protactinium activation products. The target processing was optimized for rapid, high yield and high radiopurity chemical separations. Column chromatography was used for the separation and the final chemical processing procedure is based on a Dowex 1x8 column in HCl media. The chemical studies showed that titanium was an ideal target backing material due to its chemical behavior and dissolution properties. CL resin (TrisKem International) was considered for the target processing, and, while ultimately not used, it was characterized further and batch studies are presented for radium, actinium and thorium in HCl and HNO_3 as well as radium, thorium and protactinium in HF. Six column separation studies were also performed with thorium, radium, actinium and protactinium in a variety of solution conditions. Further extraction studies were done with radium and actinium using Pb resin (Eichrom) and Rose Bengal. Both radium and actinium show a strong affinity (k' >10,000) for the resin at intermediate pHs from solutions with Rose Bengal with the pH range and

magnitude of uptake significantly increased by the presence of Rose Bengal compared to basic solutions without this large counter ion.

Thorium and protactinium tracer isotopes were necessary for all of the chemical development studies and were produced with isotope generators. A ^{237}Np/^{233}Pa isotope generator was made and extensively characterized. It was in continual use for over a year with an average yield of ∼75% before breakthrough occurred. A ^{227}Ac/^{227}Th isotope generator was also made based on an existing procedure described in the literature.

Nuclear data measurements were done for several relevant protactinium isotopes, including half-life measurements for ^{228}Pa and ^{229}Pa, and modern measurements of the major gamma-ray emissions from the decay of ^{231}Pa. For many of these measurements, the error envelopes have been significantly decreased compared to previous measurements, while remaining in good agreement with the existing literature values.

The ^{230}Th enriched targets were irradiated at the Center for Accelerator Mass Spectrometry at Lawrence Livermore National Laboratory with proton energies ranging from 14.1 to 16.9 MeV. Excitation functions in this energy range are reported for the first time in the literature for the ^{230}Th(p,2n)^{229}Pa and ^{230}Th(p,3n)^{228}Pa reactions. The peak measured value of the ^{230}Th(p,2n)^{229}Pa reaction was 182 ± 12 mb at 14.4 ± 0.1 MeV. Based on the measured ^{230}Th(p,2n)^{229}Pa reaction cross section, this reaction could reasonably be used for ^{225}Ac production, although significant amounts of relatively isotopically pure ^{230}Th would be needed for significant production.

Contents

List of Figures

List of Tables

Acknowledgments

I would like to thank everyone that has been involved in the completion of my dissertation. In particular, I would like to thank my graduate thesis advisor at UC Berkeley, Professor Jasmina Vujic, for her continual support and encouragement as well as the opportunities she has provided me. I would also like to thank my technical advisor at LLNL, Dr. Dawn Shaughnessy, for providing the opportunity for me to conduct my research at LLNL and for her guidance throughout this process. Thank you to the other members of my dissertation committee, Professor John Arnold and Professor Rebecca Abergel, as well.

This thesis was performed with considerable support from LLNL, including funding, laboratory space and the invaluable help and advice I received from researchers at LLNL. I greatly appreciate the assistance of the whole Nuclear and Radiochemistry group at LLNL. In particular, I'm grateful for the laboratory support and advice of Dr. John Despotopulos, Dr. Ken Moody and Dr. Roger Henderson.

I would like to thank the CAMS facility staff at LLNL, particularly Dr. Scott Tumey, for providing beam time. Special thanks to Rachel Lindvall, for making mass spectrometry measurements and for providing uranium ore, as well as Keenan J. Thomas and Todd Wooddy at the Nuclear Counting Facility at LLNL for their expert help with the counting systems.

Thank you to everyone at UC Berkeley that provided knowledge and advice in support of my dissertation and academic work, especially Dr. Lee Bernstein, whose guidance in regards to nuclear data and irradiations was invaluable. I am also grateful for the support of Dr. Bethany Goldblum and the Nuclear Science and Security Consortium (NSSC), who initially gave me the opportunity to get involved in radiochemistry research as an undergraduate and continued to support me in graduate school.

Finally, I would like to thank my amazing family for being there for me. I would not have been able to do this without the endless support of my parents and I am grateful for their unconditional love and encouragement throughout graduate school and beyond.

Lawrence Livermore National Laboratory Funding Auspice Statement and Disclaimer

This study was performed under the auspices of the U.S. Department of Energy by Lawrence Livermore National Laboratory under Contract DE-AC52-07NA27344. This work was funded by the LLNL Graduate Student Research Program. This material is based upon work supported by the Department of Energy National Nuclear Security Administration through the Nuclear Science and Security Consortium under Award Number DE-NA0003180. Neither the United States Government nor any agency thereof, nor any of their employees, makes any warranty, express or limited, or assumes any legal liability or responsibility for the accuracy, completeness, or usefulness of any information,apparatus, product, or process disclosed, or

represents that its use would not infringe privately owned rights. Reference herein to any specific commercial product, process, or service by trade name, trademark, manufacturer, or otherwise does not necessarily constitute or imply its endorsement, recommendation, or favoring by the United States Government or any agency thereof. The views and opinions of authors expressed herein do not necessarily state or reflect those of the United States Government or any agency thereof.

Copyright Notice for Previously Published Work

Chapter 1

Introduction

1.1 Background

Actinium-225 shows enormous potential for use in targeted alpha therapy (TAT) for cancer treatment [1–5]. Targeted alpha therapy uses radiation to kill tumor cells by complexing an alpha emitting radionuclide to a chelator and antibody, which is designed to attach to tumor antigens [1, 6]. When the isotope decays at the tumor site, the alpha particle delivers a large amount of energy in a short range, which causes DNA damage to tumor cells with limited damage to the surrounding healthy cells [1, 2, 6, 7]. Actinium-225 ($t_{1/2}$ = 10 d) is ideal for TAT because it has a short-lived decay chain with four alpha particles [2, 4]. Clinical trials have been done on the use of ^{225}Ac to treat leukemia [1, 2], it has shown efficacy in prostate cancer treatment [3] and animal studies have been done to investigate its use in ovarian cancer treatment [8]. The ^{213}Bi daughter of ^{225}Ac (Fig. 1.1) has also been studied for use as a TAT agent itself [4, 7, 9]. One of the benefits of using ^{213}Bi for TAT is that its decay emits a 440 keV gamma ray, which allows for its distribution to be monitored in-situ using single-photon emission computerized tomography (SPECT) scanning techniques [4, 10]. It has been used successfully in the treatment of patients with neuroendocrine tumors [10].

Currently, ^{225}Ac for clinical trials is obtained from the decay of ^{229}Th, a long-lived daughter of ^{233}U (Fig. 1.1), a fissile isotope produced in nuclear programs for weapons and reactors [1, 4, 11, 12].

However, the current global supply of ^{225}Ac is not sufficient to allow for wide scale use, or even trials, of this isotope [2, 11, 12]. Today, only the US, Germany and Russia have sources of ^{229}Th with enough activity to provide significant quantities of ^{225}Ac [2, 4], as shown in Table 1.1, and the three sources from these countries generally produce 1.7 Ci of ^{225}Ac per year [2, 7]. However, demand is significantly higher, $\sim$5 Ci per year [9], as the activity of ^{225}Ac given to patients in clinical trials is about 100 to 1000 μCi per patient per dose [2, 4]. Demand is expected to further increase as ^{225}Ac treatments progress through clinical trials and get approved for wider use [9].

More ^{225}Ac is unlikely to be produced in this manner as the production and purification

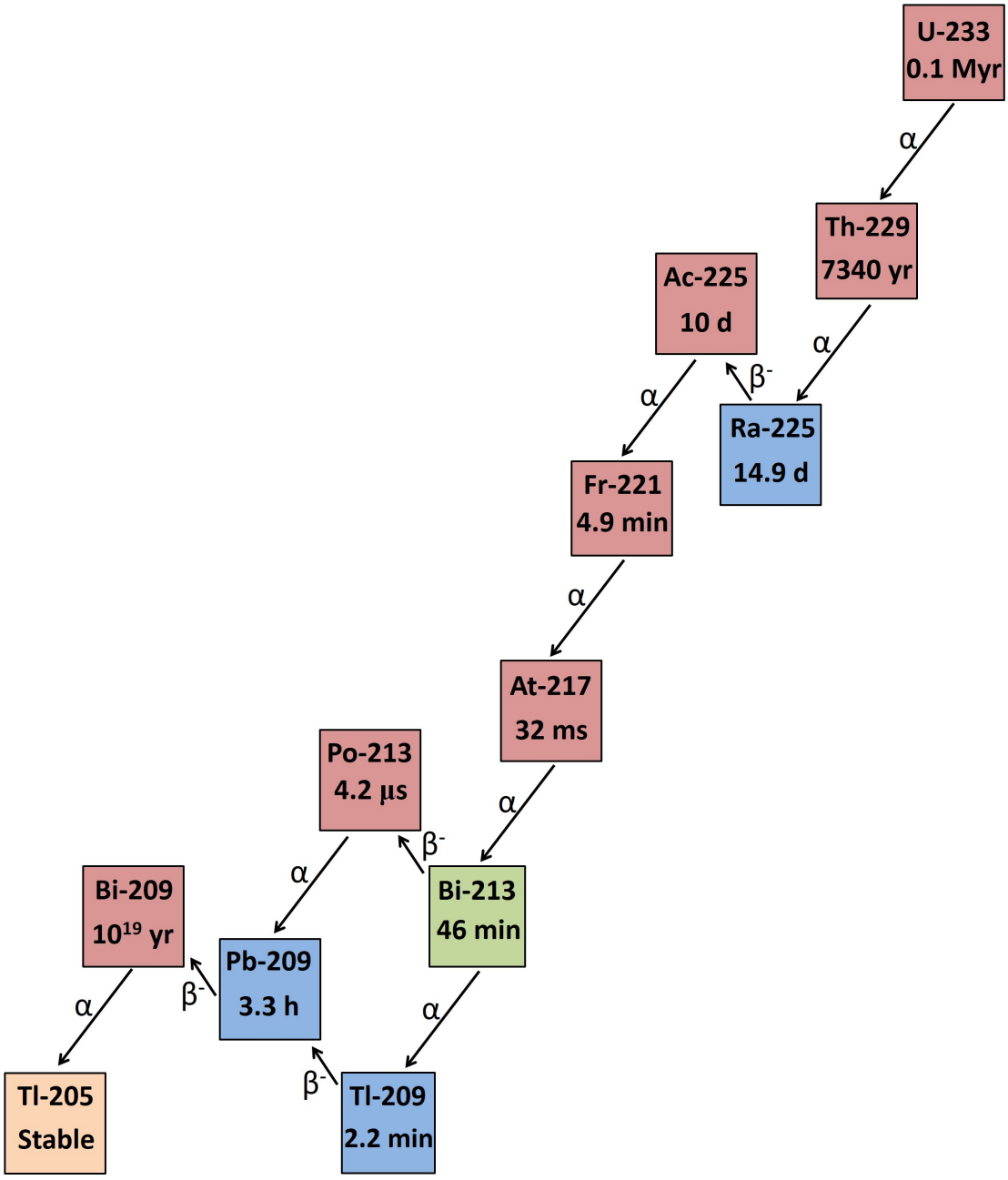

Figure 1.1: Decay Chain of ^{233}U. In this figure, pure alpha emitters are shown in pink, pure beta emitters in blue, stable isotopes in pale orange and isotopes that decay by multiple decay pathways are shown in green.

Table 1.1: Worldwide yearly production of ^{225}Ac from ^{229}Th [11].

Institute	Country	^{225}Ac yearly production
Oak Ridge National Laboratory (ORNL)	USA	720 mCi
Institute of Physics and Power Engineering	Russia	Unknown, reportedly similar to ORNL
Institute for Transuranium Elements (ITU)	Germany	350 mCi

of ^{233}U ($t_{1/2} = 1.592 \times 10^5$ y) to provide ^{229}Th ($t_{1/2} = 7{,}917$ y) is impractical due to both time constraints, as the in-growth of ^{229}Th is limited by the half-lives involved, and regulatory limits on producing and processing the material under nuclear safeguards [11, 13, 14]. In addition, the US Department of Energy (DOE) did not permit the extraction of more ^{229}Th before beginning to down-blend its supplies of ^{233}U in 2005 for disposal, making it impossible to increase ^{225}Ac production from existing sources of ^{233}U/^{229}Th in the US [9]. Therefore, research is being done on alternative methods of ^{225}Ac production to meet current and future demands [4].

The production of ^{225}Ac is only one of the scientific challenges that must be solved to allow for the regular use of ^{225}Ac in TAT [5, 9]. The binding of ^{225}Ac by a treatment-appropriate, *in vivo* stable chelator is a necessity as well and this has proven difficult [5, 9]. Actinium chemistry is not well understood and the large size and low charge density of actinium make it kinetically labile with small binding stability constants [5]. Currently, DOTA (1,4,7,10-tetraazacyclododecane-1,4,7,10-tetraacetic acid) is typically used to bind ^{225}Ac as it has medical approval for a variety of radiotherapies and binds 3+ ions fairly well [5]. Other ligands that may bind to ^{225}Ac more strongly and under milder conditions are being considered as well [4, 5]. Significant work in the area of actinium chelation and ligand development is needed for successful use of ^{225}Ac in TAT; however, the biomedical aspects of successful *in vivo* actinium chelation are not the focus of this work.

1.2 Proposed Methods of ^{225}Ac Production

Current research into methods of ^{225}Ac production can be broadly grouped into two categories: direct production, where ^{225}Ac is directly produced by a nuclear reaction, or in-direct production, where ^{225}Ac parent isotopes, such as ^{229}Th or ^{225}Ra, are produced and decay to ^{225}Ac.

Two main methods have been proposed for the direct production of ^{225}Ac: proton spallation of ^{232}Th targets and proton-induced reactions on ^{226}Ra targets [9]. The thorium proton spallation method produces ^{225}Ac by irradiating ^{232}Th targets with high-energy (>70 MeV), high current (100-200 μA) proton beams, inducing the breakup of thorium nuclei into many lower mass number particles [11, 12]. This can only be done at two places in the US: the Brookhaven Linac Isotope Producer (BLIP) at Brookhaven National Laboratory (BNL) and

the Isotope Production Facility (IPF) at Los Alamos National Laboratory (LANL). Currently, these accelerators can produce about 1.5 Ci of ^{225}Ac from a 10 day irradiation [11]. However, the fission and spallation of the ^{232}Th target resulting from the high energy irradiation produces thousands of Curies of other isotopes in the production of Curies of ^{225}Ac [12]. This makes the radiochemical separation of the actinium difficult and results in the production of other, undesirable, actinium isotopes besides ^{225}Ac [4, 11, 12].

Most other actinium isotopes are not a concern as they are short-lived and lack particularly harmful radiation in their decay chains. However, ^{227}Ac ($t_{1/2}$ = 21.773 y) is a particularly problematic contaminant in ^{225}Ac due to its long half-life, which results in a long-term dose to the patient and complicates the disposal of medical waste [4, 12, 15]. There is skepticism in the medical community that the use of ^{225}Ac produced via ^{232}Th spallation could be made safe and practical due to the presence of ^{227}Ac [4, 9]. It has been proposed instead to use ^{225}Ra also made in spallation for a ^{225}Ra/^{225}Ac isotope generator, which decreases the ^{227}Ac/^{225}Ac ratio by a factor of ∼104, but this comes with a significant reduction in yield compared with the direct production [4, 9, 15]. Actinium-226 ($t_{1/2}$ = 29.4 h) can be a concern as well due to its decay chain emissions, which cause a higher than desired whole body dose [12], but due to its half-life it can be eliminated through decay during the separation and purification of ^{225}Ac, so may or may not be a concern depending on the processing time [9, 15, 16].

The use of isotope separation techniques to obtain ^{225}Ac produced in thorium spallation has been considered [9]. Isotopically pure ^{225}Ac has been produced in Canada at TRIUMF from their Isotope Separator and Accelerator (ISAC) and Isotope Separation On-Line (ISOL) facilities, which are capable of irradiating thorium targets with 480 MeV protons and separating the volatized reaction products by mass number [9]. It may be possible for this production route to be scaled up with significant facility upgrades and dedicated beamtime in the future, if it becomes a priority for TRIUMF [9]. This method is also being developed further in Europe at the proposed Medical Isotopes Collected from ISOLDE (Isotope Separator On Line Device) facility (MEDICIS), but this is not expected to meet widespread clinical demands, merely to provide small amounts of rare isotopes for pharmaceutical development [9].

Actinium-225 production from ^{226}Ra is possible via the ^{226}Ra(p,2n)^{225}Ac reaction [9]. This reaction is considered highly promising as it has the potential to be scaled up for significant ^{225}Ac production [2] and does not co-produce ^{227}Ac [4, 9]. The cross section for this reaction is reasonable (710 mb) at low energies (∼17 MeV), so production can be done with existing medical cyclotrons [1, 4, 9]. The theoretical yields of this production method are high, up to 108 Ci per month with a 1 g ^{226}Ra target.

However, radium targets of this size would be very difficult to handle as radium is air and water reactive, has high associated dose rates and is highly toxic [4, 7, 9]. It is thought that the fabrication of large radium targets would require new facility infrastructure for isotope production [9]. Current experiments have been limited to targets with around 30 mg of ^{226}Ra, which result in tens of mCi of ^{225}Ac production [7]. Sources of the target material are limited as well, but it has been proposed that ^{226}Ra could be obtained from old medical

sources or extracted from uranium mining waste streams as it is part of the ^{238}U decay chain (Fig. 2.2) [9].

The production of ^{225}Ac parent isotopes, rather than direct ^{225}Ac production, has been investigated as well [9, 11]. Nuclear reactor production is common for medical isotopes, but the production of ^{229}Th and ^{225}Ra in this manner is generally considered impractical [9]. Reactor production of ^{229}Th is largely limited by target materials. The irradiation of 1 g ^{226}Ra can theoretically produce ∼2.7 mCi ^{229}Th per month, but this is a very low yield considering the difficulty in obtaining and handling ^{226}Ra targets [9]. While ^{228}Ra and ^{227}Ac targets could have higher yields, these target materials are not available in significant quantities [9]. Production of ^{225}Ra ($t_{1/2}$= 14.9 d) in reactors has been proposed via the ^{226}Ra(n,2n)^{225}Ra reaction but never experimentally validated [9]. The main complication is that this reaction requires a neutron spectrum dominated by high neutron energies (about 7 MeV) with limited low energy neutrons, as these lead to significant ^{227}Ac co-production, and this type of spectrum is not found in typical reactors [9]. However, promising results for ^{225}Ac production via the ^{226}Ra(n,2n)^{225}Ra reaction were obtained recently by Bernstein, et. al. using a beam of neutrons from deuteron breakup, which allows for the irradiation of ^{226}Ra with a higher energy neutron spectrum [17].

Accelerator production of ^{229}Th has been proposed as well, with particular interest in the ^{232}Th(p,4n)^{229}Pa reaction as ^{229}Pa ($t_{1/2}$ = 1.5 d) decays to ^{229}Th. However, the cross section, 162 mb at 29.8 MeV, would require high current irradiations for significant production and cannot be done with standard medical cyclotrons, which generally do not go above 20 MeV. Furthermore, there is competition from the (p,2n) and (p,3n) reactions which have similar or higher cross sections that this energy [9, 11].

The ^{226}Ra(γ,n)^{225}Ra reaction has been used for ^{225}Ac production on a small scale, producing tens of μCi of ^{225}Ac from the decay of ^{225}Ra, but the feasibility has not been demonstrated on a large scale [9]. As mentioned previously, radium targets are extremely difficult to work with and, while some existing facilities have beams that could perform this irradiation and theoretically produce Curies of ^{225}Ac a month, it has never been done and would likely require building new target handling/processing capabilities [9]. Other studies have dismissed this method as entirely impractical due to low yields and it does not appear this method is currently being widely pursued [11].

Finally, the production of ^{225}Ac via ^{230}Th irradiation has also been considered via the following reactions: ^{230}Th(γ,n)^{229}Th [9, 18, 19], ^{230}Th(n,2n)^{229}Th [19], ^{230}Th(p,2n)^{229}Pa [20], ^{230}Th(p,pn)^{229}Th [20], ^{230}Th(p,d)^{229}Th [20], ^{230}Th(p,2p)^{229}Ac [20]. However, due to a lack of ^{230}Th, there has not been significant work in this area [9, 18], though ORNL has conducted some irradiation experiments with ^{230}Th targets, which are discussed in a 2011 presentation [20]. However, as the experiments described in Ref. [20] were conducted over 9 years ago and never published in a peer-reviewed journal, the results of this work are unclear. A later publication by the same authors references a ^{230}Th irradiation along with a measurement of the ^{232}Th(p,4n)^{229}Pa excitation function, but the paper consists solely of details on the ^{232}Th irradiation with no further reference to ^{230}Th apart from the abstract [21].

1.3 The ^{230}Th(p,2n)^{229}Pa Reaction

The ^{230}Th(p,2n)^{229}Pa reaction is shown in Fig. 1.2. It produces ^{225}Ac via the decay of ^{229}Pa, which decays by electron capture and alpha decay with both decay routes ultimately going through ^{225}Ac. However, as mentioned previously, studies with ^{230}Th have been limited due to a lack of material availability [9, 18] and there is little nuclear reaction data available on this isotope. The neutron induced fission of ^{230}Th has been studied [22–24] and proton bombardment on ^{230}Th has been used to assess the nuclear structure of ^{229}Pa [25, 26] and ^{227}Ac [27], but there is no ^{230}Th(p,xn) reaction cross section data available in the literature.

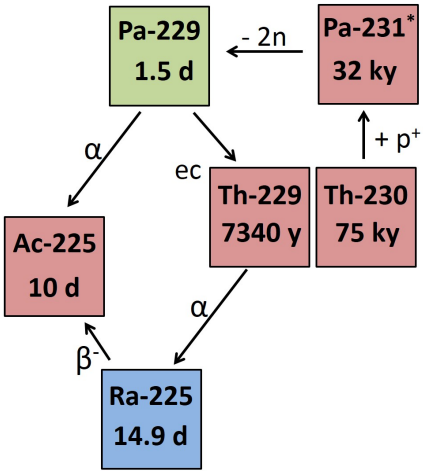

Figure 1.2: Reaction schematic for the production of ^{225}Ac via the ^{230}Th(p,2n)^{229}Pa reaction. Compound nucleus indicated with a *; data from [14]. In this figure, pure alpha emitters are shown in pink, pure beta emitters in blue and isotopes that decay by multiple decay pathways are shown in green.

Calculations of the proton-induced reaction cross sections on ^{230}Th show this reaction may be reasonable cross section for isotope production. These cross sections have been calculated by the nuclear code TALYS, which outputs a TENDL library bi-annually [28–30]. The calculated cross sections from the TENDL 2015 and TENDL 2017/2019 libraries are compared in Fig. 1.3. There was no change in calculations for ^{230}Th(p,xn) reactions between the TENDL 2017 and 2019 libraries [29, 30].

As can be seen from Fig. 1.3, the TENDL 2015 calculation is significantly different than the TENDL 2017 and 2019 calculations. The TENDL 2015 library (Fig. 1.3a [28]) predicts a peak cross section of 2.06 b at 13 MeV for the ^{230}Th(p,2n)^{229}Pa reaction, which is exceptionally high and very promising for isotope production. However, the more recent calculations from TENDL 2017 and 2019 (Fig. 1.3b [29, 30]) predict a peak ^{230}Th(p,2n)^{229}Pa reaction cross section of 256 mb at 14 MeV, which is more reasonable considering similar reactions on ^{232}Th (Fig. 1.4) but less practical for isotope production.

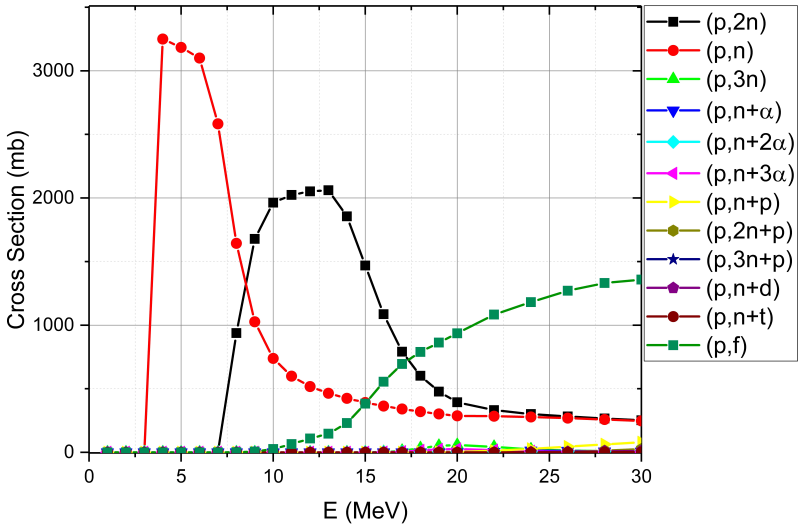

(a) TENDL 2015

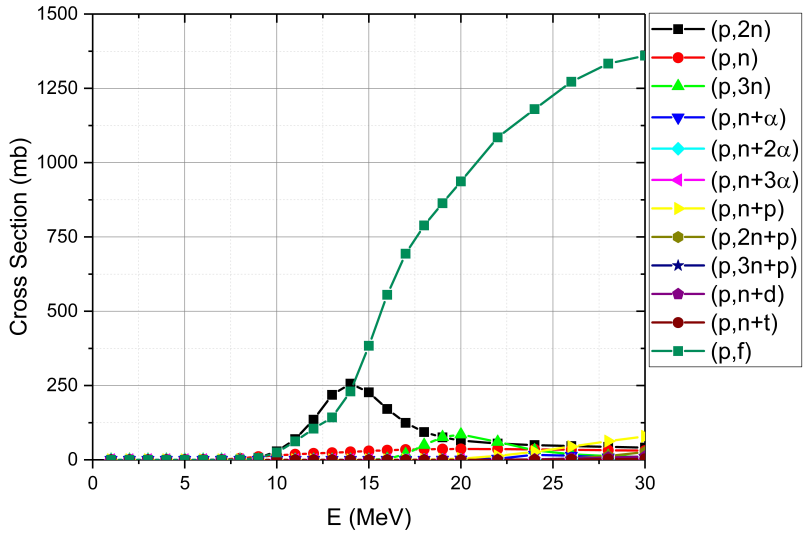

(b) TENDL 2017/2019

Figure 1.3: TENDL calculations for ^{230}Th(p,x) reactions. Data from Refs. [28–30].

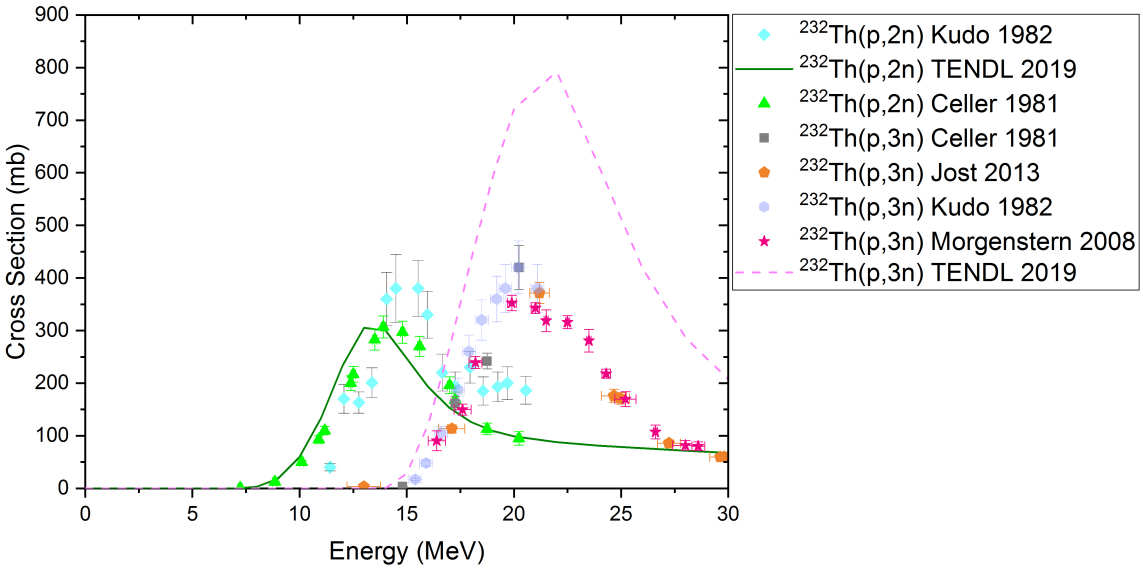

Figure 1.4: Comparison of measured cross sections and TENDL 2019 calculations for the ^{232}Th(p,2n)^{231}Pa and ^{232}Th(p,3n)^{230}Pa reactions.

Production of ^{225}Ac via the ^{230}Th(p,2n)^{229}Pa reaction has many potential advantages. The isotopic purity of ^{225}Ac produced with this reaction would be significantly improved over that of ^{225}Ac produced from ^{232}Th spallation as there are few other significant reactions channels around this energy (Fig. 1.3), which allows for targeted production of ^{229}Pa. Furthermore, due to the separation of ^{229}Pa, the parent of ^{225}Ac, from the target rather than ^{225}Ac itself, decay rather than chemical separations is relied upon to ensure isotopic purity. Thorium-230 targets would be far simpler to handle and process than radium targets and the need for lower energy beams results in less target activation than from spallation, which makes the target processing simpler. Furthermore, proton irradiations in the range of 10 to 16 MeV can be done with commercially available medical cyclotrons [31], which would greatly increase the number of facilities capable of producing ^{225}Ac, reducing the demands on individual facilities.

However, there are several disadvantages as well. The target material, ^{230}Th, is not commercially available, despite being a naturally occurring isotope as part of the ^{238}U decay chain (Fig. 2.2). As the primary decay branch of ^{229}Pa ($t_{1/2}$ = 1.5 d) is electron capture decay (99.52 ± 0.05%) to ^{229}Th rather than alpha decay (0.48 ± 0.05%) to ^{225}Ac, immediate production of ^{225}Ac is low and long-term production is limited by the long half-life of ^{229}Th [14]. A large cross section would be essential for isotope production from this reaction as a large amount of ^{229}Pa would need to be produced to reach significant activities of ^{225}Ac soon after the irradiation. Therefore, to make any real assessment of the feasibility of ^{225}Ac production via this reaction, the cross section needs to be determined.

Work performed as part of this dissertation will seek to determine the feasibility of ^{225}Ac production via the ^{230}Th(p,2n) ^{229}Pa reaction. The excitation function for the ^{230}Th(p,2n) ^{229}Pa reaction will be measured for the energy range of 14 to 17 MeV, based on the TENDL 2019 calculations (Fig. 1.3b) of the peak cross section. From the measured cross section results, an assessment will be made of the feasibility of isotope production and the isotopic purity of the resultant ^{225}Ac.

For these experiments, the ^{230}Th target material will be extracted from uranium ore as there is no commercial source from which to acquire enriched (natural or isotope separated) ^{230}Th. Another possible natural source of ^{230}Th would be the waste streams of uranium ore processing as ^{230}Th is a major component in mining waste [32]. However, the use and disposal of such waste is highly regulated, though it has been proposed as a possible source of both ^{230}Th and ^{226}Ra, which is also a member of the ^{238}U decay chain, for ^{225}Ac production. While isotope separation would be ideal to produce high isotopic purity ^{230}Th for nuclear data measurements and isotope production, isotope separation is very expensive and not commonly done with thorium. Isotope separation of ^{230}Th from ^{232}Th was performed with electromagnetic separation techniques at ORNL in the 1950s and 1960s with hundreds of milligrams of >80% ^{230}Th produced [33–35]. However, changes to the enriched isotope production programs at ORNL were made in the 1990s [36] and very few actinide isotopes are now produced by isotope separation [37]. Furthermore, ^{230}Th is no longer available from the DOE Isotope Program [37].

Any natural thorium material will have numerous thorium isotopes particularly ^{232}Th, the dominant natural thorium isotope. However, once separated from the uranium ore, the thorium material used in this work will be allowed to decay for a year, at which point only ^{232}Th, ^{230}Th, and trace ^{228}Th will remain in the material as the other isotopes will have gone through more than 12 half-lives (see Table 2.1). The presence of ^{232}Th in the material is not problematic for making the ^{230}Th(p,2n)^{229}Pa reaction cross section measurement as the interfering reaction, ^{232}Th(p,4n)^{229}Pa, has a high threshold (19.5 MeV) [38–40] and all irradiations in this work will be conducted at $\leq$17 MeV. Isotope production from the trace ^{228}Th is negligible.

The protactinium separated from the irradiated targets will contain several protactinium isotopes (Table 1.2). All of these isotopes decay to an actinium daughter product, however, due to the half-lives and branching ratios, the actinium production from most of these isotopes is negligible. The branching ratio of the decay of ^{230}Pa to ^{226}Ac is very small (0.0032%) [14]; the long half-life of ^{231}Pa inhibits the in-growth of ^{227}Ac; the alpha decay branching ratio of ^{228}Pa is small (1.85%) [14] and the short half-lives of this isotope and its daughter, ^{224}Ac ($t_{1/2}$ = 2.78 h) [14], would result in these isotopes rapidly decaying to negligible levels post-irradiation and the decay of ^{232}Pa to ^{228}Ac is inhibited by the long half-life of the intermediary daughter product, ^{232}Th. Based on these factors and the known cross sections of the ^{232}Th(p,xn) reactions, it is likely that the isotopic purity of ^{225}Ac produced from a mixed ^{230}Th/^{232}Th target would be higher than that of ^{225}Ac produced from ^{232}Th spallation, but to determine that the relevant ^{230}Th(p,xn) cross sections need to be measured.

Table 1.2: Protactinium isotopes produced from ^{230,232}Th(p,xn) reactions. Reactions included only if cross section is over 1 mb and the threshold is ≤17 MeV. Data from [14] and [41].

Isotope	Reaction	Half-life
^{228}Pa	^{230}Th(p,3n)	22 h
^{229}Pa	^{230}Th(p,2n)	1.5 d
^{230}Pa	^{230}Th(p,n); ^{232}Th(p,3n)	17.4 d
^{231}Pa	^{232}Th(p,2n)	32,760 y
^{232}Pa	^{232}Th(p,n)	1.31 d

1.4 Summary of Experimental Work

The first step in this work was obtaining ^{230}Th from uranium ore. There has been work done in the literature to separate ^{230}Th from uranium mining waste streams [32, 42–44]. However, the chemical composition and concentration of thorium in a mining waste stream is far different than that in ore and most of these papers concern industrial scale purification, so have limited relevance to the separation of thorium from unprocessed ore at a laboratory scale. Therefore, a novel procedure was developed to extract the ^{230}Th directly from unprocessed uranium ore, which was available as legacy material from Lawrence Livermore National Laboratory (LLNL). Due to the high uranium and low "natural thorium" (^{232}Th) content of this ore, the ^{230}Th/^{232}Th isotope ratio is 0.0922 ± 0.00150, several orders of magnitude larger than ^{230}Th/^{232}Th isotope ratios in typical minerals (∼10^{-6} to 10^{-5} [45, 46]), making it naturally enriched in ^{230}Th.

From the thorium separated from the uranium ore, thorium targets were made by electrodeposition. It was necessary to make thick (∼1 mg Th/cm^2), highly uniform targets with stable, adherent deposits on a backing material with good heat transfer properties and limited activation. Extensive optimization studies were done to determine a method for making acceptable targets. Glassy carbon, titanium and platinum were considered as backing materials with the final selection determined based on the quality of the target, irradiation performance and chemical properties relevant for the post-irradiation target processing.

To accurately measure the activity of ^{229}Pa produced in the irradiations, chemical processing of the irradiated targets was necessary. Due to the short half-life and weak gamma-ray emissions of ^{229}Pa (discussed further in Chapter 7) [14], the chemical processing had to be rapid, high yield and high radiopurity. Experiments for the development of chemical procedures for target processing were done in two stages, first using tracer isotopes, then irradiated ^{232}Th targets. The separation was optimized based on a number of parameters including the target backing material, dissolution chemistry, chromatographic resin, elution pattern and number of columns. The use of anion exchange and extractant based resins were considered, including CL resin (Triskem International). While CL resin was not chosen for

the final target processing procedure, further batch studies were done to better characterize the behavior of radium and the early actinides on this resin as there is limited data available in the literature.

To produce tracer isotopes for the chemistry development and electrodeposition studies, two isotope generators were made and characterized. A ^{237}Np/^{233}Pa isotope generator was made, an elution procedure established, and the elution curve and lifetime of the generator were characterized. From an existing procedure in the literature, the ^{231}Pa decay chain was used to make an ^{227}Ac/^{227}Th isotope generator.

The electrodeposition of ^{231}Pa was also studied in anticipation of needing to develop a procedure for making protactinium alpha sources for activity measurements as part of the cross section measurement experiments. While alpha spectroscopy was ultimately not used for this purpose, nuclear data studies were done with the ^{231}Pa alpha sources that were made as the evaluated nuclear data for this isotope is lacking; many previous measurements have large uncertainties and only two measurements are used to determine the absolute intensities. Therefore, new measurements of the gamma-ray energies and intensities of the decay of ^{231}Pa to ^{227}Ac were done as part of this work.

To measure the ^{230}Th(p,2n)^{229}Pa reaction cross section, three irradiations were conducted at the Center for Accelerator Mass Spectrometry (CAMS) at LLNL with proton energies of 15, 16 and 17 MeV. Each target stack contained several thorium targets, spacer foils to degrade the energy and a flux monitor. The target stacks were modeled using the Stopping and Range of Ions in Matter (SRIM) 2013 [47] to assess the energy change through the target stack and determine the optimal geometry for the target stack, including the position of the targets and additional foils (beam stop, spacer foils, etc.). The ^{230}Th(p,3n)^{228}Pa reaction cross section, which has a threshold energy of 15 MeV [39, 40], was measured along with the ^{230}Th(p,2n)^{229}Pa reaction cross section where possible.

Finally, preliminary extraction studies were done on the behavior of radium and actinium in basic solutions with Pb resin and Rose Bengal (RB), a large anion that has been shown to increase barium extraction in certain conditions. Batch, kinetics and column studies were done to determine the affinity for radium and actinium to the resin under acidic, neutral and basic conditions with and without the presence of RB.

All experiments described in this work were done in specialized facilities designed for the safe handling and containment of long-lived and/or highly radioactive isotopes. Appropriate safety precautions were taken for work involving radionuclides as well as hazardous, toxic, corrosive and carcinogenic chemicals.

Chapter 2

Separation of Thorium from Uranium Ore

2.1 Introduction

Thorium-230, historically known as ionium, is part of the ^{238}U decay chain. There are many research areas today where this isotope is relevant. It is an essential component of uranium-thorium dating, which uses disequilibria between the parent isotope ^{238}U and its daughter ^{230}Th to date carbonate materials [48]. This dating method relies on the chemical differences in solubility between uranium and thorium, which leads to their separation during geological processes [48]. Recent work has been done to better characterize ^{230}Th nuclear data to improve the accuracy of this dating method [49] as well as provide information for the designs of advanced thorium fueled fast reactors [50].

Many isotopes of interest can be produced from ^{230}Th. Via the ^{230}Th(p,2n) reaction, it can be used to produce ^{229}Pa and its daughter ^{225}Ac. Both of these isotopes have important research applications: ^{229}Pa is a pear-shaped nucleus that is a candidate for more sensitive studies on nuclear properties, like parity violation [51], and ^{225}Ac is a medically relevant isotope that is a potential agent for TAT cancer treatment as discussed in Chapter 1 [1].

Despite the interest in ^{230}Th for nuclear data measurements and isotope production, it is not available in sufficient quantities for research [9, 52]. This necessitates that it be obtained from the ^{238}U decay chain where it is naturally occurring. The purpose of this chapter is to develop a method for the extraction of significant quantities of ^{230}Th from uranium ore for use in isotope production experiments.

There has been work done in the literature to separate ^{230}Th from uranium mining waste streams [32, 43, 44, 53], but the chemical composition and concentration of thorium in a mining waste stream is far different than that in ore. Furthermore, most of these papers describe industrial scale purification and have limited relevance to the separation of thorium from unprocessed ore on a laboratory scale. The separation of milligrams of thorium from kilograms of unprocessed uranium ore has not been presented in the literature and, therefore,

a novel process for this separation was developed.

Uranium ore is classified by grade, with high-grade ore containing 1 to 4 wt.% uranium, medium-grade with 0.1 to 0.5 wt.% uranium and low-grade with less than 0.1 wt.% uranium [54]. In high-grade ores, uranium is often found in the form of uranite, a mix of uranium oxide compounds previously known as pitchblende [54, 55]. Lower-grade ores can have a number of different uranium containing minerals; in the United States, vanadates and phosphates are common [54, 55].

The uranium ore used in this work is legacy material from LLNL and is extremely high-grade. The main components are quartz (α-SiO_2), lead uranium oxide (PbU_3O_9), and uranium oxide (U_4O_9); clay ($(Mg_{11.06}Fe_{0.94})$ $((Si_{5.22}Al_{2.78})O_{20}(OH)_{16})$) and iron oxide ($Fe_5O_7(OH) \cdot 4H_2O$) are present in smaller amounts. The ore was previously determined to have 39.1 ± 1.8 wt.% uranium by a Davies and Gray titration and was characterized by mass spectrometry for trace element composition. Figure 2.1 shows a sample of the ore as it was received. Relevant isotopic ratios were determined with mass spectrometry; the $^{230}Th/^{232}Th$ ratio is 0.0922 ± 0.00150 and the $^{235}U/^{238}U$ ratio is 0.0072579 ± 0.0000075.

Figure 2.1: Uranium Ore.

Any natural source of uranium contains the three primordial actinide decay chains, ^{238}U, ^{235}U and ^{232}Th (Figs. 2.2, 2.3 and 2.4), and all of these have two thorium isotopes in their decay chains, therefore, the final product will contain six thorium isotopes (Table 2.1). Three of these have half-lives less than a month ($^{227,231,234}Th$), and, therefore, can be reduced to negligible amounts in the final product by allowing it to decay for a year as they will have gone through more than 12 half-lives. This leaves $^{228,230,232}Th$ present in the final product, which cannot be altered without isotope separation. Although ^{228}Th has a half-life of 1.91 years [14], it is in secular equilibrium with ^{232}Th ($t_{1/2} = 1.4 \times 10^{10}$ y) so the amount cannot be reduced by waiting for it to decay. However, ^{228}Th and ^{232}Th are well characterized isotopes in regard to nuclear data [14] and should not significantly interfere with the previously mentioned uses for ^{230}Th.

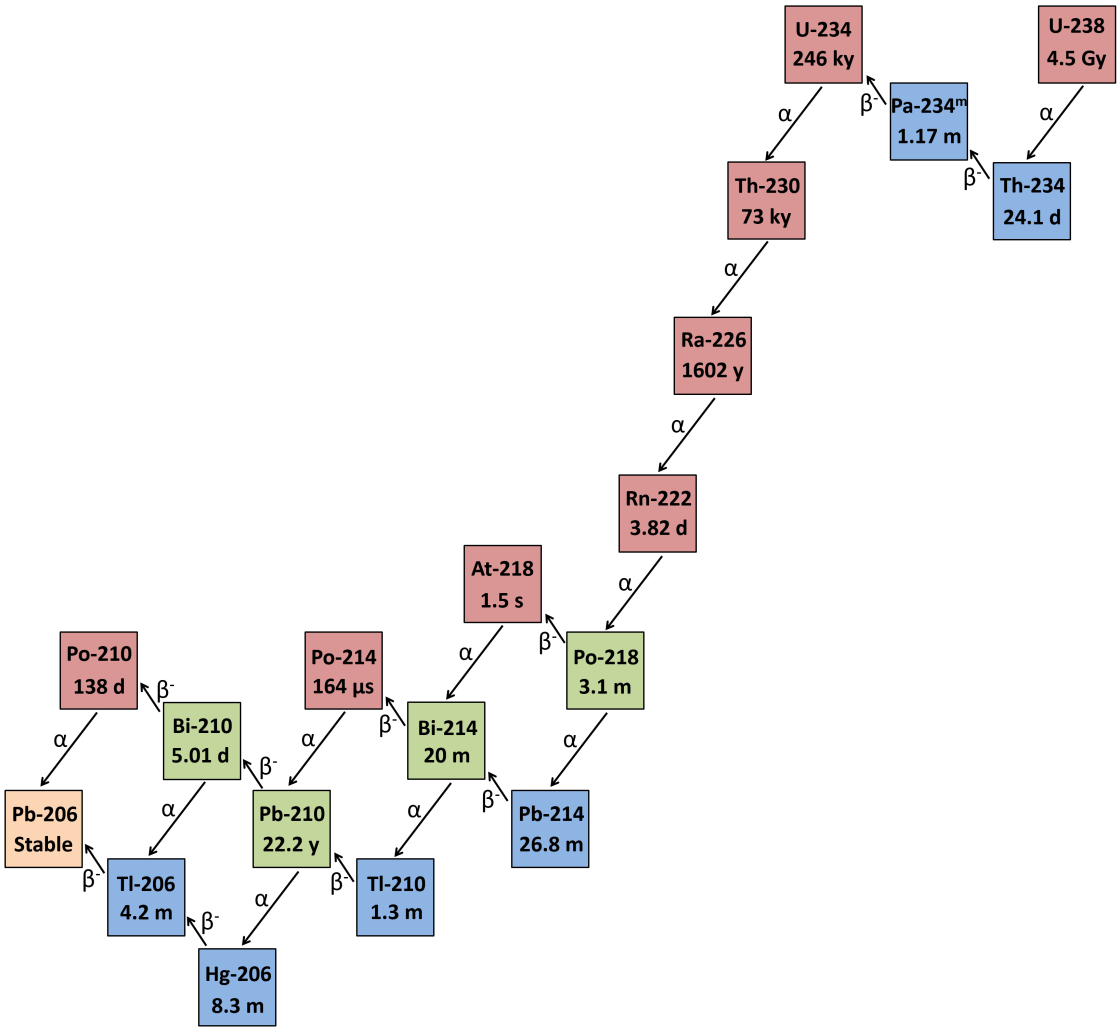

Figure 2.2: Decay chain of ^{238}U. In this figure, pure alpha emitters are shown in pink, pure beta emitters in blue, stable isotopes in pale orange and isotopes that decay by multiple decay pathways are shown in green.

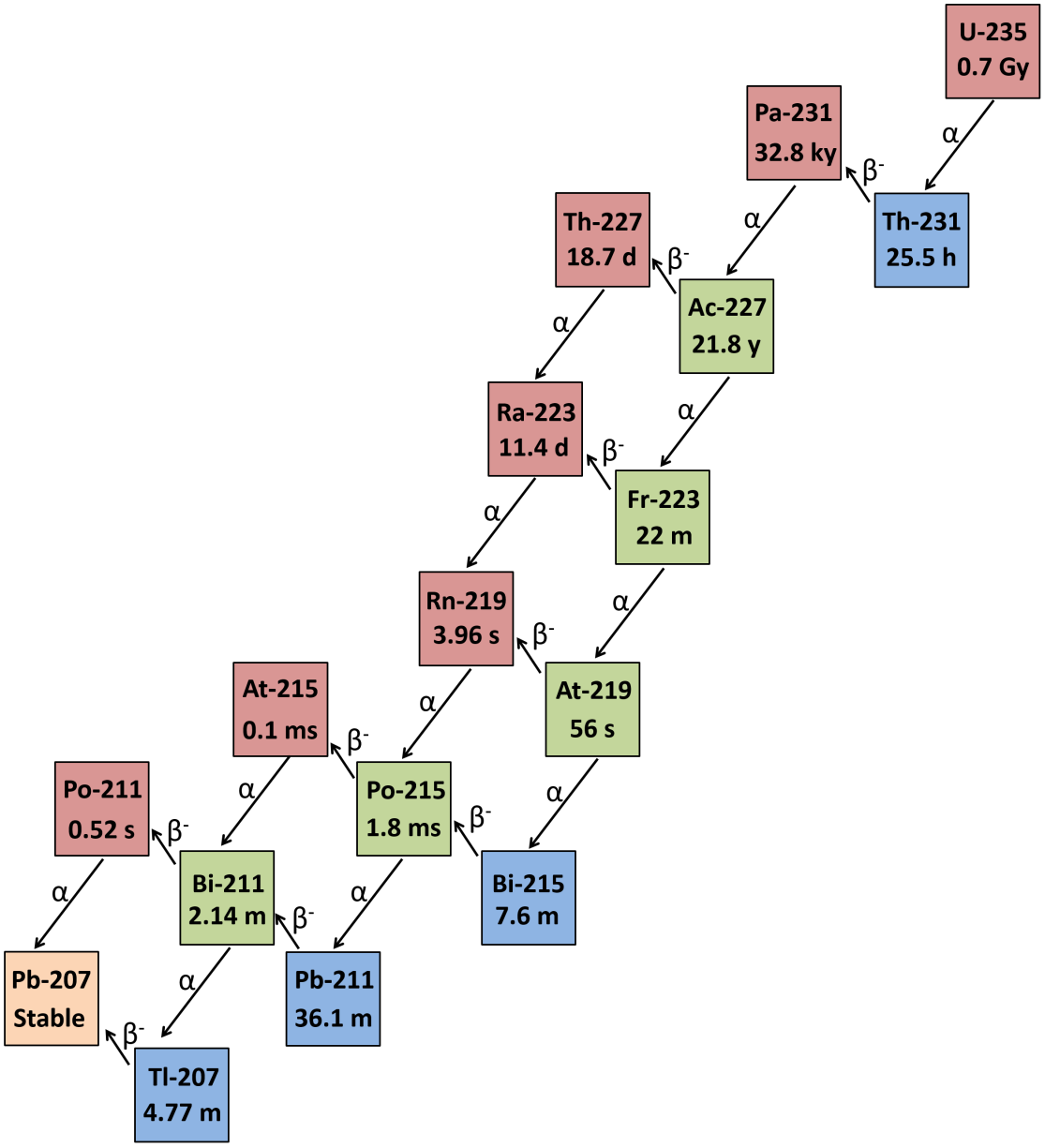

Figure 2.3: Decay Chain of ^{235}U. In this figure, pure alpha emitters are shown in pink, pure beta emitters in blue, stable isotopes in pale orange and isotopes that decay by multiple decay pathways are shown in green.

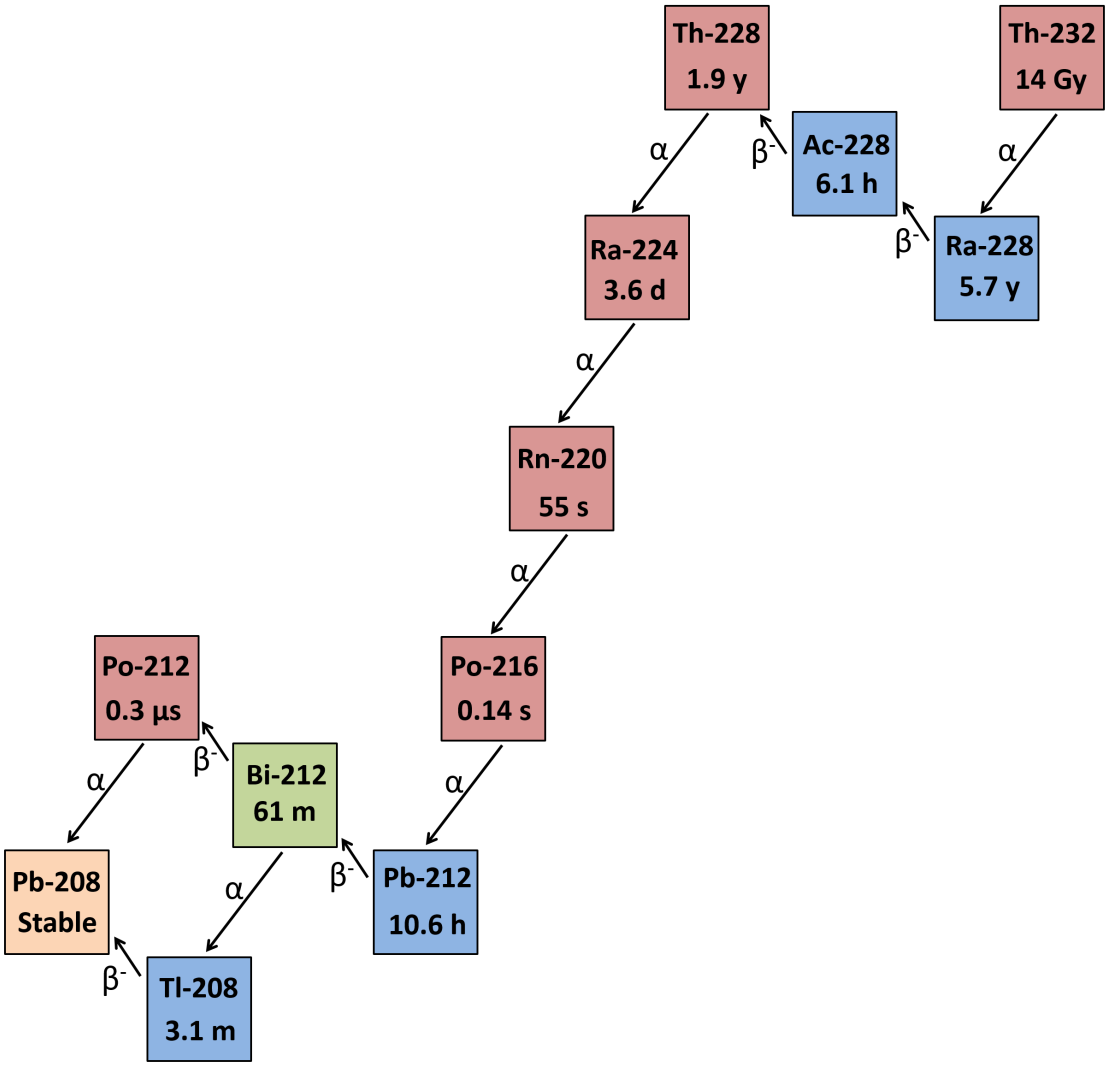

Figure 2.4: Decay Chain of ^{232}Th. In this figure, pure alpha emitters are shown in pink, pure beta emitters in blue, stable isotopes in pale orange and isotopes that decay by multiple decay pathways are shown in green.

Table 2.1: Naturally occurring thorium isotopes. Half-lives from Ref. [14].

Primordial Isotope	**Thorium Isotopes in Decay Chain**	**Half-Life**
^{238}U	^{234}Th	24.10 d
	^{230}Th	75,380 y
^{235}U	^{231}Th	25.52 h
	^{227}Th	18.68 d
^{232}Th	^{232}Th	1.405×10^{10} y
	^{228}Th	1.9116 y

In the mining industry, uranium ore is first leached to dissolve out the uranium [55]. The leaching process can be done under acidic or alkaline conditions and uses the solubility of U(VI) as a sulfate or a carbonate [54] to dissolve the uranium into sulfuric acid or a sodium carbonate/bicarbonate solution, respectively [55]. In either case, if the ore contains U(IV), which has limited solubility, an oxidant is added to convert it to U(VI), which is highly soluble in the aforementioned solutions [54, 55]. Common oxidants are iron, manganese dioxide (MnO_2) and hydrogen peroxide (H_2O_2) [54, 55]. Leaching is followed by more selective purification methods, like solvent extraction or ion exchange chromatography, to remove other elements and minerals that also dissolve under the leaching conditions [54, 55].

Acidic leaching is generally preferable as it is faster and requires fewer processing steps than alkaline leaching, which is only used under very specific conditions when the minerals in the ore have a high acid consumption. Therefore, it was decided to do acidic leaching for this experiment [55]. It was not desirable to use sulfuric acid in this process for several reasons. Uranium sulfate forms more favorably than thorium sulfate, so this method is not optimal for thorium recovery. Furthermore, sulfuric acid has a high density, high viscosity and very low pH, resulting in the need for large volumes of base for neutralization and slow evaporation. All of these factors make sulfuric acid unfavorable for leaching thorium, particularly in a non-industrial setting. Therefore, for this work, a novel, multi-step leaching procedure using nitric acid (HNO_3) was developed as an alternative to the once-through sulfuric acid-based leaching that is common in industry.

After leaching, a liquid-liquid extraction was chosen as the first separation step to remove the thorium from the bulk of the ore mass. Ion exchange chromatography and precipitation were considered but were not practical for the first separation step due to the scale. While chromatography is extremely selective, very large ion exchange columns are needed for large masses and these are not available in most non-industrial settings. Precipitation does not work well when the masses are highly disparate. In this case, since uranium is by far the largest mass component in the solution, precipitating uranium would likely carry the other actinides, or carrier would need to be added to precipitate thorium, which would add mass to the system and create the same problem in the next processing step.

Liquid-liquid extraction is ideal because it can be highly selective and significantly reduce mass for later separation steps. For this experiment, tri-butyl phosphate (TBP), Fig. 2.5, was chosen as the extractant.

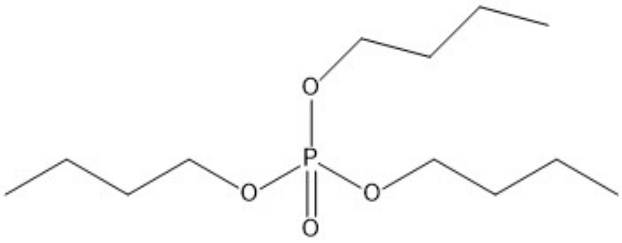

Figure 2.5: Tri-butyl phosphate

The extraction of uranium, and thorium from aqueous solutions with TBP has been extensively studied in the literature [42, 56–60]. Tri-butyl phosphate extractions are commonly applied to ore processing as well [32, 43, 44, 53]. In HNO_3-TBP systems, TBP complexes uranium and thorium, as shown in Eqns. 2.1 and 2.2 [56], and extracts them into the organic phase, separating them from the other constituents of the ore.

$$UO_2(NO_3)_{2\ (aq)} + 2TBP_{(org)} \rightleftharpoons UO_2(NO_3)_2 \cdot 2TBP_{(org)} \tag{2.1}$$

$$Th(NO_3)_{4\ (aq)} + 2TBP_{(org)} \rightleftharpoons Th(NO_3)_4 \cdot 2TBP_{(org)} \tag{2.2}$$

The literature gives a variety of conditions for extracting thorium from aqueous HNO_3 solutions of uranium ore waste: Ref. [43] recommends an aqueous phase of 1 M HNO_3 (8 M total nitrate) with 30% TBP in kerosene as the organic phase, Ref. [53] used 0.4 M HNO_3 with pure TBP and Ref. [44] recommends oxalic acid ($C_2H_2O_4$) with pure TBP for a high yield extraction and 0.4 M HNO_3 (3 M total nitrate) with pure TBP for a sufficient extraction.

Reference [56], which presents a comprehensive study of thorium extraction by TBP, was used as a basis for the forward-extraction in this work because it was desirable to extract thorium directly from the conc. HNO_3 leaching solution, rather than dilute to a lower HNO_3 concentration, to keep volumes to a minimum. Although Ref. [56] is limited to concentrations from 1 to 11 M HNO_3 (see Fig. 2.6a and 2.6b), the procedure outlined in this reference was tested with conc. HNO_3 as the aqueous phase and performed extremely well. Therefore, Ref. [56] was used to as a basis to determine the conditions for the liquid-liquid extraction in this experiment, particularly diluent concentration and relative phase volumes. However, the procedure ultimately developed for the bulk liquid-liquid separations has not been reported in the literature in the volumes or concentrations that were used in this process.

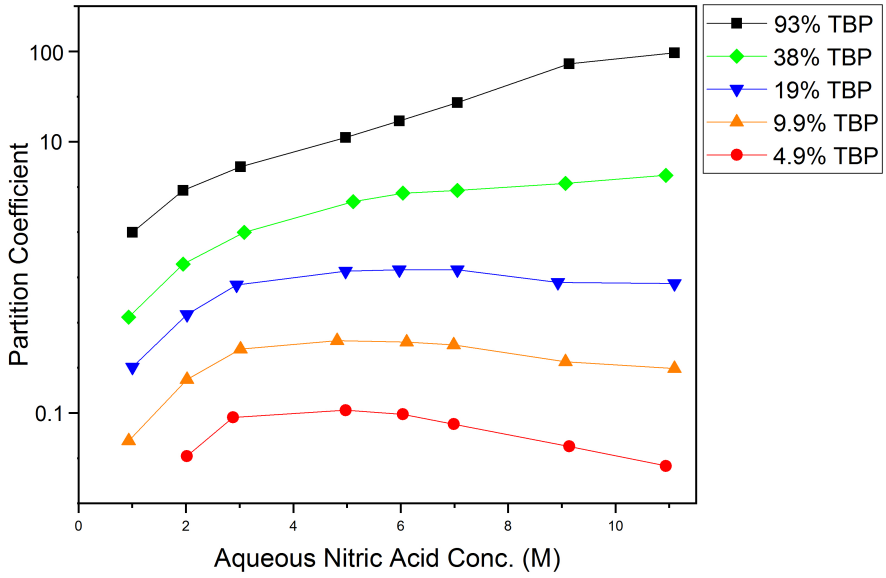

(a) Thorium

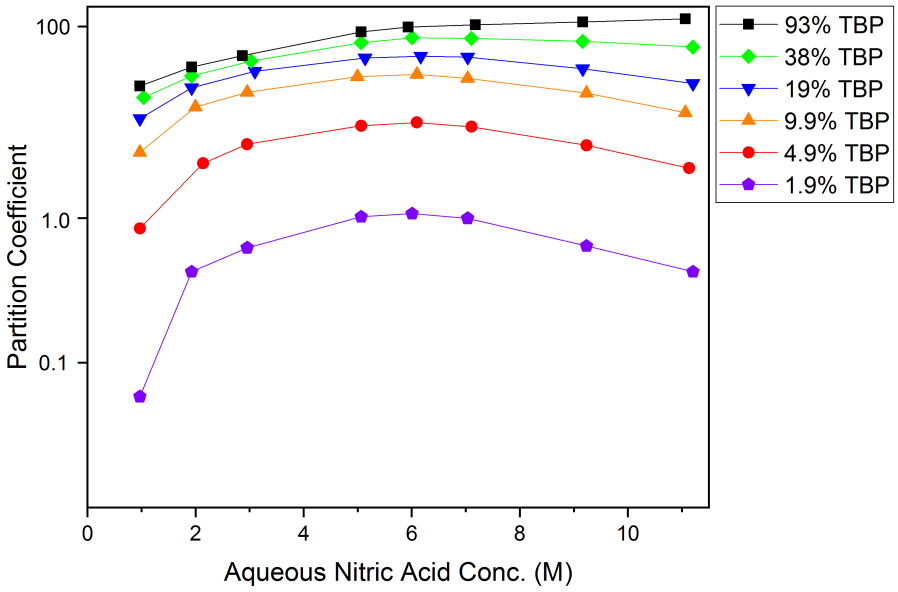

(b) Uranium

Figure 2.6: Partition coefficients of uranium and thorium in HNO_3. Data from Ref. [56]; the diluent was kerosene.

As with the extraction from aqueous solution into TBP, the literature gives a variety of ways to back-extract thorium and uranium from TBP into an aqueous solution. Reference [56] suggests back-extraction of thorium with 6 M hydrochloric acid (HCl), while Ref. [53] uses 1 M hydrofluoric acid (HF) and Ref. [43] uses 0.1 M HNO_3. The options for uranium back-extraction are similarly varied with Ref. [56] using 10 wt.% ammonium carbonate ($(NH_4)_2CO_3$), while Ref. [57] suggests 3 M acetic acid (CH_3COOH). For this experiment, many options for the aqueous phase were considered and tested on a small scale. Ultimately, HF was chosen as the aqueous phase for the back-extraction based on Ref. [53]; initial tests with HCl and HNO_3 back-extractions had low to no yield of thorium.

Once the thorium and uranium are separated from the bulk mass, an anion exchange column was used for a more selective separation. Anion exchange was chosen rather than cation exchange because thorium tends to bind irreversibly to cation exchange resins due to slow kinetics and an extremely high distribution coefficient. It displays similar behavior on anion exchange resins in HF as well. Finally, since the back-extraction solution contains a significant amount of the uranium mass, an optimal separation system would bind the thorium, a much smaller mass, and allow the uranium to pass through the column thus decreasing the amount of resin needed.

Considering these conditions, the column separation used in this experiment was based on the thorium-uranium separation in Ref. [61], which loads uranium and thorium in 8 M HNO_3 on a Dowex 1x8 column.

2.2 Description of Experimental Work

The ore for this experiment is described above. Before processing, it was dry-crushed with a ball mill (see Fig. 2.7). All chemicals were purchased from Sigma-Aldrich and were ACS grade or higher; acids were diluted as necessary with Millipore Milli-Q deionized water (18.2 MΩ cm). An overview of the ore processing procedure is given in Fig. 2.8 and is described in the following sections.

All mass spectrometry measurements were performed with a Thermo Scientific iCAP quadrupole ICP-MS (Inductively Coupled Plasma Mass Spectrometry). Full quantitative analysis was done with a linear calibration curve based off external standards. An internal standard was used to correct for matrix signal suppression and instrument drift. Samples were analyzed in triplicate and the reported error is the standard deviation of the measurements.

A high purity germanium (HPGe) detector with Ortec NIM electronics and ASPEC multi-channel analyzer was used to monitor the ore processing in several steps and to make relative measurements. Maestro software (Ortec) was used to analyze the resultant spectra and all measurements were made using the same HPGe detector and in the same geometric configuration. Quantitative gamma-ray spectroscopy was performed by the Nuclear Counting Facility (NCF) at LLNL.

Figure 2.7: Uranium ore after ball-milling.

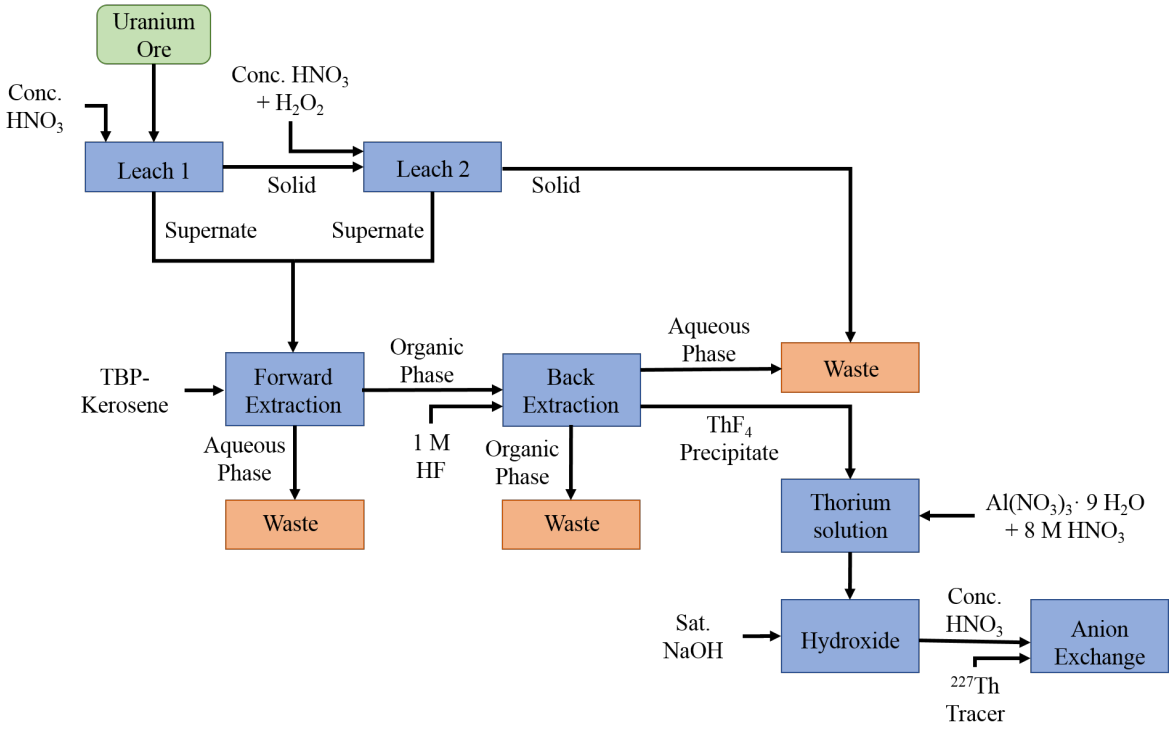

Figure 2.8: Simplified chemical processing scheme.

Leaching

A sequential leaching process was developed to remove the elements of interest from the ore. Three tests of novel leaching methods were done on a small sample of ore and the most efficient method was scaled up for bulk processing.

The initial leaching tests were done simultaneously under identical conditions to compare the leaching efficiency of conc. HNO_3, conc. HCl and aqua regia. Each test used 20 g of ore in a Teflon beaker and consisted of multiple leaching steps. The solution for each step was allowed to react for 24 hours total and between steps the solutions and remaining ore/precipitates were centrifuged for 2 minutes and 10 seconds at 4500 rpm. The solution was then decanted and the solid was dried at 95 °C for 2.5 hours before the next solution was added.

Initially, 20 mL of the acid solution of interest was added to each beaker and heated at 80 °C on a hot plate for six hours under observation. An additional 20 mL of acid was added after 3 hours. Upon adding acid, it was observed that the HNO_3 beaker bubbled and evolved a significant amount of brown gas, identified as NO_2, and the solution was dark yellow. The HCl beaker turned forest green with no gas emission or bubbles. The aqua regia beaker was dark yellow-green, violently fizzed and evolved brown gas. After heating, the beakers sat for 18 hours, after which it was seen that the HNO_3 beaker had the least amount of ore mass remaining along with a yellow solution and a white precipitate. The HCl beaker had leached the least, with a significant amount of ore mass remaining in a dark green solution along with a black precipitate. The aqua regia beaker was between the other two with some ore mass remaining, a yellow-green solution and white and black precipitate present.

For the second step, 1 mL unstabilized H_2O_2 was added to serve as an oxidant and allowed to react for 3 minutes before the addition of 25 mL of the initial acid. After the leach was completed, the aqua regia beaker was observed to have the most solid remaining; due to this and the initially more vigorous reaction (the fizzing was judged to be too risky on a large scale) this method was disregarded without further testing. The HNO_3 beaker again had the least amount of solid remaining, and the HCl beaker had solid remaining at an amount between the HNO_3 and aqua regia beakers.

For the third step, 40 mL conc. HCl was added to the beaker that originally contained conc. HNO_3 and 40 mL conc. HNO_3 were added to the beaker that originally contained HCl. This third leach was treated in the same manner as the first. The beaker that went from conc. HNO_3 to conc. HCl had a dark green supernatant and a little solid remaining. The beaker that had gone from conc. HCl to conc. HNO_3 had a yellow solution and not as much dissolution with a black and white precipitate and pieces of the initial ore were still visible.

Finally, the fourth step in the leaching test was another leach with the initial acids, this time 30 mL. This was done in the same manner as the previous steps, and after the leach, the HNO_3 beaker had a pale-yellow solution and white precipitate, which contained lead and radium (identified by gamma-ray spectroscopy). The HCl beaker was green with a black precipitate and some white precipitate and ore remaining.

From these results, a final leaching procedure consisting of four steps was established for use with the bulk ore. The total mass of ore processed was 1.7 kg. It was done in five batches, each in a 4 L glass beaker: three of the beakers had about 400 g each of ore and the other two contained about 200 g each of ore. For each step in the leach process, the solution was mixed with a stir bar for 48 hours then, after the reaction was complete, the solution was removed with a peristaltic pump and the ore dried overnight (65 to 80 °C).

Leach one used 2.5 L conc. HNO_3 for the beakers with 400 g ore and 1.5 L conc. HNO_3 for the beakers with 200 g ore. This was an extremely exothermic reaction and acid was added carefully over the course of about two hours. After all the acid was added, the solution was observed to boil under the reaction heat. A large amount of brown gas, assumed to be NO_2, was evolved. The beakers were heated at 80 °C during the second day for 8 hours. The resulting solution was dark yellow-brown, presumably due to uranyl nitrate (see Fig. 2.9).

After removing the solution and drying the ore, as described above, the second leach began. Leach two used 30 mL unstabilized H_2O_2 initially and, after the reaction had ceased, conc. HNO_3 was added to each beaker in the following volumes: 2.5 L to the beakers with 400 g of ore and 1.5 L to the beakers with less mass. Gas was evolved during this step as well, though not as much as in the first step; the solution was yellow, again due to uranyl nitrate.

Leach three used conc. HCl, 2 L for the beakers with more mass and 1 L for the beakers with less. The solution was forest green; no gas or bubbles were observed. Leach four used conc. HNO_3 with the same volumes as the third leach step. The solution was pale yellow and no visible NO_2 gas was observed. Each step in this process is shown in Fig. 2.9. Analysis was done with ICP-MS as described above and gamma-ray spectroscopy was done at the NCF at LLNL.

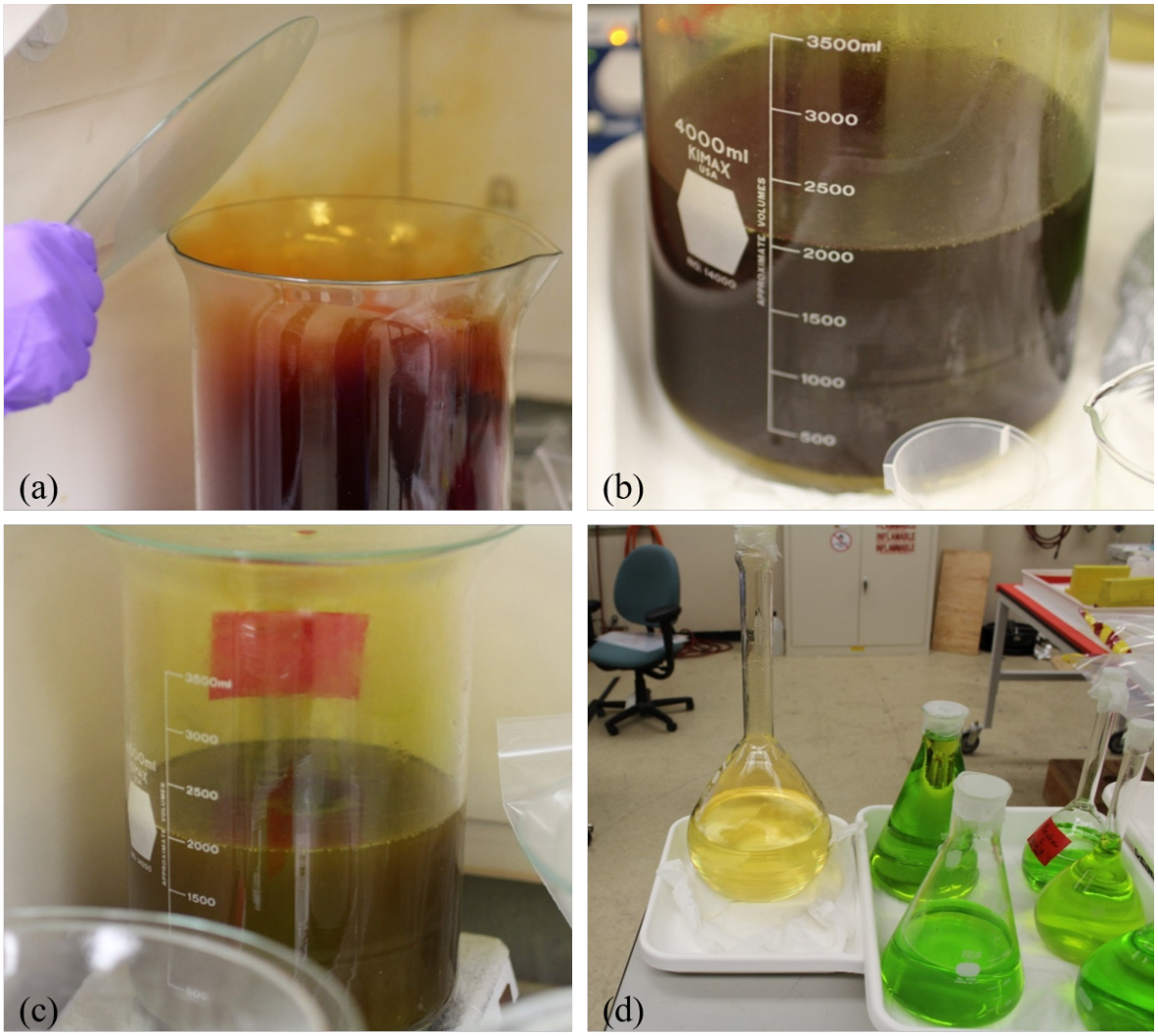

Figure 2.9: (a) Significant NO_2 gas evolution from adding conc. HNO_3 to ore in leach one (b) Leach one (conc. HNO_3) after reaction has ceased (c) Leach two (H_2O_2 + conc. HNO_3) while mixing; note the reduction in gas evolution compared to leach one (d) Leach four (conc. HNO_3) on the left and leach three (conc. HCl) on the right.

Liquid-Liquid Extraction

A liquid-liquid extraction was used to remove the thorium from the bulk ore. As leaches one and two contained 90.8 ± 15.4% of the thorium initially present in the ore (Fig. 2.12), only these two contained enough thorium to be worth further processing. The extraction was tested on a small scale before being scaled up to treat the bulk solutions. For these tests, a 20 mL aliquot of the first leach solution was added to a 50 mL centrifuge tube containing an equal volume of 93% tributyl phosphate, which was diluted with kerosene and preequilibrated with an equal volume of conc. HNO_3 immediately before the extraction. The phases were mixed by manually shaking for 10 minutes then separated by centrifugation (2000 rpm, 4 minutes) and the organic phase removed by pipette. Each phase was counted by gamma-ray spectroscopy. The back-extraction was tested with several different aqueous phases: 10 wt.% ammonium carbonate, 3 M acetic acid, 0.2 M HNO_3, 1 M HF, dil. HCl, dil. HNO_3. For each test, the organic phase was back-extracted with an equal volume of aqueous phase in the same manner as the forward-extraction. The back-extraction with 1 M HF had the best results for thorium. The full extraction process was repeated eight times on 20 mL aliquots to characterize the percent extraction.

Based on these results, a procedure was developed for the bulk extractions. First, 750 mL of the leach solution was added to a 2 L Nalgene separatory funnel, then 750 mL 93 % TBP in kerosene (pre-equilibrated with an equal volume of conc. HNO_3) was added. This was mixed for two hours with a Heidolph overhead mixer equipped with a propeller type stirring rod made of Teflon-coated stainless steel. The mixed phase separated under gravity overnight; 12 hours was the minimum time for phase separation. The aqueous phase of the forward-extraction was removed and 750 mL 1 M HF was added. This was mixed for two hours with a 12 hour phase separation time. The HNO_3 phase and organic phase were discarded after processing. Phase separation for the forward-extraction and back-extraction is shown in Fig. 2.10. Analysis for the back-extraction solution was done with ICP-MS as described above.

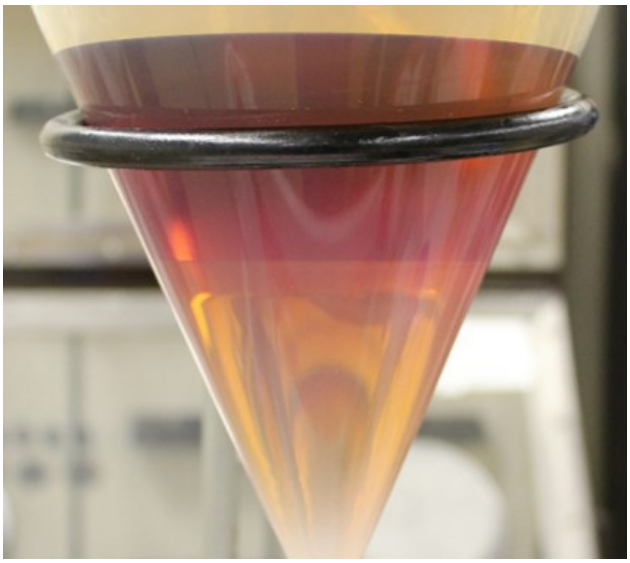

(a) Forward-extraction phase separation (TBP organic phase on top; HNO_3 aqueous phase on bottom).

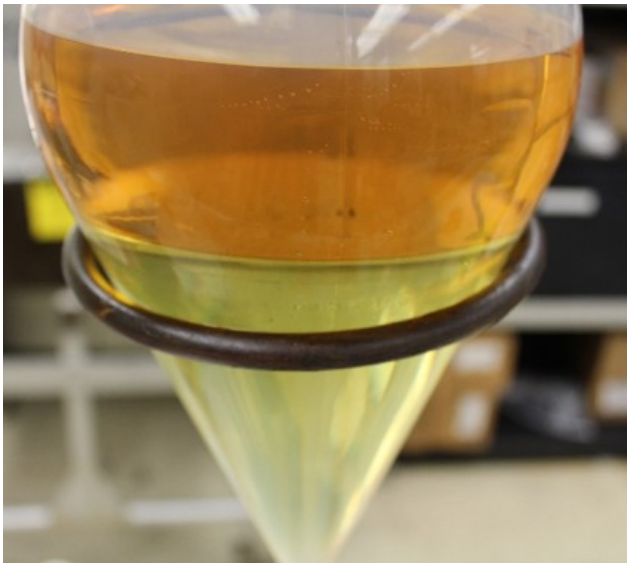

(b) Back-extraction phase separation (TBP organic phase on top; HF aqueous phase on bottom).

Figure 2.10: Forward- and back-extractions of the liquid-liquid extraction.

Precipitation and Ion Exchange Chromatography

The back-extraction solution in 1 M HF was centrifuged to remove thorium tetrafluoride (ThF_4), which precipitates, although not quantitatively. This is a white, highly insoluble salt; gamma-ray spectroscopy determined that some uranium and protactinium were carried with the precipitate, which was dissolved into a nitrate solution composed of an equal volume of sat. aluminum nitrate ($Al(NO_3)_3 \cdot 9H_2O$) and 8 M HNO_3. To this, sat. sodium hydroxide (NaOH) was added until the solution had a pH of 14. This process precipitates the actinides as hydroxides. The solution was centrifuged (4000 rpm, 2 minutes) and the supernate was decanted. The supernate was discarded and the actinide hydroxides were dissolved in conc. HNO_3. The dissolved hydroxide precipitate was analyzed with ICP-MS.

This solution was divided into twelve, 40 mL aliquots and each aliquot was loaded onto a 5 mL (7.5 cm by 9.3 mm) Dowex 1x8 column (100-200 mesh) that had been pre-washed with eight bed volumes (40 mL) of 8 M HNO_3 to convert the resin to NO_3^- form. Each column was then washed with 100 mL 8 M HNO_3 to remove the transition metals, lanthanides, protactinium and uranium. Thorium was stripped with 40 mL 10 M HCl (Fig. 2.11). The thorium fractions from all of the columns were combined, evaporated to dryness and reconstituted in conc. HNO_3. The final product was analyzed by ICP-MS and HPGe gamma-ray spectroscopy.

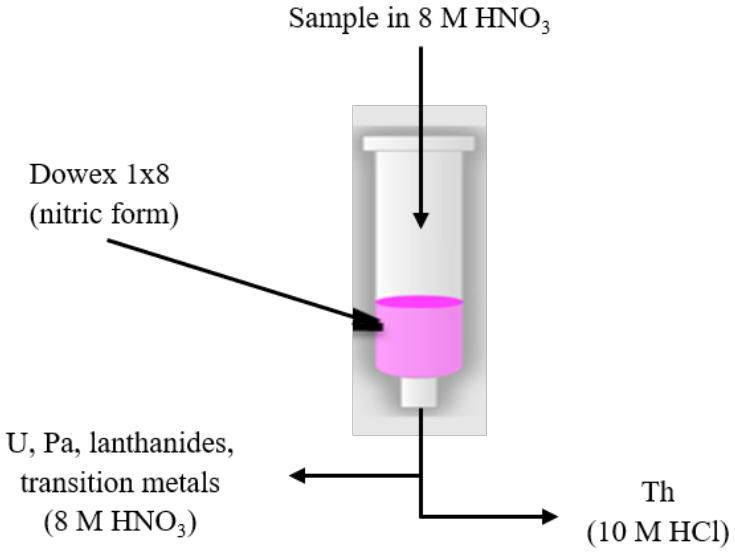

Figure 2.11: Schematic for HNO_3 anion column separation.

For the ion exchange chromatography, a ^{227}Th tracer was added to follow the progress of the bulk thorium through the column as the main thorium isotopes present (^{228}Th, ^{230}Th, ^{232}Th) have no readily detectable gamma-ray signatures and the naturally occurring ^{227}Th

had already decayed out when the column separation was done. The tracer was separated from legacy ^{231}Pa from LLNL (see Chapter 3). As mentioned previously a schematic of the full separation process is shown in Fig. 2.8.

2.3 Results and Discussion

Leaching

Yields for each leaching step were calculated from ICP-MS data for each leaching solution as compared to mass spectrometry data for the ore prior to processing. The calculated yields for each leach are shown in Fig. 2.12. For protactinium and radium, mass spectrometry data was not gathered as these elements are prone to having interferences with the actinides. Therefore, gamma-ray spectroscopy data is shown in Fig. 2.12 for ^{231}Pa and ^{226}Ra. The yields for uranium were calculated with both mass spectrometry and gamma-ray spectroscopy (using the 185 keV line from ^{235}U); the results were within error. For Fig. 2.12 and all other mass spectrometry plots, the data has been simplified to show periodic trends rather than values for individual elements, see Appendix A (Figs. A.1 to A.4) for full mass spectrometry data.

From Fig. 2.12, it can be seen that thorium was leached with a high yield in leaches one (74 $\pm$ 15%) and two (16.8 $\pm$ 3.4%), and less well in leaches three (6.9 $\pm$ 1.4%) and four (1.57 $\pm$ 0.32%). The large error bars on the thorium yields are largely due to the error on the initial value for thorium in the unprocessed ore. The other actinides and the lanthanides also have high yields in the first leach along with some of the early transition metals, particularly scandium and yttrium (see Fig. A.1). The early transition metals have a chemistry analogous to thorium in solution, so this behavior was expected. Thorium is stable in the 4+ oxidation state in solution and behaves like a d^0 metal, giving it similar chemistry to the d^0 early transition metals like scandium, yttrium, and zirconium. This tendency for scandium and yttrium to follow thorium is seen in both the leaching and the liquid-liquid extraction; more selective methods are required to separate these metals.

As the s- and p-block elements and late transition metals either do not form nitrate complexes as favorably or are bound in minerals that require harsher methods to dissolve, these groups have much lower leaching yields.

Based on these results, as well as the time required to process the leaching solutions, only leaches one and two were selected for further purification, as mentioned previously.

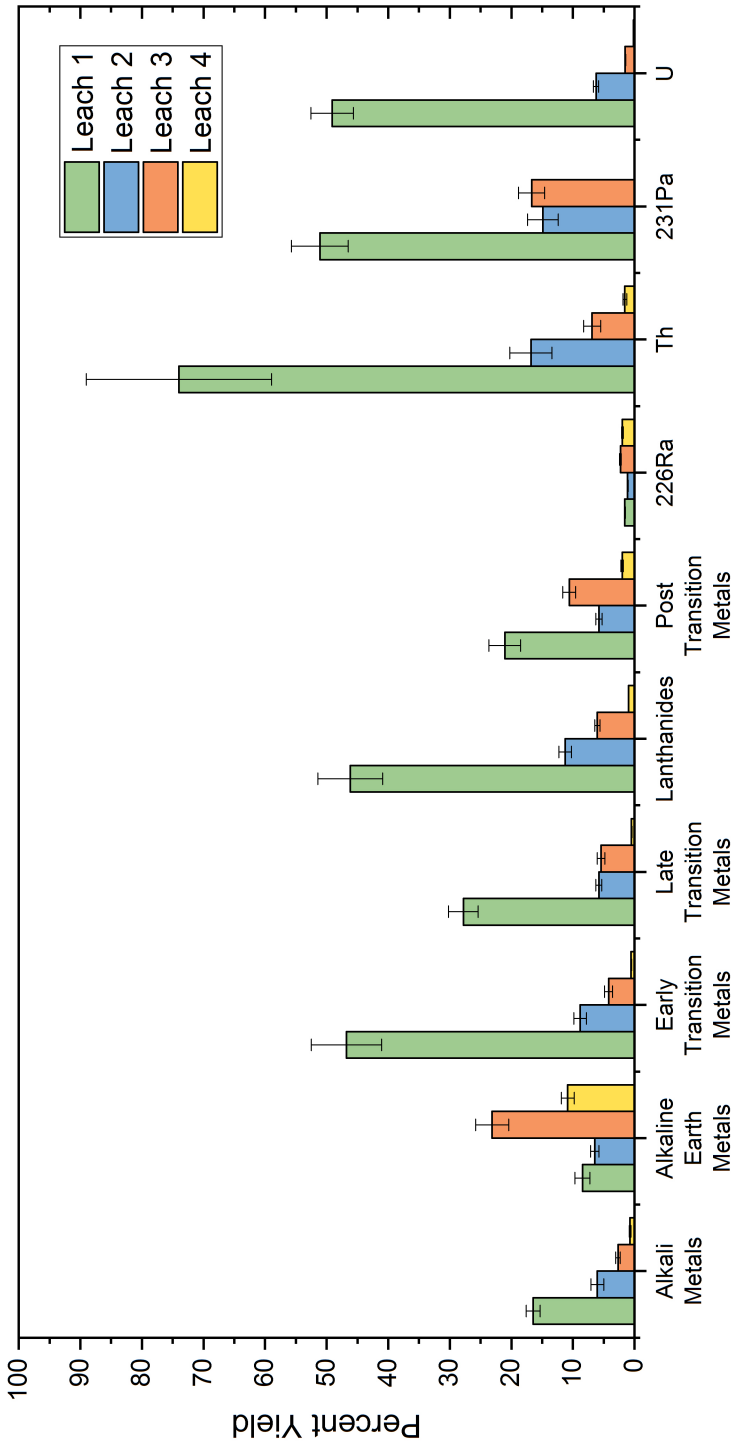

Figure 2.12: Ore leaching yields.

Liquid-Liquid Separation

Data for the TBP liquid-liquid separation for the initial, small-scale (20 mL) characterization appears in Table 2.2. The speciation of uranium and thorium in TBP is well known: two TBP molecules bond to the actinide in the axial positions through the terminal oxo group on the phosphorus [62]. In the equatorial positions, thorium has four bidentate nitrate ligands and uranium has two trans bidentate nitrates and two trans terminal oxo ligands [62].

Table 2.2: Data for small-scale TBP liquid-liquid separation. Values are an average percent extraction for eight independent trials; the error is counting error.

Element	**Forward-Extraction (%)**	**Back-Extraction (%)**
Th	98.01 ± 7.51	99.27 ± 7.21
Pa	98.89 ± 5.59	100 ± 3.46
U	76.59 ± 2.24	31.26 ± 1.85

It can be seen that the yields for thorium and protactinium are extremely high, while the yields for uranium are lower for both the forward- and back-extractions. These particular conditions were selected for high thorium yields and it was expected for protactinium to act similarly. In acidic solution, both thorium and protactinium are small, highly charged cations that complex with the conjugate base of the acid. Uranium, however, exists as uranyl (UO_2^{2+}) in solution, resulting in very different chemical behavior. This is particularly apparent in the back-extraction since Th(IV) and Pa(V) are both hard and highly Lewis acidic, while uranyl is softer and less acidic. Therefore, Th(IV) and Pa(V) complex very strongly to fluorides, which are hard and very Lewis basic, resulting in extremely high yields for the back-extraction, protactinium more so than thorium as it has a higher charge state but similar size making it harder and more Lewis acidic. Uranyl being softer and less acidic, does not complex as strongly to fluorides and subsequently has a lower yield. Since the goal of the liquid-liquid extraction is to purify the thorium but also to remove mass from the system to simplify later separations, the low extraction yields for uranium, one of the largest mass components in the ore, are advantageous.

Mass spectrometry data for the back-extraction solution is given in Fig. 2.13. It should be noted that this is taken from the back-extraction solution after removal of the ThF_4 precipitate and, therefore, is not representative of the extraction as a whole. The highest mass concentrations in the back-extraction solution are iron (27.3 ± 0.71%) and uranium (68.6 ± 1.4%). While this data cannot be considered quantitative due to the removal of fluoride precipitate, from this data and the composition of the hydroxide precipitate (Fig. 2.15), it can still be seen that the back-extraction has largely separated the actinides from the bulk of the ore mass. The main mass components in the back-extraction solution are uranium and iron; all others are present at less than 2% by mass (see Fig. A.2). In the dissolved hydroxide precipitate, the main mass components are scandium, yttrium, lanthanides, tho-

rium and uranium; all others are present at less than 1% except aluminum, which was added by the chemistry. The lanthanides, scandium and yttrium are well known to pass through TBP extractions with the actinides. Furthermore, they also form low solubility fluorides and therefore tend to follow the ThF_4 precipitate. Uranium appears at a higher mass concentration in the back-extraction solution than the precipitate, which is to be expected since uranyl fluoride is highly soluble, unlike thorium tetrafluoride. Some uranium appears in the dissolved hydroxide precipitate likely because some of the uranium is entrained in the ThF_4 mass, not due to a co-precipitation.

Iron appears in the back-extraction solution and the hydroxide precipitate most likely because it was present in such large amounts in the ore that even if only a few percent are being held in the organic phase, and subsequently in the ThF_4 precipitate by mass effects, it would still be a significant amount.

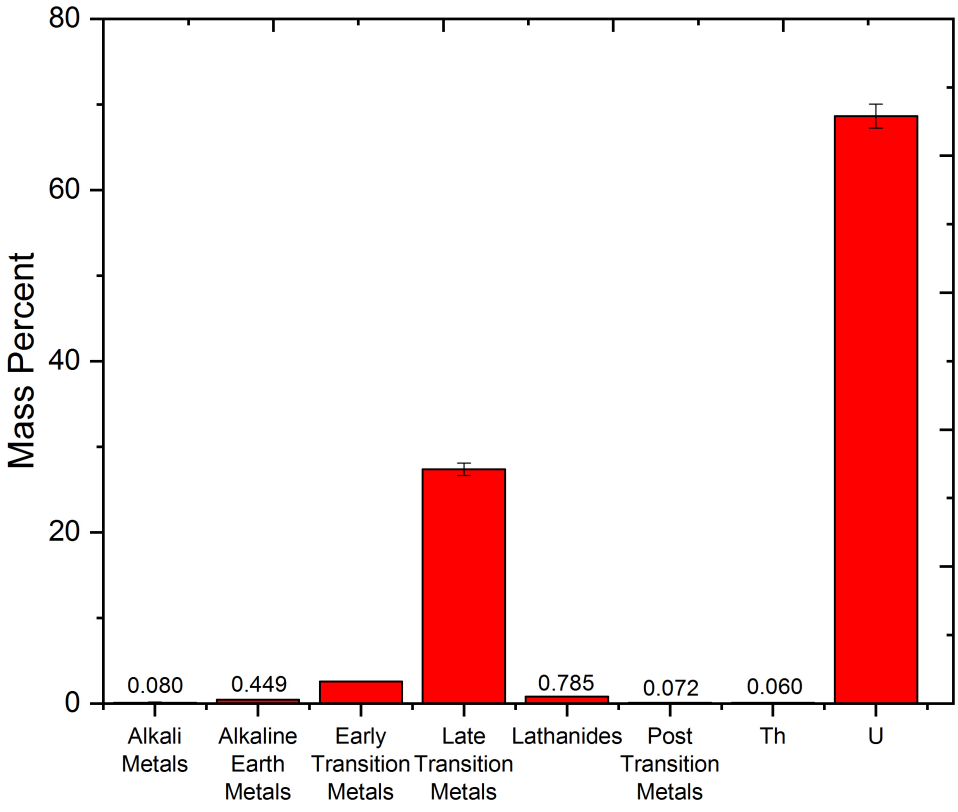

Figure 2.13: Mass spectrometry data for the HF back-extraction solution after removal of ThF_4 precipitate.

Precipitations

Thorium, like many actinides, has limited solubility in HF solutions and as a result, the back-extraction solution precipitates ThF_4, which can only be readily dissolved in solutions with a fluoride grabber, here $Al(NO_3)_3 \cdot 9H_2O$ [63, 64]. The aluminum removes the fluorides complexed to metal ions in solution, converting them to nitrates with the production of aluminum difluoride (AlF_2^+). This works well for thorium and the remaining uranium; however, protactinium is not converted to a nitrate in this process. This is evidenced by the behavior of protactinium later in the purification process: it elutes directly from the Dowex 1x8 anion exchange column, showing no affinity for the resin. If protactinium had been converted to a nitrate, it would elute only with sufficient washing as its distribution coefficient would be non-negligible [65] and it tends to hydrolyze readily without sufficient fluorides, resulting in retention on resins and plastic (such as pipettes or test tubes) [66]. Protactinium(V) bonds very strongly with fluorides and it is very difficult to convert protactinium from a fluoride, so this behavior was expected.

After dissolution in the nitrate solution, sat. NaOH was used to precipitate the actinides as hydroxides. The speciation plot for this precipitation is shown in Fig. 2.14, as the pH increases to above about 8, both uranium and thorium precipitate as hydroxides. Thorium hydroxide has been noted in the literature to be a gelatinous precipitate and that was observed here [64].

The precipitation removes the actinides from the bulk of the aluminum mass, which remains in the supernate as AlF_2^+. The hydroxide precipitate was dissolved in conc. HNO_3; mass spectrometry data for the dissolved hydroxide is shown in Fig. 2.15. Along with thorium, uranium, scandium, yttrium, and iron are present in significant amounts (see Fig. A.3), having been carried in the ThF_4 precipitate and then precipitating themselves as hydroxides. Scandium and yttrium in particular are present in large amounts as they were present in the initial ore at a higher mass concentration than thorium and have closely followed thorium throughout the processing. Iron hydroxide precipitates under these conditions, it is often used as a carrier for thorium, so it is present at a significant mass as well [64]. The post transition metals are a large mass fraction solely due to aluminum, which was present in significant mass in the solution and partially entrained in the hydroxide; the rest of the post transition metals are present in negligible amounts. The behavior of protactinium was not quantitatively accounted for in the precipitation as it was not measured with mass spectrometry. It was observed with gamma-ray spectroscopy, and since protactinium is readily carried during precipitations [66], it is assumed to have been carried along with the other actinides as a fluoride. It should be noted that Fig. 2.15 does not include data for sodium as it was present in excess since NaOH was used for the precipitation.

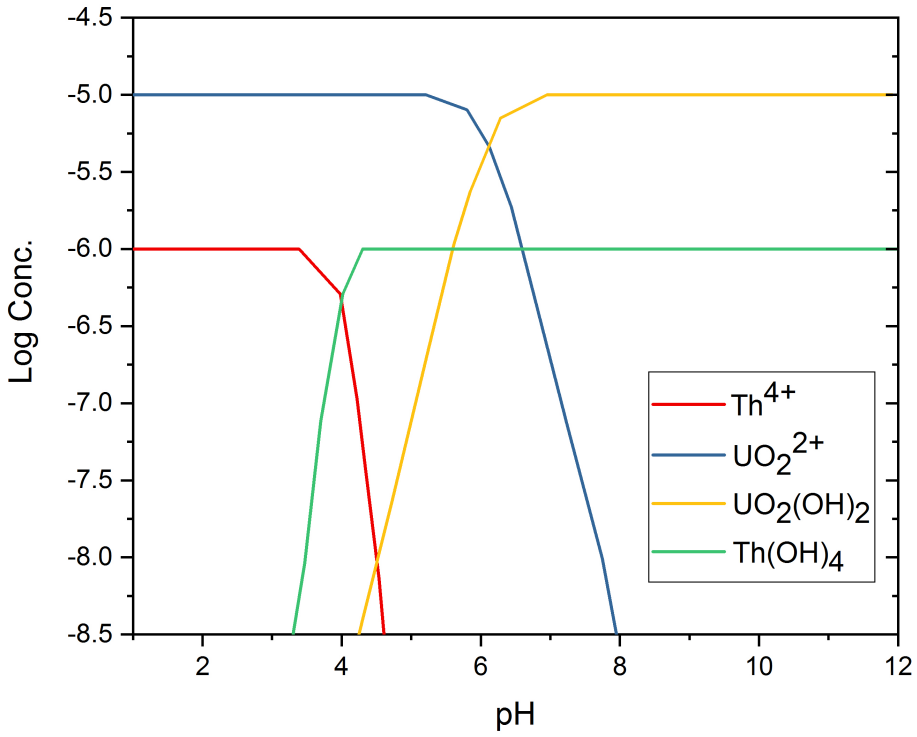

Figure 2.14: Speciation of thorium and uranium in aqueous solution. Data from Ref. [67].

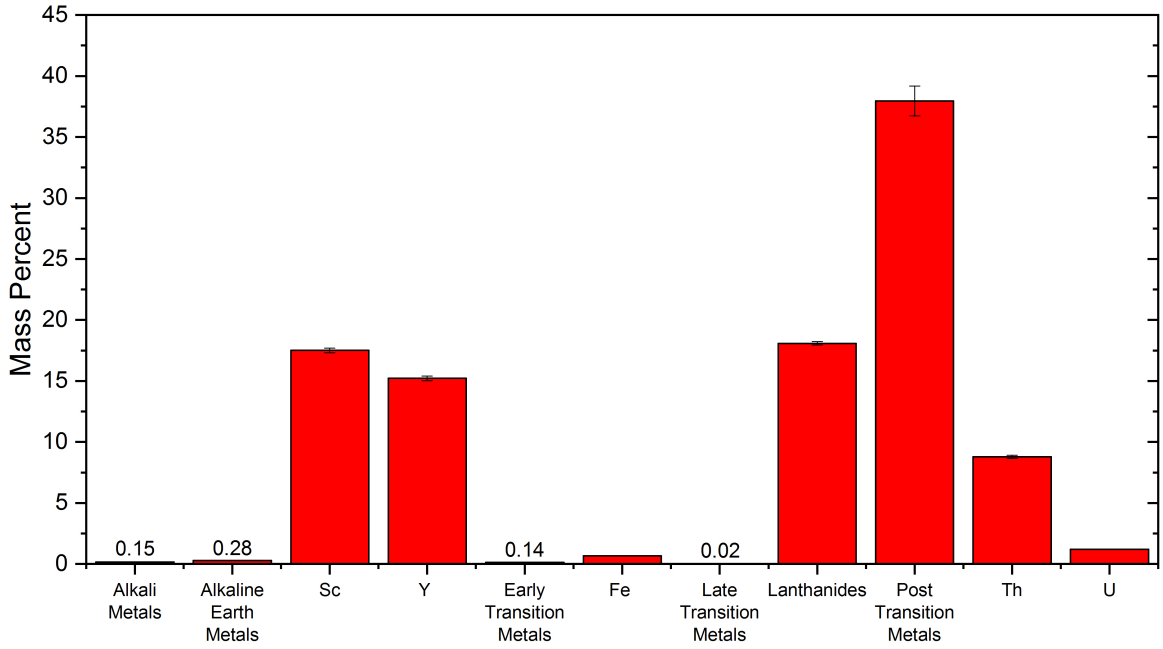

Figure 2.15: Mass composition of dissolved hydroxide precipitate as determined by mass spectrometry. Sodium not included.

Ion Exchange Chromatography

An ion exchange separation was done with Dowex 1x8 resin loaded in 8 M HNO_3. At this concentration, the lanthanides and transition metals form cationic complexes and, therefore, run through the column. The actinides (thorium, protactinium and uranium) all have some affinity for the resin in nitrate form, though protactinium and uranium less so than thorium, which bonds strongly as $Th(NO_3)_6^{2-}$ [61, 68]. Therefore, sufficient washing of the column with 8 M HNO_3 separates the thorium from uranium and protactinium. As discussed previously, protactinium would have had a significant affinity for the resin had it been converted to a nitrate; however it was observed to elute immediately, indicating it was not converted from the fluoride in the previous steps. The column was trialed on a small scale before the bulk processing and the fractions are shown in Fig. 2.16.

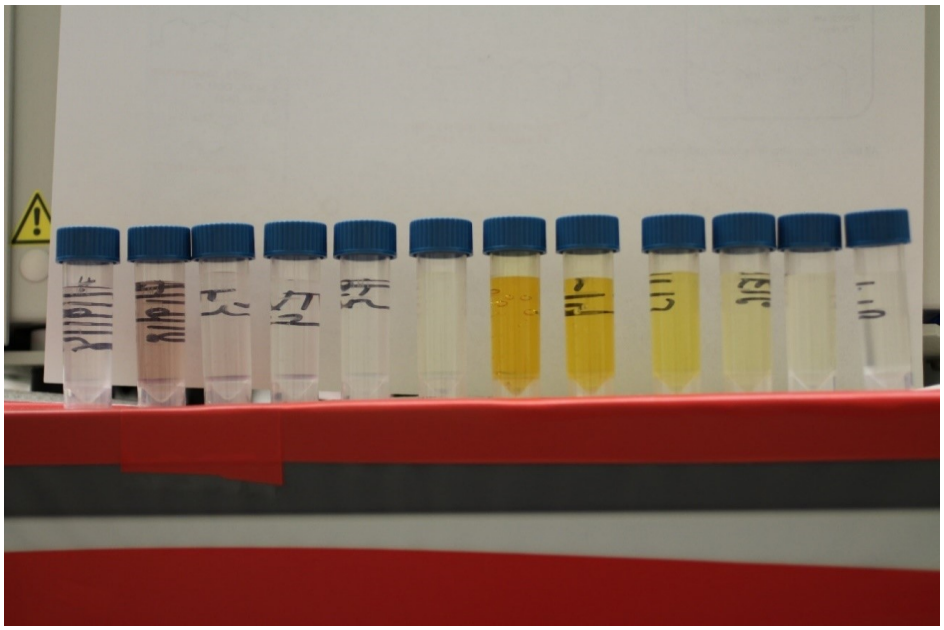

Figure 2.16: Fractions of HNO_3 Dowex 1x8 column. Transitions metals are eluted in the second fraction causing the purple color. Thorium is eluted in the seventh fraction, which appears yellow due to conc. HCl and conc. HNO_3 mixing on the column.

After the ion exchange column, the final product was 99.5 ± 1.2 wt.% thorium. The main impurities are alkali and alkaline metals along with iron and uranium. The impurities are shown by mass percent in Fig. 2.17. Sodium and aluminum, both used in the precipitation chemistry, dominate the alkali metals and post transition metals, respectively, and explain the high mass concentrations of these groups (see Fig. A.4). As before, protactinium is not included in mass spectrometry data due to interferences, however in the final sample there was no detectable ^{231}Pa. The total mass of thorium recovered was 91.32 ± 0.77 mg: 83.67 ± 0.76 mg of ^{232}Th and 7.65 ± 0.10 mg of ^{230}Th. The amount of ^{230}Th present in the ore

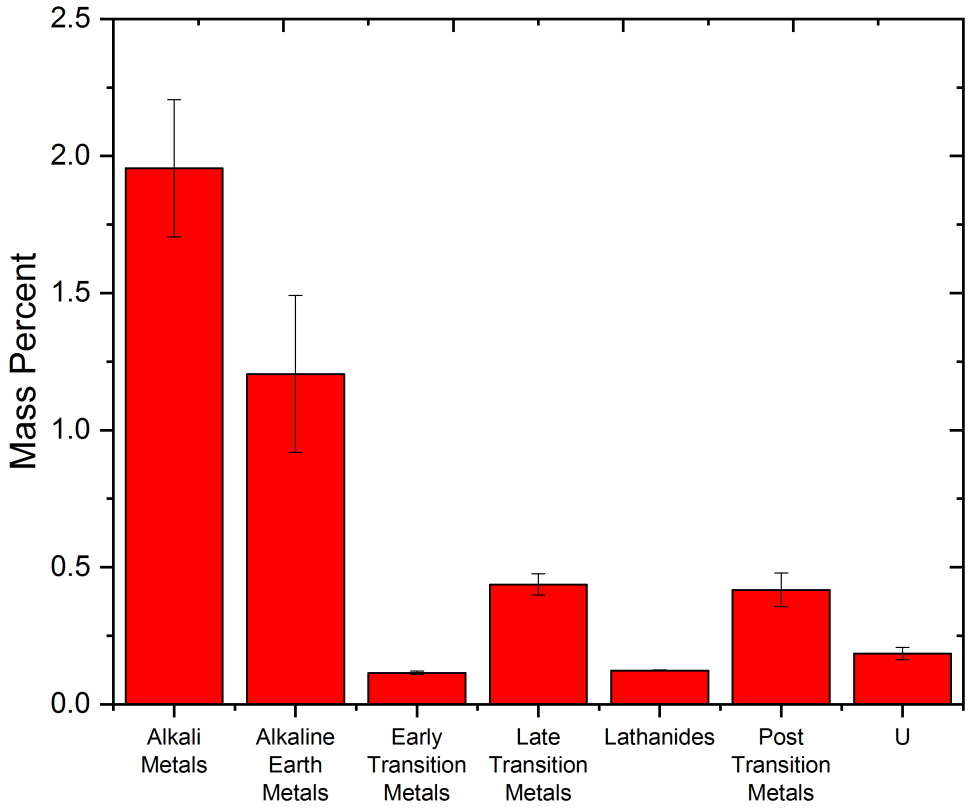

Figure 2.17: Mass percentages of impurities in thorium product.

initially can be calculated from the mass of uranium and $^{235}U/^{238}U$ ratio; this gives a result of 10.8 ± 0.8 mg ^{230}Th, indicating an overall yield of 71.1 ± 5.4% for thorium recovery. The yield can also be calculated based on mass spectrometry data for the initial ore, which measured 86.7 ± 17.7 mg of ^{232}Th. This indicates a yield of 96.5 ± 19.8%, which is within error of the yield calculation for ^{230}Th, but with an extremely large error bar arising from uncertainty on the thorium mass concentration measured in the initial ore.

The main impact on the yield is the precipitation of ThF_4 from the back-extraction solution. The leaching had an extremely high yield (about 90%) and the ion exchange chromatography can be assumed to have a high yield as well as there was no detectable thorium in the other fractions or remaining on the column. However, as shown in Fig. 2.13, there was some thorium remaining the in back-extraction solution after the precipitation, which was not recovered. Therefore, the yield could be improved by evaporating the remaining back-extraction solution to induce the precipitation of more ThF_4, which could be treated in

the same manner as described above. However, the recovery was determined to be sufficient for this work, therefore, further processing was unnecessary.

2.4 Conclusion

Thorium-230 has many research applications including radiometric dating and isotope production. Despite being a long-lived and naturally occurring isotope, there is no commercial source of ^{230}Th and, therefore, it must be acquired through separation from uranium ore. A procedure to leach high-grade uranium ore and separate the thorium on a laboratory scale was established. A sequence of HNO_3-based leaches followed by a liquid-liquid extraction from conc. HNO_3 using TBP-kerosene as the organic phase and HF for the back-extraction solution was developed and fully characterized with concentrations and on a scale not previously reported in the literature. From the back-extraction solution, thorium was precipitated as ThF_4, then dissolved with $Al(NO_3)_3 \cdot 9H_2O$ and re-precipitated as a hydroxide. Finally, anion exchange chromatography was used as a final purification step. The ultimate recovery of ^{230}Th was 7.65 $\pm$ 0.10 mg, which is adequate for nuclear data and isotope production purposes. The overall yield for ^{230}Th was 71.1 $\pm$ 5.4%, which is largely due to the non-quantitative ThF_4 precipitation following the liquid-liquid extraction. This could be improved by further processing of the back-extraction solution; however, the yield obtained was sufficient for the experiments involved in this work.

Chapter 3

Isotope Generators

3.1 Introduction

Tracer isotopes for protactinium and thorium were necessary for many aspects of this work. As most naturally occurring thorium isotopes (^{228,230,231,232,234}Th) do not have readily detectable gamma-ray lines [14], a thorium tracer was necessary for most experiments involving bulk thorium, including the final steps in the thorium purification from the uranium ore (Chapter 2), electrodeposition of ^{232}Th (Chapter 4) and the development of chemical procedures for the target processing (Chapter 6). For samples of highly pure ^{230}Th/^{232}Th, the 67 keV line from ^{230}Th [14] is detectable in the absence of other activity and with good counting geometry (as the line is easily attenuated), so a tracer was not necessary for the target preparation step of the cross section measurement itself. A protactinium tracer was needed for the electrodeposition studies on protactinium (Chapter 4), the development of chemical procedures for the target processing (Chapter 6) and as a yield tracer for the target processing to make the cross section measurement (Chapter 7).

To have readily available supplies of tracer isotopes at sufficient activity levels, two isotope generators were made as part of this work. The first used ^{237}Np ($t_{1/2}$ = 2.144 $\times 10^6$ y) to produce ^{233}Pa to serve as a protactinium tracer, and the second used ^{227}Ac ($t_{1/2}$ = 21.772 y) to produce ^{227}Th for use as a thorium tracer [14] . The half-lives and major gamma-ray lines for these isotopes are shown in Table 3.1.

3.2 Background Information

Chemical tracers are used to monitor chemical processes and provide a way to follow some component of interest in a sample that would be difficult to detect on its own. The chemical tracer must behave the same as the component that it is following (the "determinand") in the relevant chemical processes and there must be an equilibrium between the tracer and determinand at all stages of the process [69]. For analytical yield tracers, which are used when processing a sample where the initial concentration of the determinand is unknown, it

Table 3.1: Nuclear data for thorium and protactinium tracer isotopes used in this work [14].

Isotope	Half-Life (d)	Energy (keV)	Intensity (%)
^{227}Th	18.68	235.96	12.9
		256.23	7.0
^{233}Pa	26.975	300.13	6.63
		311.9	38.5
		340.48	4.45

must also be possible to determine the absolute amount of the yield tracer and determinand independently, so the yield (as given by the tracer) can be related to the total, previously unknown, amount in the sample [69].

Tracers do not need to be radioactive [70], however, radiotracers of the element of interest are particularly useful because two isotopes of the same element can be assumed to behave identically and rapidly establish an equilibrium in most chemical processes. Since these are the only type of tracers employed in this work, the following discussion will be limited to radiotracers. Along with the general requirements for tracers, ideal radiotracers are also easy to prepare and readily detectable [71]. Radiotracers are commonly used in analytical chemistry [72] for studies such as biological exposure assessments [71] and environmental studies [71] as well as in chemical industries such as petroleum refining [70].

Tracer isotopes are commonly produced with isotope generators [72, 73]. A typical isotope generator has a long-lived parent isotope that decays to a short-lived daughter isotope of interest [74, 75]. To create an isotope generator, the parent isotope is retained on a chromatography column and the daughter is eluted periodically, based on its half-life and the activity levels needed [75]. Isotope generators are a simple, rapid and inexpensive way to routinely produce short-lived radioisotopes [75] with high radiopurity [74, 76], high yields [74, 76] and no carrier added [77]. There are many applications for isotope generators beyond tracer isotope production, including medical imaging [76, 78, 79], medical treatment [74] and chemical studies [77].

The in-growth of the daughter product from the decay of any isotope is given by the Bateman equations (Eqns. 3.1-3.4) where t is the time elapsed, N_n is the number of atoms of the n^{th} isotope in a given decay chain, N_1^0 is the number of atoms of the first isotope in the decay chain at $t = 0$, and λ_n is the decay constant of the n^{th} isotope in the decay chain. In these equations, it is assumed that the daughter isotopes are radioactive and not present initially (at $t = 0$, $N_2...N_n = 0$).

$$N_n(t) = C_1 e^{\lambda_1 t} + C_2 e^{\lambda_2 t} + ...C_n e^{\lambda_n t} \tag{3.1}$$

$$C_1 = \frac{\lambda_1 \lambda_2 ... \lambda_{n-1}}{(\lambda_2 - \lambda_1)(\lambda_3 - \lambda_1)...(\lambda_n - \lambda_1)} N_1^0 \tag{3.2}$$

$$C_2 = \frac{\lambda_1\lambda_2.....\lambda_{n-1}}{(\lambda_1-\lambda_2)(\lambda_3-\lambda_2)...(\lambda_n-\lambda_2)}N_1^0 \tag{3.3}$$

$$C_n = \frac{\lambda_1\lambda_2.....\lambda_{n-1}}{(\lambda_1-\lambda_n)(\lambda_2-\lambda_n)...(\lambda_{n-1}-\lambda_n)}N_1^0 \tag{3.4}$$

For the decay of an isotope where the half-life of the parent is longer than that of the daughter isotope, there are two types of equilibrium that can be established between the parent and daughter activities: secular or transient equilibrium. In secular equilibrium, the half-life of the parent is much longer than that of the daughter, typically by a few orders of magnitude. In this case, the daughter grows-in until the activity of the daughter (A_2) is equal to that of the parent (A_1) and then the daughter isotope appears to decay with the half-life of the parent isotope. This relation is given in Eqn. 3.5 [80]. Both of the isotope generators presented in this chapter have parent-daughter isotopes in secular equilibrium.

$$A_1 = A_2 \tag{3.5}$$

In transient equilibrium, the half-life of the parent is longer than the daughter, usually about 10 times longer. In this case, the ratio between the parent and daughter activity remains constant once equilibrium is achieved with the activity of the daughter slightly higher than that of the parent and the daughter isotope appears to decay with the half-life of the parent. This relationship is given in Eqn. 3.6 [80] where λ_1 and λ_2 are the decay constants of the parent and daughter isotopes, respectively.

$$\frac{A_1}{A_2} = \frac{\lambda_2-\lambda_1}{\lambda_2} \tag{3.6}$$

Isotope generators can be made for parent-daughter isotopes that are in secular equilibrium [74] or transient equilibrium [75]. In either case, it takes one half-life of the daughter for the daughter activity to grow in to 50% of its maximum value and full equilibrium takes about 10 daughter half-lives [80]. The elution period is chosen depending on the activity level needed for the specific application. The useful life time of the isotope generator is theoretically dictated by the half-life of the parent, but often is practically determined by the chemical and radiation resilience of the chromatography column. Damage to the column can lead to elution of the parent isotope with the daughter product [73], which is referred to as breakthrough.

3.3 Protactinium-233 Isotope Generator

Introduction

Protactinium-233 is commonly used as a tracer isotope for protactinium with applications ranging from spectroscopy and nuclear data measurement [81–83] to geochemistry [84, 85] and neutron activation analysis [86]. For use as a tracer, ^{233}Pa ($t_{1/2}$ = 26.975 d) [14] is

usually obtained by separation from its parent, ^{237}Np ($t_{1/2}$ = 2.144 $\times 10^6$ y) [14, 83, 87, 88], though it can also be produced via the β-decay of ^{233}Th ($t_{1/2}$ = 22.3 m), which is produced from neutron capture on ^{232}Th [14, 89].

Neptunium-237 and ^{233}Pa can be separated by many methods including column chromatography [87, 90] and liquid-liquid extraction [83, 88]. However, neither of these methods are ideal for the repeated separation of ^{233}Pa in a laboratory setting. Liquid-liquid extractions can be time consuming and produce a lot of waste [91], and methods of ion exchange separations for neptunium-protactinium separations are often multi-step and complex [87]. Therefore, the production of ^{233}Pa with an isotope generator created using commercially available resin would be advantageous as it would be a rapid and simple method of producing ^{233}Pa.

Most protactinium-neptunium chromatography separations presented in the literature are based on retaining ^{233}Pa and, therefore, are not appropriate for an isotope generator [90–92]. In addition, most of these rely on extraction chromatography, which is not as stable as ion exchange chromatography over long periods of time, therefore not suitable for an isotope generator [91, 92].

A ^{237}Np/^{233}Pa isotope generator using Dowex 50x8, a cation exchange resin that is more chemically and radiation resistant [93] than anion or extractant-based resins, has been mentioned in the literature [94], however it was not characterized and, with the minimal information that was presented, the elution procedure was not found to be reproducible. The purpose of this chapter is to develop and fully characterize an isotope generator capable of producing ^{233}Pa for tracer studies.

The ^{237}Np decay chain is notable due to the long half-life of the granddaughter isotope, ^{233}U ($t_{1/2}$ = 159.2 $\times 10^3$ y) [14], which has a half-life very close to that of ^{237}Np, as well as the great-granddaughter, ^{229}Th ($t_{1/2}$ = 7340 y) [14]. The ^{233}U decay chain in shown in Fig. 1.1. These isotopes prevent this decay chain from coming to full equilibrium on a laboratory timescale. In the period of 1000 days (2.7 years), only ^{233}Pa grows in to a significant amount; it reaches secular equilibrium with ^{237}Np after 668.7 days (Fig. 3.1).

For any isotope generator, the parent isotope needs to be retained on the column while the daughter product of interest elutes. Here, that requires ^{237}Np to be retained on the column while ^{233}Pa elutes. While the other daughter products do not grow-in to any significant degree, it would be advantageous for the isotope generator to retain uranium and thorium as well to ensure the purity of the protactinium product over an extended period of time.

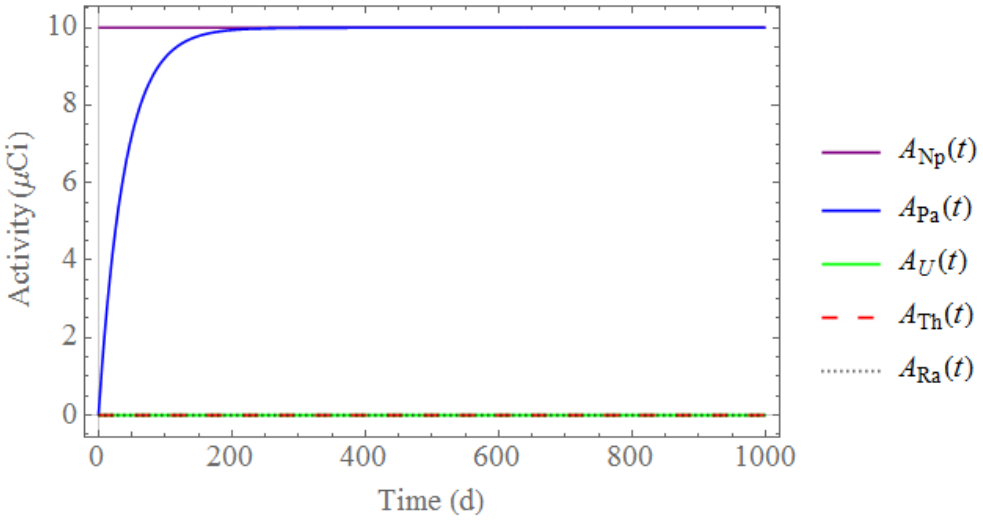

Figure 3.1: Activity curves based on the Bateman equations for the in-growth of the first four ^{237}Np daughters (^{233}Pa, ^{233}U, ^{229}Th and ^{225}Ra) in 1000 days after purification of 10 μCi ^{237}Np. Only ^{233}Pa grows-in to detectable levels during this time, the activities of ^{233}U, ^{229}Th and ^{225}Ra remain about zero.

Description of Experimental Work

All reagents used were of trace metal grade or higher; acids were diluted as necessary with Millipore Milli-Q deionized water (18.2 MΩ cm). Neptunium-237 was obtained in a nitric acid solution as legacy material from LLNL. Due to the long half-life of the ^{237}Np, its granddaughter, ^{233}U, and its great-granddaughter, ^{229}Th, it was not necessary to clean the ^{237}Np of its decay chain daughter products before preparing the isotope generator as the daughters below ^{233}Pa were not detectable. The ^{237}Np sample was evaporated to dryness and brought up in 1 mL 0.1 M HNO_3.

From this stock solution, 250 μL was removed to serve as a standard and was counted via gamma-ray spectroscopy at the NCF at LLNL to determine the activity. The remaining 750 μL (containing 248 $\pm$ 10 nCi ^{237}Np) was evaporated to dryness and brought up in 200 μL 0.1 M HNO_3. On 26 September 2019, this was loaded onto a 2 mL Dowex 50x8 (100-200 mesh) column, which had been prepared and washed with 8 mL 0.1 M HNO_3. Six 1 mL fractions of 0.01 M HF were collected to elute ^{233}Pa. The column was then washed with 2 mL H_2O before capping. The isotope generator was eluted in this manner every week to evaluate the time before breakthrough, which occurred on 15 December 2020, the 46^{th} elution. During the first year of operation, the isotope generator was eluted 35 times instead of 52 due to the COVID-19 pandemic, which shutdown laboratory work at LLNL for over four months. No difference in the yield or elution pattern was observed when elutions were resumed after the laboratory shutdown.

The relative activity of the standard and load solution was measured with an HPGe detector with Ortec NIM electronics and ASPEC multi-channel analyzer; Maestro software (Ortec) was used to analyze the resultant spectra. After elutions, the fractions were all counted relative to the standard using the same HPGe detector and in the same geometric configuration. The 311 keV (38.5 ± 0.4%) and 340 keV (4.45 ± ± 0.05%) lines were used to determine the ^{233}Pa activity while the 86 keV line was used for ^{237}Np [14]. Overlap between the 86.477 ± 0.010 keV (12.4 ± 0.3%) ^{237}Np line and the 86.595 ± 0.005 keV (1.95 ± 0.11%) ^{233}Pa line was accounted for in all measurements based off the efficiency of the detector at this energy and the intensity of these lines for each isotope [14]. As an additional check, each ^{233}Pa fraction was counted again a week after the elution and initial counting to confirm it was decaying with the half-life of ^{233}Pa.

Results and Discussion

The elution curve of the generator is shown in Fig. 3.2. The majority of the ^{233}Pa eluted in the second 1 mL fraction, on average 98.6 ± 0.3% of the total collected. The average total yield was 75 ± 1%. The isotope generator was eluted regularly from 26 September 2019 to 15 December 2020. The data presented here is from the first 45 elutions, as breakthrough occurred on the 46^{th} elution. Elution peaks in this chapter are fitted with bi-Gaussian functions; peak fitting is discussed further in Chapter 6 and Appendix B. The yields given are calculated from the counting data with error propagated from the counting statistics, but the same values, within error, can be determined from the area under the curve for each elution curve fit.

With weekly elutions, ^{233}Pa only grows into 16.5% of the equilibrium activity, which was ∼1500 dps. As mentioned previously, elutions were halted for 4 months due to the laboratory shutdown during which time ^{233}Pa grew in to 93.9% of its equilibrium activity. However, there was no discernable effect on the elution curve or yield when elutions were resumed. Therefore, more activity and greater longevity could likely be obtained from less frequent elutions.

The isotope generator was loaded in 0.1 M HNO_3 and at this concentration neptunium (presumably neptunium(V) as NpO_2^+) [95, 96], uranium(VI) (as UO_2^{2+}) [97] and thorium(IV) [64] are retained on the resin along with protactinium(V), which requires fluorides to elute. One advantage of this load solution is that in dilute acid, all typical, solution stable neptunium species (III, IV, V, VI) are retained on cation exchange resins [95], therefore no redox control is needed to prepare the ^{237}Np sample for the column. In 0.01 M HF, uranium, neptunium and thorium are retained on the resin [98], resulting in the selective elution of protactinium, presumably as PaF_7^{2-} or PaF_8^{3-} [89, 98].

The yield of the isotope generator was consistently around 75%. While better yields of protactinium elution from Dowex 50x8 (100-200 mesh) can be obtained with 0.1 M HF [98], it was decided to use 0.01 M HF due to longevity concerns as the K_d of Np(V) on this resin is highly dependent on fluoride concentration with a sharp drop in K_d from about 10^4 in 0.01 M HF to about 10^2 in 0.1 M HF [98]. Reference [94] recommends ^{233}Pa elution with 0.002 M

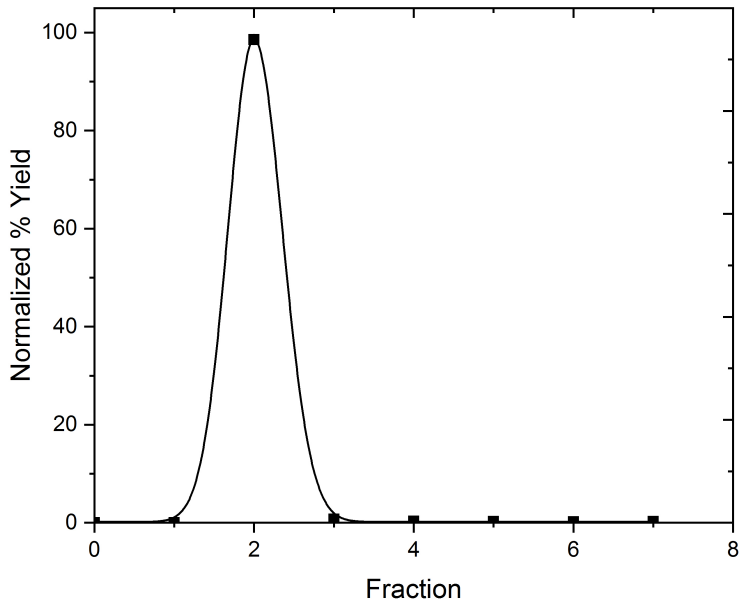

Figure 3.2: Elution curve of ^{237}Np/^{233}Pa isotope generator normalized and averaged over 45 elutions. Error bars are from counting statistics and are smaller than the data points. Fractions 0 and 7 are 2 mL H_2O fractions from the washes between elutions.

HF for this reason, and this was attempted as part of the preparation for this experiment, but the elution of 10 mL 0.002 HF on this resin did not cause ^{233}Pa to elute. Therefore, to balance the longevity of the generator with a reasonable yield and elution volume, 0.01 M HF was chosen as the eluant.

While the lifetime of the isotope generator was over a year, elutions after about 11 months of operation were visibly pink with an organic residue after evaporation and reconstitution in a small volume. This is due to contamination with resin degradation products, which was expected as the generator sees a significant amount of alpha radiation from ^{237}Np that causes damage to the resin over time, primarily by cleavage of the sulfite group [93, 99]. For applications where the presence of organic residue in the sample is problematic, the generator would likely need to be stripped after about 10 months of operation and the ^{237}Np loaded onto a new column. However, for this work, trace organics in the ^{233}Pa tracer were not an issue as they dissolved readily in concentrated acid.

3.4 Thorium-227 Isotope Generator

Introduction

There are several isotopes of thorium that are applicable for use as tracer isotopes. Historically, ^{234}Th, a β^- emitter, was commonly used as it can be obtained easily from ^{238}U [100–102]. Thorium-229 is a common tracer for alpha spectroscopy and is particularly useful for environmental purposes, as it is not naturally occurring [100, 103, 104]. However, neither of these isotopes has readily detectable gamma-ray lines, especially with a high background [14].

Thorium-227 is an alpha emitter, has several readily detectable gamma-ray lines and a reasonable half-life (Table 3.1). Since it is naturally occurring, it is not an appropriate yield tracer for any system with natural uranium, which often precludes its use in environmental studies [69]. However, in biological studies where natural ^{227}Th is negligible, ^{227}Th is a convenient tracer as it can be measured easily with gamma-ray spectroscopy [105, 106].

As ^{230}Th, ^{232}Th and ^{228}Th lack any readily detectable gamma-ray lines, ^{227}Th was used as a tracer for bulk thorium in this work for detection convenience. Its limitations as a yield tracer were taken into account: none of the thorium chemistry in this work uses ^{227}Th as an analytical yield tracer, it is used only to follow chemical processes more easily and make relative yield determinations.

Thorium-227 is produced by the decay of ^{227}Ac and is part of the ^{235}U decay chain (Fig. 2.3). It can be separated from its parent by a variety of simple methods as the properties of Ac(III) and Th(IV) are quite distinct [107]. Anion exchange chromatography in nitric acid is a common method as it can be used to elute ^{227}Ac, which is not retained at any concentration, while retaining ^{227}Th, which is removed with HCl or dil. HNO_3 [64, 106, 107]. Isotope generators for this decay chain have been reported recently for medical purposes as well, with either the elution of ^{223}Ra ($t_{1/2}$ = 11.43 d [14]) or both ^{227}Th and ^{223}Ra [108, 109].

The isotope generator used to produce ^{227}Th was made using the procedure presented in Ref. [98] because this separation is optimized for the separation of ^{231}Pa from its daughters, while simultaneously creating an isotope generator based on ^{227}Ac with only one column needed. As the only ^{227}Ac available for this work was from in-growth into a ^{231}Pa sample, this separation was ideal as it provides a method to clean ^{231}Pa of its daughter products, which was necessary for the work described in Chapter 4, and simultaneously creating the needed isotope generator to produce ^{227}Th. The in-growth of ^{227}Th and ^{223}Ra into ^{227}Ac is shown in Fig. 3.3; it takes 163.9 days for ^{227}Th to grow into secular equilibrium.

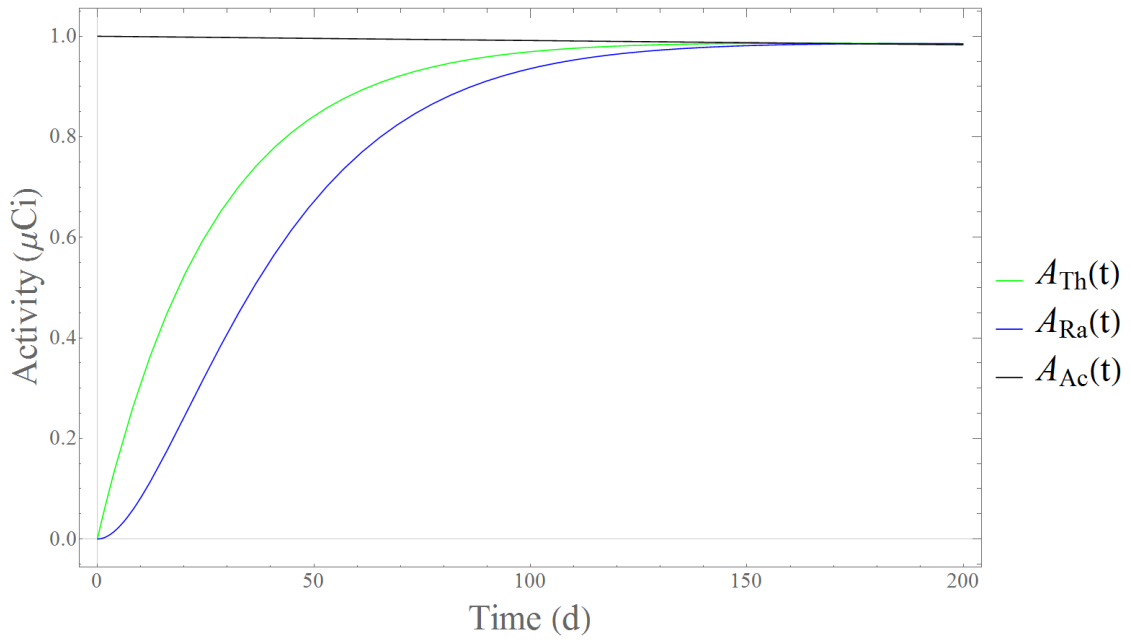

Figure 3.3: Activity curves based on the Bateman equations for the decay of ^{227}Ac to ^{227}Th and ^{223}Ra.

Description of Experimental Work

All reagents used were of trace metal grade or higher; acids were diluted as necessary with Millipore Milli-Q deionized water (18.2 MΩ cm). Legacy ^{231}Pa from LLNL was used. This material, about 1 mg ^{231}Pa in 20 M HF, had previously been cleaned of contaminants using the procedure given by Ref. [110] but the protactinium daughter products had grown in significantly since the last purification. An aliquot of the legacy ^{231}Pa solution was evaporated to dryness and reconstituted in 0.1 M HF to make a stock solution.

First, 0.25 mL of the ^{231}Pa stock was used to characterize the separation given in Ref. [98] by doing a full elution of ^{231}Pa, ^{227}Th and ^{223}Ra on a 2 mL Dowex 50x8 (100-200 mesh) column, prepared by washing with 8 mL 0.1 M HF. The column was eluted in 2 mL fractions with: 8 mL 0.1 M HF, 10 mL 0.5 M HF and 16 mL 3 M HNO_3. In this separation, ^{231}Pa elutes from the column first, followed by ^{227}Th and then ^{223}Ra; ^{227}Ac is retained on the column. Once the separation was characterized, a 5 mL aliquot of ^{231}Pa stock solution was loaded onto a 2 mL Dowex 50x8 (100-200 mesh) column pre-washed with 8 mL 0.1 M HF. The ^{231}Pa was removed with sufficient washing (12 mL) of 0.1 M HF until it was no longer detectable in the eluent, the rest of the daughters were retained on the column. For each elution of ^{227}Th, four 2 mL fractions of 0.5 M HF were collected then 2 mL H_2O was eluted to preserve the lifetime of the resin, as done with the ^{237}Np isotope generator (Section 3.3). The generator was eluted on a monthly basis for over a year with no breakthrough observed

before it was fully stripped to recover ^{223}Ra and ^{227}Ac for other applications.

Gamma-ray spectroscopy was done with an HPGe detector with Ortec NIM electronics and ASPEC multi-channel analyzer; Maestro software (Ortec) was used to analyze the resultant spectra. The fractions were all counted with the same detector and in an identical geometric configuration. All gamma spectroscopy was done with relative measurements only, no absolute activity measurements were made. The highest intensity spectral lines were used for ^{223}Ra (269.463 keV; 13.9 ± 0.3%) and ^{227}Th (235.96 keV; 12.9 ± 0.11%) [14]. For ^{231}Pa, the highest intensity lines are at 300.066 ± 0.010 keV (1.95 ± 0.11%) and 302.667 ± 0.009 keV (2.3 ± 0.3%) [14]. However, the 300 keV line overlaps with the 299.98 ± 0.03 keV (2.21 ± 0.20%) line from ^{227}Th and, therefore, cannot be used. Instead, the 302 keV line was used in conjunction with some of the minor lines (330.1 keV; 1.36 ± 0.03% and 283.7 kev; 1.65%) [14]. The absence of ^{227}Ac was determined by recounting the fractions one week after elution to ensure the absence of ^{227}Th or, for ^{227}Th fractions, that it was decaying with the appropriate half-life.

Results and Discussion

The elution curve for the full separation is shown in Fig. 3.4. Protactinium-231 elutes first as it is an anion (PaF_7^{2-} or PaF_8^{3-}) in 0.1 M HF and therefore has no affinity for the resin [98]. Thorium forms only cationic and neutral species in HF, it elutes as ThF_4 in 0.5 M HF [98]. Radium and actinium form cations in dilute HF and are retained on the column. Nitric acid (3 M) was used to elute ^{223}Ra. Although Ref. [98] calls for 7.5 M $HClO_4$ to elute radium, 3 M HNO_3 was chosen instead based on Ref. [72] for safety reasons. Actinium can be removed with 6 M HNO_3 [98], though that was not quantitatively characterized in this work.

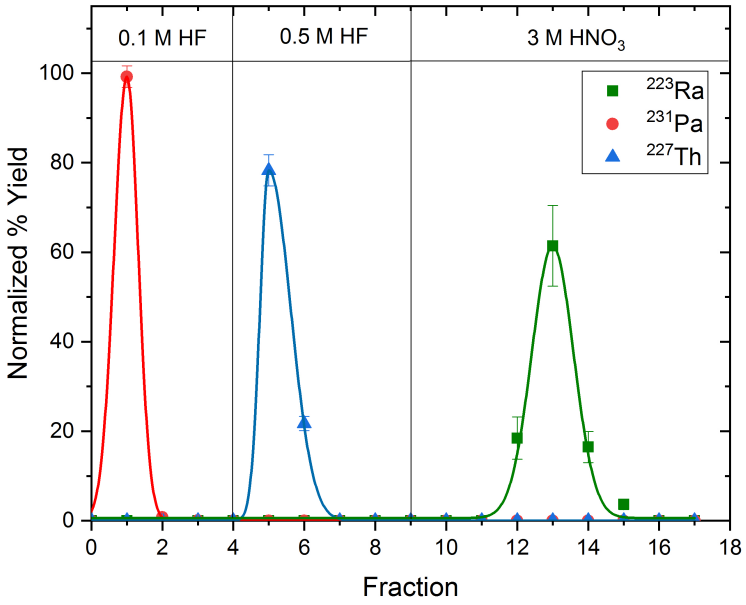

Figure 3.4: Elution curve for ^{231}Pa, ^{227}Th and ^{223}Ra from Dowex 50x8. Percent eluted is normalized, the error is from the statistical counting error.

The elution of ^{227}Th from the isotope generator is shown in Fig. 3.5. On average, 94 $\pm$ 2% of the total collected ^{227}Th activity was in the first two fractions, though there is some tailing, as was seen in the column separation (Fig. 3.4). As this isotope generator was made by replicating a procedure from the literature, it was not quantitatively characterized, all data is based on relative measurements and no absolute yield was calculated. However, the yield is assumed to be relatively consistent as each elution had about the same activity of ^{227}Th ($\sim$12 cps every 30 days) and this was consistent over the lifetime of the generator.

This isotope generator was eluted regularly for over a year and there was no breakthrough of either ^{227}Ac or ^{223}Ra. It was determined in the stripping process that this isotope generator cannot be used to continually elute both ^{227}Th and ^{223}Ra. Radium-223 is eluted under conditions where ^{227}Ac will bleed off the resin with sufficient eluant, which would result in rapid breakthrough if ^{223}Ra was regularly eluted, especially since it does not elute in a sharp peak but rather takes three to four bed volumes to fully elute (Fig. 3.4). The activity on this isotope generator was relatively low and no organic residue from resin degradation products was observed in the eluted fractions after evaporation. As with the ^{237}Np generator, discussed previously, the regular elution of the generator was impacted by the COVID-19 laboratory shutdown, and elutions were paused for about 4 months; however, it did not appear to effect the elution curve of this generator.

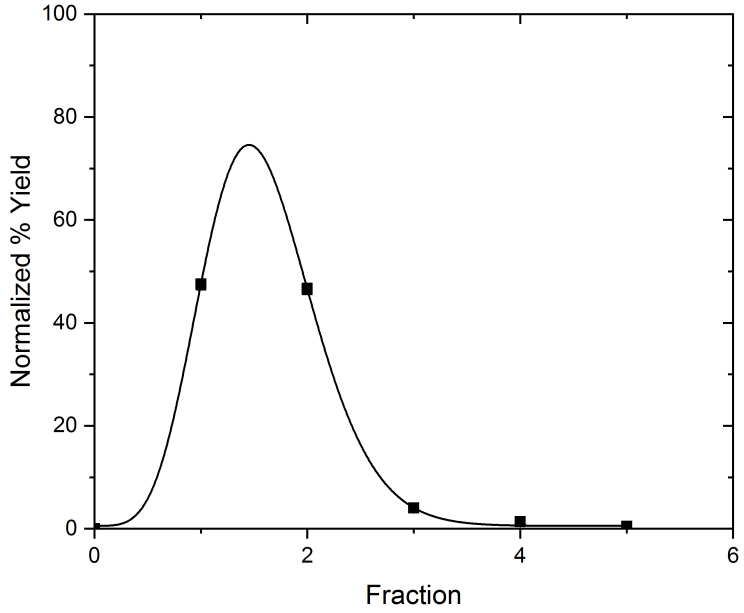

Figure 3.5: Elution curve of ^{227}Ac/^{227}Th isotope generator normalized and averaged over 16 elutions. Error bars are from counting statistics and are smaller than the data points. Fractions 0 and 5 are 2 mL H_2O fractions from the washes between elutions.

3.5 Conclusion

Two isotope generators were used in this work to produce tracer isotopes of thorium and protactinium. The first isotope generator is based on the decay of ^{237}Np and was fully characterized for the regular elution of ^{233}Pa in a small volume with a reasonable yield. The average yield for each elution was 75 ± 1% with 98.6 ± 0.3% of the total collected activity in the second fraction. The generator was in continuous operation for over a year before ^{237}Np breakthrough occurred and the yield and elution curve were consistent throughout that time.

The second isotope generator was based on the decay of ^{227}Ac and was made according to the procedure given in Ref. [98]. Thorium-227 was eluted regularly from this generator for over a year with no observed breakthrough of ^{227}Ac or ^{223}Ra. The majority of the ^{227}Th eluted in the first two fractions (on average 94 ± 2% of the total collected), but generator was not quantitatively characterized.

Both of these isotope generators are ideal for producing small amounts of tracer activity for chemical studies as they can be eluted regularly and produce tracer isotopes with reasonable half-lives and high-intensity gamma-ray lines. The ^{237}Np/^{233}Pa isotope generator

has many applications beyond this work as ^{233}Pa is a commonly used tracer in many fields, including geochemistry [84, 85] and neutron activation analysis [86]. The ^{227}Ac/^{227}Th generator has much more limited applications due to the elution in HF, which generally precludes medical applications, however, it was sufficient to produce ^{227}Th for chemical studies in this work.

Chapter 4

Target and Alpha Source Preparation by Electrodeposition

4.1 Introduction

For this work, it was necessary to fabricate thick thorium accelerator targets and thin protactinium alpha sources for nuclear data measurements. Both targets and alpha sources are commonly made using electrodeposition (ED), but each has their own specific requirements. Accelerator targets must meet strict requirements to ensure they can withstand irradiation. Targets must be uniform to prevent uneven heating as well as mechanically and thermally resilient [111, 112]. The target backing material must be pinhole free [111, 113], conductive [114], chemically resistant to the ED solution [111, 114], adherent to the target deposit [112] and, ideally, thin and low Z to minimize activation [113]. For these reasons, titanium, aluminum and carbon are common choices for backing materials [113]. In addition, impurities in the target material and target backing must be minimized [111], particularly those that can have interfering nuclear reactions. If the target is to be processed post-irradiation, the chemistry of the target deposit and backing must also be considered to ensure high yields for the recovery of the reaction products and, in the case of rare target materials, the target material itself [111–113]. Processing chemistry should also be optimized for efficiency and simplicity as well as speed in the case of short-lived activation products [111].

Sources for alpha spectroscopy have different requirements. Since alpha particles are easily attenuated, accurate alpha spectroscopy requires thin, uniform sources to ensure there is limited degradation of the alpha particle energy as it leaves the sample [114–119]. The process to make the source must have a high yield and produce a mechanically stable and adherent deposit [114]. The backing material needs to be chemically resistant and often conductive [120], depending on the method of source preparation. There are many ways of making alpha sources, which have been discussed thoroughly in the literature [114, 115], however, for precise measurements, ED is generally the accepted method for source preparation [88, 115–117, 119, 121].

4.2 Background Information

Electrodeposition is a processes where an electric potential is applied to an electrolyte containing dissolved particles or ions, which undergo an electrochemical reaction and adhere to the cathode or anode. Electroplating is a type of electrodeposition where a metal ion in solution is reduced and deposited on the cathode as a pure metal. This method is not applicable to actinides, which have too large redox potentials to be reduced to a metal by electrodeposition [118, 119]. Since actinide electrodeposition is the focus of this work, the following discussion will be limited to actinide chemistry, though the same principals apply broadly to other metals.

When a potential is applied to an electrolyte, there is an accumulation hydroxide ions (OH^-) at the positively charged cathode, forming an hydroxyl layer, accompanied by the release of hydrogen gas (H_2) [117–119]. This local change in solution chemistry leads to insoluble actinide species precipitating from solution at the cathode, forming a deposit, and over time the actinide is depleted from solution [117, 119]. The exact parameters of the solution and electrodeposition cell can have a large effect of the thickness and stability of the hydroxyl layer [119] and optimal conditions often need to be experimentally determined [114]. Electrodeposition can be done from either an aqueous solution or a polar organic solution, with the latter method historically called "molecular plating" or, less commonly, non-aqueous electrodeposition [119].

The exact species that is deposited is a matter of debate in the literature. While it is commonly accepted that ED from aqueous solutions leads to oxy-hydroxide products depositing [116, 119], it is somewhat more controversial for molecular plating. It was proposed by William Parker, who developed the concept of molecular plating and coined the term itself [119, 122], that the deposited species is the same species that is dissolved in the initial solution [115, 122], usually a nitrate or oxy-nitrate coordination complex. While this claim was repeated recently in a review article [119], more modern sources typically agree that oxy-hydroxide species are deposited in molecular plating, like in aqueous ED [112, 113]. The exact species that is deposited is generally irrelevant, however, as sources and targets are usually ignited or otherwise heated after the deposition is complete to convert the deposit to a stable oxide compound [112, 115, 116, 119].

Aqueous electrodeposition is generally done with high amperages (0.3 to 2 A/cm^2) and low voltages (<15 V) [111, 116, 123–126] as water will undergo electrolytic cleavage at high potentials, evolving O_2 and H_2 gas and eventually depleting the electrolyte. In molecular plating, there is no electrolytic cleavage of the organic electrolyte, therefore, low amperages ($\sim$0.5 mA to 10 mA) and high voltages (>50 V) are common; for actinide electrodeposition voltages are typically $\geq$500 V [111–113, 115, 127, 128]. There are many advantages to molecular plating including high uniformity [115], short deposition time [112, 115], high yield [111–113], the ability to make deposits of various thicknesses [111, 112] and a wide variety of compatible backing materials as no strongly acidic solutions are necessary [112]. These properties make molecular plating particularly suited for the fabrication of actinide targets which typically require a high degree of uniformity, high yield, thick deposits and low Z

backing materials, which are generally not as chemically resistant as other backing materials such as precious metals [111–113, 115]. After deposition, the deposit is usually ignited or heated to convert it to an oxide, as mentioned previously, and remove any remaining organic material [111, 112].

A typical molecular plating procedure for the early actinides involves a spike of an actinide solution, typically 5 to 50 μL of dilute nitric or hydrochloric acid, into an organic solvent, often isopropyl alcohol (IPA) or ethanol. The acinide is then deposited onto the cathode of an electrodeposition cell with a high voltage and low amperage [111–113, 115, 117, 128]. This method has been well characterized with regards to thorium [111, 112, 115, 117, 127–129], uranium [111–113, 115, 117, 129], plutonium [111], neptunium [111], americium [111], curium [111], californium [111] and some of the lanthanides [113, 117].

Protactinium, however, hydrolyzes readily due to its high charge state and has limited solubility in common mineral acids, like nitric and hydrochloric acid, which can lead to it retaining on the walls of vessel it is contained in rather than remaining in solution [66, 130]. Quantitative chemistry on protactinium, therefore, requires solutions with fluorides or sulfates (>0.2 M) [66, 130]. This is notably different than the solution chemistry of other early actinides, like thorium or uranium, which are stable in common mineral acids or even dissolved directly in organic solvents. Therefore, aqueous electrodeposition is commonly used for protactinium, rather than molecular plating, as it is more suited to solutions with low pH and high salt loading [88, 116, 118, 120, 123–126]. Although a couple of attempts have been made to use molecular plating with protactinium, neither had great success compared to aqueous methods [117, 121].

The geometry of electrodeposition cell itself can also have a large impact on the quality of a target or alpha source. This is discussed further in Section 4.4, which compares sources made in the same electrodeposition cell but with different anode geometries. Based on these results, no spiraled anode wires were used for electrodeposition cells in this work. In addition to the anode and cathode configuration, geometry considerations effect the shape of the deposit as well, sources and targets made by electrodeposition generally have a circular or other curved shape as sharp corners interrupt the electric field.

Due to the differences in protactinium and thorium solution chemistry, two different electrodeposition cells were used for this work. Electrodeposition of protactinium requires the use of fluorides, which highly limits the materials that can be used to construct the cell. For this work, a Teflon electrodeposition cell was designed and fabricated in-house (see Section 4.4). This cell has many advantages including a high degree of electric field uniformity, high chemical resistance and variety of acceptable backing material sizes and shapes. However, it also has significant limitations that make it non-suitable for fabricating thick thorium targets. The cell takes a long time to assemble and disassemble, and the backing material does not sit in a groove of some set size. Therefore, depositing layered targets (see Section 4.3) with this cell is challenging as it is extremely time consuming and there is no way to place the backing material in an identical position for each successive deposition to ensure the layers align.

Therefore, thorium electrodeposition was done with a conventional electrodeposition cell

[119] that was slightly modified to meet the experimental conditions (see Section 4.3). In particular, it was necessary to ensure the base of the cell fit the correct foil size (15 mm squares) and the deposition area was a 6 mm circle. This allowed the target to fit in the beam entrance window of the irradiation chamber (see Fig. 7.2) without an excess of material (a full description of the irradiation facility is given in Chapter 7). This design does not have the same degree of electrical field uniformity that the protactinium cell does, but it can be assembled and disassembled rapidly and the groove at the base of the cell ensures that the backing material is positioned similarly between depositions. The distance between the anode and cathode is adjustable to optimize the electrical field and compensate for the lack of symmetry.

4.3 Thorium Electrodeposition

Introduction

As discussed previously, there are stringent requirements that must be met by accelerator target backing materials and common materials include carbon, aluminum and titanium. For this work, simple, rapid target processing after the irradiation is also of great importance as short-lived isotopes will need to be separated from the target material and counted. A thick target is extremely important for cross section measurements [131] since the reaction rate is dependent on the areal density of the target material (Eqn. 7.8).

For this work, titanium, carbon and platinum were considered as target backing materials. Titanium (Z = 22) is one of the most commonly used backing materials and has been reported to perform better than aluminum or carbon during irradiations [113]. However, chemical processing with titanium can be difficult as evaporations can create highly insoluble titanium dioxide (TiO_2) [132]. Glassy carbon (Z = 6) is highly chemically resistant, but is brittle and not available in extremely thin foils. Despite the low Z of carbon, the thickness results in more beam attenuation than thin higher Z foils. Finally, platinum (Z = 78) is high Z, which causes significant attenuation and activation, but it can be purchased in extremely thin foils to minimize these effects and it is extremely chemically resistant.

It has been noted for molecular plating that the backing does not have a large effect on the quality of the deposit. Reference [112] used nine difference target backings ranging from aluminum to gold and noted little variation between the deposits of thorium on each backing. Similarly, Ref. [128] states that the exact backing is not a critical to the success of the deposition and had success with actinide deposition on precious metals, steel, carbon and titanium. This makes molecular plating ideal for making targets on several different backing materials, which was necessary to optimize targets for this work.

While thorium electrodeposition has been extensively characterized in the literature [111, 112, 115, 117, 127–129], the challenge for the electrodeposition of targets for this work is making a stable target with an areal mass density (conventionally referred to as "thickness" [112, 127, 131]) of about 1 mg Th/cm^2, which is not commonly done. A number of the proce-

dures outlined in these references were determined to be unsuitable on the basis of thickness. References [117], [128] and [129] deal only with thin targets. While Ref. [115] used a load solution with 1.25 mg of thorium and had reasonably high yields under certain conditions, it was not considered as there was a large variance depending on the backing material and it calls for acetone as a solvent [115]. Due to the low boiling point of acetone, it tends to evaporate significantly from the heat produced by the current flow during electrodeposition, which creates a high risk of evaporating off the solvent entirely and shorting the circuit. This is a significant fire hazard as the cell can spark under certain conditions. For this reason, other references discount acetone as a potential solvent entirely [117] and this work will not consider it either. Finally, Ref. [127] made thorium sources from 90 μg/cm^2 to 400 μg/cm^2 with an IPA electrolyte on aluminum, but noted there was poor adherence to the backing for deposits with high mass, which makes this method unsuitable for accelerator targets. Only Refs. [111] and [112] specifically address the fabrication of thick thorium targets. Both use a layering process to build up thick targets by successive deposits of about 100 μg/cm^2 and require voltages $\geq$900 V.

Most of these methods call for very high ($\geq$500 V) voltages with very low amperages (about 1 mA), which is not possible to sustain on most commercially available power supplies and requires extra safety precautions due to the dangers associated with voltages over 500 V. For this work, the power supply used, a Gwinstek 550 watt laboratory DC power supply (Model: GPR-30H100), had a maximum voltage of 400 V and a minimum amperage of 0.001 A. Therefore, only procedures with voltages <400 V could be considered.

Molecular plating of actinides with lower voltages (<500 V) is mentioned occasionally in the literature. Reference [112], which is focused on high yield, high voltage (900 V), short duration electrodeposition, states that it is possible to use a longer plating time and with a lower voltage (300 V) to make thorium targets, but does not provide details for the lower voltage method. Reference [113] uses a 150 V molecular plating method for lanthanides and uranium to achieve deposits as high as 500 μg/cm^2, but does not address thorium or thicker targets. This procedure was tested on platinum foils as part of this work, but it was extremely time consuming, taking 5 hours to deposit a single layer of 100 μg/cm^2, and, while the yield and adherence were sufficient for thin targets, targets greater than 500 μg/cm^2 were highly non-uniform with low adherence. This made thorium targets fabricated from this method unsuitable for irradiations.

After the many iterations with the method outlined in Ref. [113], the procedure in Ref. [112] was attempted at the lower voltage (300 V) that had been mentioned but not detailed in the original paper. With some modification, this method was successful and is described further in the following section. To develop and optimize an electrodeposition method for thick thorium targets, natural thorium (^{232}Th) with a ^{227}Th tracer was used and the resultant deposit evaluated for yield, uniformity and adherence. The same procedure was used on glassy carbon, titanium and platinum backings with no modifications other than the heat treatment after electrodeposition as the different materials have different thermal limits. In particular, platinum can be ignited, whereas titanium and glassy carbon are not stable in open flames as titanium combusts readily and glassy carbon is highly sensitive to

heat shock and can decompose.

Once a method for fabricating these targets was established, the natural thorium targets were irradiated to determine the in-beam performance as well as test procedures for chemically processing the targets (described in Chapter 6). Finally, ^{230}Th/^{232}Th targets were made according to the procedure developed in this chapter with the thorium material obtained in Chapter 2. These were irradiated to measure the ^{230}Th(p,2n)^{229}Pa and ^{230}Th(p,3n)^{228}Pa reaction cross sections as described in Chapter 7.

Description of Experimental Work

All acid solutions were prepared from Aristar ultra-pure acids (VWR) to ensure minimal target contamination and diluted with Aristar ultra-pure water (VWR) as necessary. The foils used as backing materials were glassy carbon (3000 °C, 0.1 mm), platinum (99.99+%, 0.025 mm) and titanium (99.9%, 0.01 mm); all were purchased from Goodfellow. To ensure the targets were pinhole free, only light tested (LT) metals were used. Before electrodeposition, each backing was washed with acetone, 0.1 M HNO_3, water and IPA then weighed three times on a Mettler Toledo ZPR6U microbalance (6.1 g maximum mass, 0.1 μg minimum mass). After electrodeposition, deposits were weighed in the same manner. Error on the mass measurements was determined from the standard deviation of three measurements.

Activity measurements were performed using an HPGe detector with Ortec NIM electronics and ASPEC multi-channel analyzer with spectra analyzed using the Maestro software (Ortec). All samples were counted relative to a standard source or electrolyte solution and in the same geometry. The 235.96 keV line (12.9%) was used for ^{227}Th [14]. Targets containing ^{230}Th were also counted with a Low-Energy Photon Spectrometer (LEPS) by the NCF at LLNL to accurately determine the activity of ^{230}Th on the target via its 67 keV line (0.38%) [14].

All targets were imaged with a VHX 5000 digital microscope with a VH-Z50L lens to assess the uniformity. The targets with ^{230}Th had sufficient activity to further characterize the uniformity with a position sensitive alpha detector (Fig. 4.1), which was used to map the activity distribution on the surface of the targets. This detector system was designed[1] and fabricated in-house and is typically referred to as the "target record player" due to the similarity in the way the detector is held over the target and how the needle on a record player is held in position. The detector itself is a small silicon detector with a 1 mm aperture that is suspended at the end of a long arm that holds it above the targets surface (Fig. 4.1b). The detector records the number of counts in a set time (2400 s) for each section (1x1 mm) of the target and the target is moved underneath the detector in a grid pattern until the entire target has been counted.

[1]Target record player system designed and maintained by Dr. Roger Henderson, who generously provided assistance with and access to the detector.

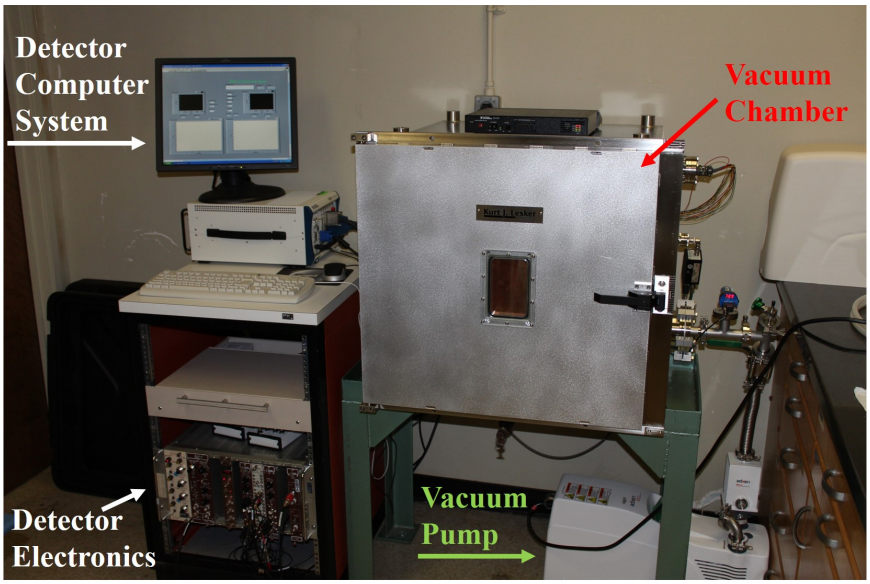

(a) External view of the target record player detector system.

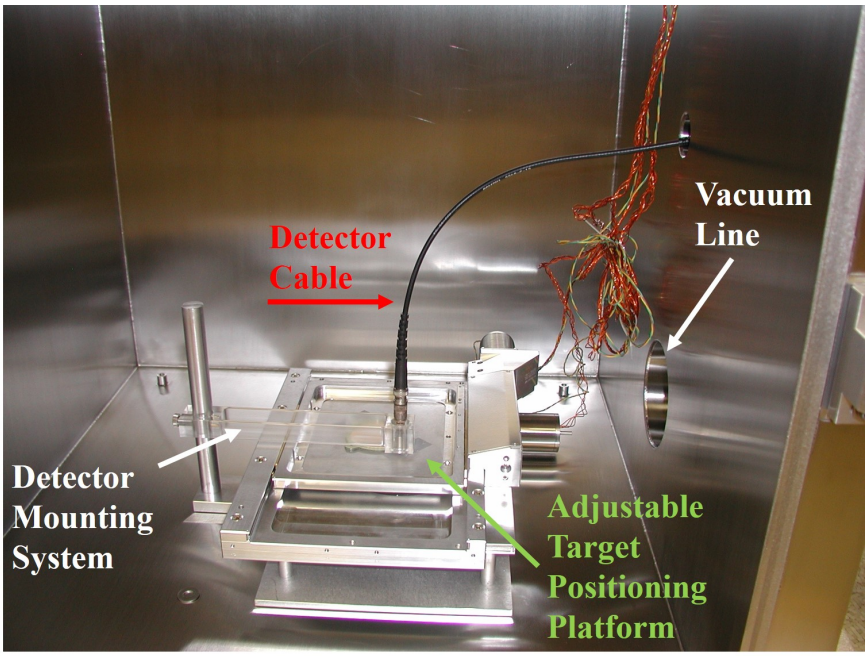

(b) Inside of the vacuum chamber of the target record player detector system. The detector itself is positioned on the underside of the end of the detector mounting arm. During operation, the vacuum chamber is evacuated and the target is automatically moved in 1 mm increments by the positioning platform.

Figure 4.1: Target record player detector system.

Thorium Preparation

A stock solution of thorium was prepared by dissolving 2.9825 g of thorium nitrate pentahydrate ($Th(NO_3)_4 \cdot 5H_2O$), legacy material (LLNL), in 30 mL 0.1 M HNO_3. A 0.9888 mL aliquot of this solution was further diluted with 0.1 M HNO_3 to make a stock solution with a concentration of 10 μg Th/μL.

A stock solution of ^{227}Th was also prepared for use as a tracer. An isotope generator was made based on the ^{231}Pa decay chain (Chapter 3) and high radiopurity ^{227}Th was eluted weekly in 4 mL 0.5 M HF. The tracer solution was evaporated down to dryness and reconstituted in 250 μL conc. HNO_3 with 250 μL sat. $Al(NO_3)_3$ to ensure the complete dissolution of ThF_4 [64]. The sample was loaded onto a 0.5 mL Dowex 1x8 (100-200 mesh) anion exchange column, pre-washed with 2 mL 8 M HNO_3. The column was washed with 4 mL 8 M HNO_3, then ^{227}Th eluted with 2 mL 10 M HCl. The ^{227}Th fraction was evaporated to dryness three times and reconstituted in 100 μL conc. HNO_3. This was repeated as necessary to acquire ^{227}Th. This extensive cleaning procedure for ^{227}Th was required because the presence of fluorides, even trace fluorides, was found to significantly lower the thorium ED yield.

Electrodeposition

To prepare the electrolyte, 10 to 80 μL of the 10 μg ^{232}Th/μL solution with a 50 to 100 μL spike of the ^{227}Th tracer was evaporated to dryness and reconstituted in IPA. For each electrodeposition, 1 mL of electrolyte was used. Electrolyte solutions were made daily in 1 to 4 mL volumes to ensure there was no effect from thorium hydrolysis. Solutions more than 24 hours old had significantly lower electrodeposition yields than solutions <12 hours old, likely due to a build up of hydrolysis products. There was no irregularity in yields for solutions $\leq$12 hours old, therefore, as a precaution all solutions were made and used within 8 hours.

The electrodeposition cell is shown in Fig. 4.2. It is composed of a plastic chimney which rests on the cathode; both are held in place by a steel frame, which also provides the electrical contact. The chimney contains the electrolyte and has a groove at the base to fit a McMaster Viton o-ring to ensure the cell does not leak. The opening of the chimney is 6 mm (dia.) circle; the area of the deposit is 0.2827 cm^2. While ED procedures often call for a spiraled platinum wire as the anode [119], better results were obtained with a straight platinum wire (see Section 4.4). The anode was suspended into the solution by a separate steel frame (Fig. 4.2b) and held 1 cm from the cathode. The base of the electrodeposition cell is designed to fit a 15 mm square backing material. Smaller sized backing materials can be accommodated, but as they do not fit exactly in the groove in the base, it is difficult to place them in the same position if layering is needed. Platinum foils (25x25 mm squares) and titanium foils (1 in. disks) were trimmed to 15x15 mm squares to fit into the ED cell; glassy carbon foils were ordered in this size. As mentioned previously, Gwinstek 550 watt laboratory DC power supply (Model: GPR-30H100) was used for all electrodepositions.

(a) Disassembled components of the cell (including the steel frame, plastic chimney Teflon cap, steel ring, screws and washers and o-ring).

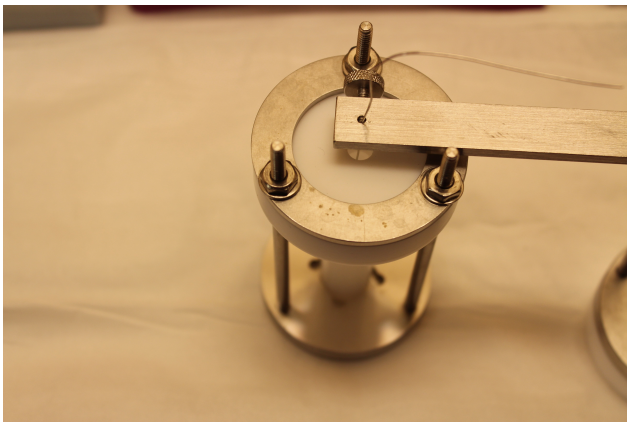

(b) The fully assembled cell with the anode wire suspended in the chimney.

Figure 4.2: Electrodeposition cell used for thorium targets.

For the initial electrodeposition, the cleaned and weighed foil was placed into the electrodeposition cell and the o-ring and chimney positioned on top. One milliliter of the electrolyte stock solution was counted with gamma-ray spectroscopy then added to the cell and the anode wire was positioned in the chimney. The power supply was turned on to 300 V ($\sim$0.002 A); all thorium electrodeposition was done with constant voltage. After 87 minutes, the current was terminated, the electrolyte removed and the target was placed on a glass petri dish to dry. Once dry, deposits on titanium and glassy carbon were placed in a furnace and baked for a total of 36 minutes: 6 minutes to heat the furnace from room temperature to 180 °C, then 30 minutes at 180 °C. Deposits on platinum were simply ignited with a Bunsen burner, with the exception of one foil that was baked first and then ignited for comparison

(discussed further in the following section). The remaining electrolyte solution was counted with gamma-ray spectroscopy and the deposit weighed with the microbalance. Layering of deposits was done in the same manner. Yields were calculated based off of the relative gamma-ray spectroscopy measurements of the electrolyte before and after the deposition. Due to the target thickness, alpha spectroscopy was not useful for yield determination as there is severe attenuation of the alpha particles through the deposit.

Target Assessment

The areal density of these targets can be expressed in two different ways: the areal density of thorium oxide (ThO_2) mass, which is representative of the total mass on the backing, or the areal density of thorium atoms, which is important for the irradiation properties of the targets. These numbers can be measured separately through spectroscopy (to determine the number of thorium atoms) or direct mass measurement (to determine the total mass of ThO_2). The areal density is then calculated by dividing the mass or number of atoms by the known area (0.2827 cm^2), which is set by the parameters of the electrodeposition cell.

Targets with ^{232}Th and trace ^{227}Th were only measured with relative gamma-ray spectroscopy, therefore, the thickness of each layer was calculated based on the measured mass only. For the targets with mixed ^{230}Th/^{232}Th, it was important to know the areal density of thorium atoms very precisely to make the cross section measurement (see Eqn. 7.8). These targets were counted with a LEPS detector and the 67 keV line from ^{230}Th used to determine the total number of ^{230}Th atoms. From this, the number of ^{232}Th atoms can be determined from the isotope ratio, which is well known from mass spectrometry (see Chapter 2), and the areal density of thorium (in μg Th/cm^2) determined from the molar mass of each isotope and the area.

For the targets with ^{230}Th, the thickness was determined independently from LEPS counting and mass measurements. The thickness as determined by LEPS counting was converted to a theoretical thickness of ThO_2 to allow for comparison with the thickness determined from the mass of the target. The two thickness measurements were in relatively good agreement for all of the ^{230}Th/^{232}Th targets, though the thicknesses determined by mass were $\sim$5% higher on average. This is likely because the low temperature heating process for the titanium backed targets is not completely effective at removing trace salts and organic contaminants.

The data in this chapter primarily concerns ^{232}Th targets, which have thicknesses reported based on mass measurements (μg ThO_2/cm^2) with a standard error of 6% to account for both the error in the mass measurement itself (the standard deviation of three measurements, <1% error) and the overestimation of thickness when determined by mass, as found for the ^{230}Th/^{232}Th deposits. Deposits with ^{230}Th/^{232}Th have the thickness reported based on the LEPS detector measurements, given as an areal density of thorium atoms (μg Th/cm^2). For ease of comparison, the calculated thickness in terms of ThO_2 is given for these targets as well, which is noted where relevant.

Results and Discussion

Electrodeposition Studies

The electrodeposition procedure was highly successful for making thick thorium targets on titanium and platinum. The targets are visually uniform (Figs. 4.3 and 4.4) and relatively mechanically resistant; they can be flexed without the target flaking and a light swipe test does not remove any detectable alpha activity. Targets were fabricated by layering thin deposits as well as single deposits of higher masses. The yield was determined from relative measurements of the initial electrolyte solution and the remaining electrolyte after deposition, as discussed previously.

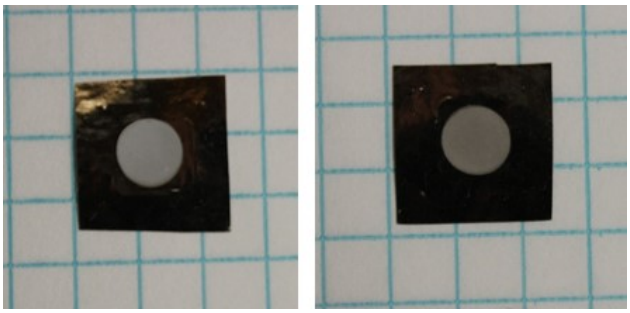

Figure 4.3: Examples of ThO_2 targets on titanium. Thicknesses are (from left to right) 1410 ± 85 μg ThO_2/cm^2 and 910 ± 55 μg ThO_2/cm^2. Total area of backing foil is 15x15 mm. Both targets irradiated with 16 MeV protons at CAMS on 3 February 2020.

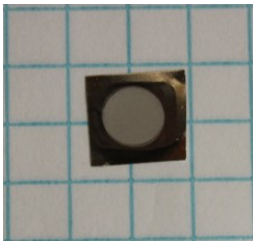

Figure 4.4: Example of ThO_2 target on platinum. Thickness is 840 ± 50 μg ThO_2/cm^2. Total area of backing foil is 10x10 mm.

Targets on glassy carbon were not successful, the deposits were highly non-uniform with low adherence. Furthermore, the mechanical stress applied to the glassy carbon foils in the electrodeposition cell created hairline cracks in the brittle material, particularly in the area compressed by the chimney and at the corners where the glassy carbon was in contact with the steel frame. These cracks lead to the targets fracturing readily with light pressure, such as that applied with tweezers to move the target or even tapping the surface. Data for these

targets could not be obtained as the process of transferring them out of the electrodeposition cell shattered the targets.

Although both platinum and titanium backed targets were fabricated successfully and eventually irradiated, most of the following section is devoted to characterization of titanium backed targets as titanium was ultimately determined to be the optimal backing material, largely due to chemical processing reasons that are discussed in-depth in Chapter 6.

Titanium Backed Targets

For initial deposits with thicknesses of about 300 to 400 μg ThO_2/cm^2, there was no detectable ^{227}Th in the remaining electrolyte, which indicates a yield greater than 98.07 $\pm$ 0.1% based on the minimum detectable activity of the detector for ^{227}Th (0.04 cps). These deposits could be layered readily and the yield remained high (90 $\pm$ 8% on average) for the second and third layers of similar thicknesses, but began to decrease by the fourth layer. Further layers were not attempted. This decrease in yield for successive layers was expected as the surface for electrodeposition gets progressively less conductive as the oxide layers build up.

Several depositions were done on titanium to determine the optimal number and thickness of layers for the targets. The thinnest layer was 330 $\pm$ 20 μg ThO_2/cm^2 and the thickest was 540 $\pm$ 30 μg ThO_2/cm^2. Initial deposits of more than 550 μg ThO_2/cm^2 were made, but not layered. Layered targets were all extremely uniform in the center of the deposit, but thicker layers had greater non-uniformity, particularly around the edges, when viewed with an optical microscope. This is shown in Fig. 4.5, which compares the uniformity of the thickest layered target (1410 $\pm$ 85 μg ThO_2/cm^2) with a slightly thinner (1100 $\pm$ 66 μg ThO_2/cm^2) but far more uniform target. The thicker target was composed of three successive layers with thicknesses of 530 $\pm$ 32, 390 $\pm$ 23 and 480 $\pm$ 29 μg ThO_2/cm^2. It was highly non-uniform at the edges due to the decreased adherence of each thick layer on the one before (Fig. 4.5a). The thinner target (Fig. 4.5b) was composed of three thinner layers (330 $\pm$ 20, 370 $\pm$ 22 and 390 $\pm$ 24 μg ThO_2/cm^2) and the uniformity, particularly at the edges, is significantly improved. Therefore, for both yield and uniformity, an optimal thick layered target would have three layers of 300 to 350 μg ThO_2/cm^2, resulting in a total thickness of about 1000 μg ThO_2/cm^2.

Targets were also made by the deposition of single thick layers, but the yield decreased for thicker initial layers, with the minimum yield of $\sim$50% for single deposits around 2000 μg ThO_2/cm^2. For non-layered irradiation targets, the thinnest was 670 $\pm$ 40 μg ThO_2/cm^2 and the thickest was 2200 $\pm$ 132 μg ThO_2/cm^2. The non-layered targets were also stable, uniform and adherent. A surface map of a non-layered target is shown in Fig. 4.6. This was a ^{230}Th/^{232}Th target with a thickness of 1116.291 $\pm$ 0.004 μg Th/cm^2 ($\sim$1270 μg ThO_2/cm^2). Due to the high activity of the targets ($\sim$2 μCi), the detector registered counts even outside of the geometrical bounds of the target, therefore, the physical size of the deposit is indicated in Fig. 4.6 with an arrow. As mentioned previously, the targets with trace ^{227}Th/^{232}Th did not have sufficient activity for measurements with the target record player system.

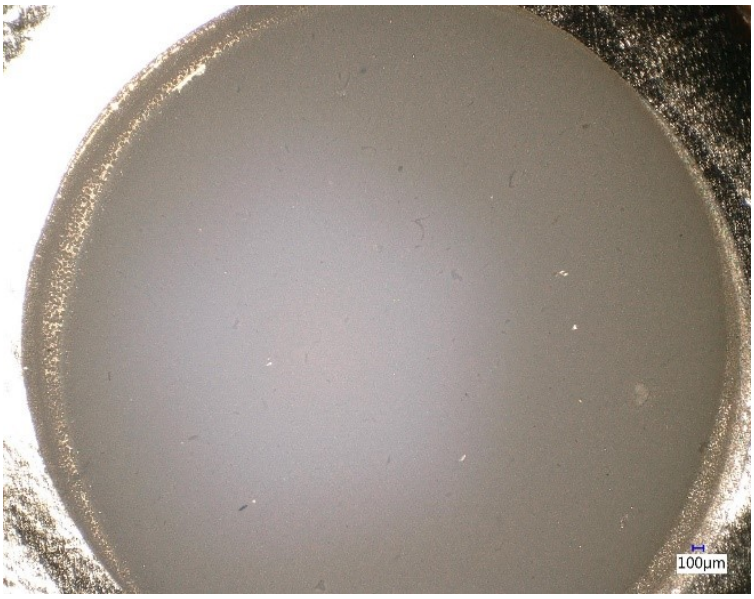

(a) ThO_2 (1410 ± 85 $\mu g/cm^2$ ThO_2) on titanium with low adherence at the edges. The overlapping circle pattern is created by inexact placement of the o-ring between successive depositions.

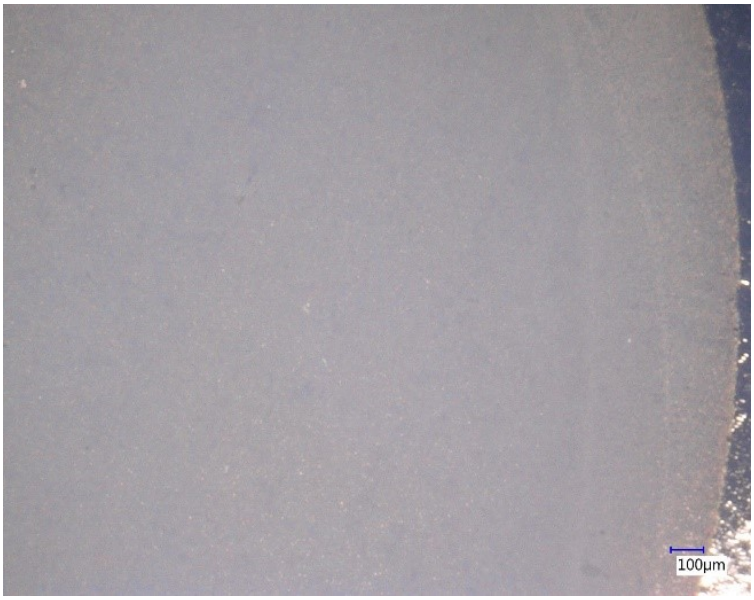

(b) ThO_2 (1100 ± 66 $\mu g/cm^2$ ThO_2) on titanium. Faint circular arcs from inexact placement of the o-ring are visible, but with no loss of target quality at the edges.

Figure 4.5: Comparison of edge uniformity of thorium targets on titanium backing foils.

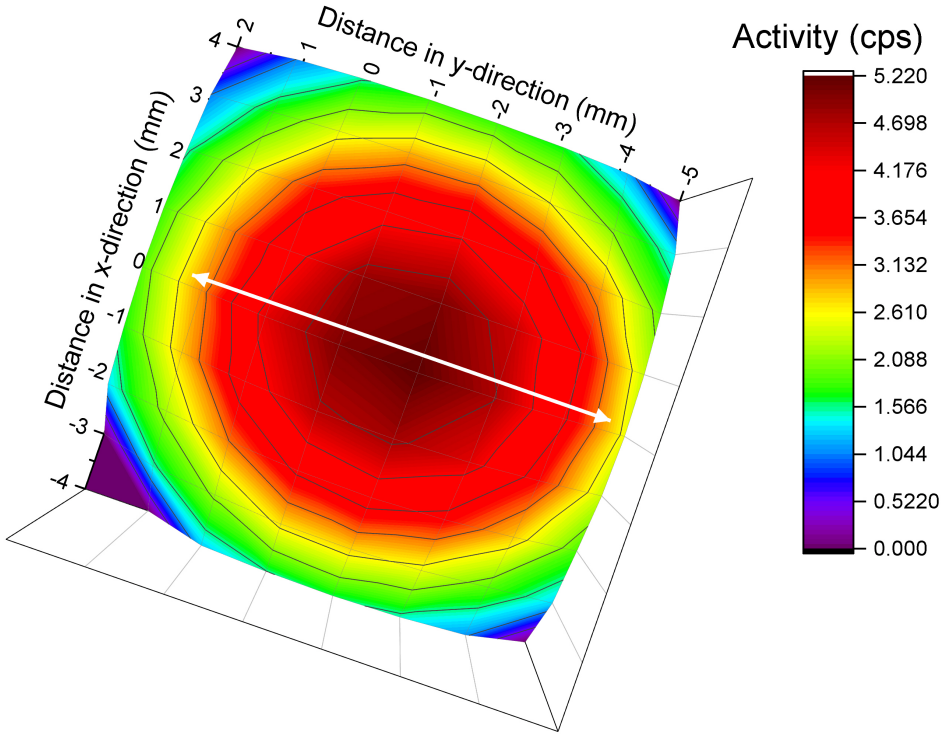

Figure 4.6: Activity map of the surface of a ^{230}Th/^{232}Th target. The geometrical size of the target (6 mm dia. circle) is indicated with a white arrow.

Platinum Backed Targets

The effect of igniting targets was examined with the platinum backed targets. A platinum backed target is shown in Fig. 4.7 before and after ignition. It can be seen that the target quality is highly improved by ignition with the number of defects and cracks reduced. Ignition improves target quality and increases uniformity by ensuring that any organic material or salt remaining on the target is destroyed and the deposit is fully converted to an oxide. Furthermore, ignition strengthens the target by creating an extremely resilient high-fired thorium oxide, which has enhanced mechanical stability and scratch resistance. High fired thorium oxide is typically described as thorium oxide heated to $\geq$1000 °C [133, 134], which is readily accomplished with a Bunsen burner as methane burns at 1950 °C [135]. Deposits on titanium cannot be heated at high temperatures to form a high-fired oxide as titanium burns in air, but rather are baked to form a low-fired oxide, which is not as resilient [133]. However, creating a high fired thorium oxide also makes the deposit more difficult to dissolve [133, 136, 137], which can be problematic for targets that will need chemical processing after irradiation (see Chapter 6).

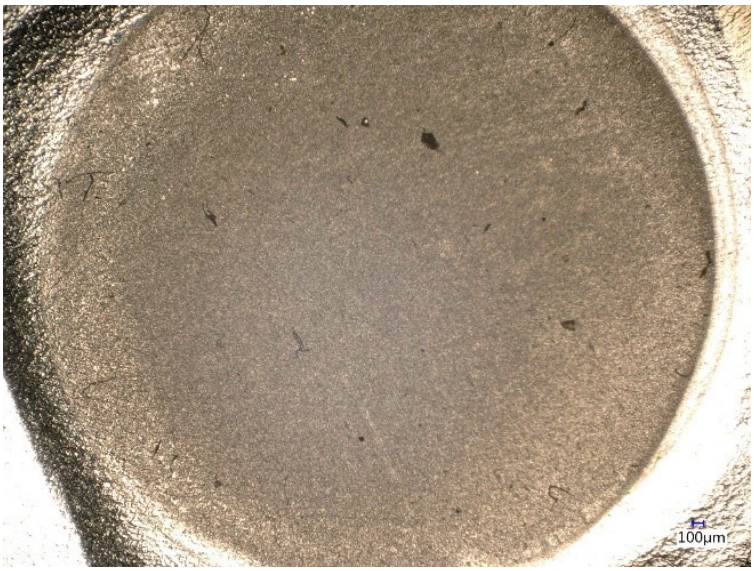

(a) ThO_2 (840 ± 50 $\mu g/cm^2$) on platinum, some defects visible.

(b) Same target after igniting with a natural gas Bunsen burner, defects significantly reduced.

Figure 4.7: Changes in uniformity after ignition of ThO_2 target on platinum backing foil.

Irradiations

To determine the effect of irradiation on the targets as well as develop chemical procedures for the target processing, four platinum backed and eight titanium backed thorium targets of varying thicknesses were irradiated in three separate irradiations with 16 MeV protons for 5 hours at CAMS. The experimental details of the irradiations are discussed in Chapter 6.

The targets performed well on both backings with no cracking, flaking or other structural damage to the target. Targets had a slight burn mark in the center from the beam, however, it did not seem to compromise the integrity of the target. There was no other observable change in the targets after the irradiation. It was noted that in the target stacks for these irradiations (Fig. 4.8), some activity from the target could rub off on the back of the previous foil while tightly compressed in the target stack. While this would not impact the chemistry development, a loss of activity or cross contamination between foils would greatly affect the cross section measurement. To ensure this did not happen during the cross section measurement experiments, thin titanium spacer foils were placed in front of the targets for these irradiations (Fig. 7.4) and then dissolved with the target in the post-irradiation processing.

For the cross section measurement experiments, eight ^{230}Th/^{232}Th targets were made on titanium foils based on the electrodeposition procedure described above. Details of these targets, irradiation conditions and cross section measurements are given in Chapter 7.

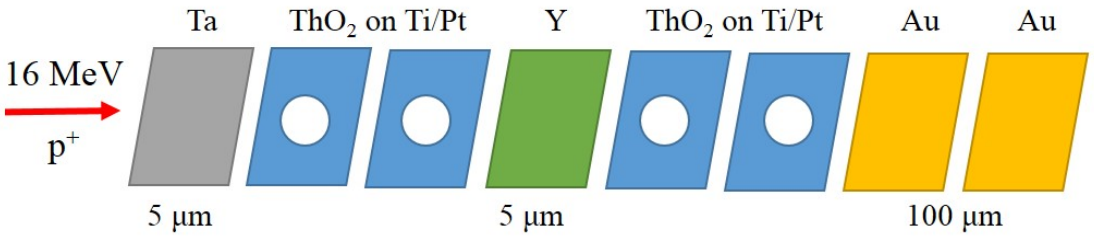

Figure 4.8: General beam stack for first three CAMS irradiations; the gold foils were associated with a different experiment. Experimental details for each irradiation given in Chapter 6.

4.4 Protactinium Electrodeposition

Introduction

While several methods for electrodepositing protactinium sources have been presented in the literature, no generally accepted method is prevalent as for the other actinides. The lack of information available on protactinium electrodeposition chemistry can be partly attributed to the tendency of protactinium to hydrolyze in aqueous solution, which makes electrodeposition

difficult [116, 121]. Therefore, a survey of present electrodeposition methods for protactinium was done.

Initially, there were two goals of this work, determining an optimal method for making a 1 μCi source of ^{231}Pa for nuclear data purposes as well as determining a method to rapidly electrodeposit alpha sources for the measurement of short-lived protactinium isotopes produced in the thorium target irradiations, particularly ^{229}Pa. Ultimately, alpha spectroscopy as a route to measure ^{229}Pa was abandoned as it was determined that a combination of gamma-ray and X-ray spectroscopy could be used to determine the activity of ^{229}Pa, as well as its daughters, with reasonable error and the combination thereof was faster and simpler than making electrodeposited alpha sources. Therefore, only the deposition of ^{231}Pa sources was finalized and a source was made for nuclear decay measurements, which are discussed further in Chapter 5.

Table 4.1 shows a list of the major papers that have been published on the topic of electrodepositing protactinium. The bulk of the work on non-tracer amounts of protactinium was done in the 1960s and 1970s and has not been revisited in the literature since then. A few recent papers have been published that involve electrodepositing trace protactinium, either for the purposes of radiochronology [124] or bioassays for worker exposure [125], and while these methods are less applicable to making a 1 μCi source, they were studied as well.

A number of the methods listed in Table 4.1 were determined to be unsuitable for this work. The methods outlined by Refs. [88, 120] are not applicable for thin alpha sources because they employ co-deposition of protactinium with uranium and lead, respectively, which would result in increased self-attenuation of the alpha particles as the sample would be thicker and have more mass than necessary. This is particularly important as the relatively low energy alpha particles from ^{231}Pa are readily attenuated [66]. The method in Ref. [121] was not considered because the paper internally noted that the final source was inferior to the previous work by Shimojima and Takagi [116].

Reference [123] does not specify either concentration of the electrolyte or time for the electrodeposition, therefore, it could not be reproduced with any accuracy and was not considered. The procedure in Ref. [117] was not attempted because it follows the typical actinide molecular plating procedure (see Section 4.2) and, as discussed previously, protactinium is well known to be unstable in nitric or hydrochloric acid solutions [66, 130]. Finally, the method presented in Ref. [126] was not considered as it was optimized for considerably more mass, 32.8 mg of ^{231}Pa, and employs an exceptionally high current, which, when tested in the electrodeposition cell used in this work, made it too difficult to reliably control the electrolyte volume as evaporative losses occurred rapidly. Therefore, only the methods given in Refs. [116], [118], [124] and [125] were tested. To accurately characterize the electrodeposition trials, a ^{233}Pa tracer was used in conjunction with ^{231}Pa.

The results for the different methods were compared on the basis of yield and uniformity. The uniformity is particularly important as alpha particle attenuation is minimized by creating a thin, even layer of activity. Non-uniformity would create areas of higher mass, and therefore more attenuation, which is undesirable for a source where the alpha activity needs to be determined very precisely (see Chapter 5). The attenuation and uniformity were

Table 4.1: Literature methods of electrodepositing protactinium.

Reference	**Year**	**Electrolyte**	**Application**
Shimojima and Takagi [116]	1963	H_2SO_4, HCO_2NH_4	Source preparation
Kim, et. al. [117]	1965	Ethanol with trace HCl	Study of actinide electrodeposition
Sakanoue, et. al. [118]	1965	NH_4HCO_2/H_2SO_4	Study of Pa electrodeposition
Wakita, et. al. [120]	1967	Co-deposit with PbO_2 in HNO_3/H_2SO_4	Geochemistry of Earth's mantle
Prakash and Ramanish [121]	1972	Isopropyl alcohol with trace HCl/HF	Study of Pa electrodeposition
Burnett, et. al. [123]	1988	H_2SO_4/HF	U-series age-dating
Price, et. al. [126]	1992	NH_4F	Source preparation
Prabhu, et. al. [125]	2010	$(NH_4)_2SO_4/H_2SO_4$, buffer	Trace bioassay
Knight, et. al. [124]	2014	$Na_2SO_4/NaHSO_4$, buffer	U-series age-dating
Smith and Barnett [88]	1965	NH_4F, NH_4Cl, oxalic acid, HNO_3	Source preparation

assessed by both typical alpha spectroscopy as well as finer measurements with the position sensitive alpha detector (target record player) discussed in the previous section.

Description of Experimental Work

All reagents used were analytical grade or higher and obtained from J.T. Baker or Sigma-Aldrich; Millipore Milli-Q deionized water (18.2 MΩ cm) was used for dilutions when necessary. Electrodeposition was done on virgin platinum planchets (1 inch dia.), which were legacy material from LLNL.

As before, gamma-ray spectroscopy was performed using a HPGe detector with Ortec NIM electronics and ASPEC multi-channel analyzer with spectra analyzed using Maestro software (Ortec). All samples were counted in the same geometry. The 302 keV ($2.3 \pm 0.3\%$) line was used for ^{231}Pa, while the 311 keV ($38.5 \pm 0.4\%$) and 340 keV ($4.45 \pm 0.05\%$) lines were used for ^{233}Pa [14]. Both isotopes have a significant line at 300 keV (^{231}Pa: $2.14 \pm 0.05\%$; ^{233}Pa: $6.63 \pm 0.06\%$), which was taken into account when analyzing the spectra [14].

Alpha spectroscopy was done with an Ortec Alpha Duo Spectrometer coupled with a vacuum pump; Maestro software (Ortec) used to analyze the spectra. The Alpha Duo system includes a built-in multichannel analyzer and the vacuum is computer-controlled through Maestro. Protactinium-233 is a pure beta emitter, so does not interfere with alpha spectroscopy of ^{231}Pa. Targets were also assessed with the target record player system described in Section 4.3. For the protactinium sources, the count time was 600 s per section of the target; the detector step size was 1 mm, as before.

The final source which was used for nuclear data measurements was also characterized with a low geometry alpha detector and extensive counting with Ge(Li) detectors, this is described in detail in Chapter 5.

Preparation of ^{231}Pa and ^{233}Pa Tracer

Legacy ^{231}Pa from LLNL was used for all of the protactinium electrodeposition studies. This material was used to fabricate the ^{227}Ac/^{227}Th isotope generator described previously; a description of the material and the procedure used to clean it are given in Chapter 3. The ^{231}Pa fractions were combined into a stock solution in 0.1 M HF with about 0.85 μCi ^{231}Pa per mL. There was no detectable ^{227}Th or ^{223}Ra in the cleaned ^{231}Pa sample.

For each electrodeposition, a 2 mL aliquot of the ^{231}Pa stock solution was spiked with about 780 dps of ^{233}Pa in 0.01 M HF from the ^{237}Np generator described in Chapter 3. This solution was evaporated to dryness at 97 °C and reconstituted in 100 μL of the electrolyte solution, this was repeated three times. On the final evaporation, the sample was reconstituted in 10 mL of the stock electrolyte solution. Before electrodeposition, the stock electrolyte was counted with gamma-ray spectroscopy and a 50 μL aliquot taken and dried on a stainless steel planchet at 35 °C; this was also counted with gamma-ray spectroscopy for direct comparison to the final protactinium deposit.

Electrodeposition

The electrodeposition cell used for the protactinium experiments is shown in Fig. 4.9; it was designed and fabricated in-house at LLNL. To accommodate solutions with fluorides, the cell is constructed entirely of Teflon. It is fully symmetric to maximize electric field uniformity with virgin platinum planchets as both the anode and cathode; the deposit spot size is 1 cm^2. The cathode and anode were replaced for each electrodeposition. Between uses, the electrodeposition cell was thoroughly cleaned with deionized water. The power source used was a Gwinstek 550-watt laboratory DC power supply (Model: GPR-30H100) as before.

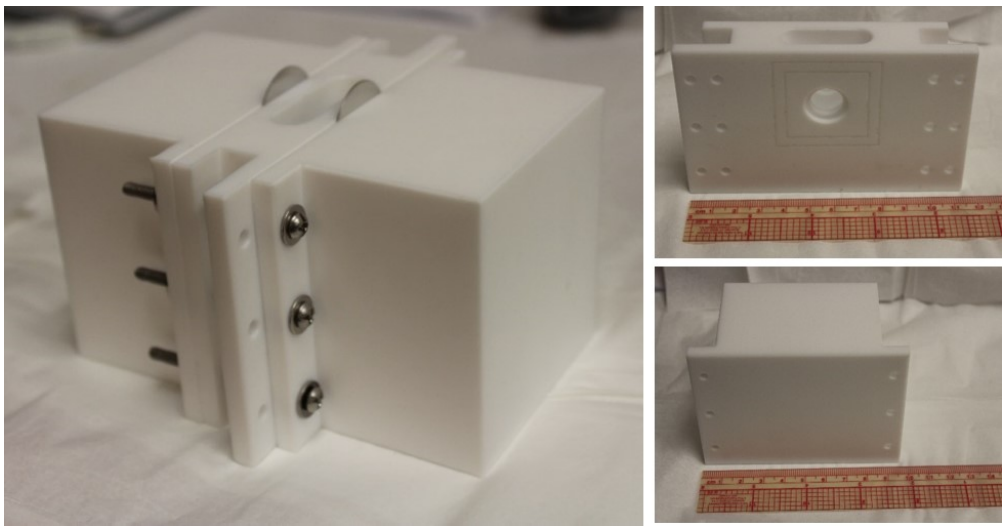

Figure 4.9: Electrodeposition cell used for protactinium electrodeposition (left) with view of center section (upper right) and side section (lower right).

To standardize the different literature procedures, a general electrodeposition procedure was developed, varying only the time and electrolyte solution according to each literature method. The total solution for each electrodeposition was 13 mL: 10 mL of the stock electrolyte solution and three 1 mL transfer rinses using the electrolyte solution. The final concentration of electrolyte solution as given in the original paper was maintained regardless of the original volume. If the procedure called for a transfer rinses with water, rather than the stock electrolyte solution, the dilution was accounted for in the electrolyte solution used here.

Before electrodeposition, the platinum anode and cathode discs were rinsed with water, ethanol then water again and the cell was checked for leaks using water. The 10 mL electrolyte solution containing $^{231}Pa/^{233}Pa$ was transferred to cell with three 1 mL rinses of the stock electrolyte solution and the power source turned on. If needed, water was added during the electrodeposition to compensate for evaporative losses. After the electrodeposition was completed, the remaining electrolyte solution was removed and the cell was rinsed with two 1

mL rinses of 5% ammonium hydroxide (NH_4OH) per the procedure in Ref. [124]. The anode and cathode planchets were rinsed with 1 mL each of: 5% NH_4OH, ethanol, and acetone then ignited. The remaining electrolyte solution, and rinses of both the cell and planchets were collected and counted with gamma-ray spectroscopy. Both anode and cathode planchets were counted with gamma-ray spectroscopy as well as alpha spectroscopy. The electrolyte solution, time and current for the four electrodeposition methods tested are given in Table 4.2; all protactinium electrodeposition was done with constant current.

Table 4.2: Protactinium electrodeposition experimental conditions.

Source Number	**Electrolyte**	**Duration**	**Current or Voltage**	**Reference**
1	0.05 M H_2SO_4 – 0.1 M HCO_2NH_4	8 hr	80 mA	[116]
2	0.94 M H_2SO_4 – 0.14 M HCO_2NH_4	4 hr	500 mA	[118]
3	0.5 M H_2SO_4 – $(NH_4)_2SO_4$ (pH 1.4)	2.5 hr	300 mA	[125]
4	1.1 M Na_2SO_4 – 0.42 M $NaHSO_4$	96 min	500 mA (5 min); 750 mA (91 min)	[124]

Results and Discussion

For each electrodeposition procedure, the yield was calculated from gamma-ray spectroscopy of the final source relative to the stippled aliquot of the stock solution in the same geometry. As a secondary check, the remaining electrolyte solution and rinses of the cell and planchets were also counted with gamma-ray spectroscopy to ensure the amount remaining in the electrolyte and the amount deposited agreed with the initial amount. The absolute ^{231}Pa activity of each source was determined with alpha spectroscopy. The yield and final ^{231}Pa activity of each of the four electrodeposition attempts is shown in Table 4.3. For all of the sources, the rinses of the planchets had no detectable activity above background, which indicates the deposits are highly stable.

Table 4.3: Results for protactinium electrodeposition trials. The remaining percent is the activity remaining in the electrolyte after the electrodeposition was complete.

Source Number	**Yield (%)**	**Remaining (%)**	**^{231}Pa Activity (μCi)**
1	101 ± 7	0.36 ± 0.12	1.81 ± 0.04
2	103 ± 12	0.1 ± 0.2	1.68 ± 0.04
3	97 ± 6	1.6 ± 0.4	1.66 ± 0.04
4	26.3 ± 1.9	80 ± 3	0.411 ± 0.009

The first source (based on Ref. [116]) had an extremely high yield and reasonably sharp peaks in the alpha spectrum (Fig. 4.10). The original procedure was done with 0.1 μg of ^{231}Pa in 5 mL and had a yield of 80 ± 2% [116]. Here a larger volume was used and the mass was considerably higher (about 30 μg), but no modifications to the procedure were required to achieve an exceptionally high yield. There are several reasons that may explain the increased yield compared to the original paper. For one, a cleaning process was used in this work to ensure the platinum cathode was free of any organic reside (which is known to disrupt electrodeposition [112]) and cleaning is not mentioned in the original paper. Another may be the increased electric field uniformity in the electrodeposition cell used in this work, which is important for effective deposition. However, as the original paper predates this work by nearly 60 years, the actual cause of the improved result is difficult to determine.

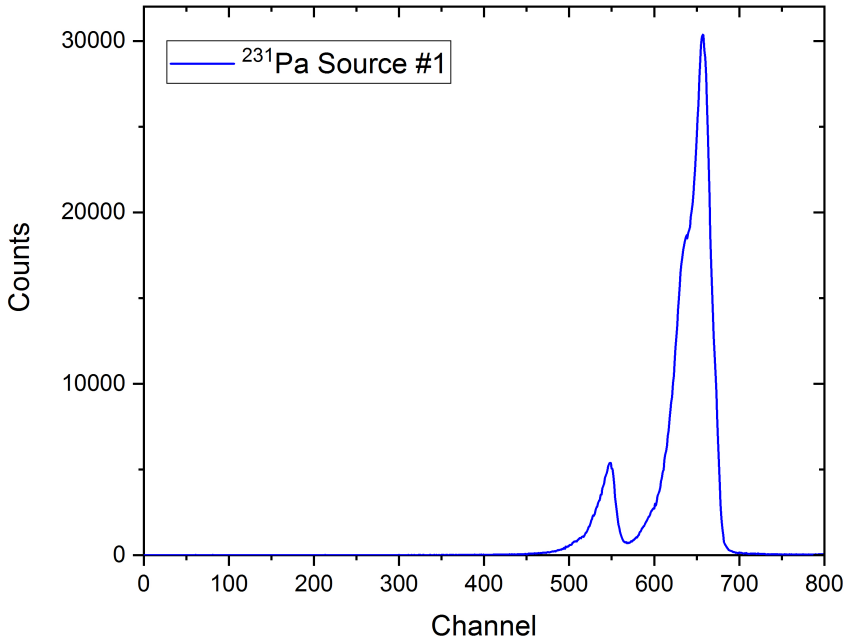

Figure 4.10: Alpha spectrum for source 1; count time was 120 s. For all ^{231}Pa alpha spectra presented in this chapter, all of the peaks arise from the alpha decay of ^{231}Pa to ^{227}Ac. The large peak around channel 650 is composed of the 5.014 and 5.028 MeV alpha emission lines with a shoulder from the 4.951 MeV alpha emission line, while the smaller peak is from the 4.736 MeV alpha emission line.

The second source (based on Ref. [118]) had a high yield but significant attenuation in the alpha spectrum (Fig. 4.11). The yield obtained here was within error of the original paper which reported the yield as greater than 90% [118]. The activity in the original experiment is given as 102 to 103 dpm/mL (1 to 10 dps/mL), while here it was >104 dps/mL, which is significantly higher. It is notable that this procedure is exceptionally similar to Ref. [116] but with a higher sulfuric acid concentration, higher current and shorter time. It has been noted in the literature that small changes to the electrodeposition conditions, which do not greatly affect the yield, can have a large impact on the deposit uniformity, which seems to be the case with the two methods given by Refs. [116] and [118].

The third source (based on Ref. [125]) had a high yield and reasonable alpha spectrum (Fig. 4.11), like the first source. The original paper does not give an electrodeposition yield specifically, only a total yield of 94.1 ± 2.4% for a full bioassay procedure, which cannot be directly compared to the yield in this work, which just includes electrodeposition. However, it does indicate the original paper had a high electrodeposition yield, which was replicated

here. It should be noted that this procedure was altered slightly from the original, which was done with 0.010 Bq or less ($\sim 6 \times 10^{-6}$ μg), whereas $\sim$1.6 μCi ($\sim$34 μg) was used here. To accommodate the increase in mass by seven orders of magnitude, a pH of 1.4 was used rather than 2.2. The pH of the electrolyte is known to increase during electrodeposition [118], therefore, to ensure the electrochemical reaction did not seize during the process, a lower starting pH was determined to be necessary.

A comparison of the alpha spectra of sources 2 and 3 is shown in Fig. 4.11. Since the two sources had the same activity (within error), the shape of the alpha spectrum is largely determined by the attenuation and the difference between the two sources is clearly visible. The activity distribution on these sources, as determined by the target record player detector, is shown in Fig. 4.12. It can be seen that the uniformity of sources 2 and 3 are similar, though the count rate is slightly lower for source 2, indicating more attenuation as was observed from the alpha spectra. Since sources 1 and 4 had higher and lower activities, respectively, than sources 2 and 3, their raw alpha spectra cannot be directly compared.

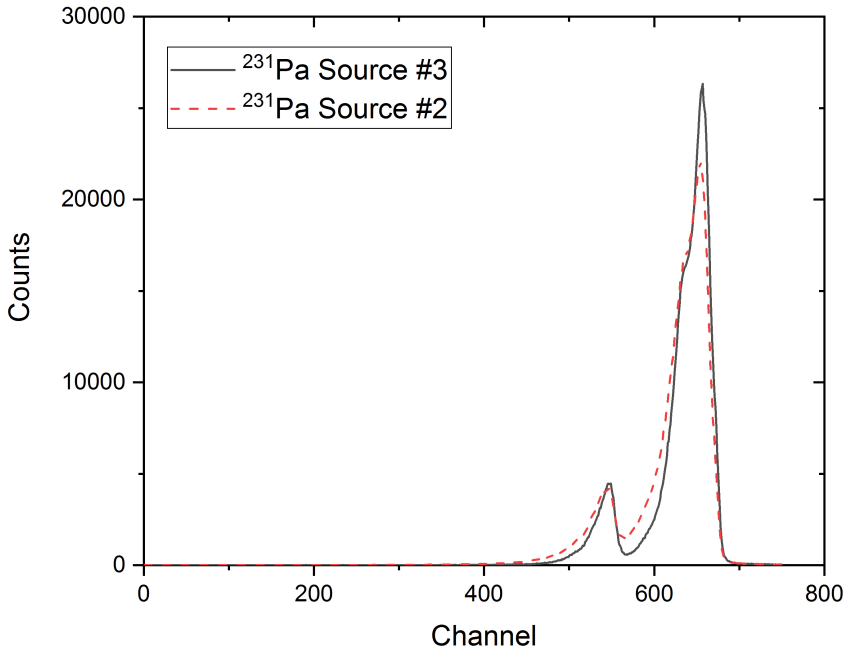

Figure 4.11: Comparison of two ^{231}Pa sources alpha spectrum. Source 3 has less attenuation than source 2 for the same activity (within error); count time was 120 s for both sources.

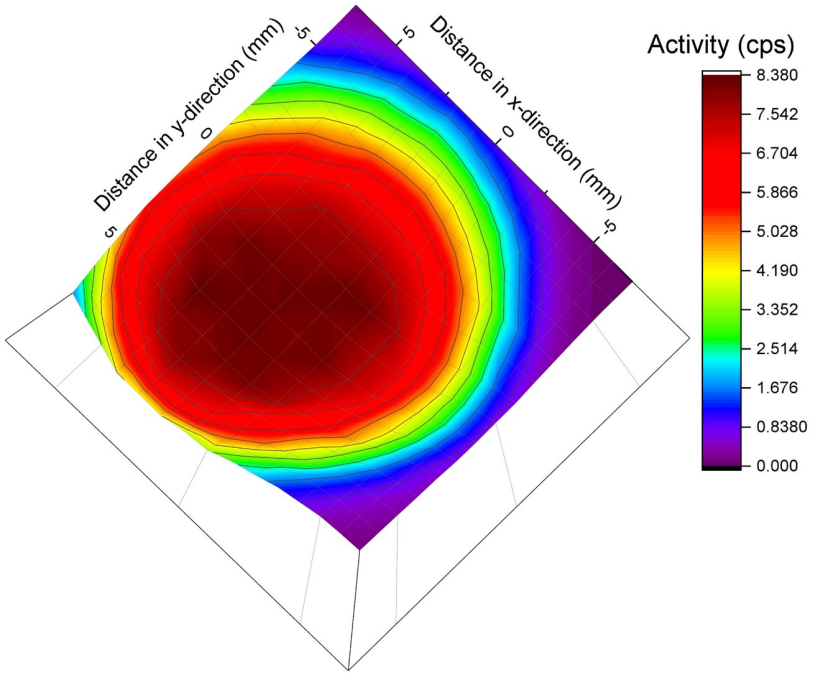

(a) Source 2

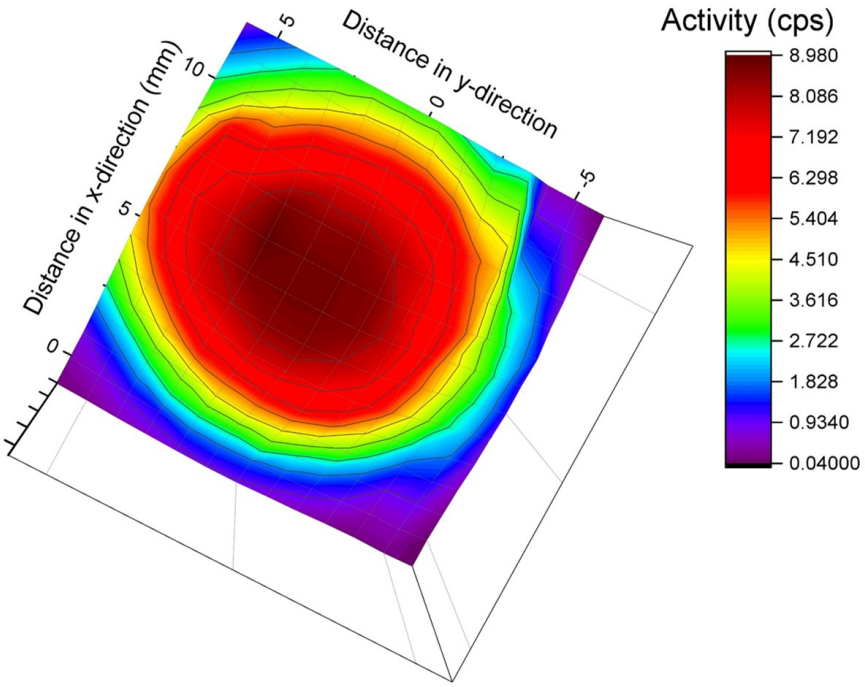

(b) Source 3

Figure 4.12: Comparison of source uniformity for protactinium sources 2 and 3.

The fourth source, made based on Ref. [124], had a low yield, making it not ideal for source preparation. The peaks in the alpha spectrum (Fig. 4.13) are sharp, but as the mass of this source is much lower than the other sources, it is difficult to make a reasonable comparison. The radiochemical yield given in the paper is $85 \pm 12\%$, which was not replicated here [124]. The procedure in the original paper was extremely clear, unlike some of the others, and was followed exactly except for an increase in volume (13 mL versus 12.5 mL). There was a large increase in activity, ~50,000 Bq here versus trace activity (~18 Bq) in the original procedure [124], but for the other sources, similar increases in activity did not impact the yield. The sharp decrease in yield may be due to the cathode as the original paper used a stainless steel cathode which has very different electrical properties than the platinum cathode used here. To keep all of the electrodepositions procedures consistent, only platinum cathodes and anodes were used for the protactinium electrodeposition studies. Furthermore, stainless steel is not resistant to fluoride corrosion and, therefore, is not an ideal cathode for the protactinium solutions used here which may have trace fluorides remaining from the protactinium purification procedures.

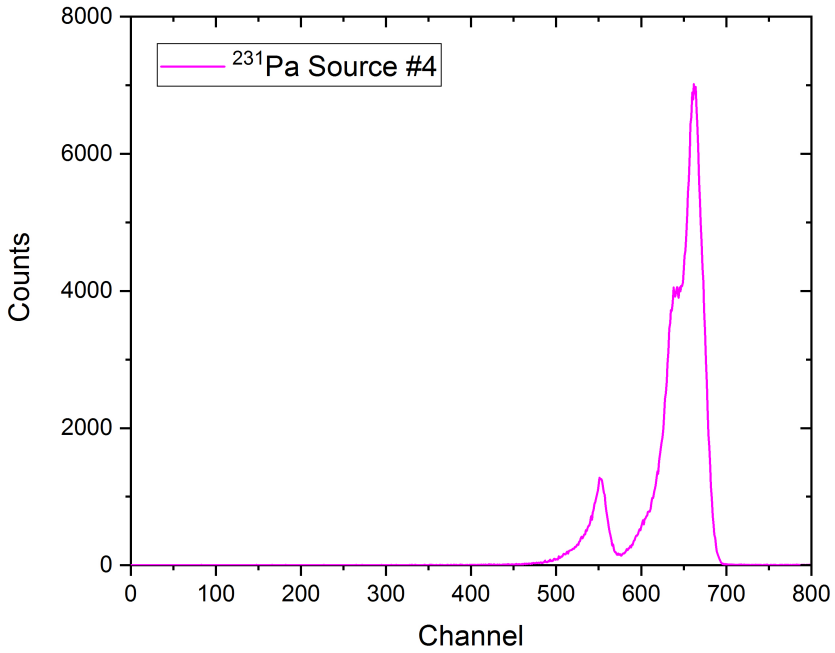

Figure 4.13: Alpha spectrum for source 4; count time was 120 s.

As mentioned previously, both the anode and cathode planchets were counted with gamma-ray spectroscopy after each electrodeposition. This was done to characterize the adherence of activity on the anode, which has been observed with some actinides before,

including protactinium [116]. However, all of the anode planchets were near background, indicating no significant deposition or adherence to the anode. It is hypothesized that this observed effect is largely driven by hydrolysis effects rather than an electrochemical reaction, particularly for low yield depositions where protactinium is not particularly stable in the electrolyte.

Based on the results of the protactinium electrodeposition studies, the electrodeposition procedures based on both Refs. [116] and [125] (sources 1 and 3) would be suitable to make a ^{231}Pa source for nuclear data measurements as they had high yields and reasonable alpha spectra. The method from Ref. [125] was chosen for convenience as it required far less time than the method in Ref. [116]. To make a source for nuclear data measurements, a 2 mL aliquot of the ^{231}Pa stock solution was taken and cleaned again using the Dowex 50x8 cation exchange separation described previously (Chapter 3) and the time of separation noted so the in-growth of the decay daughters could be rigorously accounted for. It was then prepared and electrodeposited as described above, except the ^{233}Pa tracer was not added as it would have interfered with the nuclear data measurements. The details of the source and nuclear data measurements are given in Chapter 5. An activity map of this source is shown in Fig. 4.14 and it can be seen that the uniformity is very high.

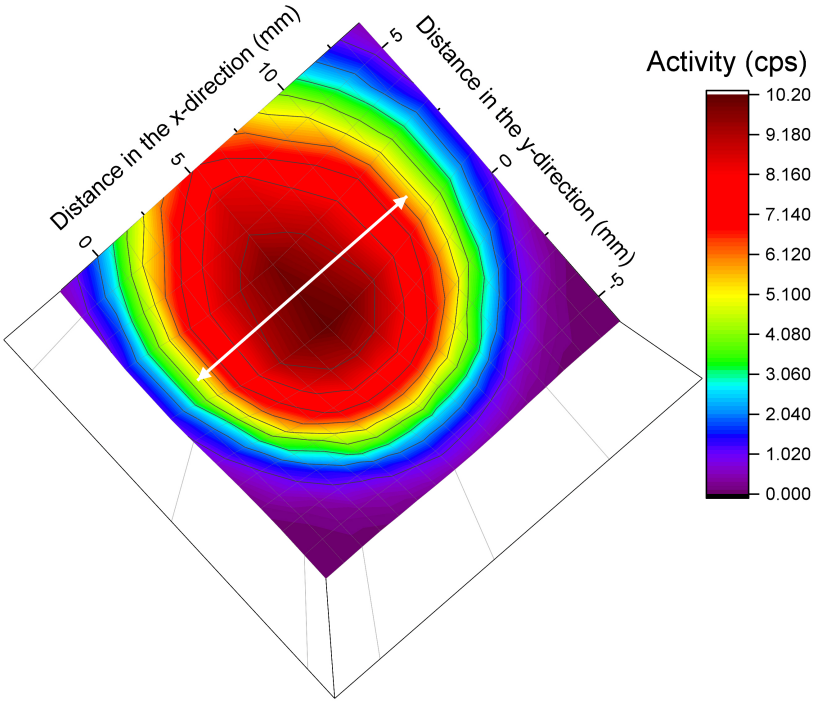

Figure 4.14: Activity distribution of ^{231}Pa on alpha source for nuclear data measurements. As before, the geometric size of the target is indicated with a white arrow.

Effect of Electrodeposition Cell Geometry

To characterize the effect of the geometry of the electrodeposition cell, two low activity ^{231}Pa sources were electrodeposited in the same electrodeposition cell using the procedure from Ref. [125] with same distance between the anode and cathode, but with a different anode geometry.

The first source (Fig. 4.15a) was deposited with a spiraled platinum wire anode and the spiral shape was mapped onto the source itself, leading to a high degree of non-uniformity. The second source (Fig. 4.15b) was made with a straight platinum wire anode, and there is significantly better uniformity. Based on these results, no spiraled anodes were used, the protactinium electrodeposition cell was fully symmetric and the thorium electrodeposition cell had a straight wire anode.

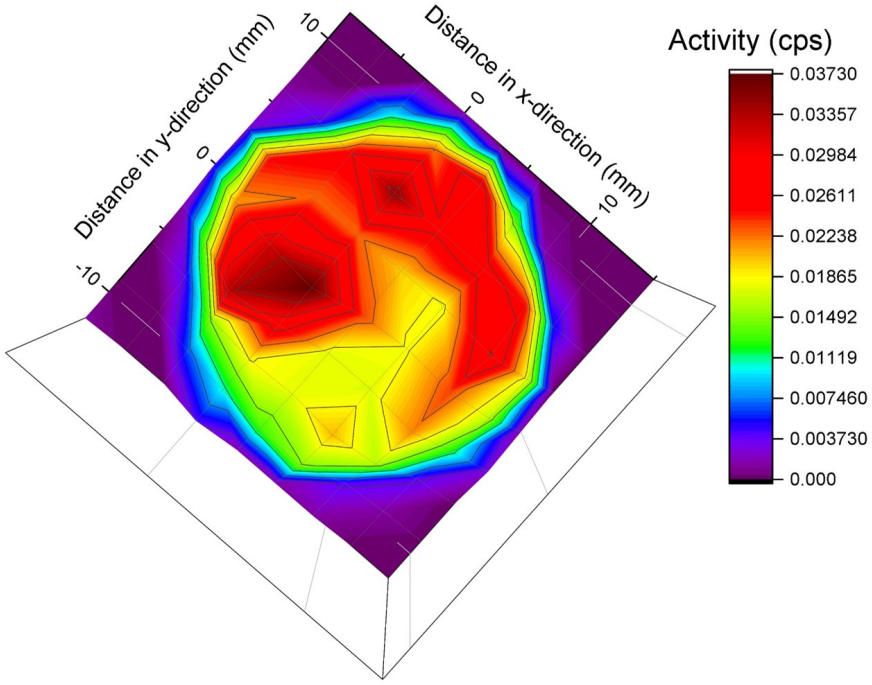

(a) Source made with a spiraled platinum wire anode.

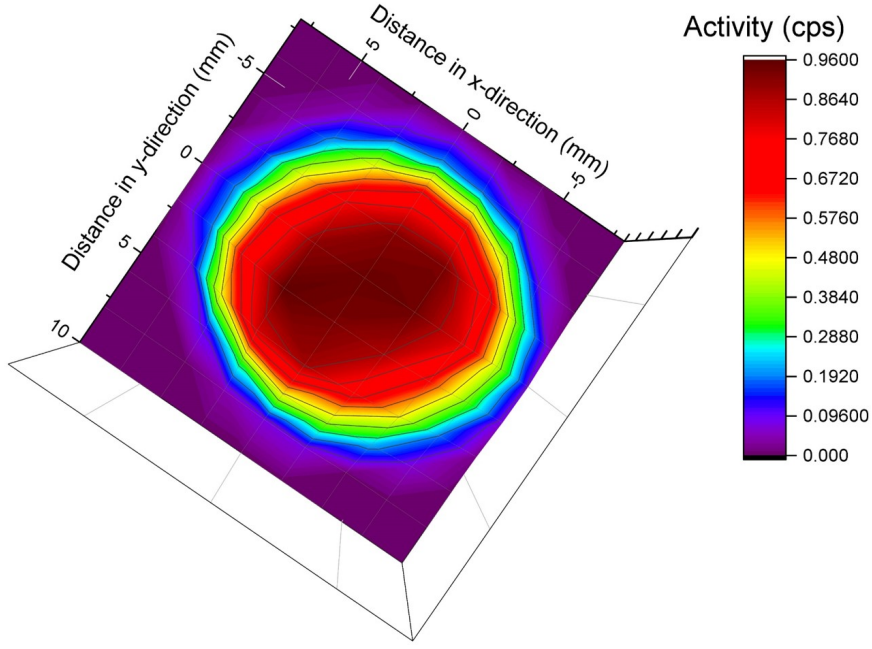

(b) Source made with a straight platinum wire anode.

Figure 4.15: Effect of anode geometry on the uniformity of low activity (<0.1 μCi) electrodeposited ^{231}Pa alpha sources.

4.5 Conclusion

Literature methods for the electrodeposition of thorium and protactinium were surveyed and experiments performed to optimize procedures for fabricating thick thorium accelerator targets and thin protactinium alpha sources.

Thorium targets were made in a wide variety of thicknesses on both platinum and titanium backing materials. Deposition on titanium was more extensively characterized as this backing material was ultimately selected to make targets for the cross section measurement. Single layer deposits ranging from 670 ± 40 μg ThO_2/cm^2 to 2200 ± 132 μg ThO_2/cm^2 and layered targets with thicknesses of 910 ± 55 μg ThO_2/cm^2 to 1410 ± 85 μg ThO_2/cm^2 were deposited on titanium. An ideal layered target would have three layers with thicknesses of 300 to 350 μg ThO_2/cm^2, resulting in a total thickness of about 1 mg ThO_2/cm^2. Yields were high for deposits of 300 to 400 μg ThO_2/cm^2, but decreased for thicker layers as well as for successive layers. The maximum number of layers was four due to this decrease in yield.

Targets were uniform, adherent and mechanically resilient; there was no structural damage to any of the targets, either layered or single deposit, during the irradiations. Furthermore, the targets were considerably thicker than targets that have been described in the literature, which usually have thickness of 500 to 1000 $\mu g/cm^2$, as discussed previously. The targets made in this work were characterized up to thicknesses of 2000 $\mu g/cm^2$ and were made with low voltage electrodeposition, which is far safer and more accessible than typical thick thorium electrodeposition procedures that call for high voltages (∼900 V). Using the procedure developed in this chapter, targets with mixed $^{230}Th/^{232}Th$ were made and irradiated at CAMS to measure the $^{230}Th(p,2n)^{229}Pa$ reaction cross section.

Protactinium electrodeposition was also studied to make a source appropriate for nuclear data measurements. While electrodeposition and alpha spectroscopy techniques were not used in the process of making the cross section measurement, these studies were applied to the fabrication of a source for ^{231}Pa nuclear data measurements. Four literature methods were tested and the compared on the basis of yield and uniformity. Two methods successfully produced highly uniform, high activity sources and one of these was chosen to fabricate a ^{231}Pa source to make nuclear data measurements of the gamma-ray energies and intensities from the decay of ^{231}Pa. Improving the nuclear data on this isotope has a number of applications, which are detailed in the following chapter.

Chapter 5

New Measurements of Gamma-ray Energies and Absolute Intensities from the Decay of ^{231}Pa

5.1 Introduction

There are two naturally occurring protactinium isotopes, ^{231}Pa from the ^{235}U decay chain (Fig. 2.3) and ^{234m,g}Pa from the ^{238}U decay chain (Fig. 2.2). Due to the short half-lives of ^{234}Pa ($t_{1/2}$ = 6.70 h) and ^{234m}Pa ($t_{1/2}$ = 1.17 m), this isotope has limited uses, but it can be used to estimate enrichment of uranium fuel [138–140]. The half-life of ^{231}Pa ($t_{1/2}$ = 32,760 y) [138] is significantly longer and this isotope has a number of uses including isotope production [87, 124, 125], nuclear forensics [139–143], archeological dating [144] and geochronology [120, 123, 145]. It decays exclusively by alpha emission to ^{227}Ac [14, 138].

In geochronology, modern dating techniques based on the ^{231}Pa/^{235}U ratio often employ mass spectrometry as naturally occurring ^{231}Pa can be difficult to accurately measure with decay counting [145]. This dating method is commonly used as a secondary check for ^{230}Th dating rather than an independent method because it has a limited range and lower precision compared to ^{230}Th dating [146]. However, ^{231}Pa/^{235}U dating is very useful in nuclear forensics when the concentration of uranium, particularly ^{235}U, is high [87].

While both multi-collector inductively coupled plasma mass spectrometry (MC-ICPMS) and alpha spectroscopy can be used for ^{231}Pa/^{235}U measurements, MC-ICPMS is often used rather than alpha spectroscopy due to its significantly lower uncertainty [87, 142, 143]. However, both alpha spectroscopy and mass spectrometry are destructive analytical methods that require time consuming and complicated sample preparation. An alternative analytical method is gamma-ray spectroscopy which is simple, rapid and non-destructive [141].

Gamma-ray spectroscopy has been used for ^{231}Pa dating, notably for uranium and thorium ores [141, 147] and archeological dating [144], however, its use is limited by the available nuclear data. The gamma-ray lines from the decay of ^{231}Pa most suitable for dating, i.e.

those with limited interferences and high abundance, are the 283.69 keV (1.65%) and 302.6 keV (2.3(3)%) lines [14, 141]. However, these lines have large uncertainties in their intensities [148], which severely limits their practical use in nuclear forensics as the intensity is vital for calculating the ^{231}Pa/^{235}U ratio.

The nuclear data for the gamma-ray lines associated with the decay of ^{231}Pa to ^{227}Ac was last evaluated in January 2016 by the International Network of Nuclear Structure and Decay Data Evaluators and is compiled in the Evaluated Nuclear Structure Data File (ENSDF) database [148]. The accepted gamma-ray energies and intensities are weighted averages of a number of measurements [148] with all intensities relative to the 283.7 keV line, which is normalized to have an intensity of 100 by convention [148]. The majority of the nuclear data compiled by ENSDF for the decay of ^{231}Pa was measured in the 1970s or earlier, with only one more recent reference (from 1986 [149]). The absolute intensities are calculated based on the relative intensities and the measured absolute intensity of the 283.7 keV reference line. However, the absolute intensity of the 283.7 keV reference line is based on only two measurements, one of which has a large error bar (4.7% [150]).

The work described in this chapter was undertaken to make accurate, modern measurements of the major gamma-ray emissions associated with the decay of ^{231}Pa to ^{227}Ac. For this, a thin, uniform ^{231}Pa source with an activity of about 1 μCi was prepared and characterized with gamma-ray spectroscopy to determine the energies and relative intensities of the main gamma-ray emissions. To determine the absolute intensities, the source was also characterized with alpha spectroscopy to determine the absolute decay rate and, from that, calculate the absolute gamma-ray intensities.

5.2 Description of Experimental Work

Source Preparation

The procedure to make the ^{231}Pa source is described in Chapter 4. The deposition yield was 89(6)%; the activity of the source was 1.578(1) μCi ^{231}Pa (58,370(40) dps) as determined by low-geometry alpha spectroscopy (described below).

Nuclear Decay Measurements

Gamma-ray spectroscopy was done at the NCF at LLNL. The ^{231}Pa source was counted six times on three different Ge(Li) detectors; a short count (1 day) and a long count (3 to 7 days) were done on each detector. The detectors were calibrated with a ^{154}Eu source using nine of its highest intensity gamma-ray lines with energies ranging from 52 to 1461 keV; for all counts the distance between the detector and the source was 8.45 cm. The code GAMANAL [151] was used to analyze the resultant spectra.

Alpha spectroscopy was done with a low-geometry detector made in-house. The detector was a 200 mm^2 silicon barrier detector; the total geometry factor[1] was 1220.8. The ^{231}Pa source was counted six times for 1.5 to 2.5 hours. The background was 0.120(5) cps. No spectra were collected, only an absolute count rate was measured. Alpha activity from the ^{231}Pa daughters was minimal due to the long half-lives of ^{231}Pa and ^{227}Ac, but, to account for this, the ratio of alpha activity arising from the daughter products to the total alpha activity was calculated using the Bateman equations and the known time of the separation of ^{231}Pa from its daughters. Using that ratio, the alpha activity from the daughter products was subtracted from the total decay rate to determine the absolute ^{231}Pa decay rate.

5.3 Results

The absolute gamma-ray energies and intensities measured are given in Table 5.1. The energies were measured independently for each count on each detector and an average energy was determined for each gamma-ray line. The uncertainty on the energy measurements was determined from the standard deviation of several measurements and the systematic uncertainty from the calibration of the detectors. Each intensity was calculated independently by dividing the absolute count rate of each peak by the total decay rate of the source. The uncertainty on each value includes the uncertainty from counting statistics as well as the systematic uncertainty from the calibration of the detectors.

5.4 Discussion

The average energies and intensities from ENSDF, along with the accepted ENSDF references, are compared to those measured in this work and given in Table 5.2; the measured intensity data has been normalized per the convention in ENSDF so the 283 keV reference line has an intensity of 100. The error on the relative intensity measurements is dominated by the counting statistics because the efficiency function for the detectors is extremely well-characterized and the ratios of gamma-ray intensities can be measured very precisely.

The gamma-ray energies reported in ENSDF are a weighted average of three to five values derived from Refs. [150, 153, 154] and supplemented by Refs. [155, 156] when a value is available. The measured energies in this work are all in agreement with the average energies reported in ENSDF within one standard deviation except for the 277.09(2) keV, 283.64(2) keV and 330.00(3) keV lines, which agree within two standard deviations. In the case of the 277.09(2) keV line, the measured value agrees within one standard deviation with three of the five values included in the ENSDF average (Refs. [150, 153, 154]) but does not agree with Refs. [155, 156], which measured higher values.

[1] In a low-geometry detector, the total geometry factor is expressed as $1/w$, where w is the solid angle subtended by the detector [152].

Table 5.1: Measured energies and absolute intensities for major gamma-ray emissions from the decay of ^{231}Pa to ^{227}Ac. The error on the energies is a standard deviation of several measurements and the error on the intensities is from counting error; both errors also include systematic uncertainty from the detector calibration.

Energy (keV)	**Intensity**
243.1(1)	0.00037(1)
255.90(4)	0.00120(2)
260.22(2)	0.00183(3)
273.16(3)	0.000592(8)
277.09(2)	0.000672(9)
283.64(2)	0.0163(2)
300.02(3)	0.0239(3)
302.62(3)	0.0242(3)
312.93(3)	0.00100(1)
327.17(3)	0.000387(6)
330.00(3)	0.01347(2)
340.77(3)	0.00175(2)
354.54(4)	0.00095(1)
357.10(4)	0.00167(2)
379.25(5)	0.000488(6)
407.83(5)	0.000354(5)

Similarly, the measured energy for the 283.64(2) keV line agrees with Refs. [150, 153, 154] but not Refs. [155, 156], which again measured slightly higher values. The 330.00(3) keV line agrees with Refs. [153–155] but not Refs. [150, 156]. It can be seen that Ref. [156] is usually on the high end of the previously reported values, this may be because it was the only study done with curved crystal spectrometers. This work, as well as Refs. [150, 153–155], used Ge(Li) detectors for gamma-ray energies above 150 keV. The errors on energies measured in this work are comparable to or better than errors on previously measured energies.

Of the 16 gamma-ray lines that were considered in this work, the measured intensities of six of them agree with the ENSDF average and have significantly improved error (the 273 keV, 277 keV, 300 keV, 341 keV, 357 keV and 379 keV lines). Two measured intensities agree with the ENSDF average, but the error is only slightly improved (the 354 keV and 408 keV lines). One measured intensity agrees with the ENSDF average, but the error is slighly larger. One intensity was the normalization factor so cannot be compared.

Four of the meaured intensities agree with the ENSDF average in two standard deviations: the 243 keV line, which agrees with Refs. [150, 153] but not with Refs. [149, 157, 158]; the 260 keV line, which agrees with Refs. [150, 153, 154], but not Refs. [149, 158]; the 313 keV line, which agrees with only Ref. [150] and not Refs. [153, 154, 158]; and the 330 keV line,

which agrees with all other measured values (Refs. [149, 150, 153, 154, 157]) except for Ref. [158]. The measured intensity for the 327 keV line only agrees with the average within three standard deviations. It agrees with Refs. [153, 154, 158], but not Refs. [149, 150]. Finally, the intensity of the 225.90(4) keV line has a wide range of measured values, from 6.34 to 8.1. The ENSDF average is significantly lower than the value measured here, which only agrees with Ref. [158], making this measured data point questionable. The cause of this may be in-growth from ^{227}Th, which has gamma-ray emissions at both 254.63(3) keV (0.71(14)%) and 256.23(2) (7.0(6)%) and could be overlapping with the ^{231}Pa lines making the measured intensity artificially high [14]. Note that Ref. [155] does not include error on its intensity measurements, which tend to deviate considerably from the average. These values were not included in comparisons here as there can be no error comparison, but these values were included in the ENSDF average.

The ENSDF data uses only two measurements to determine absolute intensities, Ref. [149], which measured an absolute intensity of 0.01649(27) for the 283 keV line, and Ref. [150], which measured an absolute intensity of 0.0169(8) for the same line. In this work, the absolute intensity of every major gamma-ray emission was measured directly (Table 5.1) and the intensity of the 283 keV line was 0.0163(2), which is in agreement with both of the previous measurements.

5.5 Conclusions

Accurately measuring ^{231}Pa activity via gamma-ray spectroscopy is important for non-destructive analysis for radiochronology and nuclear forensics, but existing nuclear data on the decay of ^{231}Pa is often inadequate for making highly accurate measurements. To reduce the error associated with the intensities of these gamma-ray emissions, the energies and absolute intensities of the major gamma-ray emissions associated with the decay of ^{231}Pa to ^{227}Ac have been remeasured. The data is in good agreement with previous measurements with a reduction in error for many of the major gamma-ray lines. For several lines, the errors measured here are an order of magnitude smaller than previous measurements.

Table 5.2: Nuclear data for gamma-ray emissions with relative intensities above 1% arising from the decay of ^{231}Pa to ^{227}Ac. Comparison of the values measured in this work with the ENSDF weighted average and the values measured in previous works (which are included in the ENSDF average [148]). Errors on the measured energies are given as a standard deviation, while error on the measured intensities is counting error; both errors also include systematic uncertainty from the detector calibration. If the publication did not measure a certain value it is indicated "nm" (not measured).

ENSDF Average		**This work**	**Ref.**					
			[153]	**[150]**	**[154]**	**[155]**	**[158]**	**[149]**
E_γ	I_γ	I_γ	I_γ	I_γ	I_γ	I_γ *	I_γ	I_γ
243.08 (9)	2.04(14)	2.25(4)	2.5 (7)	2.18(20)	2.97(24)	5.7	2.51(43)	1.87(4)
255.78 (7)	6.42(6)	7.38(7)	8.1 (16)	6.4(5)	6.34(41)	6.3	7.00(48)	6.41(6)
260.19 (8)	11.01 (13)	11.24(6)	11.3 (24)	10.9(7)	11.39(57)	19	11.03(14)	10.97(13)
273.15 (6)	3.50(5)	3.63(1)	4.4(11)	3.65(22)	3.48(24)	0.27	3.48(18)	3.50(5)
277.22 (7)	4.12(6)	4.12(2)	5.0(11)	4.24(28)	3.88(25)	0.065	4.59(58)	4.12(6)
283.682 (16)	100†	100†	100†	0.0169(8)‡	100 †	100†	100†	0.01649(27)‡
300.066 (10)	146.1(18)	146.5(2)	144(22)	144(10)	149.6(75)	230@	143.2(55)	146.3(18)
302.667 (9)&	149.3(18)	148.5(2)	144(22)	148(10)	140(11)	See above	149(20)	149.6(18)
312.92 (5)	5.98(7)	6.14(2)	6.9(16)	6.0(5)	7.05(56)	4.1	5.93(17)	5.97(7)
327.14(7)	2.18(4)	2.37(2)	2.5(13)	1.88(14)	2.27(28)	nm	2.19(44)	2.22(4)
330.055 (15)	82.3(10)	82.6(1)	81(16)	82.4(48)	81.9(65)	34	82.1(12)	82.4(10)
340.71 (6)	10.72(13)	10.71(3)	10.0(28)	10.5(7)	10.9(13)	3.7	10.62 (16)	10.80(13)
354.48 (5)	5.83(8)	5.83(2)	6.00(42)	6.3(15)	5.07(56)	nm	5.92(16)	5.81(8)
357.11 (8)	10.16(12)	10.23(2)	9.4(22)	10.9(7)	9.67(82)	nm	10.35 (46)	10.14(12)
379.35 (7)	3.01(5)	2.991(8)	2.5(10)	3.12(26)	2.89(23)	0.65	2.96(10)	3.03(5)
407.806 (28)	2.154(30)	2.17(1)	1.3(7)	2.29(2)	2.13(18)	0.34@	2.07(16)	2.156(30)

* No error reported on these values.

† All data normalized by setting the intensity for this gamma-ray line to 100.

‡ Measured absolute intensity.

@ Ref. [155] reports one value for the collective intensities of closely spaced lines (300.5+303.2 keV and 408.1+410.5 keV).

& The gamma-ray emission at 302.7 keV arises from two separate nuclear levels. The measured intensity in previous publications as well as this work does not differentiate between emissions from these different levels in reporting the intensity at this energy. However, ENSDF does differentiate between the emissions from different levels and calculates an intensity for each [148].

Chapter 6

Development of Chemical Procedures for Target Processing

6.1 Introduction

In order to measure a cross section, it is necessary to be able to measure the activity of the reaction product with high precision and accuracy. For the measurement of the ^{230}Th(p,2n)^{229}Pa reaction cross section, target processing is necessary to detect the protactinium activation products over the background of fission products and activation products from the target backing material. The most important considerations for this work are rapid chemical processing and high yields of both protactinium and the thorium target material.

Since the isotope of interest, ^{229}Pa, has only a 1.5 day half-life [14], the target dissolution, chemical separations and initial gamma-ray spectroscopy need to be optimized to take as little time as possible, preferably less than 36 hours (one half-life). There must be high recovery of ^{229}Pa to have sufficient counting statistics for the cross-section measurement, and the target material should be recoverable for further experiments as there is a limited amount available. Column chromatography was chosen for the chemical separations as it is a rapid and highly selective separation technique [54] that is commonly employed for fission product separations as well as protactinium separations [66, 159]. The main parameters that were optimized in the development of the chemical processing system were: the target backing material, conditions for target dissolution, load solution for the columns, chromatographic resin, elution pattern, evaporation conditions and number of column separations.

The target backing material is of particular importance as it adds considerable mass to the chemical system and dictates the conditions needed for full dissolution of the target. Based on the electrodeposition studies (Chapter 4), titanium and platinum were potential backing materials as both were suitable for the fabrication of thick, uniform thorium targets. Titanium has well-characterized chemical behavior and relatively low activation, though it readily forms TiO_2 on contact with air, which is difficult to dissolve and can complicate chemical procedures. Platinum has very high activation but is relatively inert, and therefore

the target could theoretically be dissolved off the backing, which limits the mass added to the system. However, if full dissolution is necessary, the need for aqua regia to dissolve the platinum backing complicates chemical procedures and necessitates lengthy evaporation steps.

As well as dissolving the target material, solutions must be optimized to dissolve protactinium, which requires the presence of HF since protactinium has limited solubility in other mineral acids [66]. Excessive HF, however, will precipitate the highly insoluble thorium tetrafluoride (ThF_4) as well as result in protactinium eluting immediately from columns rather than retaining on the resin. It is common to add aluminum salts to solutions with protactinium before running columns [66] as the addition of aluminum allows protactinium to stay solubilized as a fluoride, while minimizing the free fluorides in solution through the formation of AlF_2^+.

For all irradiation experiments, ^{233}Pa was used as a chemical yield tracer for protactinium. It was an ideal tracer for both the chemical processing development studies and the cross section measurement experiments as it has several strong gamma-ray lines (see Appendix C Table C.1 and Ref. [14]) and can be easily obtained from an isotope generator on a regular basis (Chapter 3). Furthermore, production of ^{233}Pa from nuclear reactions on ^{232}Th and ^{230}Th is negligible at these energies since the ^{232}Th(p,γ) reaction cross section is insignificant ($<$400 μb) [160, 161] and there is no route to ^{233}Pa from proton reactions on ^{230}Th.

The separation of protactinium from thorium and fission products has been discussed in the literature. For this work, only anion or extractant based chromatography resins were considered to ensure a high yield of thorium as it has a tendency to retain irreversibly on cation exchange resins, as discussed in Chapter 2. The *Radiochemistry of Protactinium* (1959) [66] discusses four ways of separating ^{233}Pa from thorium based on different initial thorium matrices. In recent times, there has been renewed interest in this separation as the production of ^{230}U from ^{230}Pa (produced by the irradiation of thorium targets) is medically relevant [162]. Based on these historic and recent studies, Dowex 1x8 anion exchange resin, in both hydrochloric acid and nitric acid mediums, and CL resin (Triskem International) (Fig. 6.1a) were considered for the initial separation step. A secondary separation step with normal DGA resin (Eichrom) (Fig. 6.1b) was also considered based on Ref. [162]. In addition, as the behavior of CL resin with actinides is not well established, further batch study experiments were done to better characterize the resin, these are discussed in detail in Chapter 8.

Development of chemical procedures for the target processing was done in two stages. Initially, experiments were done using natural thorium nitrate with tracer isotopes of ^{227}Th, ^{233}Pa and long-lived fission products. To further optimize the chemical procedures, later experiments were done with proton irradiated natural ThO_2 targets and the procedure tested under the same conditions that would be present for the cross section measurement experiments. The results for each of these stages of chemical procedure development are presented separately in the following sections. There were many research paths in this process that were not successful, these are summarized in the following sections as well with reasons for the experimental failures.

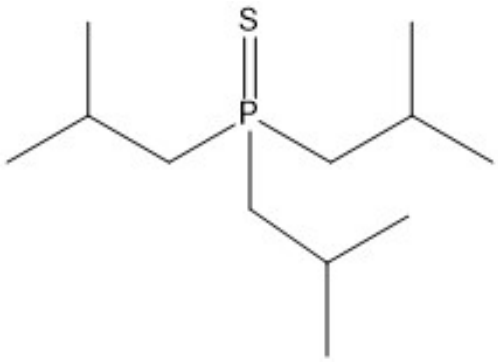

(a) CL resin

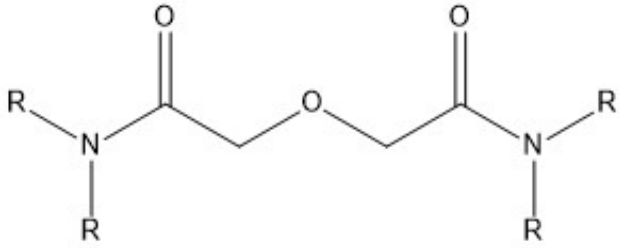

(b) DGA resin

Figure 6.1: Extractant molecules of CL resin (Triskem International), triisobutylphosphine sulfide [162] and normal DGA resin (Eichrom), N,N,N',N'-tetra-n-octyldiglycolamide [163].

6.2 Studies with Tracer Isotopes

Description of Experimental Work

All chemicals were purchased from Sigma-Aldrich and were ACS grade or higher; acids were diluted as necessary with Millipore Milli-Q deionized water (18.2 MΩ cm). Load solutions were prepared with 1 mg of natural thorium (^{232}Th) and tracer isotopes (^{227}Th, ^{233}Pa, ^{103}Ru, ^{140}La, ^{140}Ba, ^{137}Cs, and ^{147}Nd). Actinide tracers (^{227}Th, ^{233}Pa) were obtained from the isotope generators discussed in Chapter 3. As the actinide tracer isotopes are both eluted from their respective isotope generators in HF, a stock solution was prepared with both tracers in conc. HF. Natural thorium nitrate ($Th(NO_3)_4 \cdot 5H_2O$) was available as legacy material from LLNL. It was dissolved in water to make a stock solution of 20 μg Th/μL. The fission product tracers were obtained from the waste stream of another process and were in 6 M HNO_3.

An HPGe detector with Ortec NIM electronics and ASPEC multi-channel analyzer combined with Maestro software (Ortec) was used to analyze the resultant spectra. All samples were counted in the same geometry. For each isotope, the gamma-ray line with the highest intensity was used to determine the activity (Table 6.1).

Table 6.1: Half-lives, photopeaks and intensities of tracer isotopes used in the development of chemical procedures for target processing; data from [14].

Isotope	**Energy (keV)**	**Intensity (%)**
^{227}Th	235.96	12.9
^{233}Pa	311.9	38.5
^{103}Ru	497.09	91
^{140}Ba	537.26	24.4
^{140}La	487.02	45.5
^{137}Cs	661.66	85.1
^{147}Nd	531.02	13.4

For the studies in HNO_3, two stock solutions were prepared. For each, a 50 μL spike of the thorium nitrate stock solution was added to 0.5 mL of fission product tracer solution (containing ∼5 to 30 cps each of ^{103}Ru, ^{140}La, ^{140}Ba, ^{137}Cs, and ^{147}Nd). This was brought down to dryness and reconstituted in 5 mL conc. HNO_3. To this, 20 μL conc. HF with ^{227}Th and ^{233}Pa (∼10 cps each) was added. The solution was diluted to 10 mL with water (2.483 mL) and sat. $Al(NO_3)_3 \cdot 9H_2O$ (2.497 mL) for a final concentration of 8 M HNO_3 - 0.06 M HF - 0.6 M $Al(NO_3)_3$. Each stock solution was counted with an HPGe detector and loaded onto a 5 mL Dowex 1x8 (100-200 mesh) column that had been washed with 20 mL 8 M HNO_3. The columns were eluted in 10 mL fractions: six fractions of 8 M HNO_3, then two fractions of 10 M HCl and, finally, two fractions of 9 M HCl - 0.1 M HF.

For the studies in HCl, two stock solutions were prepared in a similar manner. For the first sample, a 50 μL spike of the thorium nitrate stock solution was added to 0.5 mL of fission product tracer solution (containing ∼5 to 30 cps each of ^{103}Ru, ^{140}La, ^{140}Ba, ^{137}Cs, and ^{147}Nd). This was brought down to dryness three times and reconstituted in 5 mL conc. HCl. To this, 35.7 μL conc. HF with ^{227}Th and ^{233}Pa (∼18 cps each) was added. The solution was diluted to 10 mL with a mixture of 2.719 M $AlCl_3$ (1.471 mL), conc. HCl (3.33 mL) and water (160 μL) for a final concentration of 10 M HCl - 0.1 M HF - 0.4 M $AlCl_3$. To determine if scaling down the volumes and column altered the elution, the second sample was prepared identically, but with the volumes reduced by a factor of five, resulting in a 2 mL load solution.

The 10 mL HCl sample was loaded onto a 5 mL Dowex 1x8 (100-200 mesh) column that had been prepared and washed with 20 mL 10 M HCl. The column was eluted in 10 mL fractions: six fractions of 10 M HCl, followed by two fractions of 6 M HCl fractions and, finally, two fractions of 9 M HCl - 0.1 M HF.

The 2 mL HCl sample was loaded onto a 2 mL Dowex 1x8 (100-200 mesh) column that had been prepared and washed with 8 mL 10 M HCl. The column was eluted in 2 mL fractions: six fractions of 10 M HCl, followed by two fractions of 6 M HCl fractions and, finally, four fractions of 9 M HCl - 0.1 M HF.

The second HCl column was followed by a DGA column. The protactinium fractions from this column, which had trace ^{103}Ru and were in a solution of 9 M HCl - 0.1 M HF, were combined and evaporated to dryness. The sample was reconstituted in 250 μL 10 M HNO_3 and loaded onto a 2 mL pre-packed DGA cartridge, which had been pre-washed with 5 mL 10 M HNO_3. The column was eluted under vacuum in 2 mL fractions. The first 5 fractions were 10 M HNO_3 and the last 5 were 4 M HCl - 0.1 M HF.

Nitric Acid Studies: Results

The elution curve for each HNO_3 column is shown in Fig. 6.2 (a and b). The average yields are given in Table 6.2. Elution curves were fitted with various peak functions as appropriate for the peak shape [164, 165] unless otherwise noted; peak functions and fitting is discussed in-detail in Appendix B. The yields given in this chapter are calculated from the counting data with error propagated from the counting statistics, but the same values, within error, can be determined from the area under the curve for each elution curve fit. Some elution curves, particularly those where the analyte bleeds off in several fractions due to mixed speciation or poor retention on the resin, do not fit a normal chromatographic function and those peaks are plotted with lines to guide the eye only. The fact that some peaks cannot be described well with standard mathematical functions was expected as there is no unified model for fitting chromatographic peaks [164, 165] and the difficulty associated with fitting mathematical functions to real, experimental chromatographic peaks is well known [164].

Table 6.2: Average yields for tracer isotope separation in HNO_3. Errors are propagated from counting statistics and are large because initial activities were low.

Isotope	**Average % Yield**
^{227}Th	83 ± 13
^{233}Pa	124 ± 19
^{103}Ru	101 ± 15
^{140}Ba	111 ± 17
^{140}La	105 ± 16
^{137}Cs	127 ± 47
^{147}Nd	98 ± 19

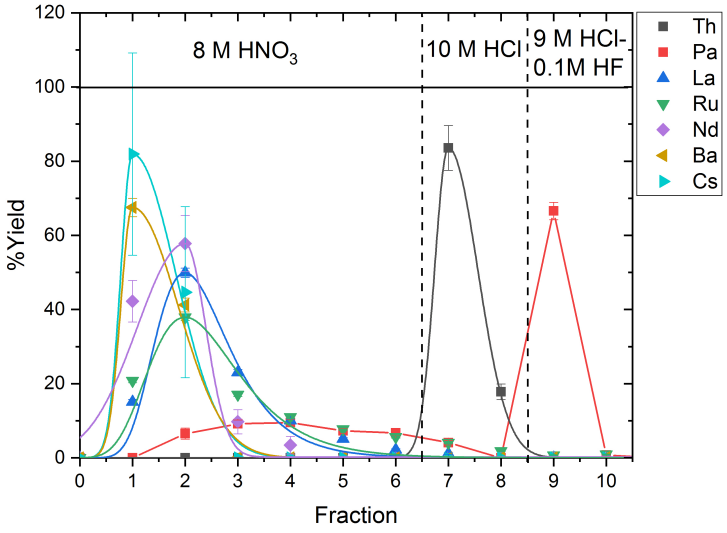

(a)

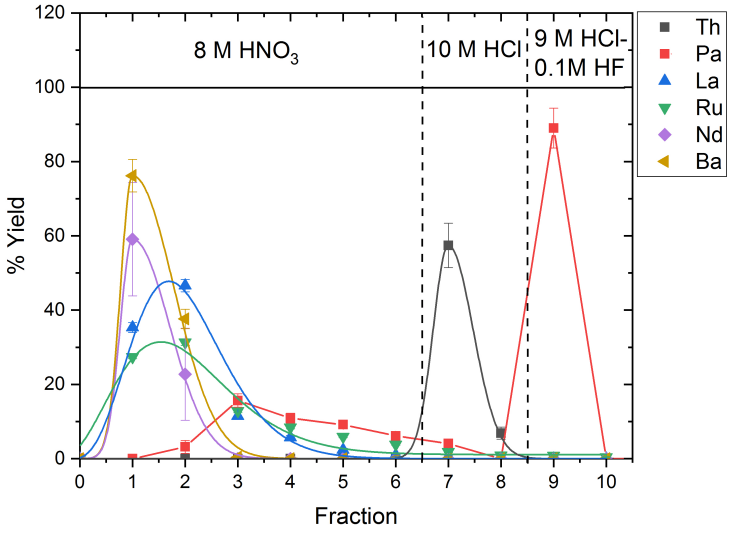

(b)

Figure 6.2: Elution curves for two tracer isotope separations in HNO_3 with Dowex 1x8; 10 mL load volume and fraction volumes. Elution curves fitted with peak functions Origin 2018 (OriginLab) except for protactinium, which does not fit a peak function and the lines simply connect the points to guide the eye.

Hydrochloric Acid Studies: Results

The elution curve for the first HCl column is shown in Fig. 6.3a. The second HCl column, which had a smaller load volume and more fractions is shown in Fig. 6.3b. The average yields are given in Table 6.3. By the time the second HCl separation was performed, some of the fission products had decayed to background, therefore, only thorium, protactinium, lanthanum and ruthenium were followed in the second separation. More fractions were added relative to the first column to ensure the full protactinium band was eluted as some had tailed into the second 9 M HCl - 0.1 M HF fraction in the first separation.

Table 6.3: Average yields for tracer isotope separation in HCl. Errors are propagated from counting statistics and are large because initial activities were low. Isotopes marked with an * were only present on the first column, therefore only the yield from the first column can be shown rather than an average.

Isotope	**Average % Yield**
^{227}Th	97 ± 15
^{233}Pa	112 ± 17
^{103}Ru	35 ± 5
^{140}Ba*	108 ± 17
^{140}La	97 ± 15
^{137}Cs*	99 ± 27
^{147}Nd*	64 ± 18

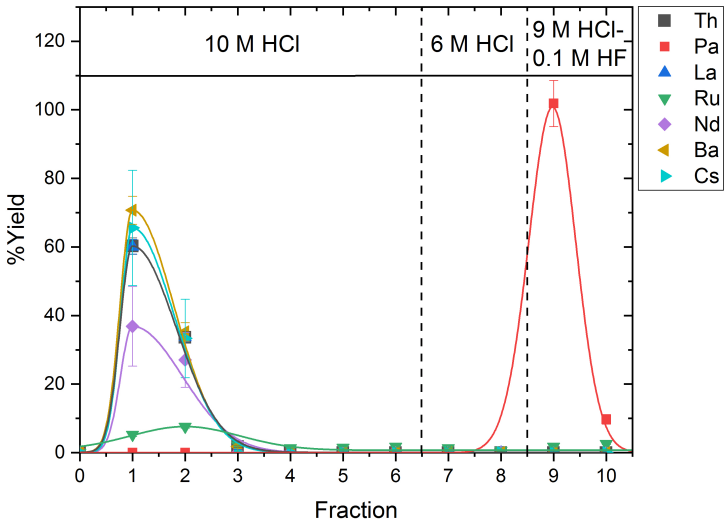

(a) Elution curves for first tracer isotope separation in HCl; 10 mL load volume and fraction volumes.

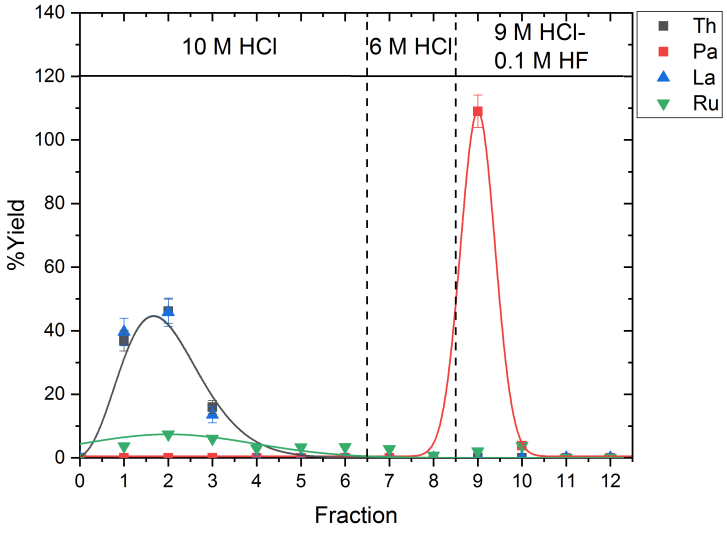

(b) Elution curves for second tracer isotope separation in HCl; 2 mL load volume and fraction volumes. Elution curves for thorium and lanthanum overlap, only the thorium (grey) is shown.

Figure 6.3: Elution curves for two tracer isotope separations in HCl with Dowex 1x8. Elution curves fitted with Origin 2018 (OriginLab).

Fractions 9 and 10 from the second HCl column were further processed with a DGA column after evaporation and reconstitution in 10 M HNO_3 (based on Ref. [162]). Only ^{233}Pa and ^{103}Ru were present in these fractions and the elution curve is shown in Fig. 6.4. The yields were low for both isotopes, 52 ± 2% for ^{233}Pa and 60 ± 3% for ^{103}Ru.

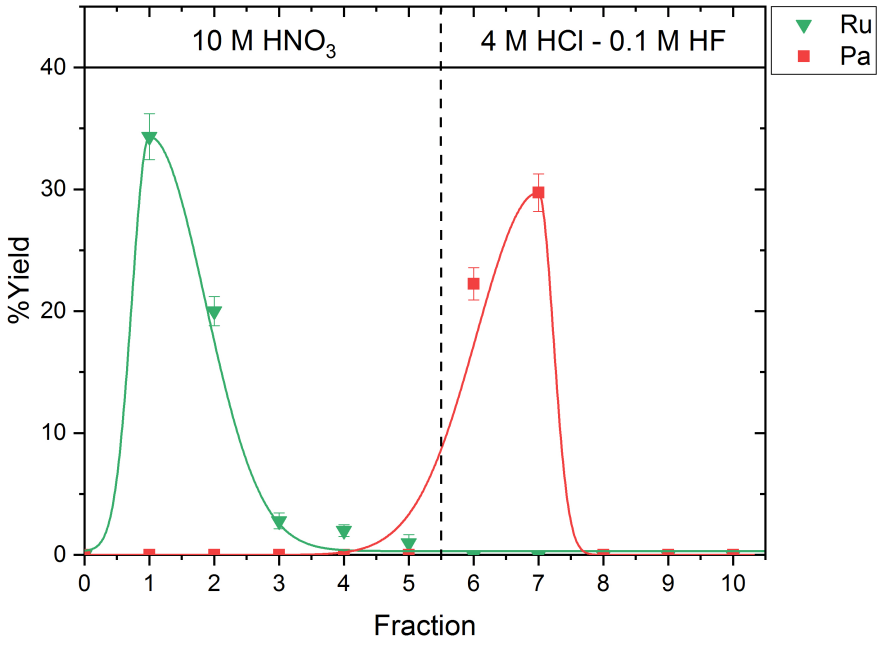

Figure 6.4: Elution curves for tracer isotope separation in HNO_3 with DGA resin; 250 μL load volume and 2 mL fraction volumes. Elution curves fitted with Origin 2018 (OriginLab).

Discussion

The separation in HNO_3 was highly reproducible, but it had a lower than desired yield for thorium, with the remainder retained on the resin, and, while the overall yield of protactinium was high, the yield in the clean protactinium fractions was low. In this separation, the fission products were largely removed by washing with 8 M HNO_3 as they are cationic or neutral in 8 M HNO_3. Ruthenium, which was likely present as several different coordination complexes, was the only exception and bled off the column in all acid concentrations. Thorium was removed with 10 M HCl as this converts the anionic $Th(NO_3)_6^{2-}$, which is strongly retained on the column, to the neutral $ThCl_4$, which elutes. The majority of the protactinium was removed when HF was added, however, about 30% bled off the column in the 8 M HNO_3 fractions, resulting in the low yield for the cleaned protactinium fractions.

While it may be possible to resolve some of these issues by adjusting the solution chemistry and elution pattern, the preliminary studies in HCl (see below) had much better results, so further iterations of this separation were not done.

The elution curves for the two HCl columns (Figs. 6.3a and 6.3b) are very similar, despite the change in the load volume and fraction volume. The yields for thorium and protactinium were high and the radiopurity of the protactinium fractions was also high with only trace ruthenium present. On this column, the fission products and thorium were removed by washing with 10 M HCl as they are neutral or cationic at this concentration. Again, the only exception was ruthenium, which bled off the column in all acid concentrations. This can be explained by the speciation of ruthenium in HCl. At concentrations of 9 to 10 M HCl, ruthenium is mainly complexed as $RuCl_6^{-3}$, which is strongly retained by the resin, but about 30% is present as $[RuCl_5(H_2O)]^{2-}$, which has less affinity for the resin [166]. The complexation chemistry in 6 M HCl is similar, $[RuCl_5(H_2O)]^{2-}$ is the dominate form but ∼20% of the ruthenium is complexed as $RuCl_6^{-3}$ and another ∼20% as $[RuCl_4(H_2O)_2]^{-}$ [166]. Therefore, at all concentrations some ruthenium bled off the column, but the majority was retained, resulting in a low yield.

With only these tracer isotopes, the elution of 6 M HCl has little effect, however, the irradiated targets will have zirconium present, which should be largely stripped in this concentration [66] and it was desirable to simulate the processing for the irradiated targets as closely as possible even in these initial chemical studies. Since thorium remained with the bulk fission products, another separation would be necessary to recover the target material, however, since the half-life is long, this is not a significant issue.

On the DGA column, ruthenium bled off in the early fractions, similar to the previous columns, and protactinium was eluted in in the first two fractions with HF present. For both isotopes, the yield was low because a significant amount stayed in the tube containing the load solution. This is common for solutions of protactinium without sufficient fluorides in which protactinium has a tendency to be "sticky" (hydrolyze) [66]. The addition of more fluorides along with aluminum, as discussed previously, is likely necessary to ensure the stability of protactinium in the solution and allow for the full transfer of protactinium from the load solution tube to the column.

From these preliminary trials, it was determined that the HCl separation was preferred as an initial separation for the target processing due to the high yield and radiopurity of the separated protactinium. The DGA column may be useful secondary separation step as it potentially could separate protactinium from zirconium and niobium along with ruthenium [162, 167]. However, for this column to be effective, it needs to be rapid with high yield and high decontamination factors, which was not demonstrated with the tracer studies.

While these studies were useful for initial characterization of the chemistry, they included only a limited subset of fission products, and the effect of the target backing material and target dissolution were not considered. Therefore, further optimization was needed to better characterize the separation chemistry. To fully simulate the experimental conditions present in the cross section measurement experiments, further studies used irradiated natural ThO_2 targets with platinum and titanium backings.

6.3 Thorium Oxide Targets on Platinum

The chemical processing was not successful for irradiated ThO_2 targets on platinum backings and no results were obtained. The experimental conditions and the reasons for the failure of these experiments are discussed below.

Summary

Four ThO_2 targets, all with thicknesses of about 500 μg ThO_2/cm^2, were made on 25 μm platinum foils following the method given in Chapter 4: each target was made with three to four layers of 100 to 200 μg ThO_2/cm^2 and was ignited with a natural gas Bunsen burner between layers to create a high fired ThO_2 deposit.

These targets were irradiated at CAMS with 16 MeV protons for 5 hours with a beam current of about 150 nA on 13 December 2019. The foil stack (Fig. 4.8) contained a 5 μm tantalum foil, followed by the four ThO_2 targets and two 100 μm gold foils, which were for another experiment. The beam was terminated at 4:00 pm and the targets were brought to the laboratory at 5:30 pm. The targets were extremely radioactive; at 1.5 hours post-irradiation, the targets had a dose rate of 140 mR/h at 2 cm and 170 mR/hr on contact. The activity was largely from platinum activation products, including gold isotopes, such as ^{194,196,198}Au, from proton induced reactions as well as radioisotopes of platinum, iridium and osmium, such as ^{195m}Pt, ^{194}Ir and ^{183}Os, from neutron reactions on platinum, which occured due to the substantial neutron flux in the beam stack as a result of (p,xn) and fission reactions.

High fired thorium oxide is difficult to dissolve [168] and it had been determined previously that the high fired ThO_2 targets fabricated in this work could not be readily dissolved by either HCl - HF or HNO_3 - HF mixtures at room temperature within a reasonable time frame (<12 hours). To ensure a rapid dissolution without boiling, which would off-gas considerable amounts of fission products, solutions of 1 mL aqua regia with 0.1 M HF were required.

In these solutions, the thorium deposit was dissolved off the platinum backing after 2 hours, but a considerable amount of the platinum was also dissolved. Furthermore, this dissolution procedure necessitated an evaporation step prior to column separations as nitrates were present, which is undesirable for the column chemistry. As the column separation is based on a HCl - HF load solution, the presence of nitrates in the load solution could change the elution behavior of some of the elements. Therefore, the solution was brought down to dryness three times prior to loading on the column, but the evaporation was slow due to the large amounts of mass from both thorium and platinum. Furthermore, a significant amount of yellow crystals, likely platinum salts, formed during the evaporation and were difficult to re-dissolve. After the final evaporation, the target solution was reconstituted in 1 mL conc. HCl - 0.2 M HF and immediately diluted to 2 mL with the addition of $AlCl_3$, conc. HCl and water, for a final solution that was 10 M HCl - 0.1 M HF - 0.4 M $AlCl_3$.

Each target solution was loaded onto a 2 mL Dowex 1x8 (100-200 mesh) column, which was pre-washed with 8 mL 10 M HCl. Fractions were collected in 2 mL increments: six

fractions of 10 M HCl, followed by two fractions of 6 M HCl and, finally, four fractions of 9 M HCl - 0.1 M HF. All fractions were counted immediately after elution on an HPGe detector in an identical configuration. It was not possible to determine the activity of the fission products or protactinium activation products in the target or the load solutions before the separation as the background from platinum activation products was too high.

The separation failed for all the targets; all of the activity eluted immediately, contrary to what was expected based on the previous separation studies with tracer isotopes. There are two main reasons why this may have occurred: the capacity of the column was exceeded due to the platinum mass or the high-fired thorium oxide was not fully dissolved, but suspended in solution and entrained the activation products. In 10 M HCl, platinum has a log distribution coefficient of 2, therefore, ∼90% of the platinum would be expected to be retained on the resin [169]. The total mass of the foil was ∼34 mg, so this is a considerable mass loading for the resin if all, or most, of the target backing dissolved.

After the unsuccessful initial separation, all fractions for each target were recombined, evaporated to dryness three times and brought up in 10 M HCl - 0.2 M HF. The samples were combined into two load solutions and each was loaded onto a 2 mL Dowex 1x8 (100-200 mesh) column and eluted as described above.

The results of the second separation aligned with the previous tracer experiments and the protactinium fractions had no detectable containments. However, these two separations were performed at five and six days post-irradiation when the activity had significantly decreased and the solution chemistry was very different than what had been original obtained from the dissolved targets, so the results were inconclusive. The second separation presumably was successful either because the first column removed the bulk of the platinum mass (and therefore the mass loading was much lower the second time) or the high-fired thorium oxide dissolved fully over the few days since the irradiation.

Overall, there were numerous issues with this procedure. The procedure for a rapid dissolution required a solution that would dissolve both the target and the platinum backing, adding considerable mass to the solution. The use of nitrates necessitated an evaporation before loading the column, which was time consuming due to the mass in the solution. To account for the platinum mass, a larger column would likely be necessary, but this is undesirable because a larger column would require more time and volume to elute as well as more time to evaporate before further processing or in preparation for counting.

Dissolution in a milder solution that would not dissolve the platinum, such as the HCl - HF load solution, would be too time consuming or would require boiling, which is undesirable for a fission product solution. Furthermore, it would be difficult to determine the yield of the dissolution if the target was dissolved off of the platinum backing as the platinum activation products were too high activity and too long-lived relative to the protactinium activation products to allow for counting of the backing material after dissolution to determine if any protactinium remained on the backing material. This assessment of the yield would not be aided by the addition of a tracer during the dissolution because the tracer and the determinand would not be seeing the same chemical environment at all stages in the chemical process as the tracer would be fully solubilized initially while the determinand would be

entrained in a highly insoluble oxide that may not fully dissolve.

Several modifications to the procedure need to be made to mitigate these issues for future irradiations. To ensure rapid dissolution and short sample preparation time, the thorium oxide target should be low fired, rather than high fired, and the backing material should readily dissolve in HCl - HF mixtures and not interfere with the separation, ideally having no affinity for the resin in 10 M HCl. Protactinium is stable in solutions of 0.1 M HF [66, 98], therefore, the fluoride concentration in the dissolution solution can be reduced by a factor of two, which allows the aluminum concentration to be reduced as well, decreasing the mass dissolved in the solutions. Finally, while the total activation of the targets was extremely high, it was largely due to platinum activation products. The areal density of thorium was low and there was not sufficient production of either fission or activation products, indicating that thicker targets ($\sim$1 mg Th/cm^2) are needed for future studies.

The use of a thin titanium backing with a low fired (180 °C) thorium oxide deposit was determined to be the optimal method to solve these chemistry issues. Titanium(IV) has a negligible affinity for anion exchange resins in 10 M HCl [169] and dissolves readily in conc. HCl solutions with HF [159] as does low fired ThO_2. This would allow for a rapid dissolution with no required evaporation before loading the column, significantly speeding up the separation procedure while ensuring that the column remains small, as the backing material would elute immediately rather than retain on the resin. As the fabrication of thick ThO_2 targets on thin titanium is readily achievable (see Chapter 4), further irradiation studies were done with titanium backed targets.

6.4 Thorium Oxide Targets on Titanium: Irradiation One

Description of Experimental Work

As with the previous experiments, all chemicals were purchased from Sigma-Aldrich and were ACS grade or higher; acids were diluted as necessary with Millipore Milli-Q deionized water (18.2 MΩ cm). Actinide tracers (^{227}Th, ^{233}Pa) were obtained from the isotope generators discussed in Chapter 3.

Relative activity measurements were done with an HPGe detector with Ortec NIM electronics and ASPEC multi-channel analyzer; Maestro software (Ortec) was used to analyze the resultant spectra. All samples were counted in the same geometry. Quantitative gamma-ray spectroscopy was done at the NCF with HPGe detectors; the code GAMANAL [151] was used to analyze the resultant spectra.

Irradiation: 3 February 2020

Four ThO_2 targets, with thicknesses ranging from about 500 μg/cm^2 to 1000 μg/cm^2, were made on 10 μm titanium foils as described in Chapter 4. The targets were irradiated at

CAMS with 16 MeV protons for 5 hours with an average beam current of about 130 nA on 3 February 2020. The foil stack (Fig. 4.8) contained a 5 μm tantalum foil, followed by two ThO_2 targets, a 5 μm yttrium foil, two ThO_2 targets and two 100 μm gold foils. The yttrium foil served as a flux monitor, the gold foils were associated with different experiment. The beam current was terminated at 4:00 pm, the targets were removed from the target chamber and arrived at a laboratory by 5 pm. The first three thorium targets were placed in separate 5 mL plastic tubes. To each target, 950 μL conc. HCl, 50 μL of a ^{227}Th tracer ($\sim$5 cps) in conc. HCl, and 10 μL of a ^{233}Pa tracer ($\sim$10 cps) in conc. HF were added to dissolve the target and backing material.

Within 30 minutes of adding the acids, the targets turned black and begin to fragment, after 70 minutes, there was no visible solid remaining. The targets were left to dissolve overnight (14 hours). The fourth thorium target was not dissolved and instead was counted with gamma-ray spectroscopy at the NCF at 2.8, 3.7, 4 and 12.5 hours post-irradiation; the yttrium flux monitor was counted at 3.2 hours post-irradiation.

Chemical Processing: 4 February 2020

The next morning (4 February 2020), one target solution was diluted to 2 mL with 148 μL $AlCl_3$ (2.741 M), 666 μL conc. HCl and 176 μL water, giving a final concentration of 10 M HCl - 0.14 M HF - 0.2 M $AlCl_3$. The final solution was pale purple. A 2 mL Dowex 1x8 (100-200 mesh) column was prepared and washed with 8 mL 10 M HCl, and the target solution loaded with two 500 μL rinses of the empty tube. The time from dilution to loading the column, which is the reaction time for the aluminum, was 45 minutes. Fractions were collected in 2 mL increments: six fractions of 10 M HCl, two fractions of 6 M HCl and finally four fractions of 9 M HCl - 0.1 M HF. All fractions were counted immediately after elution on an HPGe detector in an identical configuration.

Fraction 10 contained the majority of the protactinium activity, and was sent to the NCF for absolute gamma-ray spectroscopy and spectrum analysis along with fractions 3, 5, 7 and 12. Fraction 9, which contained about 40% of the protactinium activity, was evaporated to dryness at 95°C and brought up in 250 μL 10 M HNO_3 in preparation for another separation with DGA resin. However, the DGA column ultimately was not performed as the fission product activities were too low for a conclusive result.

Chemical Processing: 5 February 2020

The Dowex 1x8 separation was repeated with the second target solution. A 2 mL Dowex 1x8 column was prepared, and the target solution was diluted and loaded onto the column as described previously. The time from the dilution to the column loading was 60 minutes. Fractions were collected in 2 mL increments: six fractions of 10 M HCl, four fractions of 6 M HCl and finally four fractions of 9 M HCl - 0.1 M HF. All fractions were counted immediately after elution on the same HPGe detector in an identical configuration. The majority of the

protactinium activity (∼85%) was in fraction 12, the second fraction of 9 M HCl - 0.1 M HF, as before.

Chemical Processing: 6 February 2020

The third target solution was diluted in the same manner as the others. This was loaded with two 500 μL rinses onto a pre-packed, 2 mL Triskem CL resin cartridge which had been washed with 10 mL 10 M HCl (further details of CL resin given in Chapter 8). The column was run under vacuum at a rate of 0.8 mL/min. Four fractions were eluted based on the procedure in Ref. [162]. The first fraction was 5 mL 10 M HCl, the second was 20 mL 10 M HCl and the final two were 5 mL 4 M HCl - 0.1 M HF.

Additional Tracer Studies

As mentioned previously, a sample was prepared for separation with DGA resin on 4 February 2020 but by the next day, the activity was too low to obtain a conclusive result and the column was not performed. Therefore, tracer studies were done with ^{233}Pa, ^{89}Zr and ^{48}V to better characterize this separation. As before, ^{233}Pa was obtained from an isotope generator; ^{89}Zr was separated from the yttrium flux monitor foil used in this irradiation and ^{48}V was obtained from the first fraction of the 4 February 2020 column. A stock solution with these three tracer isotopes was prepared in conc. HCl - 0.1 M HF and then divided into three samples to serve as load solutions for three column separations. Each sample was evaporated to dryness three times at 95 °C and 50 μL conc. HNO_3 added between evaporations. On the final evaporation, the load solutions for the first two columns were reconstituted in 250 μL 10 M HNO_3 with a drop of sat. $Al(NO_3)_3$ and the final sample, for the third column, reconstituted in 250 μL 10 M HNO_3 with 50 μL sat. $Al(NO_3)_3$. For each column, a pre-packed, 2 mL Eichrom DGA cartridge was prepared by washing with 10 mL 10 M HNO_3. The load solution was added, followed by a rinse of 750 μL 10 M HNO_3. Fractions were collected in 5 mL increments (see Figs. 6.7-6.9 for elution pattern for each column).

Results and Discussion

Separation with Dowex 1x8

The thorium targets were highly radioactive after the irradiation from thorium activation and fission products as well as titanium activation products. Titanium has several stable isotopes and produces numerous activation products, mainly isotopes of scandium and vanadium. In particular, there was significant production of ^{48}V, ^{44m,g}Sc, ^{46}Sc and ^{47}Sc (see Table 6.4 for gamma-ray emission and reaction pathways). Most of the other activation products do not have strong gamma-ray emissions other than the 511 keV annihilation peak associated with β^+ decay. The count rate in the 511 keV channel for the fourth target was $1.32 \pm 0.012 \times 10^6$ photons/s at 2.8 hours post irritation. As fission products are neutron-rich and mainly

decay by β^- decay, this activity is mainly from the titanium activation products. The total number of fissions was estimated to be about 10^{8-9}.

Table 6.4: Titanium activation products with significant gamma-ray lines; nuclear data from [14].

Isotope	Reaction(s)	Half-Life	Gamma-ray Lines and Intensity
^{48}V	^{47}Ti(p,γ); ^{48}Ti(p,n); ^{49}Ti(p,2n)	15.97 d	983.5 keV (99.98%); 1312.1 keV (98.2%)
^{44}Sc	^{47}Ti(p,α)	3.97 h	1157.0 keV (99.9%)
^{44m}Sc	^{47}Ti(p,α)	58.61 h	271.2 keV (86.7%)
^{46}Sc	^{47}Ti(p,2p); ^{49}Ti(p,α)	83.79 d	889.3 keV (99.98%); 1120.5 keV (99.98%)
^{47}Sc	^{50}Ti(p,α)	3.3492 d	159.4 keV (68.3%)

The elution curve for the first target separation (on 4 February 2020) with Dowex 1x8 is shown in Fig. 6.5. The data is from the relative gamma-ray spectroscopy measurements and samples with particularly high activities were not able to be counted. Therefore, fractions 1 and 2, which contained the bulk of the fission products, titanium activation products and thorium, are not shown as these fractions had a dead time of over 80% on the HPGe detector and the data was poor. In addition, only relative yields are shown as the load solution had a dead time of over 90% so an initial count was not possible. For fission products with multiple high yield isotopes (e.g. ^{133,135}Xe, ^{46,47}Sc), only the data for the highest activity isotope is plotted, but the data for all isotopes was compared to ensure the elution curve was consistent between isotopes of the same element. Parent-daughter isotope pairs are plotted together for isotopes where the decay is rapid and the parent isotope has few gamma-ray lines (^{99}Mo and ^{112}Pd).

In this separation, protactinium eluted in the first two fractions of 9 M HCl - 0.1 M HF with about 40% of the activity in the first fraction and the remainder in the second fraction. The total protactinium yield was ∼90% for each separation, as determined from the ^{233}Pa tracer. The contaminants in the protactinium fractions were ^{97}Zr, ^{97}Nb, ^{135}Xe, ^{115}Cd/^{115}In, ^{47}Sc, ^{48}V and ^{112}Pd/^{112}Ag. Figure 6.6 shows the elution curve for this separation for only protactinium and these contaminants.

The presence of ^{97}Zr and ^{97}Nb was expected as zirconium and niobium are difficult to separate from protactinium [66, 162]. Both isotopes began to elute in fraction 7, the first fraction of 6 M HCl, and peak in fraction 9, the first fraction of 9 M HCl - 0.1 M HF. Based on

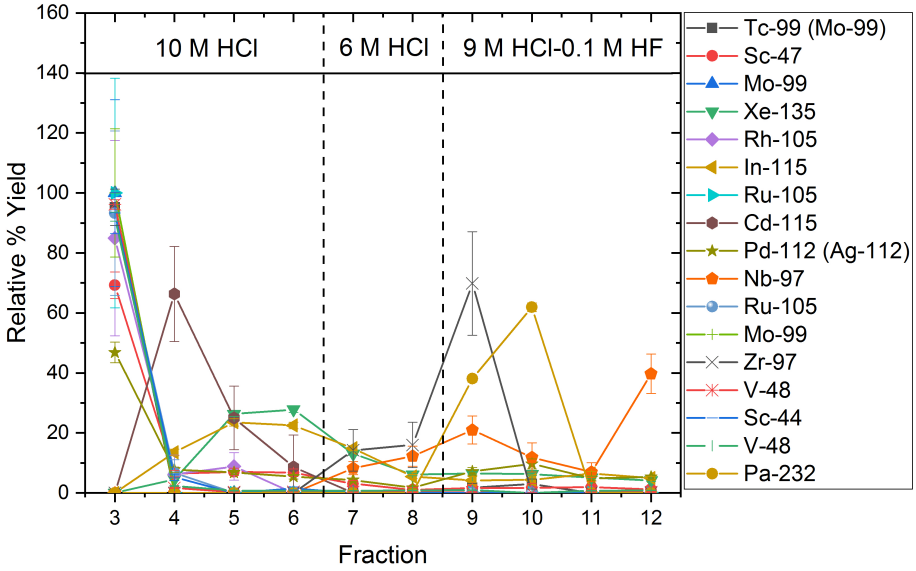

Figure 6.5: Elution curve for fractions 3 to 12 of first target separation from 3 February 2020 CAMS irradiation. As the elution curve is incomplete, with fractions 1 and 2 not shown, no fitting was done and lines are to guide the eye only.

this behavior, the addition of more fractions of 6 M HCl should increase the radiopurity of the protactinium as more of the ^{97}Zr and ^{97}Nb should elute before the elution of protactinium.

The presence of xenon, cadmium/indium and palladium/silver was unexpected as these elements do not share many chemical similarities with protactinium. Their presence was due to their tendency to bleed off the column over several fractions, which can be explained by their log distribution coefficients. On this column, ^{135}Xe and ^{115}Cd/^{115}In eluted in broad bands, beginning around fraction 4, that tailed into the protactinium fractions. Cadmium and indium have log distribution coefficients in 10 M HCl of about 1 and 0.5, respectively, and higher log distribution coefficients in 6 M HCl, about 2.5 and 1, respectively [169]. Therefore, these isotopes began to bleed off in the 10 M HCl fractions in broad peaks followed by a decrease in elution for the 6 M HCl fractions, and a slight increase in the final 9 M HCl fractions. While the behavior of xenon on anion exchange resins is not well characterized, its iodine parent has a log distribution coefficient of about 1 in 6 M HCl and less than 0.5 in 10 M HCl [169], which is similar to the trend in log distribution coefficients for cadmium and indium leading to similar behavior in this separation system.

The elution of ^{112}Pd/^{112}Ag peaked in the early fractions but there was tailing throughout all fractions, though with a decrease in the 6 M HCl fractions. This is expected since palladium has a log distribution coefficient of 2 in 6 M HCl and about 1 in 10 M HCl, so it elutes in broad bands in fractions with a high HCl concentration (10 M and 9 M) and

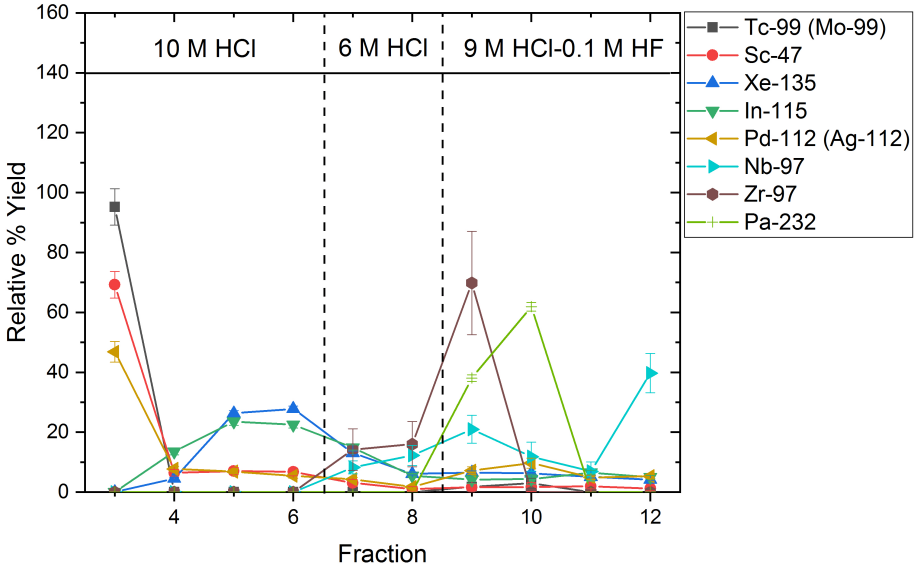

Figure 6.6: Elution curve from the first target separation showing the elution of protactinium and a subset of the fission products. As before, the elution curve is incomplete (showing only fractions 3 to 12), therefore, no fitting was done, and lines are to guide the eye only.

less so in the 6 M HCl fractions [169]. Silver follows a similar patter though with lower log distribution coefficients, less than 0.5 in 6 M HCl and negligible in 10 M HCl [169].

While adding more fractions of 10 M HCl may remove slightly more of the ^{135}Xe, ^{115}Cd/^{115}In and ^{112}Pd/^{112}Ag, these elements are highly volatile and can be quantitatively removed from the protactinium fractions by evaporation. Furthermore, they are present in low quantities and do not interfere with protactinium gamma-ray spectroscopy. Therefore, changing the column elution is unnecessary.

Titanium(IV) and its main activation products, ^{44,47}Sc(III) and ^{48}V(IV), have a slight affinity for the resin at all HCl concentrations [169]. The oxidation state of vanadium is indicated by its behavior, V(V) has a strong affinity for the resin in 10 M HCl, which is clearly not the case in this separation as vanadium elutes mainly in the first few fractions of 10 M HCl. However, since ^{48}V and ^{47}Sc are produced in such large amounts relative to the other activation products, even a few percent bleeding off the column in the later fractions is easily detectable, which is seen here. Eluting more fractions of any concentration may help to reduce the tailing into the protactinium fractions.

To improve this separation, the Dowex 1x8 column elution was modified and tested with another target the following day, 5 February 2020. Two more fractions of 6 M HCl were eluted to attempt to remove more ^{97}Zr and ^{97}Nb before the elution of protactinium and achieve better band separation between these elements. However, by the time this column

separation was performed, it was 40 hours post-irradiation and, by the time of counting it was 46 hours post-irradiation. Therefore, many fission products were considerably lower in activity, particularly ^{97}Zr ($t_{1/2}$ = 16.749 h), which decayed to undetectable levels along with its short-lived daughter, ^{97}Nb ($t_{1/2}$ = 72.1 min) [14].

Therefore, it could not be determined if the extra 6 M HCl fractions were sufficient to improve the separation. Of the other contaminants, the elution of ^{115}In and ^{112}Pd /^{112}Ag was unaffected by the addition of two 6 M HCl fractions, while the relative percentages of ^{135}Xe, ^{47}Sc and ^{48}V in the protactinium fractions were reduced. Decay may be playing a role in this for ^{135}Xe ($t_{1/2}$ = 9.14 h) as a couple of half-lives have passed for it and its parent, ^{135}I ($t_{1/2}$ = 6.58 h), since the previous separation, so these isotopes may simply be undetectable in the later fractions where the relative yield is lower [14]. As the data for this column was poor due to low activities and there was no significant change from the previous column (Figs. 6.5 and 6.6), the elution curve is not shown graphically.

Based on the results of these columns, the separation is effective, but it may be possible to improve it by adding more 6 M HCl fractions. These studies also showed the need for rapid chemistry to fully characterize the behavior of the short-lived fission products. The time to process the sample needs to be weighed against the radiopurity as ^{229}Pa is short-lived and must be detectable despite the activity of ^{233,232,230,228}Pa, which cannot be removed by separations. Therefore, a sample with more ^{229}Pa activity but some trace contaminants would be preferred to a highly clean sample that has less ^{229}Pa activity, provided the containments do not interfere with protactinium gamma-ray spectroscopy. Future experiments need to be timed to ensure the full chemical process is rapid enough for the detection of ^{229}Pa, and the chemistry needs to be performed immediately after the irradiations to ensure shorter-lived radionuclides can be detected reliably.

DGA resin and CL resin

The DGA column was not performed with a sample from the irradiation due to the decay of ^{97}Zr and ^{97}Nb. The evaporation process to prepare the load solution removed all detectable activity of the volatile fission products (^{135}Xe, ^{115}Cd/^{115}In and ^{112}Pd/^{112}Ag), and the activity of ^{97}Zr, ^{97}Nb and ^{47}Sc had decayed to background as it was 48 hours post-irradiation by the time the column was performed. Therefore, it was not possible to get a conclusive result from the irradiation sample, and instead additional studies were done with tracer isotopes.

The DGA separation was repeated three times with tracer isotopes (^{233}Pa, ^{89}Zr and ^{48}V). Each column had different elution conditions, which are show along with the results in Figs. 6.7-6.9. In the first elution (Fig. 6.7), vanadium eluted mainly in 10 M HNO_3, though some tailed into later fractions. Protactinium bled off in 0.1 M HNO_3 but the majority eluted in 4 M HCl - 0.1 M HF and zirconium eluted in 4 M HCl - 0.1 M HF. This was unexpected based on Ref. [170], which indicated that zirconium should elute in 0.1 M HNO_3.

For the second column (Fig. 6.8), the elution was changed to attempt to separate protactinium and zirconium by eluting protactinium first with a high concentration of HNO_3 with trace HF, a condition where zirconium should be retained on the column [167, 170],

and then elute zirconium as before. While this separation has better band separation than the previous elution, there was tailing of all three elements, and neither the vanadium nor protactinium fractions were clean with both having some amount of all three elements.

Finally, for the third separation attempt (Fig. 6.9), more fractions were added and the aluminum concentration was increased to attempt to regulate the protactinium and zirconium bleeding off in the early fractions. This was still not successful and all three elements bled into most fractions.

Based on these results, which were inconsistent and unsuccessful, as well as the time necessary to prepare the samples, it was decided that a second separation was unnecessary as the increase in protactinium radiopurity is offset by the time to prepare the sample and run the column as the containments largely decay out during this time. Furthermore, the NCF gamma-ray spectroscopy data for the protactinium fractions from the Dowex 1x8 column showed the impurities did not interfere with accurately measuring the protactinium activation products.

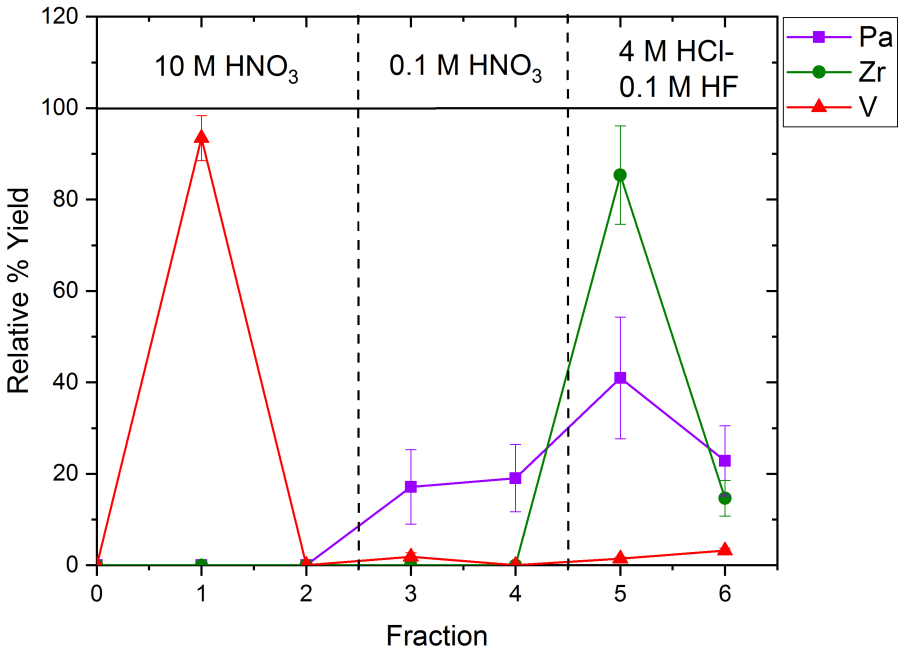

Figure 6.7: Elution curve of the first separation of protactinium, zirconium and vanadium on DGA resin. Lines are to guide the eye only; 250 μL load solution volume and 5 mL fraction volume.

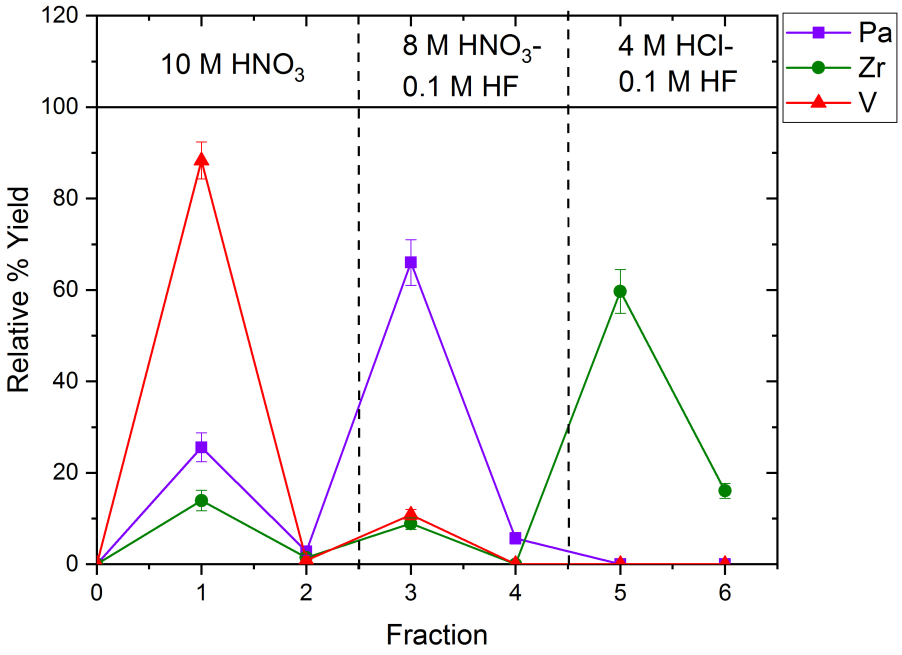

Figure 6.8: Elution curve of the second separation of protactinium, zirconium and vanadium on DGA resin. Lines are to guide the eye only; 250 μL load solution volume and 5 mL fraction volume.

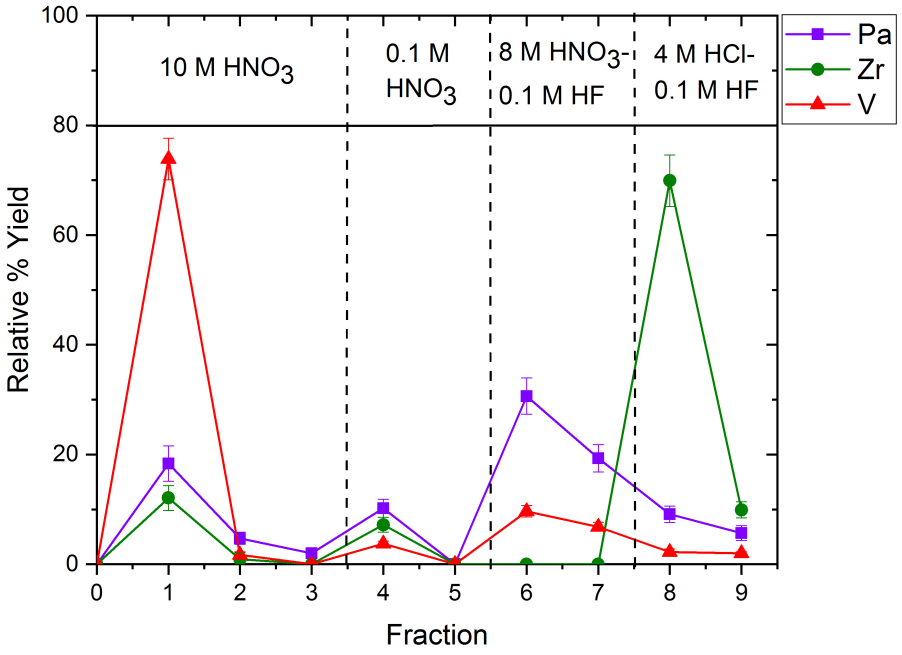

Figure 6.9: Elution curve of the third separation of protactinium, zirconium and vanadium on DGA resin. Lines are to guide the eye only; 250 μL load solution volume and 5 mL fraction volume.

A separation was also tested with CL resin, which was considered because it had been used in a similar separation in the literature [162], however, it was not as effective as the Dowex 1x8 separation. While the elution curve was very similar to that for the Dowex 1x8 resin and the containments in the protactinium fraction were similar, the contaminants were present in significantly higher quantities. Optimization of this separation would have been difficult as the behavior of very few elements is well characterized on this resin. Due to this lack of data, further studies were done with CL resin to determine its applicability for other actinide separations, see Chapter 8, but it was not pursued as a separation method for the target processing chemistry.

6.5 Thorium Oxide Targets on Titanium: Irradiation Two

Description of Experimental Work

Irradiation

Four ThO_2 targets, with thicknesses ranging from about 800 $\mu g/cm^2$ to 1100 $\mu g/cm^2$, were made on 10 μm titanium foils as described in Chapter 4. The targets were irradiated at CAMS with 16 MeV protons for 5 hours with an average beam current of 177 $\pm$ 27 nA on 3 August 2020. The foil stack (Fig. 4.8) contained a 5 μm tantalum foil, followed by: two ThO_2 targets, a 5 μm yttrium foil, two ThO_2 targets and two 100 μm gold foils. The yttrium foil served as a flux monitor, the gold foils were associated with different experiment. The beam current was terminated at 4:08 pm and the targets were removed from the target chamber and arrived at a laboratory by 4:40 pm. The yttrium foil was prepared for counting and arrived at the NCF at 5:16 pm. All four thorium targets were placed in separate 5 mL plastic tubes. To each target, 1000 μL conc. HCl and 10 μL of a ^{233}Pa tracer ($\sim$10 cps) in conc. HF was added to dissolve the target and backing material. A standard solution containing only the ^{233}Pa tracer was made in the same manner.

Chemical Processing

The targets were left to dissolve for 1.5 hours. After this time, the solutions were diluted with 148 μL $AlCl_3$ (2.741 M), 666 μL conc. HCl and 176 μL water, giving a final concentration of 10 M HCl - 0.14 M HF - 0.2 M $AlCl_3$. The dilution was done at 7:00 pm for the first two targets and 7:10 pm for the second two targets along with the ^{233}Pa standard.

Four 2 mL Dowex 1x8 (100-200 mesh) columns were prepared and washed with 8 mL 10 M HCl. After the wash, the first two target solutions were loaded onto separate columns at 8:12 pm with two 500 μL rinses each of the empty tube. As with the dilution, the loading of other two target samples was staggered by 10 minutes to simplify the processing. These samples were loaded onto columns at 8:24 pm in the same manner.

All fractions were collected in 2 mL increments: six fractions of 10 M HCl, seven fractions of 6 M HCl and finally four fractions of 9 M HCl - 0.1 M HF. The first two columns were completed around 11:50 pm and the second two around 12:20 am. All fractions and the standard were counted on an HPGe detector in an identical configuration. After the relative counting, all fractions from the separation of the first target solution were brought to the NCF at 5:30 am for quantitative gamma-ray spectroscopy, which began around 6:00 am.

Results and Discussion

The elution curve for this separation is shown in Fig. 6.10. The elution curve is similar to that from the previous irradiation, but with improved band separation between protactinium, zirconium and niobium. Only the relative yields are given as the fission products and protactinium activation products could not be detected over the titanium activation products in the load solution. The yield of protactinium was 90 ± 3%, as determined from the ^{233}Pa tracer, and it eluted mainly in fractions 14 and 15.

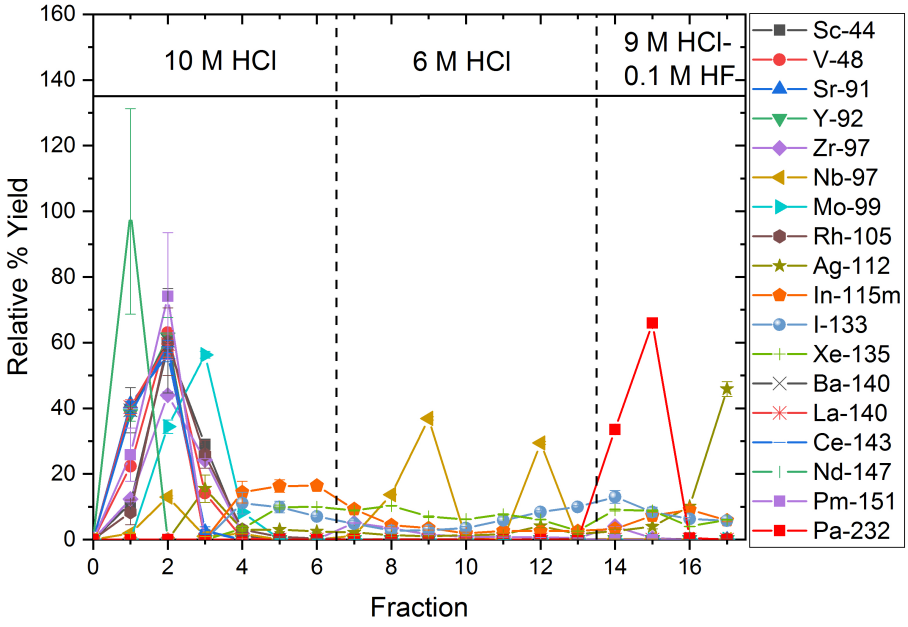

Figure 6.10: Elution curve from the first target separation from the 3 August CAMS irradiation. No fitting was done, and lines are to guide the eye only.

The majority of the protactinium eluted in fraction 15, which had a protactinium yield of 57 ± 2%. The radiopurity of this fraction was 99 ± 0.1% at 20.6 hours post-irradiation. The contaminants were ^{97}Zr, ^{97}Nb, ^{112}Pd/^{112}Ag, ^{115}Cd/^{115}In, ^{117}Cd/^{117}In, ^{133,135}I and ^{135}Xe; all

were present in trace quantities as indicated by the radiopurity. Figure 6.11 shows the elution curve for this separation again with only protactinium and a subset of fission productions to better show the behavior of protactinium and the contaminants. The radiopurity of fraction 14 was similar, 99 ± 0.2% at 16.3 hours post-irradiation, but the yield was lower (32 ± 1%). Finally, fraction 16 has a protactinium yield of only 0.42 ± 0.05% and fraction 17 had no detectable protactinium.

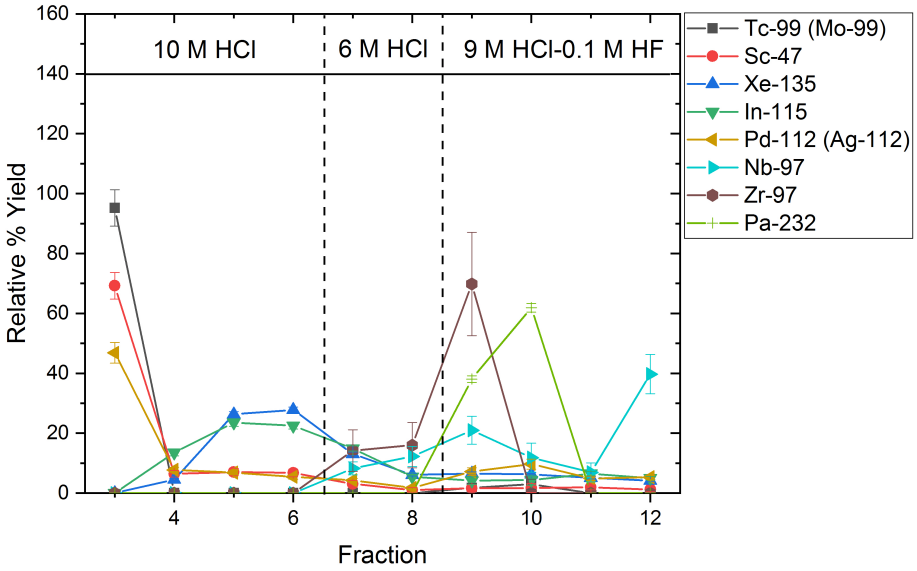

Figure 6.11: Elution curve of protactinium and a subset of the fission products from the first target separation from the 3 August CAMS irradiation. No fitting was done, and lines are to guide the eye only.

The samples were removed from the irradiation facility and the separation chemistry complete in ∼8 hours, which is ideal for the measurement of a short-lived isotope. The yield and radiopurity of the protactinium fractions, particularly fraction 15, were high. Based on this these results, it was determined that this separation and dissolution process was sufficient for the chemical processing of irradiated thorium targets for the measurement of the ^{230}Th(p,2n)^{229}Pa reaction cross section.

It was observed that as the mass of the dissolved target increased, the chemical yield of protactinium decreased. There were also issues with the salting out of aluminum chloride in some of the solutions. Both of these factors could lead to a decrease in protactinium yield as protactinium has a tendency to follow mass in chemical processes, particularly if there is some hydrolysis, which may be possible due to the low F^- concentration. Therefore, the loss in yield is likely due to protactinium being carried by the precipitation of the aluminum salt or with the thorium and titanium mass as it elutes from the column. It may be possible to

resolve these issues with careful solution control, but the reduction in yield was not significant enough for that be necessary.

6.6 Conclusion

Numerous different separation systems were considered in the development of a chemical processing system for this work. Measurement of the ^{230}Th(p,2n)^{229}Pa reaction cross section necessitates rapid, high yield and high radiopurity chemical separations due to the short half-life of ^{229}Pa. Separation systems were first studied with tracer isotopes followed by experiments with irradiated ^{232}Th targets, and the effect of the target backing material on the dissolution and the separation chemistry was studied. Anion exchange resin, in HNO_3 and HCl media, and extractant based resins were considered for the initial separation. A secondary separation step with DGA resin was considered as well.

A final chemical processing system was established based on a Dowex 1x8 column in HCl media. The time from the end of the irradiation to the completion of the chemical processing was about 8 hours. The total yield of protactinium was 90 $\pm$ 3%, with 57 $\pm$ 2% present in fraction 15, which had a radiopuritry of 99 $\pm$ 0.1% at 20.6 hours post-irradiation. Titanium was determined to be a better target backing material than platinum due to the ease of dissolution and lack of affinity for Dowex 1x8 in 10 M HCl, which allow for faster, simpler separations as the target backing dissolved quickly in the column load solution and did not interfere with the separation.

While similar separations have been presented in the literature before, the unique parameters of the target, target backing and need for rapid chemistry meant that extensive optimization of chemical processing procedures was necessary to meet the requirements for this experiment. The chemical processing procedure demonstrated here was successfully used to in the ^{230}Th(p,2n)^{229}Pa and ^{230}Th(p,3n)^{228}Pa cross section measurement experiments, as discussed in the following chapter.

Chapter 7

Cross Section Measurements

7.1 Introduction

As discussed in Chapter 1, ^{225}Ac is of interest for medical isotope production and there is on-going research into methods of producing ^{225}Ac, either directly or via the decay of its parent isotopes (^{229}Th, ^{229}Pa, and ^{225}Ra). Production of ^{225}Ac and ^{229}Th via reactions on ^{230}Th, particularly the (p,2n) reaction, has been considered [18, 38]. However, there is limited nuclear data available on ^{230}Th reaction cross sections and no ^{230}Th(p,xn) reaction cross section data available in the literature.

To assess the feasibility of using the ^{230}Th(p,2n)^{229}Pa reaction for ^{225}Ac production via the decay of ^{229}Pa (Fig. 7.1), experimental measurements of the cross section were performed. As the ^{230}Th(p,2n)^{229}Pa reaction has been predicted to peak around 14 MeV to 15 MeV (see Chapter 1 and Refs. [26, 30]), experiments in this work focused on measuring the cross section between 14 MeV and 17 MeV. A limited portion of the excitation function of the ^{230}Th(p,3n)^{228}Pa reaction, which has a threshold at 15 MeV [39, 40], was also measured in this energy region.

While the availability of ^{230}Th is limited [18], it can be obtained from uranium ore or uranium ore-byproducts (Chapter 2) as it is naturally occurring in the ^{238}U decay chain. As described in Chapters 1 and 2, the ^{230}Th used in this work was separated from a high grade uranium ore (39.1 $\pm$ 1.8 wt. % uranium) that was naturally enriched in ^{230}Th with a ^{230}Th/^{232}Th isotope ratio of 0.0922 $\pm$ 0.00150, several orders of magnitude larger than ^{230}Th/^{232}Th isotope ratios in typical minerals, which are on the order of 10^{-6} to 10^{-5} [45, 46]. To ensure there was no interference from the ^{232}Th(p,4n)^{229}Pa reaction, all irradiations were conducted well below the threshold for that reaction (19.5 MeV) [38–40]. The ^{232}Th(p,n)^{232}Pa reaction cross section, which is fairly well-known and has no interfering reaction from ^{230}Th, was measured simultaneously with the ^{230}Th(p,2n)^{229}Pa and ^{230}Th(p,3n)^{228}Pa reactions for all measurements to validate the experimental conditions.

Cross section measurements were made with three proton irradiations at varying energies and the excitation functions for the ^{230}Th(p,2n)^{229}Pa, ^{230}Th(p,3n)^{228}Pa and ^{232}Th(p,n)^{232}Pa

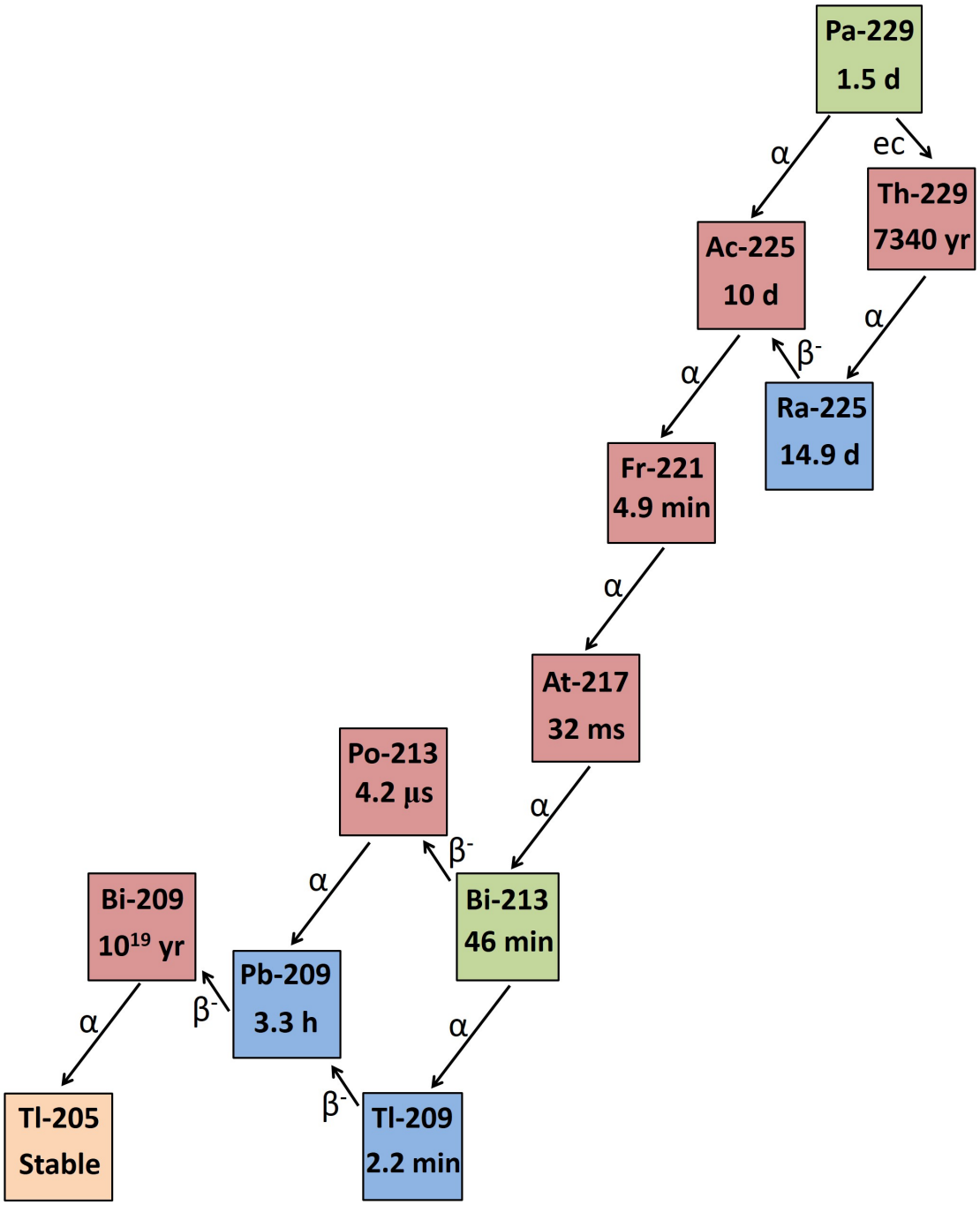

Figure 7.1: Decay chain of ^{229}Pa. In this figure, pure alpha emitters are shown in pink, pure beta emitters in blue, stable isotopes in pale orange and isotopes that decay by multiple decay pathways are shown in green.

reactions are reported from 14.1 to 16.9 MeV. The excitation functions for the ^{230}Th(p,2n)^{229}Pa and ^{230}Th(p,3n)^{228}Pa reactions shown here have not been previously presented in the literature. The cross section results are compared with the theoretical calculations from TENDL 2019 [19], the output library of the nuclear code TALYS (see Chapter 1), as well as existing nuclear data for the ^{232}Th(p,n)^{232}Pa reaction.

The half-lives of ^{229}Pa and ^{228}Pa were also measured as part of the cross section measurement experiments. While the ^{229}Pa half-life measured in this work does not improve upon past measurements, measuring the ^{229}Pa activity repeatedly over several half-lives was valuable for verifying the activity of ^{229}Pa, which has few, weak gamma-ray lines, and the measured half-life agrees well with existing literature values. The measured half-life of ^{228}Pa is slightly shorter than the value currently accepted by ENSDF, which is based on one historical measurement from 1952 that was made with alpha pulse spectroscopy. The measurement presented here was made with gamma-ray spectroscopy and provides a new data point for an isotope with limited available nuclear data.

7.2 Background Information

Nuclear reactions[1] have important applications in many areas of chemistry and physics. They can be used to study nuclear structure as well as understand and describe nuclear reactions, such as those in nuclear reactors or stellar nucleosynthesis. Activation analysis, which relies on neutron-induced nuclear reactions, can be used to determine the elemental composition of various materials. Nuclear reactions are fundamental to isotope production and the study of super heavy elements as well.

A nuclear reaction occurs when there is an interaction between a projectile particle (or gamma-ray) and target nucleus. In typical laboratory setting, the target nucleus is stationary and a light projectile (proton, alpha particle, gamma-ray, etc.) is accelerated towards the target, though it is possible to have heavy ion projectiles and/or both the projectile and target in motion. The discussion of nuclear reactions in this chapter will be limited to low energy reactions ($\sim$10 MeV per nucleon) with stationary targets and focus on the aspects relevant to isotope production.

Nuclear reactions are described by the projectile, target and reactions products, which are generally a light particle (or gamma-ray for a radiative capture reaction) and a heavy nucleus. This is shown in Eqn. 7.1 where the target and projectile are T and p, respectively, and the reaction products are X and y. There are many different types of nuclear reactions, including scattering, radiative capture, nuclear photoeffect (if the projectile is a gamma-ray) and transfer reactions. The reactions studied in this work are compound nucleus reactions, a type of nuclear reaction where the projectile nucleus and target nucleus merge for a short period of time, forming a highly excited compound nucleus, before a light particle is emitted.

[1]The explanation of nuclear reactions given in this section is based on Refs. [54] and [171], unless otherwise noted.

$$T(p,y)X \tag{7.1}$$

All nuclear reactions are governed by the conservation of total energy (the sum of the rest-mass energy and kinetic energy), charge and momentum. Reactions are described by a Q value (Eqn. 7.2) which is defined as the difference between the final and initial total kinetics energies (T), or as the difference between the initial and final rest-mass energies (m). A Q value greater than zero indicates the reaction releases energy (exothermic/exoergic) while a Q value less than zero indicates the reaction would need energy input to occur (endothermic/endoergic). The energy input comes in the form of the kinetic energy of the projectile. Therefore, for a reaction with Q < 0 to be energetically allowed, the kinetic energy of the projectile plus the Q value must be greater than zero. The minimum kinetic energy required for the reaction to occur is referred to as the threshold energy.

$$Q = T_X + T_y - T_P - T_T = [m_P + m_T - (m_X + m_y)]c^2 \tag{7.2}$$

Another important property to describe nuclear reactions is the cross section. This can be expressed as a microscopic cross section (σ, cm^2), which is the areal probability per nucleon of a given reaction occurring and is distinct from the geometric area of a nucleus, or the macroscopic cross section (Σ, cm^{-1}), which is the product of the microscopic cross section and the atom number density (n, atoms/cm^3) of the target material and is useful for assessing reaction probability in a bulk material rather than per nucleon. The microscopic cross section is very important for isotope production and this is described in the following equations.

For a nuclear reaction where a parallel, collimated beam with a known intensity (I, particles/s) is incident on a thin target with a known atom number density and thickness (x, cm), the transmitted beam intensity (I_f, particles/s), which is the unreacted beam particles, is given by Eqn. 7.3.

$$I_f = Ie^{-nx\sigma} \tag{7.3}$$

The rate of nuclear reactions (R, s^{-1}) can be found from the difference between the initial beam intensity and the transmitted beam intensity as shown in Eqn. 7.4.

$$I - I_f = R = I(1 - e^{-nx\sigma}) \tag{7.4}$$

For a thin target, the only kinds of targets considered in this work, Eqn. 7.4 can be simplified with a Taylor expansion, to result in Eqn. 7.5.

$$R = Inx\sigma \tag{7.5}$$

If the reaction product of interest, usually the heavy ion, is stable, the resultant production (At_{stable}, atoms) is given by multiplying the reaction rate by the length of the irradiation (t_i, s) as shown in Eqn. 7.6.

$$At_{stable} = Rt_i = Inx\sigma t_i \tag{7.6}$$

For the case of a radioactive reaction product, the decay of the reaction product during the irradiation time must be accounted for, as shown in Eqn. 7.7 where A_0 (s^{-1}) is the activity of the reaction product at the end of the irradiation and λ is the decay constant (s^{-1}).

$$A_0 = R\left(1 - e^{-t_i\lambda}\right) = Inx\sigma\left(1 - e^{-t_i\lambda}\right) \tag{7.7}$$

In this work, the areal density of the target (N, atoms/cm^2) was well-known from the area of the target and the activity of radioactive target material (see Chapter 4), while the thickness and density were not characterized independently. Since the areal density is the product of the density and thickness, Eqn. 7.7 can be expressed as shown in Eqn. 7.8.

$$A_0 = IN\sigma\left(1 - e^{-t_i\lambda}\right) \tag{7.8}$$

From these equations, it can be seen that a cross section can be calculated from the known irradiation parameters and the measured activity post-irradiation.

7.3 Description of Experimental Work

Irradiation Facility

The irradiations were performed with a 10 MV tandem accelerator located at the CAMS facility at LLNL. A total of six irradiations were performed as part of this work: three with ^{232}Th targets to establish the procedures for target fabrication and chemical processing, and three with ^{230}Th/^{232}Th targets to measure the cross sections of interest. The experimental conditions and results of the first three irradiations are described in Chapter 6.

The final three irradiations, detailed in this chapter, were used to measure the excitation functions of the ^{230}Th(p,2n)^{229}Pa and ^{230}Th(p,3n)^{228}Pa reactions in the energy range of 14.1 to 16.9 MeV. These irradiations were performed over several months with proton energies of 15 MeV, 16 MeV and 17 MeV. The irradiations were 8 to 12 hours in length with beam currents of 185 ± 7 nA to 277 ± 13 nA (Table 7.1). For each irradiation, thorium targets, cover foils and spacer foils, described in the following section, were stacked into an aluminum holder (Fig. 7.2) that was mounted in the CAMS irradiation chamber (Fig. 7.3); the targets and foils were trimmed to 8 mm squares to fit in the holder. During the irradiations, the chamber was under vacuum and beam stop was water cooled.

Table 7.1: Irradiation conditions and target information for cross section measurement experiments.

Irradiation	**Date**	**Beam Current (nA)**	**Beam Energy (MeV)**	**Irradiation Length (hours)**	**Spacer Foils**	**Target**	**Thickness (μg Th/cm^2)**	**Incident Energy (MeV)**
1	31 August 2020	185 ± 7	16	8	-	1	1086.629 ± 0.005	15.7 ± 0.1
						2	1127.714 ± 0.005	15.6 ± 0.1
2	28 September 2020	195 ± 8	17	12	Pt, Ta	1	921.710 ± 0.004	16.9 ± 0.1
						2	1599.668 ± 0.005	16.0 ± 0.1
						3	939.179 ± 0.004	15.7 ± 0.1
3	26 October 2020	277 ± 13	15	12	Ta, Ta	1	1075.127 ± 0.005	14.9 ± 0.1
						2	1813.112± 0.005	14.4 ± 0.1
						3	1913.309 ± 0.005	14.1 ± 0.1

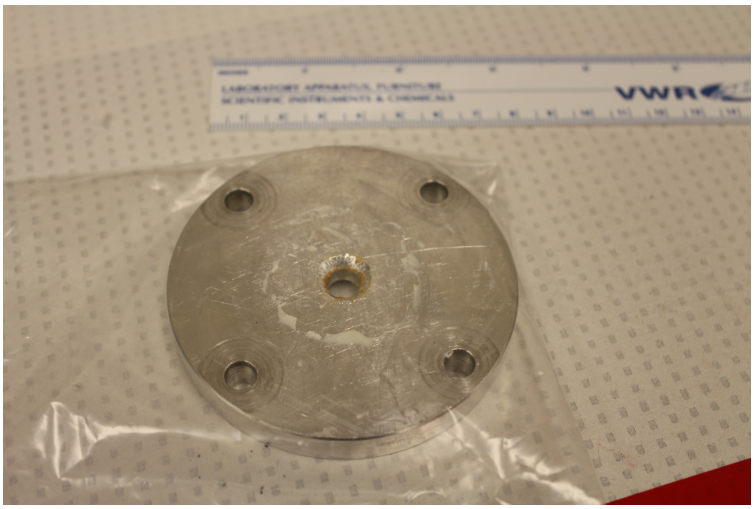

(a) Front

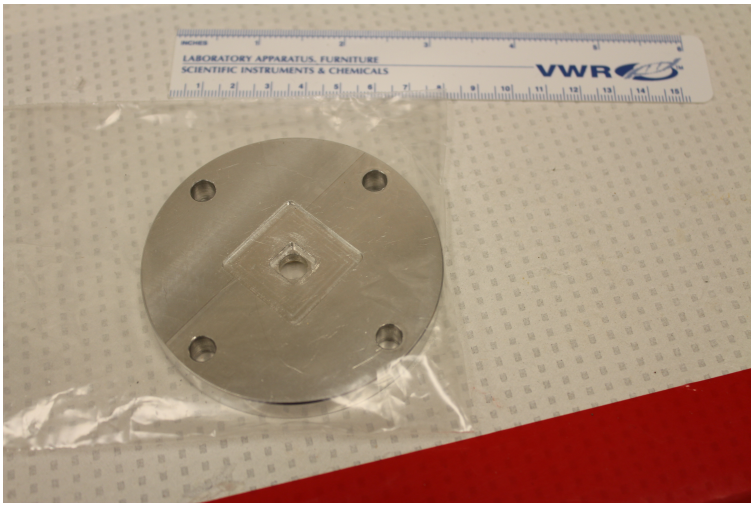

(b) Back

Figure 7.2: Aluminum CAMS holder; 6 inch ruler for scale. The beam enters through the 6 mm (dia.) circle visible on the front of the holder. For irradiations, foils are stacked into the small square opening (8x8 mm) visible on the back of the holder. The larger square (25x25 mm) visible on the back holds a 2 mm thick tantalum beam stop.

Targets

Thorium oxide targets were fabricated according to the procedure established in Chapter 4 with the thorium obtained from uranium ore as described in Chapter 2. The $^{230}Th/^{232}Th$ isotope ratio, as mentioned previously, was 0.0922 ± 0.00150 as determined by mass spectrometry (Chapter 2). A total of eight thorium targets were irradiated and processed over

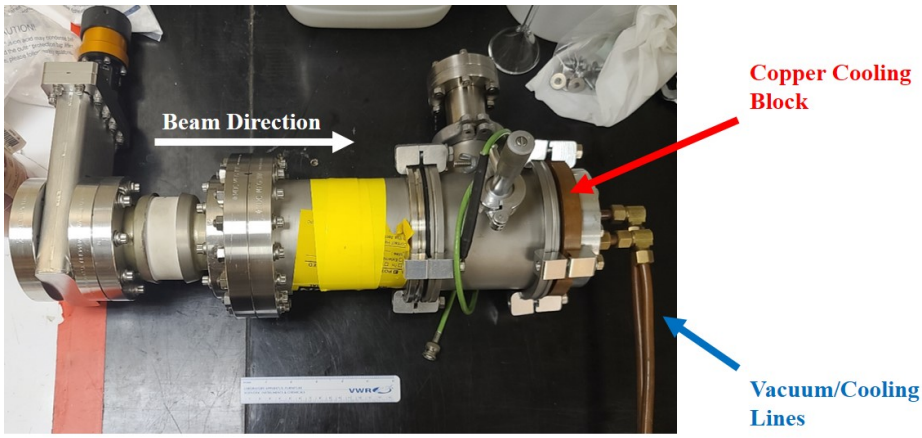

Figure 7.3: CAMS irradiation chamber. The aluminium holder is held on the copper cooling block inside the chamber (not visible).

three irradiations; target details are given in Table 7.1. The target backing material was 10 μm titanium (99.9%, LT, Goodfellow). Target thicknesses ranged from 921.710 $\pm$ 0.005 to 1913.309 $\pm$ 0.005 μg Th/cm^2. The areal density of the targets was determined with gamma-ray spectroscopy using the 67 keV gamma-ray line of ^{230}Th and target uniformity was determined with a position sensitive alpha detector, further details of target characterization are given in Chapter 4.

The proton energy through the target stack was modeled using the program SRIM 2013 [47]. Spacer foils of tantalum (10 μm, 99.9%, LT, Goodfellow) and platinum (25 μm, 99.99+%, LT, Goodfellow) were used to degrade the energy and allow the cross sections to be determined over a range of energies ($\sim$1 MeV) per irradiation (see Table 7.1). Thin titanium (2 μm, 99.99%, Lebow Company) cover foils were positioned in front of each target during the irradiations and then chemically processed with their respective target. An yttrium foil (5 μm, 99%, Goodfellow, not light-tested) was used as a flux monitor for all irradiations and a thin tantalum foil (5 μm, 99.9%, Goodfellow, not light-tested) was the first foil in each stack per the irradiation facility guidelines. The general target stack for these irradiations is shown in Fig. 7.4. The first irradiation for the cross section measurement experiments was slightly different than the other two, it had two tantalum foils at the front of the target stack, only two thorium targets and no spacer foils. Furthermore, due to issues at the irradiation facility it was 4 hours shorter than the other irradiations.

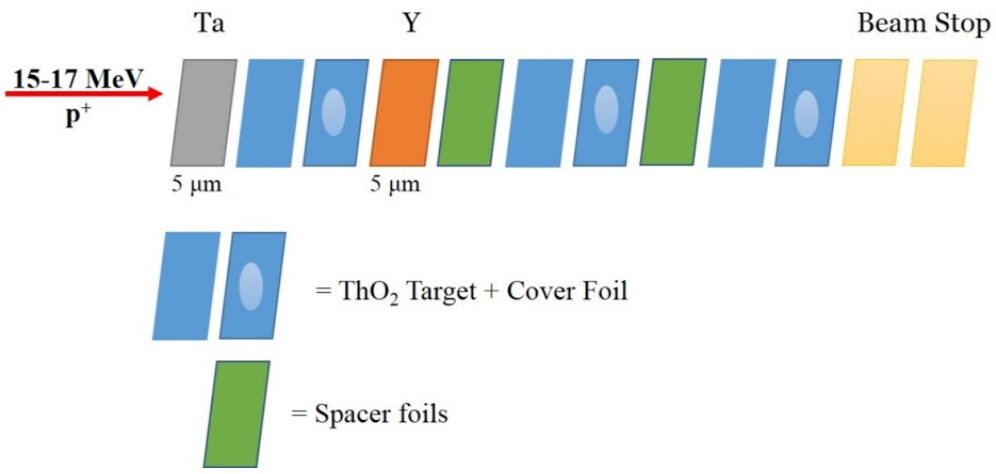

Figure 7.4: Schematic of the target stack for ^{230}Th/^{232}Th irradiations. Targets, cover foils and spacer foils are described in Section 7.3 and Table 7.1.

Target Processing

Target processing was necessary to detect the protactinium activation products over the high background from fission products and titanium activation products. The details of the chemical processing procedure are given in Chapter 6 and briefly summarized below.

After each irradiation, the targets were removed from the CAMS beamline within an hour and brought to a laboratory for chemical processing. Each target foil and its cover foil were removed from the target stack and placed in separate 5 mL plastic tubes. To each target, 1000 μL conc. HCl and 10 μL of a ^{233}Pa tracer ($\sim$1000 dps) in conc. HF were added to dissolve the target and backing material. A standard solution containing only the ^{233}Pa tracer was made in the same manner.

After the dissolution was complete (1.5 hours), the target solutions and standard were diluted to 2 mL 10 M HCl - 0.14 M HF - 0.2 M $AlCl_3$ and column chromatography was used to separate protactinium. In this separation, protactinium eluted mainly in fraction 15 (Fig. 6.10), which had a radiopurity of >99% and a protactinium yield of 63 $\pm$ 1% to 85 $\pm$ 6%, as determined from the ^{233}Pa tracer, with the higher mass targets having lower chemical yields (see Chapter 6). The remainder of the protactinium was in fractions 14 and 16 as well as the empty tube ($\sim$5-10%). After the separation, the protactinium samples were counted with gamma-ray spectroscopy. The total time from the end of the irradiation to the start of the gamma-ray spectroscopy of the separated protactinium samples was about 8 hours. For each target, fraction 15 was used for all protactinium activity measurements.

As discussed in Chapter 6, ^{233}Pa was chosen as the yield tracer because it has several strong gamma-ray lines [14] and its production from nuclear reactions in the target is negligible as the ^{232}Th(p,γ) reaction cross section is small (<400 μb) in this energy range [160, 161] and there is no route to ^{233}Pa from ^{230}Th.

For the targets irradiated at higher energies (>16 MeV), the significant ^{230}Pa production necessitated further chemical processing to measure the ^{213}Bi daughter of ^{229}Pa (Fig. 7.1) with reasonable counting statistics as ^{230}Pa (440.78 keV) and ^{213}Bi (440.45 keV) have gamma-ray emissions with similar energies (see Appendix C Table C.1 for a complete table of relevant half-lives, and gamma-ray energies and intensities) [14]. For these samples, protactinium and actinium were separated with column chromatography 35 days post-irradiation. The samples were evaporated to dryness and reconstituted in 2 mL 10 M HCl - 0.14 M HF - 0.2 M $AlCl_3$, the same load solution as used for the initial separation. As before, the separations were performed with 2 mL Dowex 1x8 (100-200 mesh) columns, which had been prepared and washed with 8 mL 10 M HCl. Samples were loaded onto the columns with two 500 μL rinses of the empty tube.

All fractions were collected in 2 mL increments: four fractions of 10 M HCl, followed by four fractions of 9 M HCl - 0.1 M HF. The average total yield of actinium on this column was $99 \pm 2\%$ as determined from three studies with tracer isotopes (^{233}Pa, ^{228}Ac) under identical chemical conditions. While the total yield was high, actinium eluted in a broad band over most fractions. As before, the cleanest fraction was selected for gamma-ray spectroscopy, which was fraction 1 with an average actinium yield of $45.6 \pm 0.2\%$.

The actinium samples were counted with gamma-ray spectroscopy after a decay period of 12 hours, which ensured ^{213}Bi and ^{221}Fr were in equilibrium with ^{225}Ac. For the targets irradiated at lower energies, there was far less ^{230}Pa produced and, therefore, the in-growth of ^{213}Bi could be measured without further chemical processing. The 218.0 keV line from ^{221}Fr was also visible in some of the samples but it was not present with reasonable counting statistics and not used quantitatively.

Gamma-ray Spectroscopy

The chemical yield was determined with relative gamma-ray spectroscopy. Each separated protactinium sample was counted relative to a ^{233}Pa standard immediately after chemical processing with an HPGe detector with Ortec NIM electronics and ASPEC multi-channel analyzer. Maestro software (Ortec) was used to analyze the resultant spectra. All samples and the standard were counted in the same geometry.

To make the cross section measurement, the protactinium samples were counted with gamma-ray spectroscopy at the NCF at LLNL. All samples were counted with an HPGe detector as well as a LEPS detector. The detectors were calibrated with a ^{154}Eu source and the code GAMANAL [151] was used to analyze the resultant spectra. Each sample was counted at approximately 10 hours post-irradiation with the LEPS detector. Gamma-ray spectra were taken with the HPGe detector at approximately 12, 18, 24, 36 and 48 hours post-irradiation followed by additional counts every 24 hours for the next 6 days. The yttrium flux monitor foil was counted with the HPGe detector immediately with two spectra measured within four hours post-irradiation. Samples were recounted with the HPGe detector, either with or without prior chemical processing, about 35 to 40 days post-irradiation.

For all protactinium samples, the activities of ^{233}Pa, ^{232}Pa, ^{230}Pa and ^{229}Pa were determined as well as ^{228}Pa, if present. The activities of ^{233,232,230,228}Pa can be readily determined with gamma-ray spectroscopy as these isotopes have several high intensity lines (see Table C.1). As ^{229}Pa has only weak, low energy gamma-ray lines, the LEPS detector was used in conjunction with repeated counts on the HPGe detector over several ^{229}Pa half-lives to make a direct activity measurement. X-ray analysis of each spectrum as well as measurements of the in-growth of ^{213}Bi were used to confirm the activity.

From the gamma-ray spectroscopy data, the activity of each isotope at the end of the irradiation (A_0) can be determined with the known, absolute intensities of its gamma-ray lines and a decay correction based on the half-life and the time since the irradiation ended. From A_0, as well as the known areal density, beam intensity, irradiation time and decay constant of the isotope of interest, the cross section can be calculated with Eqn. 7.8. The activity of ^{89}Zr in the yttrium flux monitor foil was used to determine the current using Eqn. 7.8 with the known cross section of the ^{89}Y(p,n)^{89}Zr reaction [41]. Isotope decay during counting was not relevant for any of the gamma-ray spectroscopy measurements.

7.4 Results and Discussion

Cross Section Measurements

The cross section data was gathered over three separate irradiations with a total of eight thorium targets. For each target, the ^{232}Th(p,n)^{232}Pa, ^{230}Th(p,2n)^{229}Pa and ^{230}Th(p,3n)^{228}Pa reaction cross sections were measured simultaneously. For all cross section measurements, the error was propagated from the standard deviation of several activity measurements (3-19%) as well as error from the calibration of the detectors (∼1-5%), beam current (∼4%), target thickness (∼2%) and chemical yield (∼4%). There is a standard error of 0.1 MeV on the projectile energy based on the irradiation facility conditions and SRIM modeling of the energy through the target stack. Six separate cross section measurements are shown for each reaction as three of the eight targets were irradiated at an energy of 15.66 ± 0.15 MeV (error from the standard deviation). For this energy, the cross section was calculated from the average of the three measurements with the error given by the standard deviation.

The excitation functions for the ^{230}Th(p,2n)^{229}Pa and ^{230}Th(p,3n)^{228}Pa reactions are shown in Fig. 7.5 and all measured cross section data is given in Table 7.2. The average ^{228}Pa activity was determined based on its 338, 409 and 911 keV lines in three spectra taken within the first 24 hours post-irradiation; error is from the standard deviation. The ^{229}Pa activity was determined from its 119 keV gamma-ray line (Appendix C Fig. C.1). As this is a weak emission (see Appendix C Table C.1) [14, 172], spectra were taken with HPGe and LEPS detectors five times over the 36 hours post-irradiation and the activity determined from the average and standard deviation of these measurements. As the activity measurement was based on one line, X-ray analysis and measurements of the in-growth of ^{213}Bi were also done to confirm the activity measurement. For each protactinium sample, the X-rays in the

five spectra, mentioned previously, were analyzed for their activity, interferences and decay rate of the five protactinium isotopes present (^{228,229,230,232,233}Pa), taking into account five to six major X-ray energies for each isotope as well as low energy (<150 keV) gamma-ray lines. The energy range was chosen to ensure the activities of ^{228,230,232,233}Pa could be determined separately with data from their higher energy gamma-ray lines, particularly ^{232}Pa which has a 150 keV line with a significant intensity [14]. The ^{229}Pa activity calculated from the X-ray analysis was within error of the direct activity measurement (Fig. 7.6) except for the measurement at 16.9 MeV, where the X-ray result was higher. This is likely due to increased interferences at higher energies as the ^{232}Th(p,f) and ^{232}Th(p,3n)^{228}Pa reaction cross sections increase considerably as the energy increases. The in-growth of ^{213}Bi into the protactinium samples, as determined by gamma-ray spectroscopy about 40 days post-irradiation, confirmed the direct activity measurement as well.

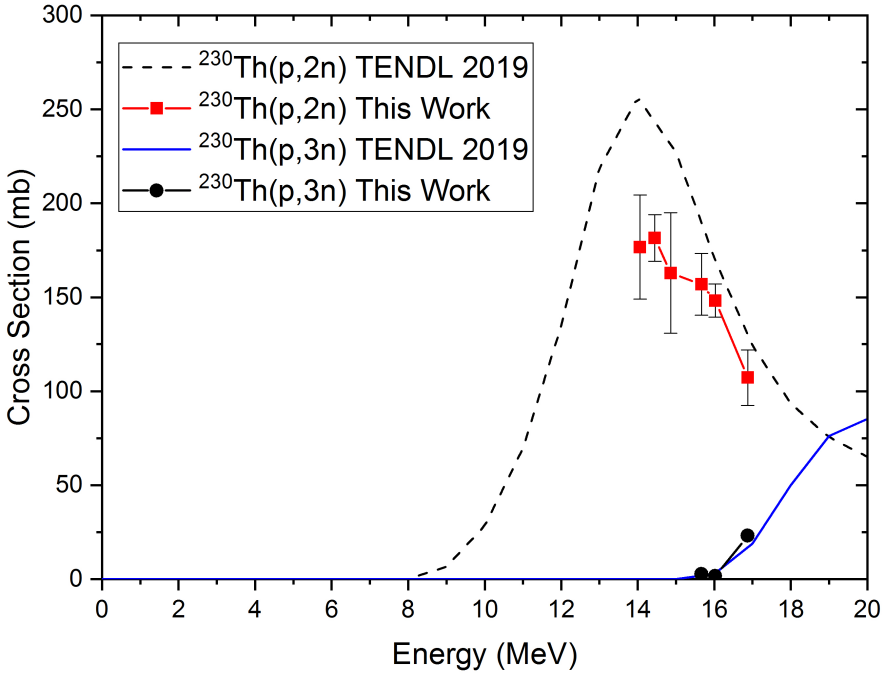

Figure 7.5: Measured excitation functions of the ^{230}Th(p,2n)^{229}Pa and ^{230}Th(p,3n)^{228}Pa reactions from 14.1 to 16.9 MeV compared to the TENDL 2019 calculations. Cross section error propagated from the standard deviation of several activity measurements. The point at 15.66 ± 0.15 MeV is an average over three measurements; the error on the cross section and the energy is given by the standard deviation.

The peak of the ^{230}Th(p,2n)^{229}Pa excitation function is between 14 and 15 MeV, but

cannot be determined more precisely from this data as the cross section measurements at 14.1, 14.4 and 14.9 MeV are all within error. However, the general shape of the excitation function can be seen as there is a clear decrease in the cross section from 14.1 MeV to 16.9 MeV. The maximum measured cross section was 182 ± 12 mb at 14.4 ± 0.1 MeV. The ^{230}Th(p,3n)^{228}Pa reaction cross section is low in this region, which was expected as the threshold is 15.0 MeV [39, 40], but it is clearly increasing as the energy increases. Due to the high threshold relative to the energy region studied, the cross section for this reaction was only measured at three energies (15.7, 16.0 and 16.9 MeV).

The measured ^{230}Th(p,2n)^{229}Pa reaction cross sections are lower than the cross sections calculated by TENDL 2019, though the measured peak appears to align well with the calculation, which puts it at 14 MeV [30]. The limited measurements of the ^{230}Th(p,3n)^{228}Pa reaction cross section appear to be in good agreement with the TENDL 2019 calculation for that reaction.

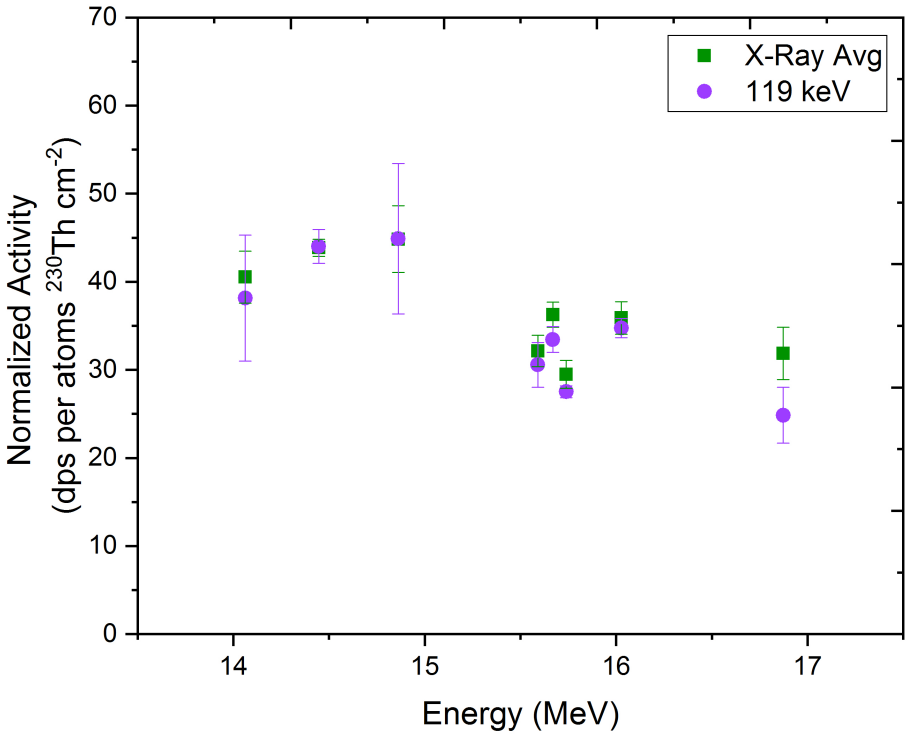

Figure 7.6: Comparison of ^{229}Pa activity calculated via direct measurement of 119 keV line and X-ray analysis. The activities were normalized by the ^{230}Th atom number areal density of the original target.

The results for the measurement of the ^{232}Th(p,n)^{232}Pa excitation function, which was used to validate the experimental conditions, are shown in Fig. 7.7. The ^{232}Pa activity was determined from its 150, 388, 581, 819 and 867 keV lines as well as the 969.32 keV line for measurements below 15 MeV where there was no production of ^{228}Pa, which has a gamma-ray line with a similar energy (968.97 keV). The activity was determined from the average activity of these five (or six) lines in three spectra taken within the first 24 hours post-irradiation; error is from the standard deviation. The measurement agrees well with the literature data for this cross section in the relevant energy range.

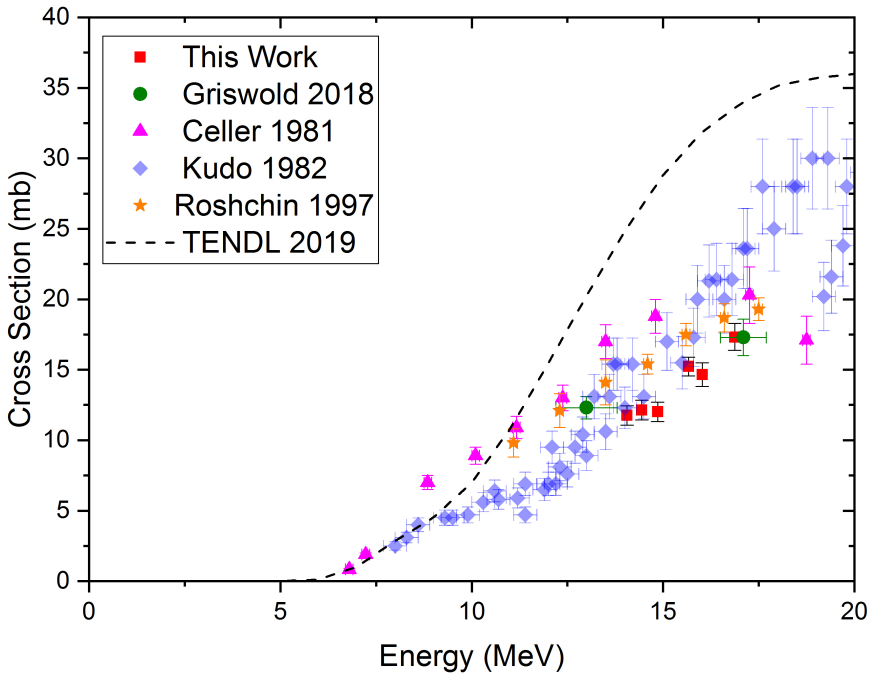

Figure 7.7: Measured excitation function of the ^{232}Th(p,n)^{232}Pa reaction from 16.8 to 14.1 MeV compared to the TENDL 2019 calculation and literature data. Cross section error propagated from the standard deviation of several activity measurements. The point at 15.66 ± 0.15 MeV is an average over three measurements; the error on the cross section and the energy is given by the standard deviation.

Table 7.2: Experimentally measured cross sections for the ^{230}Th(p,2n)^{229}Pa, ^{230}Th(p,3n) ^{228}Pa and ^{232}Th(p,n)^{232}Pa reactions.

Energy (MeV)	**^{230}Th(p,2n)^{229}Pa (σ, mb)**	**^{230}Th(p,3n)^{228}Pa (σ, mb)**	**^{232}Th(p,n)^{232}Pa (σ, mb)**
16.9 ± 0.1	107 ± 15	23 ± 1.3	17.3 ± 1.0
16.0 ± 0.1	148 ± 9	1.6 ± 0.15	14.7 ± 0.8
15.7 ± 0.14	156 ± 16	2.7 ± 1.6	15.2 ± 0.7
14.9 ± 0.1	163 ± 32	-	12.0 ± 0.7
14.4 ± 0.1	182 ± 12	-	12.1 ± 0.7
14.1 ± 0.1	166 ± 32	-	11.7 ± 0.7

Half-Life Measurements

For each protactinium sample, the 119 keV gamma-ray line from ^{229}Pa was followed over several half-lives to ensure it was decaying with the appropriate half-life. For the three samples with the highest ^{229}Pa activity, the half-life was measured based on this gamma-ray line (Fig. 7.8). The average measured half-life was 1.5 ± 0.1 days with error propagated from the statistical counting error. This agrees well with the half-life from the evaluated nuclear (1.50 ± 0.05 days [14]) as well as the recent measurement by Griswold, et. al. of 1.55 ± 0.01 days [38].

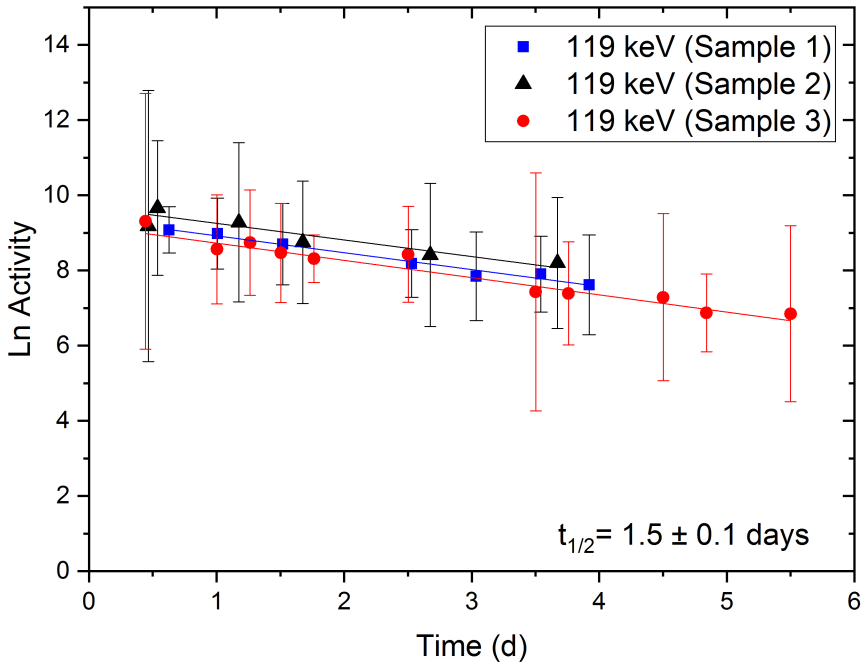

Figure 7.8: Measurement of the ^{229}Pa half-life from the 119 keV gamma-ray line for three protactinium samples. Error is statistical counting error. Least squares fit done with the program Origin 2018 (OriginLab).

The half-life of ^{228}Pa was also measured from three samples using two gamma-ray lines: 409 keV and 911 keV. While ^{228}Pa also has a 463.00 keV line with a high intensity, this line was not used as there is an interference from ^{230}Pa, which has a 463.59 keV gamma-ray line. The average measured half-life was 19.5 ± 0.4 hours (Fig. 7.9), which is smaller than the half-life given in the evaluated nuclear data (22 ± 1 hours) [173, 174].

The nuclear data for the half-life of ^{228}Pa was last evaluated in December 2012 by the International Network of Nuclear Structure and Decay Data Evaluators [173]. The half-life in ENSDF is 22 ± 1 hours [173], which is based on the measurement in Ref. [175]. Another measurement of 29 ± 1 hours from Ref. [176] is noted in ENSDF, but was not included in the final half-life assessment. The measurement from Ref. [175] was made in 1951 based on alpha pulse analysis with an argon ionization chamber using a ^{228}Pa sample known to be contaminated with the slightly longer lived ^{229}Pa. Furthermore, Ref. [175] notes that the two isotopes cannot be easily differentiated with alpha pulse analysis as their alpha emission energies are similar. Therefore, the decrease in the measured half-life is likely explained by the use of gamma-ray spectroscopy rather than alpha pulse analysis as the value from Ref.

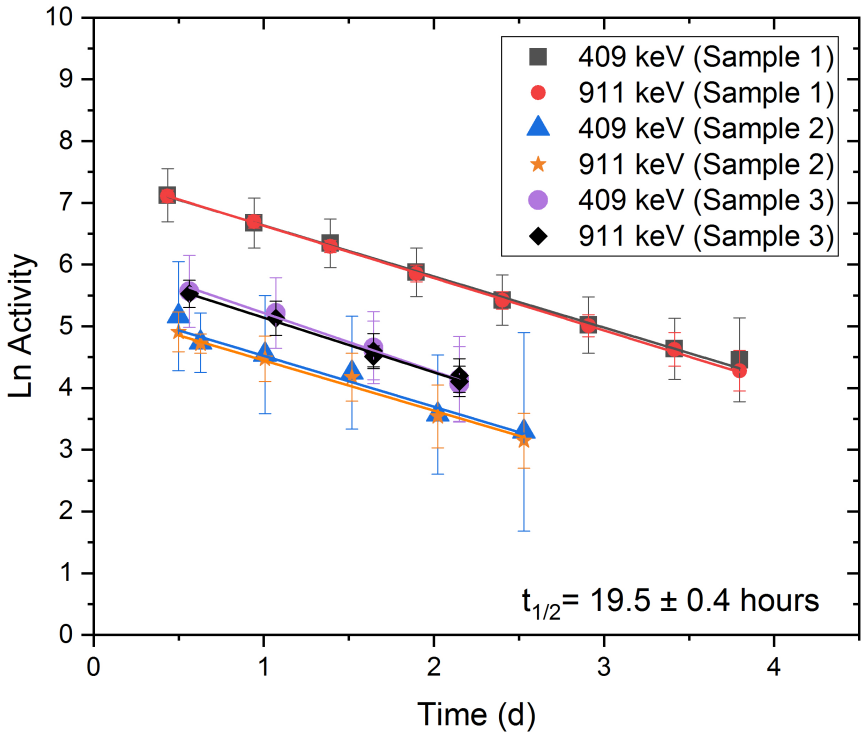

Figure 7.9: Measurement of the ^{228}Pa half-life from the 409 and 911 keV gamma-ray lines for three protactinium samples. Error is statistical counting error. Least squares fit done with the program Origin 2018 (OriginLab).

[175] may be an overestimate due to the presence of ^{229}Pa in the sample and the difficulties in resolving the alpha emission peaks of ^{228}Pa and ^{229}Pa.

Implications for ^{225}Ac Production

Based on the cross section shown in Fig. 7.5, the ^{230}Th(p,2n)^{229}Pa reaction is a reasonable method for ^{225}Ac production only if relatively large amounts of isotopically pure ^{230}Th were available, which could be obtained from the decay of ^{234}U or produced with isotope separation. As the activities required for TAT are in the range of 0.1 mCi to 1.4 mCi per patient per dose [4], current methods of ^{225}Ac production are focused on the production of around ~10 mCi ^{225}Ac/month [38]. Assuming the cross section shown in Fig. 7.5 and a target of 2 mg ^{230}Th/cm^2 (either mixed with ^{232}Th or isotopically pure), a 36 hour irradiation with a beam current of 1 μA would produce 80 μCi of ^{229}Pa but only 0.34 μCi of ^{225}Ac at its

maximum activity (see Appendix C Fig. C.2a) due to the low alpha decay branching ratio (0.48%) [14]. The production of ^{229}Th via the decay of ^{229}Pa is insignificant (<0.1 nCi) due to the long ^{229}Th half-life ($t_{1/2}$ = 7,340 years), see Appendix C Fig. C.2b [14].

As the production of ^{229}Pa saturates around 36 hours, increasing the irradiation time does not significantly impact production on a short timescale (days). Increasing the beam current to 200 μA (reasonable for isotope production facilities [4, 38]), increases the production to 16,040 μCi of ^{229}Pa but still only 9 nCi of ^{229}Th and a maximum of 68 μCi of ^{225}Ac. To overcome the low alpha decay branching ratio, the cross section would need be significantly larger, such as the ∼2 b cross section that was calculated for this reaction by TENDL 2015 (Chapter 1), which, with similar irradiation conditions, could have produced 746 μCi of ^{225}Ac with a 36 hour irradiation. However, the measured cross section is considerably lower than the TENDL 2015 calculation (Fig. 1.3a) and in much better agreement with the TENDL 2019 value, as shown above.

Despite the issues that arise from the low alpha decay branching ratio of ^{229}Pa and long half-life of ^{229}Th, production of ^{225}Ac with the ^{232}Th(p,4n)^{229}Pa reaction has been proposed via exceptionally long irradiations of thick thorium targets, presumably with the thorium target as a component of a beam stop at an accelerator facility [38]. Calculations have shown that cumulative reactions in the target would allow ^{229}Th to build up to mCi levels over a one year irradiation, producing significant amounts of ^{225}Ac, which grows in rapidly due to the short half-lives of ^{225}Ra and ^{225}Ac (Fig. 7.1) [38]. The measured peak cross section of the ^{230}Th(p,2n)^{229}Pa reaction (∼180 mb at 14.4 MeV) is comparable to the peak cross section of the ^{232}Th(p,4n)^{229}Pa reaction (∼160 mb at 30 MeV [38]), so it would be a good candidate for a similar production route, particularly as the target could be irradiated at lower energies, resulting in less activation. However, for this to be feasible it would require a thick, high purity ^{230}Th target as targets proposed for this type of production are on the order of 2 mg/cm^2 [38].

An advantage of production with the ^{230}Th(p,2n)^{229}Pa reaction, if it were feasible to scale up, would be high isotopic purity of the resultant ^{225}Ac. There are limited routes to other actinium isotopes even with mixed ^{230}Th/^{232}Th targets. The in-growth of ^{226}Ac via ^{230}Pa alpha decay (0.0032%) [14] is minor and has been neglected in past studies [4]. At sufficiently low proton energies, there would be no production of ^{224}Ac (via the decay of ^{228}Pa) and even with higher energy irradiations, the small alpha decay branching ratio of ^{228}Pa (1.85%) and short half-life of ^{224}Ac ($t_{1/2}$ = 2.78 h) [14] would result in this isotope rapidly decaying to negligible quantities post-irradiation. Actinium-227 would mainly arise from the decay of ^{231}Pa produced from the ^{232}Th(p,2n)^{229}Pa reaction as the (p,γ) and (p,α) reactions on ^{230}Th are predicted to be negligible [30]. Due to the long half-life of ^{231}Pa, the production of ^{227}Ac is low even with a considerable quantity of ^{232}Th. The irradiation of 24 mg Th/cm^2 (mixed ^{230}Th/^{232}Th with an isotope ratio similar to that of the thorium material used in this work) for 36 hours at 200 μA would result in the production of 16,040 μCi of ^{229}Pa, which decays to 68 μCi of ^{225}Ac in ∼40 days, but only 63 nCi ^{231}Pa, which decays to 0.2 nCi ^{227}Ac in the same time. This gives a ^{227}Ac/^{225}Ac ratio of 3.25 × 10^{-6}, which is significantly better than current ^{227}Ac/^{225}Ac ratios from production at IPF and BLIP, 1.8 × 10^{-3} and 2.07 × 10^{-3},

respectively [11].

7.5 Conclusion

The excitation functions determined in this work for the ^{230}Th(p,2n)^{229}Pa and ^{230}Th(p,3n)^{228}Pa reactions from 14.1 to 16.9 MeV are reported for the first time in the literature. The excitation function of the ^{232}Th(p,n)^{232}Pa reaction was also measured to verify the experimental conditions. The measured excitation functions were compared to calculations from TENDL 2019 and there is reasonably good agreement, although the measured ^{230}Th(p,2n)^{229}Pa reaction cross sections are lower than the calculation. This was expected as TENDL calculations for ^{232}Th(p,xn) reactions also tend to be slightly higher (Figs. 1.4 and 7.7) than the measured data. The peak measured cross section for the ^{230}Th(p,2n)^{229}Pa reaction was 182 $\pm$ 12 mb at 14.4 $\pm$ 0.1 MeV, though the measurements from 14.1 to 14.9 MeV were all within error, so the peak cannot be determined conclusively. This aligns well with the peak calculated by TENDL 2019 of 14 MeV [30]. Based on this cross section, production of ^{225}Ac via the ^{230}Th(p,2n)^{229}Pa reaction is only feasible with a significant amount of isotopically pure ^{230}Th as mixed ^{230}Th/^{232}Th targets from natural sources with sufficient levels of ^{230}Th would be impractically large.

Half-life measurements for ^{229}Pa and ^{228}Pa are presented, the measured half-lives are 1.5 $\pm$ 0.1 days and 19.5 $\pm$ 0.4 hours, respectively. The measured half-life for ^{229}Pa agrees well with the literature values. The measured half-life for ^{228}Pa is slightly smaller than the half-life given in ENSDF, likely due to how the half-life of ^{228}Pa was historically measured.

Chapter 8

CL Resin: Batch and Column Studies

8.1 Introduction

CL resin, made by TrisKem International as well as Eichrom Technologies Inc., is a relatively new extraction chromatography resin (commercially available since 2011) that was developed for the separation of chloride and iodide, and is also highly selective for platinum group metals [177]. The extractant molecule is triisobutylphosphine sulfide (Fig. 6.1a), which consists of a central phosphorous atom bonded to three isobutyl groups and a terminal sulfur [162].

This resin is of particular interest for the nuclear industry with applications in nuclear waste management [178, 179], nuclear medicine and isotope production [162, 180, 181], and nuclear monitoring [182]. As iodine is a high yield, highly volatile fission product, the measurement and management of iodine is extremely important for nuclear monitoring and nuclear waste management; CL resin is particularly suited for this because it provides a way to separate iodine from bulk samples, which is otherwise challenging [178, 179, 182]. In the area of nuclear medicine, this resin can be used to monitor the levels of ^{131}I, a common nuclear medicine isotope, in hospital waste [180].

As mentioned in Chapter 6, separations based on CL resin have been studied recently for isotope production and purification application beyond radioiodine, particularly for the separation of radiotherapeutic isotopes, or their parent isotopes, from irradiated thorium targets [162, 181]. So far, studies have focused on the behavior of thorium and its activation products of interest in hydrochloric acid systems, most likely because studies with thorium have shown no uptake on CL resin in hydrochloric acid solutions [181]; therefore, it can be useful for removing the bulk target material from fission product solutions [162, 181].

Literature on the behavior of thorium and its activation products on CL resin is limited to two papers [162, 181] both aimed at the removal of bulk thorium from medical isotopes of interest. Reference [162] is more extensive and reports distribution coefficients for protactinium, uranium, thorium, niobium, radium and actinium in HCl from 0.1 to 10 M HCl. Another batch study by the same authors is presented in Ref. [181], which studied the behavior of silver and ruthenium on CL resin in HCl and HNO_3 media. To better under-

stand the behavior of the early actinides and radium on CL resin and to develop separations for alternative applications, more extensive batch studies in HCl and other acid media are required and have not yet been presented in the literature.

Therefore, batch studies were done with Th(IV), Ac(III) and Ra(II) in HNO_3 and HCl as well as with Th(IV), Ra(II) and Pa(V) in HF. A wide range of acid concentrations was used and it was found that thorium has an extremely high uptake in CL resin in dilute HCl and dilute HNO_3, and a moderate uptake at intermediate concentrations of HF. The high uptake in HCl had not been previously reported in the literature as other studies did not study sufficiently low acid concentrations and it significantly broadens the applications of CL resin in regard to thorium separations. Using the data from the batch studies, numerous column separation systems are presented that provide methods for the separation of thorium from the other early actinides and radium, both on trace levels and with mass. A method for the separation of bulk or trace thorium from radium and actinium in dilute acid (HNO_3 or HCl) is presented as well as two separations of thorium and protactinium, one by retention of thorium on CL resin and the other by retention of protactinium.

8.2 Description of Experimental Work

CL resin (TrisKem International, 50-100 μm) was used for all batch and column studies; column studies were done with pre-packed, 2 mL cartridges. All acid solutions were prepared from Aristar ultra-pure acids (VWR) and diluted with Aristar ultra-pure water (VWR) as necessary. Isotopes were obtained from the decay chains of ^{232}Th, ^{231}Pa and ^{237}Np, which were legacy materials from LLNL. For the batch studies, tracer solutions of ^{228}Ac, ^{223}Ra, ^{227}Th, and ^{233}Pa were separated from their respective decay chains, ^{232}Th (^{228}Ac via ^{228}Ra), ^{231}Pa (^{227}Th/^{223}Ra via ^{227}Ac) and ^{237}Np (^{233}Pa), and prepared in solution with activities ranging from ~3 cps to ~50 cps per 20 μL. The column studies used the same isotopes as well as the direct use of ^{232}Th (where thorium mass was needed) and ^{231}Pa (as there was not sufficient ^{233}Pa remaining after the batch studies).

An HPGe detector with Ortec NIM electronics and ASPEC multi-channel analyzer was used to make activity measurements. Maestro software (Ortec) was used to analyze the resultant spectra. All samples were counted in the same geometry. For each isotope, the gamma-ray line with the highest intensity was used to determine the activity (see Table 8.1).

An Orion Star A211 pH meter calibrated with three buffers (4.00 ± 0.01, 7.00 ± 0.01 and 10.01 ± 0.01) was used to measure the pH of each HNO_3 and HCl acid solution.

Batch Uptake Studies

Batch uptake experiments were performed by adding 5 to 15 mg of dry resin to a 15 mL centrifuge tube along with 1 mL of acid. A list of acids and concentration ranges is given in Table 8.2. The resin was mixed with the acid for 30 minutes on an orbital shaker table to pre-equilibrate it, then a 20 μL spike containing the activity was added (see Table 8.2).

Table 8.1: Photopeaks and intensities used for activity measurements [14].

Isotope	Energy (keV)	Intensity (%)
^{223}Ra	269.46	13.9
^{227}Th	235.96	12.9
^{228}Ac	911.20	25.8
^{231}Pa	283.7	1.65
^{233}Pa	311.90	38.5

Table 8.2: Acid concentrations and spike concentrations for batch studies. Thorium-227 showed a significant uptake on the resin at 0.001 M HCl and HNO_3 in the initial batch studies and, therefore, it was studied in dilute acid as well. Studies done in duplicate and triplicate are marked as x2 and x3, respectively.

Acid	Concentration Range (M)	Spike Concentration (M)	Isotopes
HF	0.001 to 28	0.1	^{223}Ra (x2), ^{233}Pa (x2), ^{227}Th
HCl	0.001 to 11.19	0.1	^{223}Ra, ^{228}Ac, ^{227}Th
HNO_3	0.001 to 15.9	0.1	^{223}Ra, ^{228}Ac, ^{227}Th
Dilute HCl	10^{-5} to 10^{-3}	10^{-4}	^{227}Th (x3)
Dilute HNO_3	10^{-5} to 10^{-3}	10^{-4}	^{227}Th (x3)

Each sample was mixed for 3 hours during which time it was counted with an HPGe detector for 60 to 600 s to obtain $\geq$500 counts in the photopeak for each isotope. After the mixing period, each sample was filtered through a 0.45 μm polytetrafluoroethylene (PTFE) syringe filter to remove the resin. From each filtered solution, a 720 μL aliquot was taken and diluted to 1020 μL with de-ionized water. This was counted on the same HPGe detector, and in the same geometry as the initial sample, for 60 s to 12 hours depending on the activity. For counts longer than 30 minutes, a background subtraction was performed. All counts were decay corrected to account for decay during the experiment. For isotopes with a significant uptake on the resin and/or relatively high counting error (due to low activity in the initial batch study), batch studies were performed in duplicate or triplicate as needed. The weight distribution ratio (D_w, ml g^{-1}) was calculated from Eqn. 8.1 [183, 184], which takes into account the initial activity of the sample (A_0), the final activity of the sample (A_s), the volume (V, mL) and the weight of the resin (W, g).

$$D_w = \frac{A_0 - A_s}{A_s} \times \frac{V}{W} \tag{8.1}$$

To determine the effects of thorium hydrolysis on the batch study results, a blank study

was performed in the same manner as the batch study with no resin for thorium in 10^{-5}, 10^{-4} and 10^{-3} M HCl and HNO_3. The pH of all solutions of HNO_3 and HCl was determined with a pH meter; solutions with concentrations of 10^{-3} M and greater were below pH 3, therefore, thorium hydrolysis should be negligible in these solutions [64]. A blank study was also done for thorium in HF at all concentrations to determine the effects of microprecipitation as thorium readily forms ThF_4 in HF.

Uptake Kinetics Studies

Kinetics experiments were performed for ^{227}Th as it was the only isotope to show uptake on the resin in the batch experiments. The kinetics were studied in both HCl and HNO_3. For each acid, three standards were prepared with 1 mL 10^{-4} M acid in a 15 mL centrifuge tube and a 20 μL spike added with $\sim$2.5 cps ^{227}Th in 10^{-4} M acid. The standards were counted for 3 minutes with an HPGe detector. Samples were prepared in the same manner as before with 5-10 mg of resin in 1 mL 10^{-4} M acid. This was mixed for 30 minutes to pre-equilibrate the resin, before a 20 μL spike of ^{227}Th in 10^{-4} M acid was added. Each sample was mixed for a specific period of time (60 s, 300 s, 600 s, 30 min, 1 hour and 3 hours) before rapidly filtering to remove the resin. From the solution, a 720 μL aliquot was removed, diluted to 1020 μL with de-ionized water and counted in the same geometry as the standards. Samples in HNO_3 were counted for 180 to 300 s. Samples in HCl were counted for 30 minutes to 12 hours. For counts longer than 30 minutes, a background subtraction was performed. All counts were decay corrected to account for decay during the experiment.

Column Studies

Several column studies were done to test methods to separate ^{227}Th from ^{223}Ra, ^{228}Ac and ^{233}Pa based on the results from the batch studies. For each column, solutions containing the tracer isotopes were evaporated to dryness and reconstituted in the desired load solution and volume. The load solution was first counted with an HPGe detector and then loaded onto a 2 mL, pre-packed resin cartridge, which had been pre-washed with 8 mL of the same acid as the load solution. The columns were run using an Eichrom 12-hole polycarbonate vacuum box with a pressure regulator; the eluent flow rate was $\sim$1 mL/min ($\sim$5 mmHg). Fractions were counted with an HPGe detector in the same geometry as the load fraction. All counts were decay corrected to account for decay during the experiment. A total of six column separation systems were tested.

Two of the columns tested the separation of trace thorium from radium and actinium. For these, the load solution contained ^{227}Th, ^{223}Ra and ^{228}Ac in 1 mL 10^{-4} M acid, either HNO_3 or HCl. A load fraction and ten 1 mL fractions of 10^{-4} M acid were eluted to collect ^{223}Ra and ^{228}Ac, and then ten 1 mL fractions of 2 M acid were eluted to collect ^{227}Th.

The next column was identical to the HCl column described above, but with the addition of 1 mg ^{232}Th to the load solution and without ^{228}Ac. As before, a load fraction and ten 1

mL fractions of 10^{-4} M acid were eluted to collect ^{223}Ra, and then ten 1 mL fractions of 2 M acid were eluted to collect the thorium.

To asses whether the uptake of thorium on the resin was dependent on the pH or the concentration of Cl^-, a fourth column was done to separate ^{227}Th from ^{223}Ra, but with the addition of strontium chloride ($SrCl_2$, Sigma-Aldrich) to provide an excess of Cl^-. For this column, the load solution contained ^{227}Th and ^{223}Ra in 2 mL 10^{-4} M HCl with 1 M $SrCl_2$, making the final concentration 10^{-4} M in H^+ but 2.0001 M in Cl^-. A load fraction and four 2 mL fractions of 10^{-4} M HCl were eluted to collect strontium and ^{223}Ra, followed by four 2 mL fractions of 2 M HCl to collect ^{227}Th. After counting, the fractions were evaporated to dryness to observe the mass in each fraction; this determined that the strontium eluted in the first four fractions with ^{223}Ra, as expected.

The final two columns tested separations of ^{227}Th from ^{223}Ra and/or ^{231}Pa. The first column had a load solution of ^{227}Th and ^{231}Pa in 2 mL 0.8 M HF. A load fraction and five 2 mL fractions of 0.8 M HF were eluted to collect ^{231}Pa, followed by four 2 mL fractions of 2 M HCl to collect ^{227}Th. The second column had a load solution of ^{227}Th, ^{223}Ra and ^{231}Pa in 2 mL 10^{-4} M HCl - 10^{-4} M HF - 0.01 M H_3BO_3. A load fraction and three 2 mL fractions of 10^{-4} M HCl were eluted to collect ^{223}Ra, followed by three 2 mL fractions of 2 M HCl to collect ^{227}Th and then four 2 mL fractions of 1 M HF to collect ^{233}Pa.

8.3 Results and Discussion

Batch Studies

The results for the batch studies in HCl and HNO_3 are given in Fig. 8.1a and 8.1b. The results for the batch study in HF are given in Fig. 8.2. For all batch study results, the lower limit for measurement of the weight distribution ratio was 0.1 based on the inherent errors associated with the weight of the resin per sample and counting statistics, which cause larger variations at values near zero. The error shown is the statistical counting error, except for studies that were repeated in triplicate or duplicate, where the error is given as a standard deviation. It was observed that thorium has a strong uptake on the resin in dilute ($\leq$0.001 M) acid, though the effect is much stronger in HCl than HNO_3. Radium and actinium have no uptake on the resin at any concentration in either HCl or HNO_3 and radium and protactinium have no uptake on the resin in HF.

It was expected for radium not to interact with the resin as well since radium is notoriously difficult to complex and tends to only form simple salts [185]. Actinium did not interact with the resin either, which was expected as actinium is also difficult to complex and its complexation chemistry is poorly understood [186, 187]. Previous studies with actinium in HCl did not measure any interaction of actinium with the resin [162], and those results were replicated here.

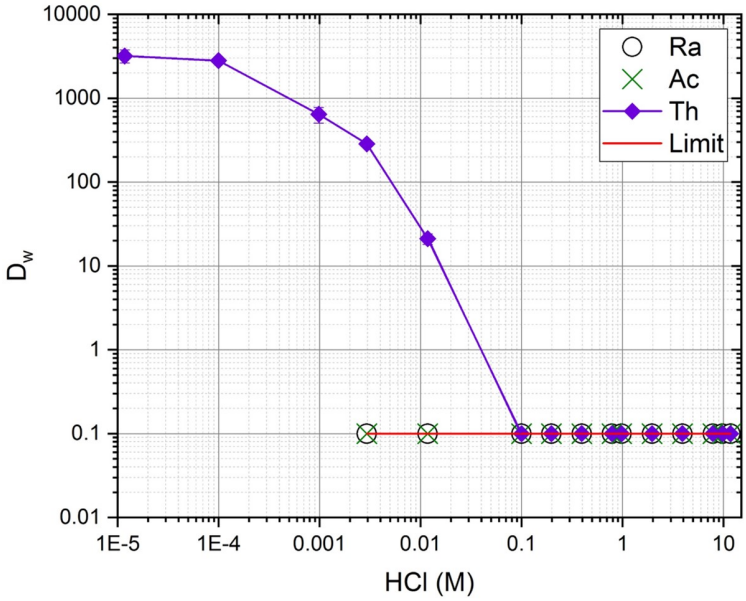

(a)

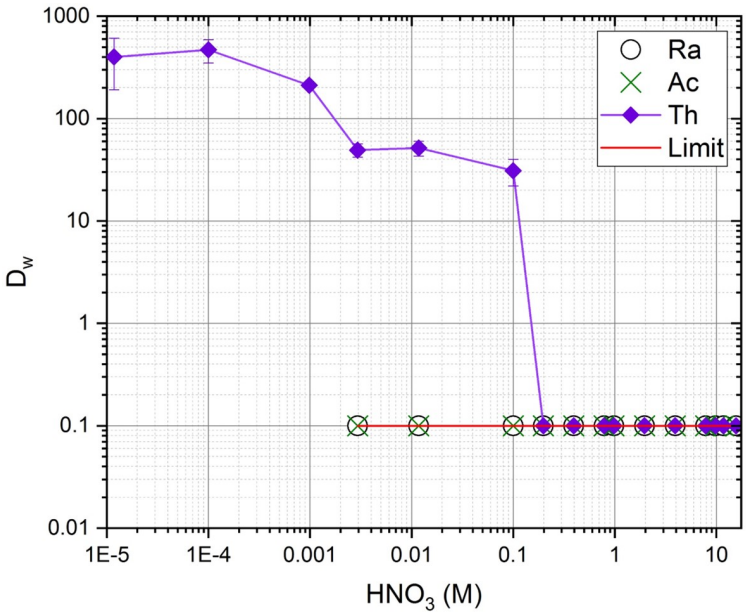

(b)

Figure 8.1: Batch uptake of thorium, radium and actinium in HCl (a) and HNO_3 (b) on CL resin. Uptake studies with thorium were repeated in triplicate for concentrations of 0.001, 10^{-4} and 10^{-5} M; for these points the error given is a standard deviation rather than the statistical counting error (as for all other data points). All data points for radium and actinium lie on the limit line at 0.1.

Reproducible chemistry involving protactinium can be difficult as it hydrolyzes readily due to its high charge state and forms colloids that adhere to glassware, silica, plastic or other solids in solution [66, 130]. As discussed previously (Chapter 4), protactinium is only significantly stable in solutions of HF or H_2SO_4 [66, 130], which provide a strong complexing anion that prevents hydrolysis, and it is not stable for extended periods of time in solutions of HCl or HNO_3 solutions [66, 130]. Therefore, it was not included in the HCl or HNO_3 batch studies. It does not interact significantly with the resin, which is to be expected as it does not typically interact with extractants in the presence of HF [66].

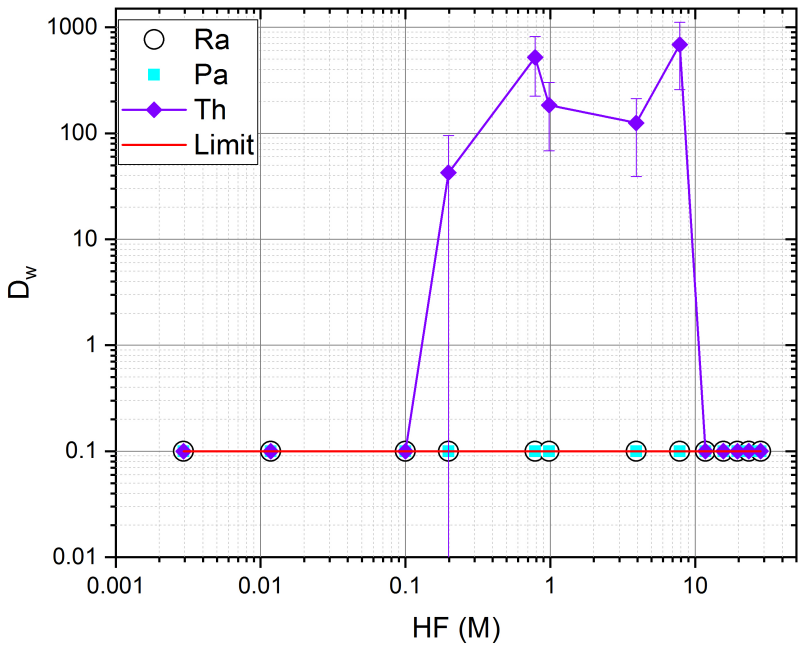

Figure 8.2: Batch uptake of thorium, radium and protactinium in HF. Studies with protactinium and radium were done in duplicate (due to low activities in the first batch study) and, as they showed no uptake on CL resin, all data points for radium and protactinium lie on the limit line at 0.1.

Thorium is known to hydrolyze in solutions with a pH greater than 3 [64], therefore a blank study was performed identically to the batch study but with no resin for thorium in solutions of 10^{-5} and 10^{-4} M HNO_3 and HCl, which had a pH greater than 3, as well as 10^{-3} M HCl and HNO_3, which had a pH just below 3. The blank study showed there was no detectable loss of thorium to the laboratory equipment (tubes, pipettes, filters, etc.) in HNO_3 or HCl solutions with concentrations of 10^{-5} to 10^{-3} M HNO_3 or HCl. Therefore, thorium hydrolysis and the presence of hydrolytic species are likely not having an effect on

the results. The lack of detectable effects from hydrolysis may be due to the timeframe in which the samples were prepared and the experiments conducted (∼6 hours). The hydrolysis of actinium and radium was not considered as these elements do not hydrolyze in solutions below pH 9 [188, 189] and no basic solutions were considered in this study.

At high concentrations of acid, the resin was observed to significantly degrade with the acid solutions appearing oily with an intense sulfur smell after extended contact with the resin. This is presumably due to a breakdown of the extractant molecule on the resin, which contains a sulfur-phosphorous bond that is likely reacting with the acid at high concentrations to form other sulfur compounds. Oxidation of this resin has been mentioned in the literature; in particular, Ref. [181] observed oxidation effects for this resin in HNO_3 ($\geq$6 M [181]), including color changes of the pre-packed resin cartridges, which turn blue in higher concentrations of HNO_3. In this work, similar color changes were observed and it was noted that the breakdown of the resin was more pronounced in solutions of HF and HNO_3, where the effects were observed at concentrations of 8 M and above. The resin appeared slightly more robust in HCl with the effects of the degradation appearing only above 10 M. Based on these results, it is not recommended to attempt separations in more concentrated acids unless it is to strip the column and further purification steps are acceptable as elutions with strong acid resulted in visible organic contamination in the final product.

In HF, thorium has a moderate uptake on the resin at intermediate concentrations, while protactinium and radium have no uptake on the resin (Fig. 8.2). Irregularities in the thorium uptake trends may be due to microprecipitation of ThF_4 as well as degradation of the resin. In HF solutions, thorium precipitates as ThF_4, an extremely insoluble white precipitate that can only be readily dissolved with the addition of an aluminum salt to complex the fluorides [64]. A blank study with thorium in HF was performed identically to the batch study but with no resin and it was found that ∼25% of the apparent extraction may be due to microprecipitation, leading to the loss of thorium to the tubes and filters, which is reflected in the large error bars for the thorium points in Fig. 8.2. In addition, the decrease in uptake after 8 M HF could also be due to the breakdown of the resin in the higher concentrations of HF as the acid solutions visibly contained an organic oil above 8 M. As the extractant is stripped off the resin by the high acid concentration, it would remain in the solution after filtration and result in an apparently low extraction. Actinium was not studied in HF as the short half-life ($t_{1/2}$ = 6.15 hours) [14] and the time necessary to complete a batch study (∼6 hours) meant sample preparation had to be minimal, and it was not possible to get it into a dilute HF solution in the necessary time frame.

As shown in Figs. 8.1 and 8.2, thorium has a strong uptake on the resin in dilute HCl and HNO_3 as well as in HF. This may be due to its smaller size and higher charge state compared to Ac(III) and Ra(II). Although molecules of the type $R_3P{=}E$ (E = C, N, O) are typically drawn as a double bonded ylene (P=E), calculations have shown that the ylide resonance form ($R_3P^+—E^-$) contributes significantly to the electronic structure [190–192]. As sulfur has even less of a tendency to form double bonds than oxygen, its lighter, smaller homolog, it is reasonable to think that the ylide resonance form would have a significant contribution to the electronic structure of the CL resin extractant (Fig. 8.3). This may explain why the

resin has a stronger uptake of the more highly cationic species, Th(IV), which can have a stronger ionic-type interaction with the extractant than the less cationic Ra(II) and Ac(III). In addition, the small size of thorium may allow it to have a stronger sorption if geometry is a factor. In the solutions of 10^{-5} and 10^{-4} M HNO_3 and HCl, hydrolytic species of thorium are likely present, however, as there was no detectable affect from hydrolysis in the blank study, these species are likely not effecting the results.

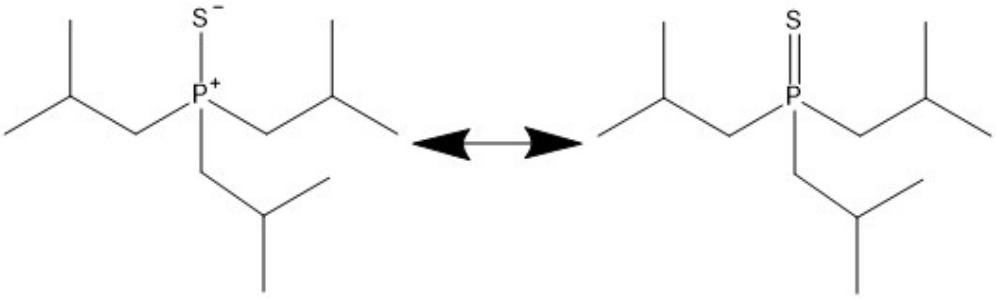

Figure 8.3: Ylide and ylene resonance forms of triisobutylphosphine sulfide.

Kinetics Studies

The results of the kinetics studies are shown in Fig. 8.4. Uptake of thorium on CL resin is rapid, particularly in HNO_3 where it is near equilibrium in ∼30 s. It takes about an hour to reach equilibrium in HCl, but the weight distribution ratio is over 1000 in ∼30 s. This shows the kinetics are sufficiently fast for a column separation. The blank study showed there was no detectable effect of hydrolysis in this timeframe.

Column Studies

Based on the results from the batch and kinetic uptake experiments, several column studies were undertaken to determine if CL resin could separate thorium, radium, protactinium and actinium. In dilute HNO_3 and dilute HCl, thorium is strongly absorbed on the resin and washing with dilute acid can readily separate both radium and actinium; thorium can then be eluted with 2 M acid (Fig. 8.5). The yields for these separations are given in Table 8.3; the recovery is within error of 100% for all three elements. No actinium or radium was detectable in the thorium fraction in either column. The elution bands were narrower and better separated in HCl, where the weight distribution ratio for thorium is higher. In HNO_3 there was some breakthrough of thorium in the radium/actinium fraction and both radium and actinium bled off over several fractions.

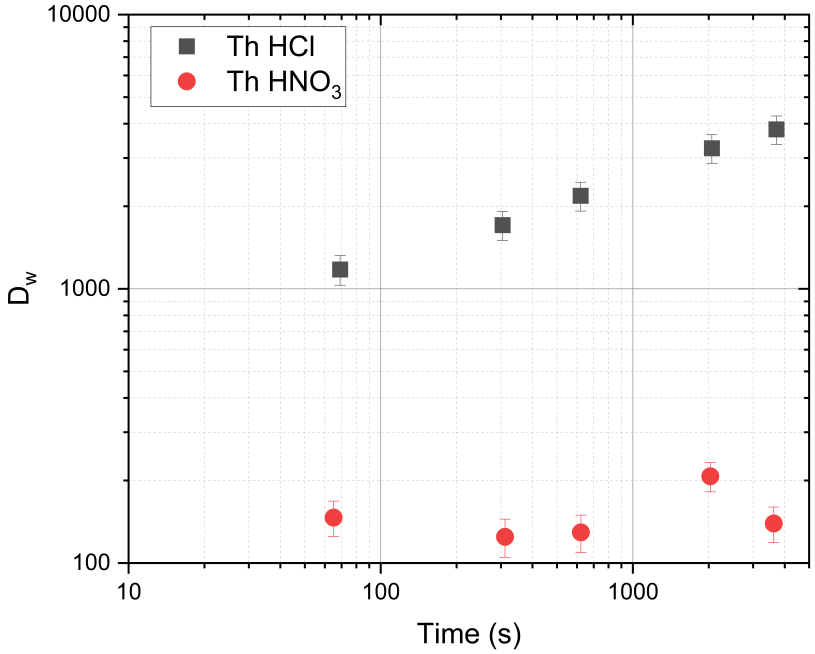

Figure 8.4: Kinetic uptake experiments of thorium on CL resin from 10^{-4} M acid; error is the statistical counting error.

Table 8.3: Yields of thorium, radium and actinium from separation on CL resin from dilute acid. Errors are from statistical counting error.

Column		**Yield**	
Load Solution	^{227}**Th**	^{223}**Ra**	^{228}**Ac**
10^{-4} M HCl	111 ± 5%	96 ± 4%	97 ± 10%
10^{-4} M HNO_3	104 ± 9%	110 ± 7%	105 ± 12%

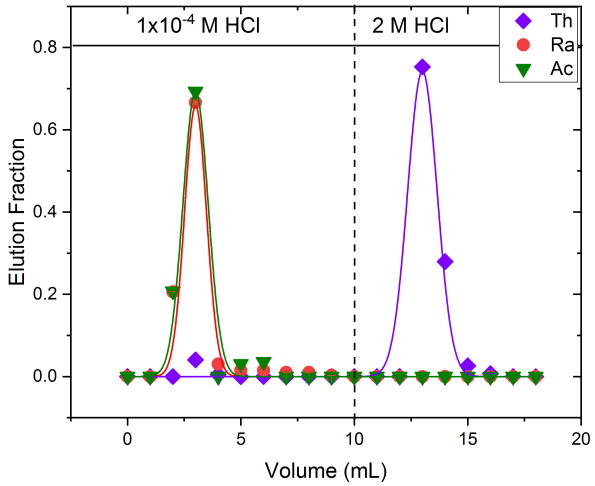

(a) HCl

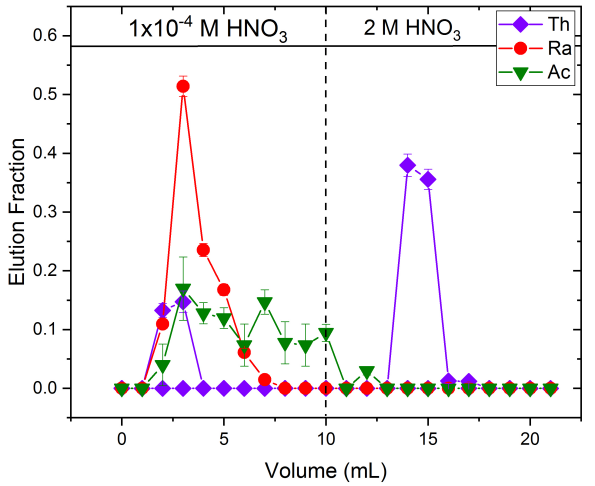

(b) HNO_3

Figure 8.5: Elution of ^{227}Th, ^{223}Ra, ^{228}Ac on CL resin in dilute acid solutions. Error is counting error, lines are to guide the eye.

As the separation of trace thorium and radium was more successful in HCl (Fig. 8.5a), this separation was also tested with the addition of 1 mg ^{232}Th to the load solution to ensure the separation would also work with mass. The elution curve is shown in Fig. 8.6, the yield was 99 ± 3% for thorium and 102 ± 4% for radium.

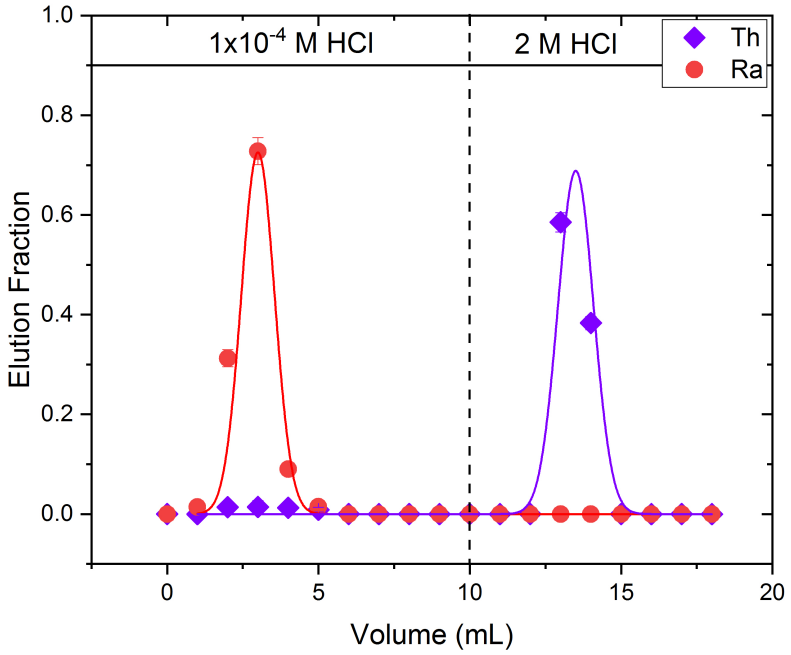

Figure 8.6: Separation of ^{223}Ra from 1 mg ^{232}Th and trace ^{227}Th. Error is counting error, lines are to guide the eye.

To determine if the Cl^- or H^+ concentration was driving the extraction of thorium, an additional column was done out of a dilute HCl solution (10^{-4} M) with ^{227}Th, ^{223}Ra and $SrCl_2$ (to provide an excess of Cl^-). Strontium was chosen as the chloride salt as it would not affect the pH (as a salt like NH_4Cl would) and presumably would have no uptake on the resin like radium, which tends to act strongly like its lighter homologs, and, therefore, not affect the separation. It can be seen from the elution curve (Fig. 8.7) that the excess Cl^- (∼2 M Cl^-) does not affect the retention of thorium on the resin or the elution curve (accounting for the larger fraction volumes in this separation). As before, the yield is high for both thorium (111 ± 11%) and radium (98 ± 2%).

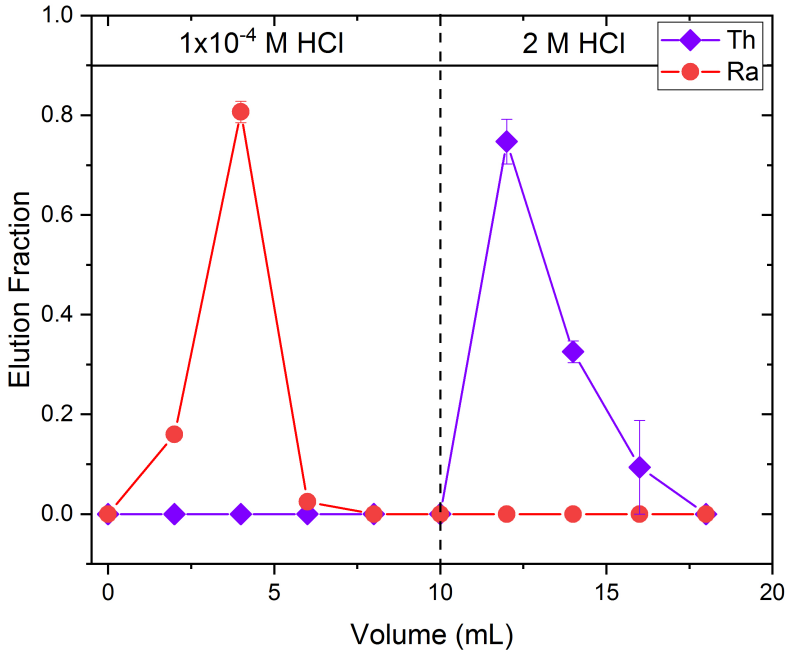

Figure 8.7: Separation of ^{223}Ra from ^{227}Th tracer in the presence of 1 M $SrCl_2$. Error is counting error, lines are to guide the eye. Evaporation was used to determine qualitatively that strontium elutes with radium; no mass was visible in the thorium fractions.

Two column separations were tested for the separation of thorium and protactinium. The first was done in an HF solution (Fig. 8.8) where thorium is retained on the resin in 0.8 M HF, while protactinium elutes. Thorium can then be eluted with 2 M HCl, as before. The yield for this column is relatively low for thorium (61 $\pm$ 7%), with much of it retained on the column, but high for protactinium (91 $\pm$ 10%). Thorium also bled slightly into the last protactinium fraction, though this could likely be improved by smaller fraction volumes (2 mL here). There was no detectable thorium in the first two protactinium fractions which contained 91 $\pm$ 7% of the total protactinium. It should be noted that this separation would likely not work on thorium samples with mass as bulk thorium would precipitate out as ThF_4. As mentioned previously, even on trace levels microprecipitation can occur and this may be why the yield is low for thorium as some may microprecipitate as ThF_4 and remain on the resin or be trapped in the frit of the column rather than elute with the 2 M HCl.

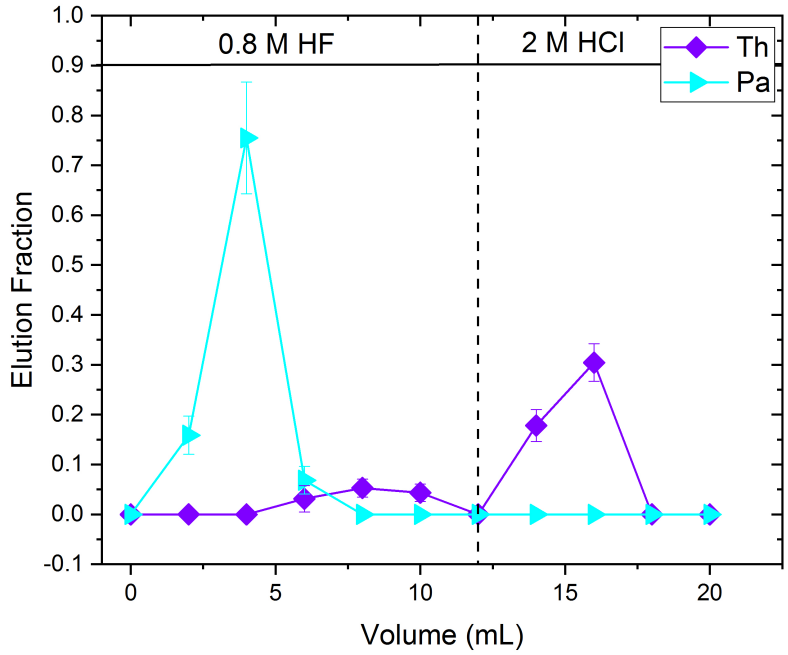

Figure 8.8: Separation of ^{231}Pa from ^{227}Th tracer in HF on CL resin. Error is counting error, lines are to guide the eye.

The second thorium/protactinium separation reverses the elution order and also separates radium from thorium and protactinium (Fig. 8.9). In this separation, the load solution was 10^{-4} M HCl - 10^{-4} M HF - 0.01 M H_3BO_3. The H_3BO_3, a fluoride scavenger, controls the free fluoride concentration to ensure that protactinium is retained on the column, a common procedure for protactinium chemistry [193]. Radium and thorium are eluted with 10^{-4} M HCl and 2 M HCl, respectively, while protactinium is eluted by adding fluorides, here in the form of 1 M HF.

Yields are low for both thorium (49 ± 7%) and protactinium (61 ± 10%) with high losses to the column and load solution tube, respectively. The yield for radium (128 ± 13%) is unchanged from previous separations. The yields for thorium and protactinium could likely be increased by more careful control of the fluoride concentration, as losses of thorium are likely due to some ThF_4 forming and remaining on the column (as seen in the HF column discussed previously) while some protactinium is likely hydrolyzing due to the low fluoride concentration and adhering to the load solution tube. It may be possible to correct this by increasing the fluoride concentration with a fluoride salt to stabilize the protactinium while also avoiding increasing the H^+ concentration (as that will decrease the uptake of thorium). The H_3BO_3 should also be given sufficient time to react with the protactinium

fluoride solution to minimize the free fluoride concentration before thorium in HCl is added. It should be noted that aluminum salts, which would dissolve ThF_4 completely and were used in previous chapters to control free F^- concentrations in solution, should not be used with CL resin as aluminum has some uptake on the resin in dilute HCl and the mass loading can affect the separation.

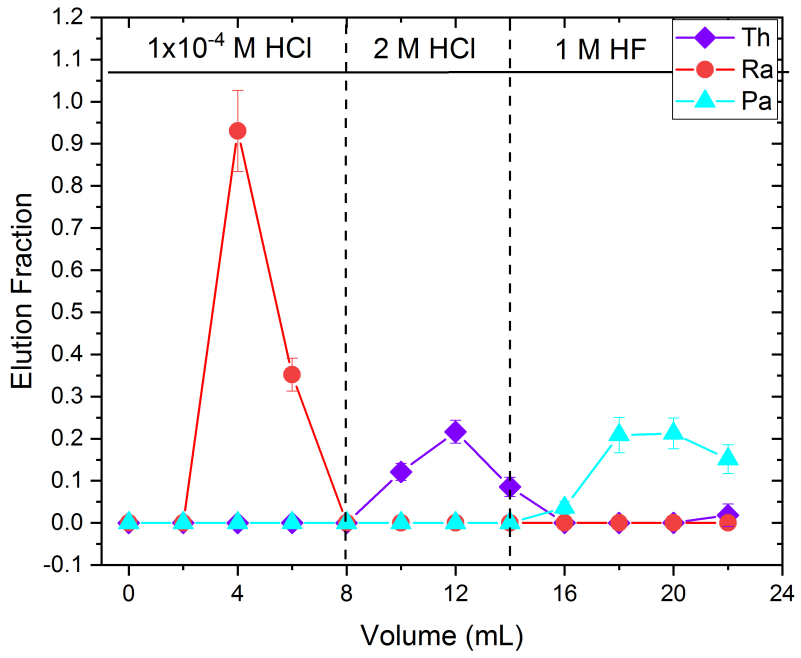

Figure 8.9: Separation of radium, thorium and protactinium from a solution of HCl-HF-H_3BO_3. Error is counting error, lines are to guide the eye.

8.4 Conclusion

Batch, kinetics and column studies of radium, actinium, thorium and protactinium on CL resin have been performed in HCl, HNO_3 and HF media. Radium and actinium show no uptake on the resin in HNO_3, HCl or HF; protactinium also shows no uptake in HF. Only thorium shows a strong uptake on the resin with weight distribution ratios over >100 in dilute HNO_3 (10^{-5} to 10^{-3} M) and >1000 in dilute HCl (10^{-5} to 10^{-3} M); kinetics studies showed the uptake is sufficient for column separations.

To the best of the author's knowledge, these are the first results in the literature for the uptake of radium, actinium and thorium in HNO_3 on CL resin as well as for radium, thorium

and protactinium in HF. Previous work in the literature had measured the uptake of radium, thorium and actinium from 0.1 to 10 M HCl [162], however, the limited acid range used in Ref. [162] meant that the strong uptake of thorium in dilute acids was not reported in that work, but it is thoroughly characterized in these studies.

Based on the results from the batch studies, six separations of thorium from radium and the other early actinides are given for HNO_3, HCl and HF media. The separations in HCl in particular are high-yield with good separation factors and can be used in a variety of solution conditions, including with thorium mass and in the presence of excess Cl^-.

Future work will include further optimization of separations of protactinium, radium and thorium as well as studies in dilute sulfuric acid as Ce(III) has been shown to have a small uptake on CL resin in 1 M H_2SO_4 [177], which may indicate that Ac(III) could uptake on the resin in H_2SO_4 as well as Ac(III) tends to behave similarly to the 3+ lanthanides [186].

Chapter 9

Extraction of Radium and Actinium with Pb Resin and Rose Bengal

9.1 Introduction

Macrocyclic ligand bonding of radium and actinium is an active area of research with applications in chemical separations [194, 195] and TAT [5, 185]. Radium and actinium are both large, relatively basic metals that are difficult to complex and the development of ligands and separation chemistry for these elements is complicated by the fact that the chemistry of radium and actinium is not well understood [5, 185]. Macrocyclic ligand bonding is promising for both elements as the macrocyclic effect significantly stabilizes radium and actinium complexes, which are usually highly labile due to the low charge density of the large cations [5, 185].

Crown ethers are a type of macrocyclic ligand and are useful for chemical separations of metal ions as they are extremely selective, separating metal ions based on size, charge and complexation chemistry [196]. They are commonly used for separations of series of elements, such as the lanthanides or alkaline earth metals [194, 197], which makes them well suited for studies on separations of radium, which is the heaviest alkaline earth metal and chemically similar to barium [185], and actinium, which has similar chemistry to lanthanum [5].

A commercially available extractant resin, Sr resin (Eichrom Technologies), containing 4,4'(5')-di-t-butylcyclohexano 18-crown-6 (DtBu18C6) (Fig. 9.1) in 1-octanol, has been employed for radium separations [194, 195] and has been shown to have potential for actinium/lanthanide separations as well [194]. However, the separation systems that have been demonstrated in the literature thus far require the use of super acids, particularly perchloric acid ($HClO_4$) and hexafluorophosphoric acid (HPF_6) [194, 195], which limits their applicability as these acids are extremely hazardous [194]. These separations rely on the ability of crown ethers to extract hydronium ions and become positively charged, allowing for an ion association extraction mechanism, as well as the large size of the counter ion, which favors the extraction of larger cations [194].

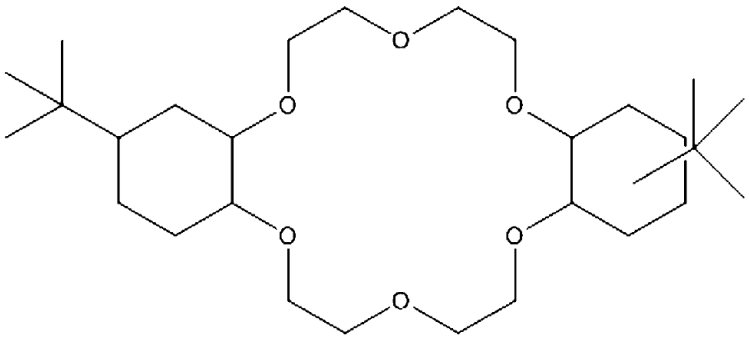

Figure 9.1: Extractant molecule of Sr resin and Pb resin (4,4'(5')-di-t-butylcyclohexano 18-crown-6).

The use of a large counter ion to stabilize the extraction of larger metal ions with crown ethers has also been demonstrated for barium separations in basic solutions with high extraction and rapid kinetics reported for the extraction of barium by 18-crown-6-Rose Bengal systems [198]. Rose Bengal (RB), shown in Fig. 9.2, is a large molecule that is doubly anionic above pH 5 with a negative charge on the carboxylic acid group as well as a delocalized negative charge on the xanthene ring [199–201].

Based on the results from these studies and the basic properties of both radium and actinium, the extraction of radium and actinium was studied with RB and Pb resin (Eichrom Technologies), an extraction chromatography resin based on the same extractant as Sr resin (DtBu18C6) [202]. Batch studies and kinetic studies were done with both blank solutions (containing no RB) and with RB. Both radium and actinium have a high uptake on Pb resin from solutions with RB, particularly radium which has a maximum k' ∼40,000. Due to the similarities in the trends of radium and actinium behavior, the applicability of these systems to radium/actinium separations is limited, though some column studies were done to determine the feasibility of separations based off differences in the kinetics of extraction. While there are many ways to separate radium from actinium, novel separations are still of interest in the literature as there are many application for such systems and the coordination chemistry of radium and actinium is not well understood, as discussed previously. Separations that retain radium, rather than actinium, are of particular interest as such systems are less commonly found in the literature.

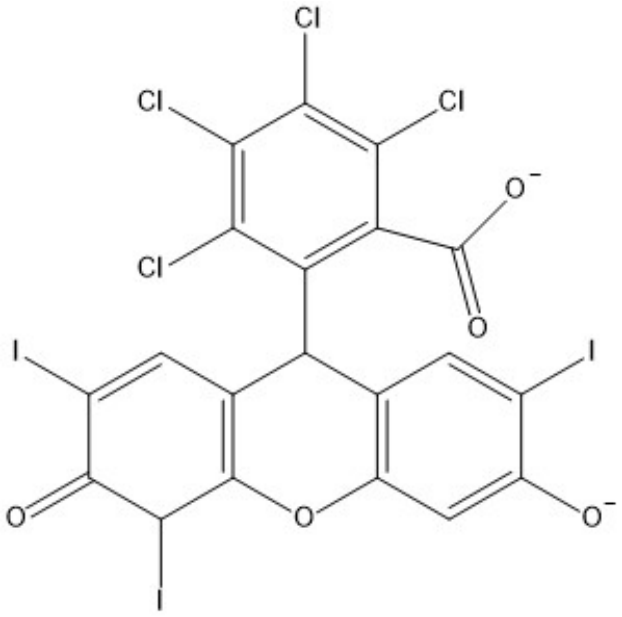

Figure 9.2: Anionic form of Rose Bengal.

9.2 Description of Experimental Work

Reagents and Materials

For all studies, Pb Resin (50-100 μm, 40% w:w, Eichrom Industries, Inc.) was used. All solutions were prepared using Aristar ultra-pure water (VWR). A 1 M LiOH stock solution was used for all basic pH adjustments and prepared with $LiOH \cdot H_2O$ (99.995%, trace metal basis, Sigma-Aldrich). Lithium hydroxide was chosen because lithium should not affect the extraction at low concentrations [198]. A 0.01 M HCl stock solution was prepared using Aristar ultra-pure acid (VWR) and used for all acidic pH adjustments. The disodium salt of Rose Bengal (Sigma-Aldrich, dye content 95%) was used as received for solution preparation.

Both tracer isotopes were individually separated from their parent isotopes with cation exchange chromatography in HNO_3: ^{223}Ra from ^{227}Ac and ^{228}Ac from ^{228}Ra. The parent isotopes (^{227}Ac, ^{228}Ra) had been previously separated from their long-lived parent isotopes, ^{231}Pa and ^{232}Th respectively, which were available as legacy materials from LLNL. Radioisotope stock solutions were prepared in 10^{-5} M HCl with 4-20 cps of the desired radionuclide per 20 μL.

Solutions and pH Measurements

Two sets of solutions were prepared for the batch and kinetics studies, with RB and without RB (blanks); for each, eleven solutions were prepared with pHs from ∼2 to ∼12.9 (see Table

9.1). Solutions were prepared in 50 mL volumes; the RB solutions were prepared using the blank solutions, then adjusted with small volumes (<100 μL) of HCl or LiOH to the final pH. The concentration of RB was 0.0001 ± 0.00002 M.

The pH of each solution was measured with an Orion Star A211 pH meter calibrated with three buffers: 4.00 ± 0.01, 7.00 ± 0.01 and 10.01 ± 0.01. The samples for each measurement (batch and kinetics studies) were prepared by adding 20 μL of the radionuclide solution to 1 mL of a stock solution; column load solutions were prepared with 20 μL of each radionuclide stock solution to 2 mL of the desired stock. The pH after these additions was measured three times for each solution and the average pH determined. The standard deviation of measurements was always within ± 0.2 pH units; therefore, this was taken as the error of the pH measurements for each study. Solutions under pH 5 containing RB needed to be made fresh each day as the stability of RB at low pH is poor and precipitation was observed at pH 4 and lower. The pH of each solution was also adjusted daily if there were any changes.

Table 9.1: Solution pH for studies. All pH numbers have an error of ± 0.2 and the pH values describe the pH of 1 mL of the stock solution after the addition of 20 μL 10^{-5} M HCl (to account for pH changes that occur when spiking in the radionuclides).

Solution #	**Acid or Base**	**pH**	
		Blank	*Rose Bengal*
1	0.01 M HCl	1.96	1.97
2	0.001 M HCl	2.95	3.04
3	0.0001 M HCl	3.38	4.16
4	0.00001 M HCl	4.35	5.21
5	Ultra-pure water	5.52	5.90
6	0.00005 M LiOH	6.80	6.27
7	0.000001 M LiOH	8.52	6.54
8	0.00001 M LiOH	9.24	7.05
9	0.001 M LiOH	10.95	7.93
10	0.01 M LiOH	12.06	10.88
11	0.1 M LiOH	12.87	12.06

Activity Measurements

Activity measurements were performed using an HPGe detector with Ortec NIM electronics and ASPEC multi-channel analyzer with spectra analyzed using Maestro software (Ortec). Table 9.2 shows the photopeaks, intensities and half-lives of the relevant isotopes. Both ^{223}Ra and ^{228}Ac have gamma-ray energies around 270 keV [14], therefore, the 144.2 keV

gamma-ray line was used for ^{223}Ra in samples with both ^{223}Ra and ^{228}Ac. All counts were decay corrected to account for decay during the experiment.

Table 9.2: Photopeaks, intensities and half-lives of isotopes used in this study [14].

Nuclide	Photopeak (keV) and Intensity	Half-life (d)
^{223}Ra	269.5 (13.7%) 144.2 (3.22%)	11.435
^{228}Ac	911.2 (25.8%)	0.2563

Batch Studies

Batch uptake studies were performed according to the procedure in Ref. [196]: 5-15 mg of dry Pb resin were added to a 15 mL centrifuge tube along with 1 mL of one of the solutions from Table 9.1. The resin slurry was mixed on an orbital shaker for 30 minutes to pre-equilibrate the resin. A 20 μL spike, containing either ^{228}Ac or ^{223}Ra, was added to each tube and the samples were mixed on an orbital shaker for 3 hours. During this time, each sample was counted for 60 to 300 s to obtain >500 counts in the photopeak for the isotope of interest. After mixing, the samples were filtered through a 0.45 μm PTFE syringe filter to remove the resin. A 720 μL aliquot of each solution was diluted to 1020 μL with ultra-pure water in order to maintain the same counting geometry. After dilution, gamma-ray spectroscopy was started immediately and these samples were counted on the same HPGe detector and in the same configuration for 60 s to 12 hours, depending on activity. All batch experiments were performed in triplicate and reported errors are propagated from the standard deviation of the replicates. The capacity factor (k') for the Pb resin was calculated from the weight distribution ratios as described in Refs. [202, 203]. Batch studies were also performed with the same spike solutions of actinium and radium in acidic solutions (HCl and HNO_3) with no RB and concentrations ranging from 0.001 to concentrated. No extraction was observed, therefore, results for these experiments are not presented graphically.

Kinetic Studies

The uptake kinetics of radium and actinium were measured in both blank and RB solutions. Counting standards for the kinetics studies were made in triplicate by adding 1 mL of the desired concentration of a blank or RB solution to a centrifuge tube, adding the 20 μL spike containing the radionuclide of interest, filtering through a PTFE syringe filter and diluting a 720 μL aliquot to 1020 μL for counting. The standards were counted with an HPGe detector until >1000 counts in the photopeak were obtained.

The samples were prepared similarly to the batch experiments: 5-15 mg of resin were pre-equilibrated for 30 minutes with the solution of interest; then a spike containing either ^{228}Ac or ^{223}Ra was added and each sample was shaken for a given time interval (25 s to 4.5 hours) before quickly filtering to isolate the solution from the resin. A 720 μL aliquot was taken and diluted to 1020 μL, to maintain the same counting geometry as the standards, and each sample was counted until there were >500 counts in the photopeak of interest. These experiments were performed only one time each and errors are propagated from the statistical counting errors.

Column Studies

The batch uptake data shows that radium and actinium behave similarly in these solutions and a column separation of these two elements should not be feasible from either the blank or RB solutions. However, column studies were still performed with a few different load solution conditions to show that these elements could be sorbed and desorbed, and to attempt separations based on the differences in uptake kinetics. The columns used were pre-packed 2 mL cartridges containing dry Pb resin; these were pre-conditioned with 5 mL of the same solution as the load solution. Load solutions were made by adding 20 μL of each radionuclide stock solution (a total of 40 μL) to 2 mL of the desired solution (to maintain the same pH as the batch study points) and each was counted with an HPGe detector until >500 counts were obtained in the photopeaks for both ^{228}Ac and ^{223}Ra. A 12-hole polycarbonate vacuum box (Eichrom, Darien, IL, USA) with a pressure regulator was used to regulate the eluant flow rate of the columns ($\sim$2 mL/min). For each column, 2 mL fractions were collected to maintain the same counting geometry as the load solution; Table 9.3 shows the elution parameters for each column.

Table 9.3: Elution parameters for the columns. Load solution and all fractions were 2 mL. Solutions are described in Table 9.1.

Column	Fraction	Solution
1	Load	RB Solution #10 (pH 10.88)
	Load Fraction, Fractions 1-2	RB Solution #10 (pH 10.88)
	Fractions 3-5	Blank Solution #10 (pH 12.06)
	Fractions 6-9	Blank solution #1 (pH 1.96)
2	Load	Blank Solution #10 (pH 12.06)
	Load Fraction, Fractions 1-4	Blank Solution #10 (pH 12.06)
	Fractions 5-8	Blank Solution #1 (pH 1.96)
3	Load	RB Solution #4 (pH 5.21)
	Load Fraction, Fractions 1-2	RB Solution #4 (pH 5.21)
	Fractions 3-6	Blank Solution #1 (pH 1.96)
	Fractions 7-10	Concentrated HCl

9.3 Results and Discussion

Batch Studies

The effect of pH on the extraction of actinium and radium by Pb resin in RB solutions is shown in Fig. 9.3. Both radium and actinium show an extremely strong affinity to the resin above pH 3 with a slight decrease in affinity above pH 8; however, even at pH 12, the extraction is still very strong. The maximum extraction for radium is a k' ∼40,000 at pH 8; the maximum extraction for actinium is ∼20,000 at pH 5.

The decrease in extraction at low pH is likely explained by the formation of the neutral lactone form of RB, which cannot act as a counter ion in the extraction. Above pH 5, RB exists as the RB^{2-} anion, as previously mentioned, but beneath pH 5, RB undergoes a lactonization reaction (Fig. 9.4), which converts the carboxylic acid group to an ester and protonates the oxygen functional groups on the xanthene ring [199–201, 204].

Currently, there is no data available for this system for either radium or actinium, although studies have been done with barium [198], which extracts as Ba(18C6) · RB and has similar chemical properties to radium. Therefore, it is assumed based on Ref. [198] that the extracted species for radium is Ra(18C6) · RB, analogous to the barium species. While the ionic radius of radium(II) (162 pm [205]) is slightly larger than barium(II) (135 pm to 161 pm, depending on the coordination number [206]), the size difference likely does not affect the structure of the extracted species. For example, cesium(I), which is slightly larger than radium with an ionic radius of 167 pm [205], also extracts in the same manner

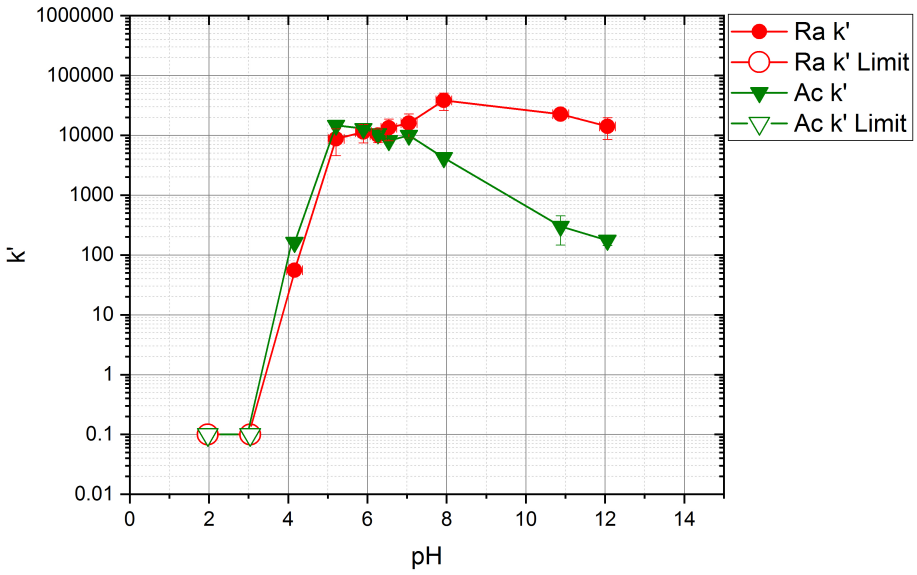

Figure 9.3: The batch uptake (k') of ^{228}Ac and ^{223}Ra as a function of pH on Pb resin with a 3 hour equilibration time from solutions containing Rose Bengal. Errors are propagated from the standard deviation of replicates.

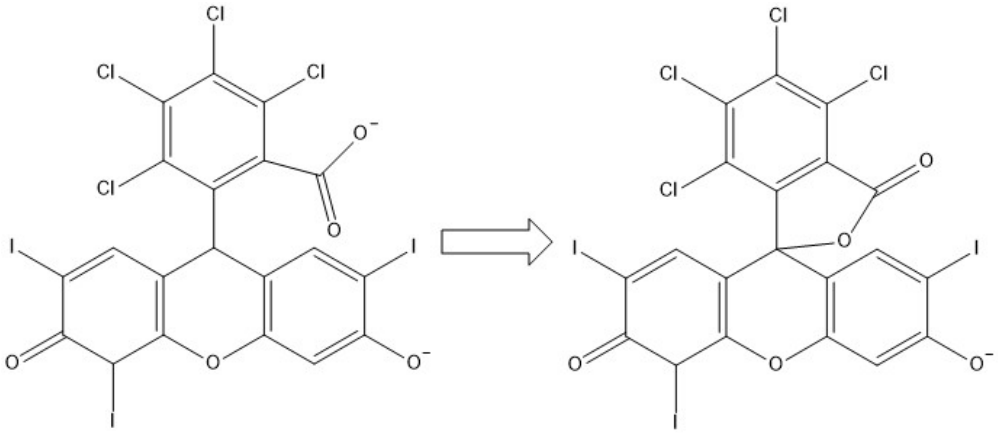

Figure 9.4: Lactonization of RB in acidic solutions.

with 18C6 and a large counter ion, forming a 1:1:1 Cs-18C6-picrate complex [207]. There is limited structure data for radium macrocyclic complexes available in the literature, but based on experimental and calculated structures of barium [208], cesium [207] and actinium [209] macrocyclic complexes, radium likely sits slightly above the ring of the macrocycle, leaving room for coordination with the RB molecule on the other side of the radium ion.

Complexation chemistry of Ac(III) is poorly understood [5], so it is difficult to assess what the extracted actinium species may be. The extraction of La(III), which has similar properties to Ac(III) [5], with 18-crown-6 and tricholoacetate (tca) has been studied in HCl solutions [197], and the extracted complex is La(18C6) · 3tca with tca providing the only counter ions and no involvement of the conjugate base anion (Cl^-). Based on that result and the extracted species of barium, Ac(III) is hypothesized to extract as $[Ac(18C6)]_2$ · 3RB, which could be reasonable due to the size and charge delocalization of RB anions. As mentioned previously, large cations like actinium tend to sit slightly above the ring of the macrocycle [207–209], leaving room for complexation with RB on the other side of the ion. Another possibility is the extraction of AcOH(18C6) · RB, as $AcOH^{2+}$ is the presumed hydrolysis product of actinium [5], but this is less likely as $AcOH^{2+}$ is very inert and likely only forms above pH ∼9.5 [5], which is around where the extraction decreases, rather than increases. However, as mentioned previously, it is difficult to make conclusions about actinium speciation in these solutions as the chelation, hydrolysis and aqueous solution behavior of actinium is not well-characterized [209–211].

As mentioned in the previous section, batch studies were carried out with radium and actinium in HCl and HNO_3 with concentrations ranging from 0.001 to concentrated and no extraction was seen, which agrees with previous results in the literature [194]. Extraction with crown ethers can occur by a cavity-based mechanism, where the metal ion fills the cavity in the crown ether, or an ion association mechanism, where a positive ion (such as a hydronium ion or potassium cation) fills the crown ether cavity and interacts with a negatively charged metal ion complex (typically the metal cation complexed to the conjugate base of the acid) [194, 196]. In HNO_3 and HCl, both cavity-based and ion associated extraction mechanisms may occur, but neither is sufficient for extraction of radium and actinium, both of which are large and relatively Lewis basic ions that are out-competed for the position in the cavity of the crown by the hydronium ion [5, 195].

To determine the effect of RB on the extraction, the batch study was also performed with the blank basic solutions as shown in Fig. 9.5. Both actinium and radium have some affinity for the resin out of basic solutions. The extracted species are most likely $Ra(OH)_2$ and $Ac(OH)_3$ interacting 1:1 with DtBu18C6 as both elements begin to extract around the pH of formation of the neutral hydroxide species. Actinium does not form hydroxides until above pH 9.41 [5, 209], and here it does not extract at pH 9.24 and below, but begins to extract at pH 10.95. There is a lack of detailed data for radium hydroxide formation as a function of pH, but it is relatively basic like actinium [212] and would be expected to behave similarly, which is seen here.

Based on the results presented in Figs. 9.3 and 9.5, it can be seen that RB not only extends the pH range in which actinium and radium can be extracted, but also significantly

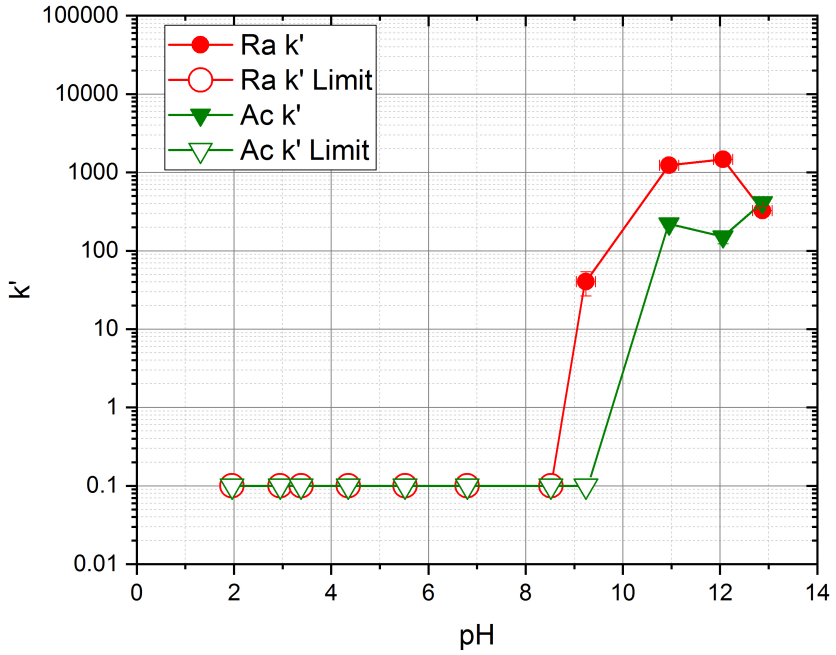

Figure 9.5: The batch uptake (k') of ^{228}Ac and ^{223}Ra from the blank solutions as a function of pH on Pb resin with a 3 hour equilibration time. Errors are propagated from the standard deviation of replicates.

stabilizes the extracted complex leading to the extremely high k' values shown in Fig. 9.3. This agrees with previous reports in the literature that the use of large counter ions with crown ethers can favor the extraction of bigger metal cations [194].

Kinetics Studies

The data from the batch studies indicated that both radium and actinium have a strong affinity for DtBu18C6 from blank basic solutions as well as the RB solutions. Kinetics studies were done in both RB and blank solutions (Fig. 9.6) to determine how rapid the extraction is and to assess the feasibility of column separations. Radium uptake from RB solutions was extremely high at the peak extraction, so to ensure that good counting statistics could be obtained from the aqueous phase, the kinetics were not measured at the peak extraction (pH 7.93), but at pH 12.06, which has a slightly lower, but still very high, extraction. Actinium uptake was not as high as radium from the RB solutions, so the kinetics were measured at both the peak extraction (pH 5.21) and a lower point (pH 10.88), which was of interest for column studies as there is a significant difference between the behavior of radium and

actinium at this point in the batch study and the kinetics would show if a column separation was feasible. The blank kinetics were measured at pH 12.06 for both radium and actinium.

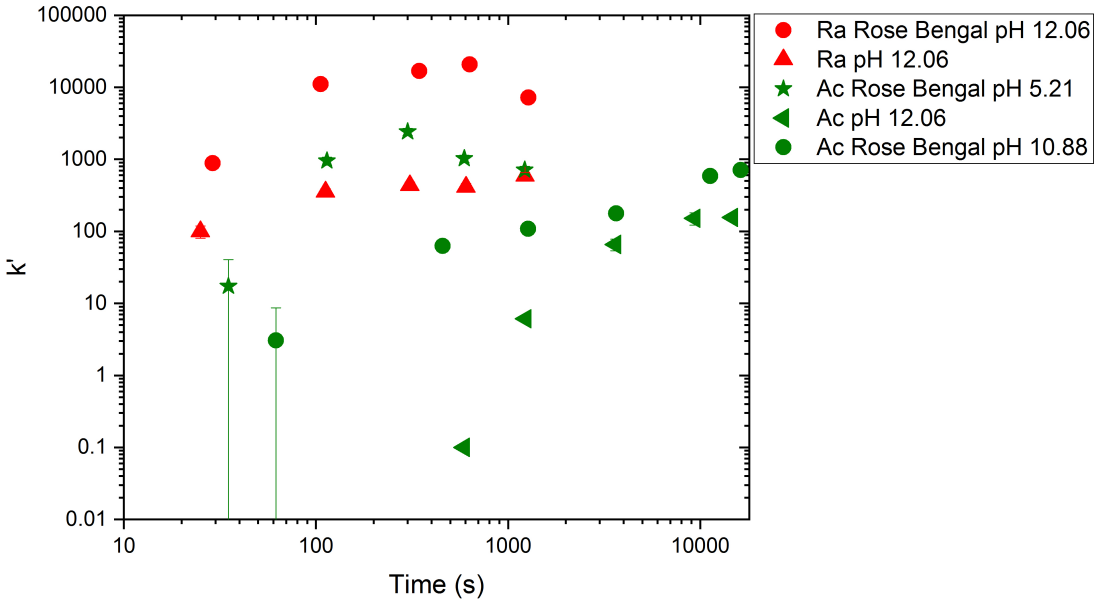

Figure 9.6: Kinetics of uptake for ^{223}Ra and ^{228}Ac at various pH values in the blank and RB solutions. Errors are propagated from the statistical counting error.

As can be seen from Fig. 9.6, even for very short mixing times (<45 s) the uptake of radium is high in both the blank and RB solutions (k' >100). As in the batch studies (Fig. 9.3), the presence of RB makes the extraction much stronger, even on a short timescale. Actinium uptake is much slower than radium and it does not begin to significantly extract in the RB solutions until more than 100 s have elapsed. In the blank solutions, the kinetics are even slower, with no significant extraction until ∼15 minutes. The slower extraction of actinium may be due to steric hindrance as Ac(III) requires more than one RB molecule to provide charge balance.

Column Studies

The batch studies showed that actinium and radium have very similar uptake parameters in this extraction system. Therefore, a column separation would be difficult as it would rely only on the differences in the kinetics of uptake between the two elements. However, columns were still performed to show the behavior of each element in a column study and to determine the feasibility of radium/actinium separations. Based on the results of the kinetics studies (Fig. 9.6), under fast flow rates (∼2 mL/min) actinium may bleed off the

column and be separated from radium, which should be rapidly and strongly retained on the resin due to its extremely high k' values and rapid uptake kinetics.

The first column (Fig. 9.7) had a load solution of RB Solution #10 (see Table 9.1), a condition where both radium and actinium have uptake on the resin, though actinium less so than radium. This column was eluted with RB Solution #10, followed by Blank Solution #10 (pH 12.06) and then stripped with Blank Solution #1 (pH 1.96). Due to the slow kinetics of extraction for actinium in the load solution, it is possible to elute 84.1 ± 6.4% of the actinium under a fast flow rate (∼2 mL/min) with no elution of radium. The remainder of the actinium activity elutes with the radium fraction. Total recovery of radium and actinium was within error of 100%; yields for all columns are given in Table 9.4.

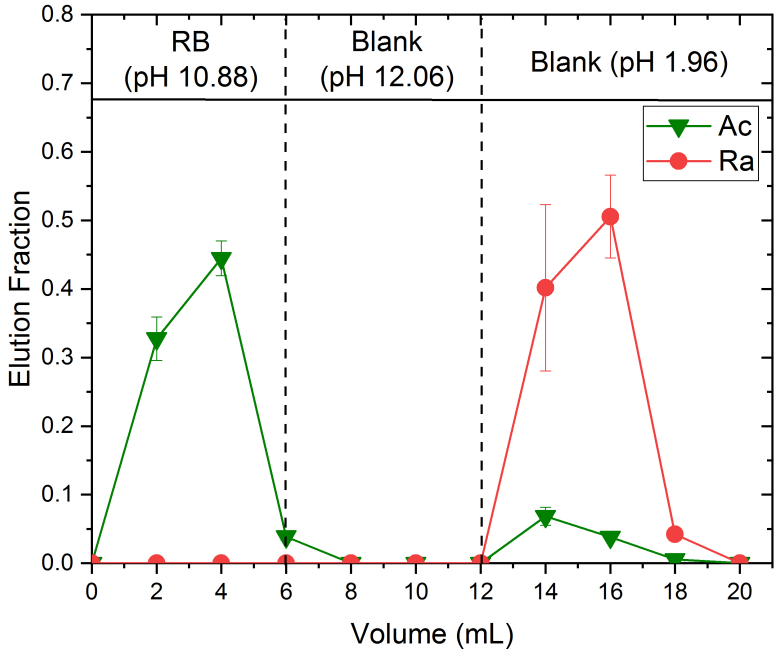

Figure 9.7: First column elution of 2 mL pre-packed Eichrom Pb resin cartridges at ∼2 mL/min flow rates; 2 mL fractions volumes. Error propagated from the statistical counting error; lines are to guide the eye.

Table 9.4: Column yields for ^{228}Ac and ^{223}Ra.

Column	**Total Yield (%)**	
	^{228}Ac	**^{223}Ra**
1	95.3 ± 8.1	95.0 ± 6.6
2	102.8 ± 5.6	77.4 ± 23.4
3	68.1 ± 10.0	69.7 ± 21.5

A second column (Fig. 9.8) was done using only the blank solutions. As with the previous column, the load solution was chosen to correspond to a point in the batch study where both radium and actinium had an affinity for the resin, but the uptake of radium was stronger. The load solution was Blank Solution #10 (pH 12.06) and, as before, the slow uptake kinetics of actinium result in 60.1 ± 5.6% of the actinium bleeding off the column immediately, with no co-elution of radium. The total yield for both actinium and radium is within error of 100% (Table 9.4), although the yield for radium has a large error due to poor counting statistics as less activity was used for this column.

The final column (Fig. 9.9) was loaded at the pH of maximum extraction for actinium, which is RB Solution #4 (pH 5.21), to determine if it was possible to retain both elements on the column. Under this condition, both radium and actinium are retained on the column, however, the elution yields for both were lower, with some retention on the column even after stripping with conc. HCl. A distinct purple-red band formed at the top of this column from the RB and, unlike first column which was also loaded with an RB solution, this band did not fully disappear with the subsequent elutions of Blank Solution #1 or conc. HCl. This band may have entrained some of the radium and actinium in a less reversible manner than when the column was loaded at a higher pH, though it is unclear why that may have occurred. Elution with nitric acid, while it was not attempted here, may have been able to remove the remaining actinium and radium through oxidation of extractant.

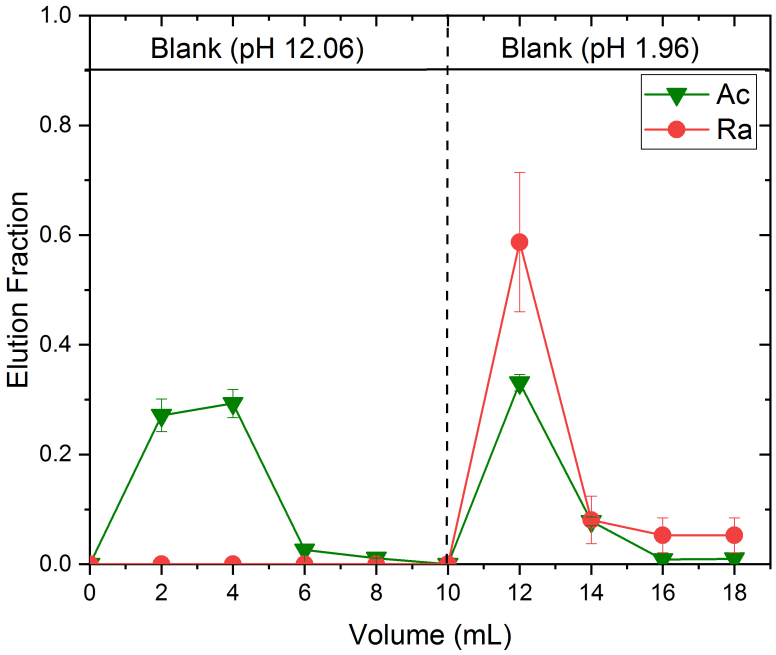

Figure 9.8: Second column elution of 2 mL pre-packed Eichrom Pb resin cartridges at ∼2 mL/min flow rates; 2 mL fractions volumes. Error propagated from the statistical counting error; lines are to guide the eye.

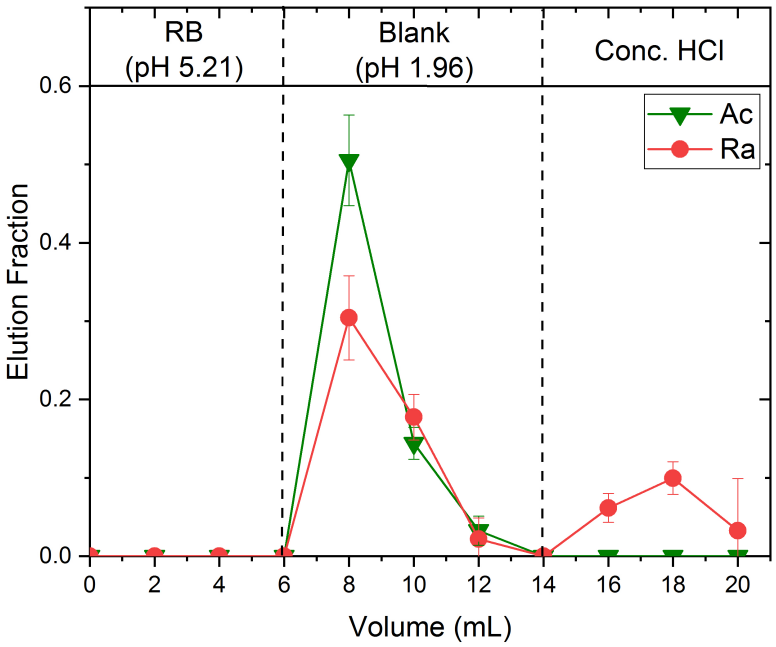

Figure 9.9: Third column elution of 2 mL pre-packed Eichrom Pb resin cartridges at ∼2 mL/min flow rates; 2 mL fractions volumes. Error propagated from the statistical counting error; lines are to guide the eye.

9.4 Conclusion

Batch and kinetics uptake studies as well as column studies were performed to evaluate the extraction of radium and actinium with crown ether-RB systems. Both radium and actinium have a high affinity for the resin and in much milder conditions than the extractions with super acids that have been demonstrated for these elements previously on this resin [194]. Batch studies show that in the blank basic solutions, radium and actinium both have some affinity for the resin, likely due to a cavity-based extraction of the neutral hydroxide species. The presence of RB in the solutions significantly increases the magnitude and pH range of uptake with high extraction (k' ∼10,000) of radium from pH 5 to 12 and actinium from pH 5 to 7. The maximum extraction for radium is at pH 8 with k' ∼40,000 and the maximum extraction for actinium is at pH 5 with k' ∼20,000. This agrees with previous reports in the literature that large counter ions favor the extraction of larger metal cations [194]. Based on analogous structures reported in the literature for lanthanum, cesium, and barium as well as calculations of actinium-macrocycle coordination complexes, the extracted forms are hypothesized to be $Ra(18C6) \cdot RB$ and $[Ac(18C6)]_2 \cdot 3RB$. The uptake kinetics for radium are extremely fast in both the blank and RB solutions, but slower for actinium, particularly in the blank solutions.

While the similar behavior of radium and actinium in this system limits the possibilities for separations of radium and actinium, column studies were performed to show both elements can be retained on a column in RB solutions. By employing a fast flow rate, actinium can be separated from radium with reasonable yields and high radiopurity. Further studies will be done to determine if the crown ether-RB extraction system studied in this work could be applied to separations of actinium and radium from the lanthanides and thorium, as these metals are significantly less basic and are expected to behave differently in these solutions.

Both radium and actinium are notoriously difficult to complex, and the vast majority of studies focus on acidic conditions [5, 185, 195]. Therefore, while the results presented here did not lead to a definitive separation of actinium and radium, they show a system which has an extremely strong binding of both metal cations, which has implications for future complexation studies of radium and actinium. These results highlight the benefits of exploring the chemistry of these relatively basic cations in neutral to basic solutions with large counter ions as a path forward for future development of separation and binding systems for radium and actinium.

Chapter 10

Conclusion

The goal of this dissertation was to measure the ^{230}Th(p,2n)^{229}Pa reaction cross section in the energy range of 14 to 17 MeV to assess the feasibility of using this reaction to produce ^{225}Ac via the decay of ^{229}Pa. This was achieved through numerous experimental steps, starting with obtaining the ^{230}Th enriched target material and culminating with gamma-ray spectroscopy of protactinium samples obtained from chemical processing of the irradiated targets.

While ^{230}Th has many research applications beyond isotope production and is naturally occurring, it is not commercially available. Therefore, the target material for this work was separated from a high grade uranium ore that was naturally enriched in ^{230}Th. A procedure to separate thorium from the ore through a multi-step chemical process was developed. The ore was leached sequentially with HNO_3 and HCl, then a liquid-liquid extraction was performed with TBP. After the liquid-liquid extraction, thorium was precipitated twice, first as a fluoride and then a hydroxide, before a final separation with anion exchange chromatography. The total yield of ^{230}Th in this process was 71.1 $\pm$ 5.4%. The final product was 91.32 $\pm$ 0.77 mg of thorium with a purity of 99.5 $\pm$ 1.2 wt. %.

After obtaining the thorium, it was necessary to determine methods to electrodeposit the material to make accelerator targets as well as develop the chemical separations that would be used to process the targets following the irradiation. These studies required tracer isotopes of thorium, since most natural thorium isotopes do not have readily detectable gamma-ray lines, and protactinium, to develop chemical separations for protactinium and serve as a yield tracer for the target processing following the irradiations. Using a procedure from the literature, ^{227}Th was obtained from the ^{231}Pa decay chain with a single column separation that removes ^{231}Pa from its daughter products and retains ^{227}Ac on a cation column, from which ^{227}Th can be regularly eluted. This isotope generator was in use for over a year without breakthrough of either ^{227}Ac or ^{225}Ra. A ^{237}Np/^{233}Pa isotope generator was also made and fully characterized. It had an average yield of 75 $\pm$ 1% and was eluted weekly for over a year before breakthrough occurred. As 98.6 $\pm$ 0.3% of the total ^{233}Pa activity was collected in the second fraction, this isotope generator was ideal for producing a tracer isotope with a small volume and high activity.

Numerous electrodeposition methods were studied to make thorium targets for the irradiations. Natural thorium oxide targets with a variety of thicknesses (∼650 to 2200 μg ThO_2/cm^2) were made on titanium and platinum. On both backings, the deposits were highly uniform, adherent and had no apparent damage after irradiation with 16 MeV protons for ∼5 hours at CAMS. The thorium targets required chemical processing after the irradiations to measure the activity of the protactinium activation products and extensive studies were performed to determine a suitable procedure. The chemistry was optimized to be rapid, high yield and high radiopurity. The targets were dissolved in HCl - HF solutions and loaded onto Dowex 1x8 anion exchange resin columns, which were eluted with HCl and HCl - HF solutions. On these columns, protactinium eluted largely in the fifteenth fraction with a reasonable yield (∼60%) and high radiopurity (∼99%). The total protactinium yield was ∼90%.

With procedures established for the target fabrication and target processing, targets were made for the ^{230}Th(p,xn) cross section measurements from the thorium material separated from uranium ore. Several irradiations were conducted at CAMS and excitation functions were measured for the ^{230}Th(p,2n)^{229}Pa and ^{230}Th(p,3n)^{228}Pa reactions from 14.1 to 16.9 MeV. The peak measured cross section of the ^{230}Th(p,2n)^{229}Pa reaction was 182 ± 12 mb at 14.4 ± 0.1 MeV. As part of the electrodeposition work, methods of electrodepositing ^{231}Pa were studied as well to characterize a method for making thin protactinium alpha sources. While this technique was not used in the process of making the cross section measurement, it was used to make measurements of the ^{231}Pa gamma-ray energies and intensities. The measured gamma-ray energies and intensities are in good agreement with previous measurements and with reduced error for the major gamma-ray lines, in some cases by as much as an order of magnitude.

Further chemical separation studies were also done with CL resin (TrisKem International) as there is little data available on this resin in the literature. It was characterized with batch, kinetics and columns studies with radium, actinium, thorium and protactinium in HNO_3, HCl and HF. The extraction of radium and actinium by Pb resin and Rose Bengal was also studied. As noted previously, actinium and radium are notoriously difficult to complex, however, high extraction (k' ∼10,000) of both elements was demonstrated with the Pb resin-Rose Bengal system in neutral to basic solutions.

In the measurement of this cross section and the associated experiments, a considerable amount of nuclear data measurements were done. Two excitation functions were reported that have not been previously presented in the literature, which could provide bench marking data for nuclear codes to improve future calculations. The half-life of ^{228}Pa, for which there are very few existing measurements in the literature, was measured based on its gamma-ray emissions. New measurements of the gamma-ray energies and intensities for the decay of ^{231}Pa to ^{227}Ac are presented with reduced error bars for some gamma-ray emissions, which may be useful for more accurate, non-destructive assays of the age of ^{235}U materials.

10.1 Implications for Isotope Production

As discussed previously, existing supplies of ^{225}Ac are limited and the demand for this isotope, as a promising TAT isotope, is high and expected to increase. Currently, there is no clear route producing ^{225}Ac on a large scale and numerous different reaction pathways have been proposed, but there have been research challenges with all of these production methods. The main production routes that have been considered are: ^{232}Th spallation, which has reasonable yields but low isotopic purity and difficult post-processing, and the ^{226}Ra(p,2n)^{225}Ac reaction, which has a high yield but several issues associated with the targets, including difficulty with obtaining the target material, fabricating and handling the targets. Therefore, other production routes and techniques are being considered, such as isotope separation or indirect production of ^{225}Ac via the decay of its parent isotopes (^{229}Pa, ^{229}Th and ^{225}Ra).

The ^{230}Th(p,2n)^{229}Pa reaction is one of the indirect production methods that has been considered, but previous studies on ^{230}Th reactions have been limited and, in particular, no ^{230}Th(p,xn) reaction cross section data is available in the literature. In this work, the excitation function of the ^{230}Th(p,2n)^{229}Pa reaction was measured from 14.1 to 16.9 MeV, with the energy range chosen based on cross section calculations in TENDL 2019. From the measured cross section data, this reaction may be reasonable for isotope production if relatively isotopically pure ^{230}Th is available.

There are several advantages to isotope production via this reaction: the isotopic purity is extremely high, the cross section peaks at a relatively low energy ($\sim$14 MeV), which is accessible on most medical cyclotrons as well as other accelerator facilities, and the target fabrication and processing is relatively simple, especially compared to thorium spallation targets or radium targets. The targets can be fabricated and transferred easily as they are non-reactive and low activity. Due to the low proton energies, there are not as many open reaction channels as in thorium spallation, so the target processing is simpler as fewer isotopes and less activity are produced. While the yield of ^{225}Ac is limited by the low alpha-decay branching ratio of ^{229}Pa and long half-life of ^{229}Th, the reaction may still be useful for significant ^{225}Ac production via long-term irradiations or for the production of small, highly pure ^{225}Ac samples for laboratory studies.

10.2 Future Work

There are many avenues for future studies based on this work. Cross sections for ^{230}Th(p,2n) ^{229}Pa and ^{230}Th(p,3n)^{228}Pa reactions could be characterized over a wider range of energies to more accurately determine the peak shapes and maxima of the excitation functions. Some studies at lower proton energies (10 to 14 MeV) may be possible as ride along experiments at CAMS in the future and could provide more data for the excitation function of the ^{230}Th(p,2n)^{229}Pa reaction. The ^{230}Th(p,3n)^{228}Pa reaction cross section is predicted to peak at 20 MeV, but, as CAMS can generally only achieve beam energies up to 18 MeV with reasonable current, further measurements of this excitation function would require the use

of another accelerator facility. The thorium material used in this work would be acceptable for studies at higher energies as the calculated peak of the ^{230}Th(p,3n)^{228}Pa reaction is well below the threshold (26.6 MeV) of the interfering reaction, ^{232}Th(p,5n)^{228}Pa [39].

Further extraction studies with radium and actinium will be the primary focus of future work. The promising results for radium and actinium extraction in neutral to basic solutions will be explored in future studies with novel extractants, particularly larger crown ethers and novel thia-crown ethers. Actinium prefers to form high coordination number complexes [5], is stable in high pH (>3) solutions and in some cases extracts better from these solutions [5, 213], is very large and shows a strong macrocyclic effect [5]. Therefore, its extraction with large macrocycles, such as 24-crown-8, and some novel thia-crown ethers, such as dibenzo-bis-oxo-tetrathia-18-crown-6, in a variety of pHs will be considered and the effect of large counter ions studied. The behavior of radium with large crown ethers (up to 30-crown-10) has been studied in acidic solutions for synergistic extractions [214], but based on the results presented in Chapter 9, its behavior in neutral to basic solutions with these crowns may be different and have the potential for greater extraction.

Bibliography

1. Elgqvist, J., Frost, S., Pouget, J. & Albertsson, P. The Potential and Hurdles of Targeted Alpha Therapy - Clinical Trials and Beyond. *Front Oncol* **3,** 324 (2013).
2. Morgenstern, A., Bruchertseifer, F. & Apostolidis, C. Bismuth-213 and Actinium-225 - Generator Performance and Evolving Therapeutic Applications of Two Generator-Derived Alpha-Emitting Radioisotopes. *Curr. Radiopharm.* **5,** 221–227 (2012).
3. Kratochwil, C. *et al.* Targeted Alpha Therapy of Metastatic Castration-Resistant Prostate Cancer with ^{225}Ac-PSMA-617: Swimmer-Plot Analysis Suggests Efficacy Regarding Duration of Tumor Control. *J Nucl Med* **795-802,** 59 (2018).
4. Morgenstern, A. *et al.* An Overview of Targeted Alpha Therapy with ^{225}Actinium and ^{213}Bismuth. *Current Radiopharmaceuticals* **11,** 200–208 (3 2018).
5. Thiele, N. & Wilson, J. Actinium-225 for targeted alpha therapy: Coordination Chemistry and current chelation approaches. *Cancer Biotherapy and Radiopharmaceuticals* **33,** 336–348 (2018).
6. Carithers, W. A Review On The Development of Targeted Alpha Therapy in the Treatment of Cancer. *Everyday Urology-Oncology Insights* **2** (2017).
7. Aliev, R. A. *et al.* Isolation of Medicine-Applicable Actinium-225 from Thorium Targets Irradiated by Medium-Energy Protons. *Solvent Extraction and Ion Exchange* **32,** 468–477 (2014).
8. Borchardt, P., Yuan, R., Miederer, M., McDevitt, M. & Scheinberg, D. Targeted Actinium-225 in Vivo Generators for Therapy of Ovarian Cancer. *Cancer Research* **63,** 5084–5090 (2003).
9. Robertson, A., Ramogida, C. F., Schaffer, P. & Radchenko, V. Development of ^{225}Ac Radiopharmaceuticals: TRIUMF Perspectives and Experiences. *Current Radiopharmaceuticals* **11,** 156–172 (2018).
10. Kratochwil, C. *et al.* ^{213}Bi-DOTATOC receptor-targeted alpha-radionuclide therapy induces remission in neuroendocrine tumours refractory to beta radiation: a first-in-human experience. *Eur J Nucl Med Mol Imaging* **41,** 2106–2119 (2014).
11. Griswold, J. *et al.* Large scale accelerator production of ^{225}Ac: Effective cross sections for 78-192 MeV protons incident on ^{232}Th targets. *Applied Radiation and Isotopes* **118,** 366–374 (2016).

12. Engle, J. *et al.* Ac, La, and Ce radioimpurities in ^{225}Ac produced in 40-200 MeV proton irradiations of thorium. *Radiochimica Acta* **102,** 569–581 (2014).

13. Boll, R., Malkemus, D. & Mirzadeh, S. Production of actinium-225 for alpha particle mediated radioimmunotherapy. *Applied Radiation and Isotopes* **62,** 667–679 (2005).

14. National Nuclear Data Center (NNDC) Brookhaven National Laboratory. Accessed: 2020-11-16. 2019.

15. Robertson, A. *et al.* ^{232}Th-Spallation-Produced ^{225}Ac with Reduced ^{227}Ac Content. *Inorganic Chemistry* **59,** 12156–12165 (2020).

16. Fitzsimmons, J., Griswold, J., Medvedev, D., Cutler, C. & Mausner, L. Defining Processing Times for Accelerator Produced ^{225}Ac and Other Isotopes from Proton Irradiated Thorium. *Molecules* **24,** 1095 (2019).

17. Bernstein, L., Batchelder, J., Morrell, J. & Voyles, A. *Systems and methods for producing actinium-225* World Intellectual Property Organization. International Publication Number: WO2020210147A1. 2020. `https://patents.google.com/patent/WO2020210147A1/en`.

18. Zhuikov, B. *et al.* Production of ^{225}Ac and ^{223}Ra by irradiation of Th with accelerated protons. *Radiochemistry* **53,** 73–80 (2011).

19. Koch, L., Apostolidis, C., Janssens, W., Molinet, R. & Geel, J. V. Production of Ac-225 and application of the Bi-213 daughter in cancer therapy. *Czechoslovak Journal of Physics* **49,** 817–822 (1999).

20. Stracener, D. *R and D on Accelerator-Based Production of ^{229}Th* in (2011 Nuclear Physics (NP) Review, Oak Ridge, TN, 2011).

21. Jost, C., Griswold, J., Bruffey, S., Miradeh, D. S. & Williams, C. Measurement Of Cross Sections For The ^{232}Th(p, 4n)^{229}Pa Reaction At Low Proton Energies. *Application of Accelerators in Research and Industry* **1525,** 520–524 (2013).

22. Boldeman, J. & Walsh, R. $\bar{v}_p$ for sub-barrier fission in ^{230}Th. *Physics Letters B* **62,** 149–152 (1976).

23. Yuen, G., Rizzo, G., Behkami, A. & Huizenga, J. Fragment angular distributions of the neutron-induced fission of ^{230}Th. *Nuclear Physics A* **171,** 614–624 (1971).

24. Sicre, A. *et al.* Fission-fragment angular distributions for ^{230}Th(n,f) in the vicinity of the 715 keV resonance. *Nuclear Physics A* **445,** 37–56 (1985).

25. Levona, A. *et al.* The nuclear structure of ^{229}Pa from the ^{231}Pa(p,t)^{229}Pa and ^{230}Th (p,2nγ)^{229}Pa reactions. *Nuclear Physics A* **576,** 267–307 (1994).

26. Grafen, V., Ackermann, B., Baltzer, H., Bihn, T. & Gunther, C. Does a $5/2^+$ - $5/2^+$ ground-state parity doublet exist in ^{229}Pa? *Phys. Rev. C* **44,** 1728 (1991).

27. Burke, D., Garrett, P. & Qu, T. Levels in ^{227}Ac populated in the ^{230}Th(p,α) reaction. *Nuclear Physics A* **724,** 274–288 (2003).

28. Koning, A. *et al.* TENDL-2015: TALYS-based evaluated nuclear data library. *IAEA, PSI, CEA Bruyeres-le-Chatel, CCFE* **26** (Dec. 2015).
29. Koning, A., Rochman, D. & Sublet, J. TENDL-2017: TALYS-based evaluated nuclear data library. *IAEA, PSI, CEA Bruyeres-le-Chatel, CCFE* **29** (Dec. 2017).
30. Koning, A. *et al.* TENDL: Complete Nuclear Data Library for Innovative Nuclear Science and Technology. *Nuclear Data Sheets* **155,** 1–55 (2019).
31. *PETtrace 800 cyclotron series* General Electric Company. Accessed: 2020-2-16. 2017.
32. Nirdosh, I. Removal of ^{230}Th by Solvent Extraction from High Grade Uranium Ore Liquid Tailings to Arrest ^{226}Ra Production in the Tailings. *The Canadian Journal of Chemical Engineering* **80,** 525–529 (2002).
33. Livingston, R. *Electromagnetic Reserach Division: Quarterly Progress Report for Period Ending September 30, 1953* (Oak Ridge National Laboratory, Oak Ridge TN, 1952).
34. Love, L. & Bell, W. *Review of ORNL Electromagnetic Separations Program, 1968 - 1969* (Oak Ridge National Laboratory, Oak Ridge TN, 1971).
35. Harmatz, B., McCurdy, H. & Case, F. *Catalog of Uranium, thorium and plutonium isotopes* (Oak Ridge National Laboratory, Oak Ridge TN, 1954).
36. Tracy, J. Status of the isotope enrichment program at Oak Ridge National Laboratory. *Nuclear Instruments and Methods in Physics Research Section A: Accelerators, Spectrometers, Detectors and Associated Equipment* **303,** 3–8 (1991).
37. *Product Catalog* National Isotope Development Center `https://www.isotopes.gov/catalog`. Accessed: 2021-03-25. 2021.
38. Griswold, J. *et al.* Production of ^{229}Th for medical applications: Excitation functions of low-energy protons on ^{232}Th targets. *Phys. Rev. C* **98,** 044607 (2018).
39. *Q-value Calculator* National Nuclear Data Center (NNDC) Brookhaven National Laboratory. Accessed: 2020-11-16. 2019.
40. Wang, M. *et al.* The AME2016 atomic mass evaluation (II). Tables, graphs and references. *Chinese Physics C* **41,** 030003 (2017).
41. Soppera, N., Dupont, E. & Fleming, M. JANIS Books. *OECD NEA Data Bank* **12** (Sept. 2020).
42. Peppard, D., Mason, G. & Gergel, M. The mutual separation of thorium, protoactinium, and uranium by tributyl phosphate extraction from hydrochloric acid. *Journal of Inorganic and Nuclear Chemistry* **3,** 370–378 (1957).
43. Kluge, E., Lieser, K., Loc, I. & Quandt, S. Separation of ^{230}Th (Ionium) from Uranium Ores in Sulfuric Acid and in Nitric Acid Solutions. *Radiochimica Acta* **24,** 21–26 (1997).

44. Carswell, D., Fletcher, J. & Clelland, D. The recovery of thorium-230 from uranium wastes. *Journal of Inorganic and Nuclear Chemistry* **5,** 147–152 (1957).

45. Meija, J. *et al.* Atomic weights of the elements 2013 (IUPAC Technical Report). *Pure and Applied Chemistry* **88,** 265–291 (2016).

46. Turner, S., van Calsteren, P., Vigier, N. & Thomas, L. Determination of thorium and uranium isotope ratios in low concentration geological materials using a fixed multi-collector-ICPMS. *J. Anal. At. Spectrom.* **16,** 612–615 (2001).

47. Ziegler, J., Biersack, J. & Littmark, U. *The Stopping and Range of Ions in Matter, New York: Pergamon Press* (1985).

48. Zhao, J., Yu, K. & Feng, Y. High-precision ^{238}U-^{234}U-^{230}Th disequilibrium dating of the recent past: a review. *Quaternary Geochronology* **4,** 423–433 (2009).

49. Cheng, H. *et al.* Improvements in ^{230}Th dating, ^{230}Th and ^{234}U half-life values, and U-Th isotopic measurements by multi-collector inductively coupled plasma mass spectrometry. *Earth and Planetary Science Letters* **371-372,** 82–91 (2013).

50. Goldblum, B. *et al.* Indirect determination of the ^{230}Th(n, f) and ^{231}Th(n, f) cross sections for thorium-based nuclear energy systems. *Phys Rev C* **80,** 044610 (2009).

51. Singh, J. A New Concept for Searching for Time-Reversal Symmetry Violation Using Pa-229 Ions Trapped in Optical Crystals. *Hyperfine Interact* **240,** 29 (2019).

52. Zhuikov, B. *et al.* Production of ^{225}Ac and ^{223}Ra by Irradiation of Th with Accelerated Protons. *Radiochemistry* **53,** 73–80 (2011).

53. Peppard, D. *et al.* Studies of the Solvent Extraction Behavior of the Transition Elements. II. Isolation of Gram Quantities of ^{230}Th (Ionium) from a Pitcheblende Residue. *J Am Chem Soc* **75,** 4576–4578 (1953).

54. Loveland, W., Morrissey, D. & Seaborg, G. *Modern Nuclear Chemistry* (John Wiley and Sons, Inc, Hoboken, NJ, 2006).

55. Council, N. R. *Uranium Mining in Virginia: Scientific, Technical, Environmental, Human Health and Safety, and Regulatory Aspects of Uranium Mining and Processing in Virginia* 96–119 (The National Academies Press, Washington, DC, 2012).

56. Sato, T. Extraction of Uranium (VI) and Thorium from Nitric Acid Solutions by Tri-n-Butyl Phosphate. *J Appl Chem* **15,** 489–495 (1965).

57. Orabi, A. Determination of uranium after separation using solvent extraction from slightly nitric acid solution and spectrophotometric detection. *Journal of Radiation Research and Applied Sciences* **6,** 1–10 (2013).

58. Ishimori, T. & Nakamura, E. *Data of Inorganic Solvent Extraction. Part I* (Japan Atomic Energy Research Inst., Tokyo, 1963).

59. Healy, T. & McKay, H. Complexes Between Tributyl Phosphate and Inorganic Nitrates. *Recueil* **75,** 730–736 (1965).

60. Steinnes, E. Precise and rapid determination of trace amounts of uranium in inorganic samples by neutron activation and TBP extraction. *Analytica Chimica Acta* **76,** 461–463 (1975).

61. Altas, Y., Tel, H. & Eral, M. Anion-exchange separation and determination of throium and uranium in Eskisehir-Beylikahir ore in Turkey. *Journal of Radioanalytical and Nuclear Chemistry* **241,** 637–641 (1999).

62. Verma, P. *et al.* Structural investigations on uranium(VI) and thorium(IV) complexation with TBP and DHOA: a spectroscopic study. *New J. Chem.* **42,** 5243–5255 (2018).

63. Brown, D. & Whittaker, B. A new simple procedure for the recovery and purification of protactinium-231. *Journal of the Less Common Metals* **61,** 161–170 (1978).

64. Hyde, E. *The Radiochemistry of Thorium* (Subcommittee on Radiochemistry National Academy of Sciences - National Research Council, Oak Ridge, TN, 1960).

65. Faris, J. & Buchanan, R. Anion Exchange Characteristics of the Elements in Nitric Acid Medium. *Anal. Chem* **36,** 1157–1158 (1964).

66. Kirby, H. *The Radiochemistry of Protactinium* (Subcommittee on Radiochemistry National Academy of Sciences - National Research Council, Miamisburg, OH, 1959).

67. Saliba-Silva, A., Linardi, M., Rocha, L. D. S. & Durazzo, M. Thorium-234 Electrodeposition Using Ionic and Aqueous Uranyl Solutions. *ECS Transactions* **66,** 11–20 (2015).

68. Gindler, J. *The Radiochemistry of Uranium* p. 215 (Subcommittee on Radiochemistry National Academy of Sciences - National Research Council, Argonne, IL, 1962).

69. Harvey, B. & Lovett, M. The use of yield tracers for the determination of alpha-emitting actinides in the marine environment. *Nuclear Instruments and Methods in Physics Research* **223,** 224–234 (1984).

70. Zemel, B. *Tracers in the Oil Field* (Amsterdam: Elsevier, 1995).

71. Blinova, O., Aliev, R. & Sapozhnikov, Y. in *Proceedings of the First International Meeting on Applied Physics (APHYS-2003), Badajoz, Spain* (2003).

72. Guseva, L. & Tikhomirova, G. Optimization of Conditions for Isolation of Short-Lived ^{211}Pb Using a Cation Exchanger and Aqueous-Organic HCl Solutions as Eluents. A ^{223}Ra-^{211}Pb Generator. *Radiochemistry* **46,** 168–171 (2004).

73. Kmak, K., Despotopulos, J. & Shaughnessy, D. ^{210}Pb/^{210}Po isotope generator. *Journal of Radioanalytical and Nuclear Chemistry* **319,** 257–261 (2019).

74. Dash, A. & Bhattacharyya, P. Preparation of a ^{90}Sr-^{90}Y generator using zirconium antimonate. *Applied Radiation and Isotopes* **45,** 415–417 (1994).

75. Lebowitz, E. & Richards, P. Radionuclide generator systems. *Seminars in Nuclear Medicine* **4,** 257–268 (1974).

76. Chajduk, E., Doner, K., Polkowska-Motrenko, H. & Bilewicz, A. Novel radiochemical separation of arsenic from selenium for ^{72}Se/^{72}As generator. *Applied Radiation and Isotopes* **70,** 819–822 (2012).

77. Despotopulos, J., Kmak, K., Moody, K. & Shaughnessy, D. Development of a ^{212}Pb and ^{212}Bi generator for homolog studies of flerovium and moscovium. *Journal of Radioanalytical and Nuclear Chemistry* **317,** 473–477 (2018).

78. Grant, P., Erdal, B. & O'Brien, H. A ^{82}Sr-^{82}Rb isotope generator for use in nuclear medicine. *Journal of Nuclear Medicine* **16** (1975).

79. Molinski, V. A review of ^{99m}Tc generator technology. *The International Journal of Applied Radiation and Isotopes* **33,** 811–819 (1982).

80. Loveland, W., Morrissey, D. & Seaborg, G. in *Modern Nuclear Chemistry, Hoboken, NJ, John Wiley and Sons, Inc.* 57–87 (2006).

81. Baas-May, A., Kratz, J. & Trautmann, N. Absence of delayed fission in the β^--decay of 23 min ^{238}Pa. *Zeitschrift fur Physik A Atoms and Nuclei* **322,** 457–462 (1985).

82. Chu, Y. & Zhou, M. Comparison of the (p,xn) Cross Sections from ^{238}U, ^{235}U and ^{232}Th Targets Irradiated with 200 MeV Protons. *IEEE Transactions on Nuclear Science* **30,** 1152–1155 (1983).

83. Sill, C. Purification of radioactive tracers for use in high sensitivity alpha spectrometry. *Anal. Chem.* **46,** 1426–1431 (1974).

84. Nakanishi, T. *et al.* Successive determinations of ^{210}Pb, ^{210}Po, ^{226}Ra, ^{228}Ra and selected actinides in seawater and sea sediment. *Journal of Radioanalytical and Nuclear Chemistry* **138,** 321–330 (1990).

85. Bacon, M., Huh, C., Fleer, A. & Deuser, W. Seasonality in the flux of natural radionuclides and plutonium in the deep Sargasso Sea. *Deep Sea Research Part A. Oceanographic Research Papers* **32,** 273–286 (1985).

86. Byrne, A. & Benedik, L. Applications of neutron activation analysis in determination of natural and man-made radionuclides, including Pa-231. *Czechoslovak Journal of Physics* **49,** 263–270 (1999).

87. Eppich, G., Williams, R., Gaffney, A. & Schorzman, K. ^{235}U-^{231}Pa age dating of uranium materials for nuclear forensic investigations. *J. Anal. At.* **28,** 666–674 (2013).

88. Smith, G. & Barnett, G. The quantitative electrodeposition of tracer protactinium. *Journal of Inorganic and Nuclear Chemistry* **27,** 975–978 (1965).

89. Kirby, H. *The Radiochemistry of Protactinium* (Subcommittee on Radiochemistry National Academy of Science – National Reseach Council, Washington, DC, 1959).

90. Inoue, Y., Tochiyama, O. & Hamashima, S. Removal of ^{233}Pa from ^{237}Np using manganese dioxide or silica gel. *The International Journal of Applied Radiation and Isotopes* **29,** 561–565 (1978).

91. Knight, A., Nelson, A., Eitrheim, E., Forbes, T. & Schultz, M. A chromatographic separation of neptunium and Protactinium using 1-octanol impregnated onto a solid phase support. *Journal of Radioanalytical and Nuclear Chemistry* **307,** 59–67 (2016).
92. Ostapenko, V. *et al.* Sorption of Protactinium(V) on extraction chromatographic resins from nitric and hydrochloric solutions. *Journal of Radioanalytical and Nuclear Chemistry* **311,** 1545–1550 (2017).
93. Marsh, F. & Pillay, K. *Effects of ionizing radiation on modern ion exchange materials* (Los Alamos National Laboratory, Los Alamos, 1993).
94. Tereshatov, E. *et al.* Isocratic anion exchange separations of Group V elements. *Journal of Radioanalytical and Nuclear Chemistry* **286,** 9–16 (2010).
95. Burney, G. & Harbour, R. *The Radiochemistry of Neptunium* (Subcommittee on Radiochemistry National Academy of Sciences – National Research Council, Washington DC, 1974).
96. Marsh, S. *et al. Cation exchange of 53 elements in nitric acid* (Los Alamos Scientific Lab., Los Alamos, 1978).
97. Strelow, F., Rethemeyer, R. & Bothma, C. Ion Exchange Selectivity Scales for Cations in Nitric Acid and Sulfuric Acid Media with a Sulfonated Polystyrene Resin. *Anal. Chem.* **37,** 106–111 (1965).
98. Guseva, L. & Tikhomirova, G. Ion exchange behavior and separation of actinides in different oxidation state on cation exchangers in dilute solutions of hydrofluoric acid. *Radiokhimiya* **35,** 103–110 (1993).
99. Specht, S., Schutz, B. & Born, H. Development of a high-pressure ion-exchange system for raid preparative separations of trans-uranium elements. *J Radioanal Chem* **21,** 167–176 (1974).
100. Wrenn, M., Singh, N., Ibrahim, S. & Cohen, N. Thorium-229 as an Isotopic Tracer for the Radiochemical Determination of Thorium Isotopes in Biological Samples. *Anal. Chem.* **50,** 1712–1714 (1978).
101. Moore, W. & Sackett, W. Uranium and thorium series inequilibrium in sea water. *Journal of Geophysical Research* **69,** 5401–5405 (1964).
102. Bhatki, K. Production of Thorium-234 Tracer. *Anal. Chem.* **39,** 401–403 (1967).
103. De Lavison, P. *et al.* The standardisation of Th-229 for an environmental yield tracer. *Applied Radiation and Isotopes* **53,** 243–249 (2000).
104. Rosholt, J. Radioisotope dilution analyses of geological samples using ^{236}U and ^{229}Th. *Nuclear Instruments and Methods in Physics Research* **223,** 572–576 (1984).
105. Kandlbinder, R., Geissler, V., Schupfner, R., Wolfbeis, O. & Zinka, B. Analysing of ^{228}Th, ^{232}Th, ^{228}Ra in human bone tissues for the purpose of determining the post mortal interval. *Journal of Radioanalytical and Nuclear Chemistry* **280,** 113–119 (2009).

106. Glover, S., Filby, R. & Clark, S. Determination of ^{232}Th in human tissues by preconcentration neutron activation analysis with yield determination using ^{227}Th. *Journal of Radioanalytical and Nuclear Chemistry* **234,** 65–70 (1998).

107. Monsecour, M., de Regge, P. & Baetsle, L. Radioanalytical methods for the accurate determination of ^{227}Ac and ^{228}Th in irradiated ^{226}Ra targets. *Journal of Radioanalytical Chemistry* **35,** 185–196 (1977).

108. Henriksen, G., Hoff, P., Alstad, J. & Larsen, R. 223Ra for endoradiotherapeutic applications prepared from an immobilized ^{227}Ac/^{227}Th source. *Radiochimica Acta* **89,** 661–666 (2009).

109. Abou, D. *et al.* Automated Production of Alpha-Emitting Therapeutic Radionuclides. *Journal of Medical Imaging and Radiation Sciences* **50,** S33 (2019).

110. Brown, D. & Whittaker, B. A new simplified procedure for the recovery and purification of Protactinium-231. *Journal of Less Common Metals* **61,** 161–170 (1978).

111. Trautmann, N. & Folger, H. Preparation of Actinide Targets by Electrodeposition. *Nuclear Instruments and Methods in Physics Research* **A282,** 102–106 (1989).

112. Aumann, D. & Mullen, G. Preparation of targets of Ca, Ba, Fe, La, Pb, Tl, Bi, Th and U by electrodeposition from organic solutions. *Nuclear Instruments and Methods* **115,** 75–81 (1974).

113. Eberhardt, K. *et al.* Preparation of targets for the gas-filled recoil separator TASCA by electrochemical deposition and design of the TASCA target wheel assembly. *Nuclear Instruments and Methods in Physics Research Section A: Accelerators, Spectrometers, Detectors and Associated Equipment* **590,** 134–140 (2008).

114. Yaffe, L. Preparation of thin films, Sources, and Targets. *Annual Review of Nuclear Science* **12,** 153–188 (1962).

115. Parker, W., Bildstein, H. & Getoff, N. Molecular plating I, a rapid and quantitative method for the electrodeposition of thorium and uranium. *Nuclear Instruments and Methods* **26,** 55–60 (1964).

116. Shimojima, H. & Takagi, J. Electrodeposition of protactinium. *Journal of Inorganic and Nuclear Chemistry* **26,** 253–255 (1964).

117. Kim, S., Noakes, J., Akers, L. & Miller, W. *Electrodeposition of Actinides and Lanthanides* (Oak Ridge Institute of Nuclear Studies, INc., Oak Ridge, TN, 1965).

118. Sakanoue, M., Takagi, T. & Maeda, M. Studies of the Adsorption and Electrodeposition of Protactinium. *Radiochimica Acta* **5,** 79–87 (1965).

119. Crespo, M. A review of electrodeposition methods for the preparation of alpha-radiation sources. *Applied Radiation and Isotopes* **70,** 210–215 (2012).

120. Wakita, H., Nagasawa, H., Uyeda, S. & Kuno, H. Uranium, thorium and potassium contents of possible mantle materials. *Geochemical Journal* **1,** 183–198 (1967).

121. Prakash, S., Singh, R. & Ramaniah, M. Electrodeposition of protactinium. *Inorganic and Nuclear Chemistry Letters* **8,** 113–117 (1972).

122. Parker, W. & Falk, R. Molecular plating: A method for the electrolytic formation of thin inorganic films. *Nuclear Instruments and Methods* **16,** 355–357 (1962).

123. Burnett, W., Baker, K., Chin, P., McCabe, W. & Ditchburn, R. Uranium-series and AMS ^{14}C studies of modern phosphatic pellets from Peru shelf muds. *Marine Geology* **80,** 215–230 (1988).

124. Knight, A., Eitrheim, E., Nelson, A., Nelson, S. & Schultz, M. A simple-rapid method to separate uranium, thorium, and protactinium for U-series age-dating of materials. *Journal of Environmental Radioactivity* **134,** 66–74 (2014).

125. Prabhu, S., Sawant, P. & Bhati, S. Standardization of radiochemical procedure for the estimation of protactinium in bioassay samples. *Radiation Protection and Environment* **33,** 137–139 (2010).

126. Price, P. *et al.* Emission of ^{23}F and ^{24}Ne in cluster radioactivity of ^{231}Pa. *Phys. Rev* **46,** 1939–1945 (1992).

127. Saettel, M. Thorium Target Thickness From Radioactivity Measurement. *Nuclear Intstruments and Methods* **200,** 87–90 (1982).

128. Fowler, M., Gursky, J. & Wilhelmy, J. Preparation of actinide targets and sources using nonaqueous electrodeposition. *Nuclear Instruments and Methods in Physics Research* **A303,** 99–101 (1991).

129. Hao, L. *et al.* Rapid preparation of Uranium and Thorium alpha sources by electroplating technique. *Kerntechnik* **75,** 381–385 (2010).

130. Takagi, J. & Shimojima, H. Studies on protactinium (V) in sulphuric acid solution - I: Centrifugation study. *Journal of Inorganic and Nuclear Chemistry* **27,** 405–409 (1965).

131. Evans, J., Lougheed, R., Coops, M., Hoff, R. & Hulet, E. The use of electrodeposition methods to prepare actinide targets for cross-section measurements and accelerator bombardments. *Nuclear Instruments and Methods* **102,** 398–401 (1972).

132. Landis, V. & Kaye, J. *The radiochemistry of titanium* (Subcommittee on Radiochemistry National Academy of Sciences- National Research Council, 1971).

133. Kateley, J., Tschetter, M. & Chiotti, P. Reaction of thoria with zirconium chloride. *Journal of the Less Common Metals* **26,** 145–155 (1972).

134. Crouthamel, C., Knapp, W., Skladzien, S. & Loeding, J. Preparation of high-density, spherical thorium oxide particles with up to 10 atom percent uranium. *Argonne National Lab.* (1961).

135. *Flame Temperatures Gases* Engineering ToolBox. Accessed: 2020-10-23. 2003. `https://www.engineeringtoolbox.com/flame-temperatures-gases-d_422.html`.

136. Chaudhury, S., Keskar, M., Patil, A., Mudher, K. S. & Venugopal, V. Studies on the dissolution behaviour of ThO_2 and (U, Th)O_2 by a solid state reaction method. *Radiochimica Acta* **94,** 357–361 (2009).

137. Takeuchi, T., Hanson, C. & Wadsworth, M. Kinetics and mechanism of the dissolution of thorium oxide in hydrofluoric acid and nitric acid mixtures. *Journal of Inorganic and Nuclear Chemistry* **33,** 1089–1098 (1971).

138. Chu, S., Ekstrom, L. & Firestone, R. The Lund/LBNL Nuclear Data Search. `http://nucleardata.nuclear.lu.se/toi/nucSearch.asp` (July 2018).

139. Pietruszewski, A., Zarnowiecki, K. & Smagala, G. in *Nuclear Safeguards Technology* (1986).

140. Sullivan, J., Rawool-Sullivan, M. & Wenz, T. $LaCl_3$(Ce) and $LaBr_3$(Ce) gamma-ray spectra with various plutonium isotopic and uranium enrichment standards. *Journal of Radioanalytical and Nuclear Chemistry* **276,** 699–705 (2008).

141. Rekha, A., Dingankar, M., Anilkumar, S. & Narayani, K. Determination of the activity ratios of ^{231}Pa to ^{235}U and ^{227}Th to ^{235}U in ore samples using gamma-spectrometry. *Journal of Radioanalytical and Nuclear Chemistry* **268,** 453–460 (2006).

142. Rolison, J. & Williams, R. Application of the ^{226}Ra-^{230}Th-^{234}U and ^{227}Ac-^{231}Pa-^{235}U radiochronometers to UF_6 cylinders. *Journal of Radioanalytical and Nuclear Chemistry* **317,** 897–905 (2018).

143. Rolison, J., Treinen, K., McHugh, K., Gaffney, A. & Williams, R. Application of the ^{226}Ra-^{230}Th-^{234}U and ^{227}Ac-^{231}Pa-^{235}U radiochronometers to uranium certified reference materials. *Journal of Radioanalytical and Nuclear Chemistry* **314,** 2459–2467 (2017).

144. Berzero, A., Caramella-Crespi, V. & Cavagna, P. Direct gamma-ray spectroscopy dating of fossil bones: Preliminary results. *Archaeometry* **39,** 189–203 (1997).

145. Edwards, R., Cheng, H., Murrell, M. & Goldstein, S. Protactinium-231 Dating of Carbonates by Thermal Ionization Mass Spectrometry: Implications for Quaternary Climate Change. *Science* **276,** 782–786 (1997).

146. Edwards, R., Gallup, C. & Cheng, H. Uranium-series Dating of Marine and Lacustrine Carbonates. *Reviews in Mineralogy and Geochemistry* **52,** 363–405 (2003).

147. Raje, N. *et al.* Preconcentration of natural protactinium (^{231}Pa) from monazite on Dowex 1X8 and subsequent determination by gamma-spectrometry. *Journal of Radioanalytical and Nuclear Chemistry* **247,** 115–120 (2001).

148. ENSDF Nuclear Data Sheets: ^{227}Ac. *Nuclear Data Sheets* **132,** 257 (2016).

149. Banham, M. & McCrohon, R. *The measurement of gamma-ray emission probabilities for the nuclides ^{231}Pa, ^{233}Pa, ^{232}U, ^{235}U, ^{237}U, and ^{237}Np* (US Department of Energy, Washington, DC, 1986).

150. De Pinho, A., da Silveira, E. & da Costa, N. High-Resolution Gamma Spectroscopy in the Decay of Pa-231. *Phys. Rev* **2,** 572 (1970).

151. Gunnink, R. & Niday, J. *Computerized quantitative analysis of gamma-ray spectrometry* (1972).

152. Samuel, J. & Vaidyanathan, S. *A Low Geometry Alpha Counter* (Government of India Atomic Energy Commission – Bhabha Atomic Research Centre, Bombay, India, 1973).

153. Leang, C. Etude des Rayonnements Gamma Accompagnant la Desintegration Alpha du Protactinium-231 (^{231}Pa-^{227}Ac). *J. Phys. France* **31,** 269 (1970).

154. Teoh, W., Connor, R. & Betts, R. The decay of ^{231}Pa. *Nuclear Physics A* **319,** 122–142 (1979).

155. Lange, R. & Hagee, G. Levels, transitions and rotational structure in ^{227}Ac. *Nuclear Physics A* **124,** 412–428 (1969).

156. Borner, H. *et al.* High Precision Measurements of Some Gamma Transitions in ^{227}Ac, ^{228}Th, ^{231}Pa, ^{232}U, ^{233}Pa, ^{239}Np, ^{239}Pu and ^{245}Am. *Nucl. Instrum. Methods* **166,** 251–255 (1979).

157. De Pinho, A., Auler, L. & da Silva, A. X rays following the alpha decay of ^{231}Pa. *Phys. Rev* **9,** 2056 (1974).

158. Anicin, I. *et al.* Levels and Transitions in ^{227}Ac. *Journal of Physics G: Nuclear Physics* **8,** 369 (1982).

159. Landis, V. & Kaye, J. *The Radiochemistry of Titanium* (Subcommittee on Radiochemistry - National Academy of Sciences, Washington, DC, 1971).

160. Roshchin, A. *et al.* Cross sections of nonfission reactions induced in Th-232 by low-energy proton. *Physics of Atomic Nuclei* **60,** 1941 (1997).

161. Szerypo, J., Szweryn, B., Hornshoj, P., Nielsen, H. L. & Luontama, M. Radiative Capture of Protons by the Deformed Nuclide Th-232. *Zeitschrift fuer Physik A* **324,** 439 (1986).

162. Mastren, T. *et al.* Separation of Protactinium Employing Sulfur-Based Extraction Chromatographic Resins. *Anal. Chem.* **90,** 7012–7017 (2018).

163. DGA Resins. *Eichrom Technologies* **1** (Dec. 2020).

164. Li, J. Development and Evaluation of Flexible Empirical Peak Functions for Processing Chromatographic Peaks. *Anal. Chem.* **69,** 4452–4462 (1997).

165. Marco, V. D. & Bombi, G. Mathematical functions for the representation of chromatographic peaks. *Journal of Chromatography A* **931,** 1–30 (2001).

166. Suzuki, T. *et al.* Speciation of Ruthenium(III) Chloro Complexes in Hydrochloric Acid Solutions and Their Extraction Characteristics with an Amide-Containing Amine Compound. *Metals* **8,** 558 (2018).

167. Despotopulos, J. *et al.* Characterization of Group 5 dubnium homologs on diglycolamide extraction chromatography resins from nitric and hydrofluoric acid matrices. *Journal of Radioanalytical and Nuclear Chemistry* **303,** 485–494 (2015).

168. Kluge, E. & Lieser, K. Dissolution of ThO_2 in HCl/HF Mixtures. *Radiochemica Acta* **29,** 167–168 (1981).

169. Kraus, K. & Nelson, F. in *Proc. Intern. Conf. Peaceful Uses Atomic Energy* Geneva, Switzerland (1956).

170. Horwitz, E., McAlister, D., Bond, A. & Barrans, R. Novel Extraction of Chromatographic Resins Based on Tetraalkyldiglycolamides: Characterization and Potential Applications. *Solvent Extraction and Ion Exchange* **23,** 319–344 (2007).

171. Krane, K. *Introductory Nuclear Physics* (John Wiley and Sons, Inc, Hoboken, NJ, 1988).

172. ENSDF Nuclear Data Sheets: ^{229}Pa ϵ decay. *Nuclear Data Sheets* **109,** 2657 (2008).

173. ENSDF Nuclear Data Sheets: ^{228}Pa. *Nuclear Data Sheets* **116,** 163 (2012).

174. Chu, S., Ekstrom, L. & Firestone, R. *The Lund/LBNL Nuclear Data Search* Lawrence Berkeley National Laboratory. Accessed: 2020-11-16. Feb. 1999.

175. Meinke, W., Ghiorso, A. & Seaborg, G. Artificial Chains Collateral to the Heavy Radioactive Families. *Physical Review* **81,** 782 (1951).

176. Gerschel, C., Pautrat, M., Ricci, R., Vanhorenbeeck, J. & Teillac, J. Etude des Series α de Protactinium 227, 228, 229 et 230. *Phys. Nucl. Annuaire,* 47 (1964).

177. *Triskem Infos No 5* Triskem International `https://www.triskem-international.com/scripts/files/59d1f4fc2b6bf5.29801126/tki5_en_binder_1.pdf`. Accessed: 2020-10-10. 2010.

178. Decamp, C. & Happel, S. Utilization of a mixed-bed column for the removal of iodine from radioactive process waste solutions. *Journal of Radioanalytical and Nuclear Chemistry* **298,** 763–767 (2013).

179. Nottoli, E., Bienvenu, P., Labet, A. D., Arnold, M. & Bertauxa, M. Accurate determination of ^{129}I concentrations and ^{129}I/^{137}Cs ratios in spent nuclear resins by Accelerator Mass Spectrometry. *Applied Radiation and Isotopes* **86,** 90–96 (2014).

180. Esparza, D. *et al.* Fast-response flow-based method for evaluating ^{131}I from biological and hospital waste samples exploiting liquid scintillation detection. *Talanta* **206,** 120224 (2020).

181. Mastren, T. *et al.* Chromatographic separation of the theranostic radionuclide ^{111}Ag from a proton irradiated thorium matrix. *Analytica Chimica Acta* **998,** 75–82 (2018).

182. Zulauf, A., Happel, S., Mokili, M., Bombard, A. & Jungclas, H. Characterization of an extraction chromatographic resin for the separation and determination of ^{36}Cl and ^{129}I. *Journal of Radioanalytical and Nuclear Chemistry* **286,** 539–546 (2010).

183. Horwitz, E., Dietz, M. & Fisher, D. Separation and preconcentration of strontium from biological, environmental, and nuclear waste samples by extraction chromatography using a crown ether. *Anal. Chem.* **63,** 522–525 (1991).

184. Horwitz, E., Chiarizia, R. & Dietz, M. A novel strontium-selective extraction chromatographic resin. *Solvent Extr Ion Exch* **10,** 313–336 (1992).

185. Gott, M., Steinbach, J. & Mamat, C. The Radiochemical and Radiopharmaceutical Applications of Radium. *Open Chemistry* **14,** 118–129 (2016).

186. Stevenson, P. & Nervik, W. *The Radiochemistry of the Rare Earths, Scandium, Yttrium and Actinium* (Lawrence Radiation Laboratory, Livermore, CA, 1961).

187. Stein, B. *et al.* Advancing Chelation Chemistry for Actinium and Other +3 f-Elements, Am, Cm, and La. *J. Am. Chem* **141,** 19404–19414 (2019).

188. Zielinska, B., Bilewicz & A. The Hydrolysis of Actinium. *Journal of Radioanlytical and Nuclear Chemistry* **261,** 195–198 (2004).

189. Brown, P. & Ekberg, C. *Hydrolysis of Metal Ions* (Wiley VHC, Weinheim, 2016).

190. Streitwieser, A., Rajca, A., McDowell, R. & Glaserlc, R. Semipolar P-0 and P-C Bonds: A Theoretical Study of Hypophosphite and Related Methylenephosphoranes. *J. Am. Chem.* **109,** 4184–4188 (1987).

191. Kocher, N., Leusser, D., Murso, A. & Stalke, D. Metal Coordination to the Formal P-N Bond of an Iminophosphorane and Charge-Density Evidence against Hypervalent Phosphorus(V). *Chemistry - A European Journal* **10,** 3622–3631 (2004).

192. Gilheany, D. No d Orbitals but Walsh Diagrams and Maybe Banana Bonds: Chemical Bonding in Phosphines, Phosphine Oxides, and Phosphonium Ylides. *Chem. Rev.* **94,** 1339–1374 (1994).

193. Kluge, E. & Lieser, K. Separation of Thorium, Protactinium and Uranium by Ion Exchange and Extraction. *Radiochimica Acta* **27,** 161–171 (1980).

194. Filosofov, D. *et al.* Behavior of Actinium, Alkaline and Rare Earth Elements in Sr-Resin/Mineral Acid Systems. *Solvent Extraction and Ion Exchange* **00,** 1–14 (2015).

195. Mohamud, H. *et al.* Progress towards the development of a rapid analytical approach for separation of ^{226}Ra using dibenzo-18-crown-6 ether functionalised silica (SiO_2) disks. *Radiation Physics and Chemistry* **140,** 57–60 (2017).

196. Despotopulos, J. *et al.* Characterization of the homologs of flerovium with crown ether based extraction chromatography resins: studies in hydrochloric acid. *Journal of Radioanalytical and Nuclear Chemistry* **310,** 1201–1207 (2016).

197. Imura, H. *et al.* Characterization of the Lathanum(III) and Europium(III) tricholoacetate complexes extracted with 18-crown-6. *Solvent Extraction and Ion Exchange* **14,** 817–832 (1996).

198. Parham, H. & Fazeli, A. Extraction-Spectrophotometric Determination of Trace Amounts of Barium by 18-Crown-6 and Rose Bengal. *Analytical Sciences* **16,** 575–577 (2000).

199. Bilski, P. & Chignell, C. Properties of differently charged micelles containing rose bengal: application in photosensitization studies. *J* **77,** 49–58 (1994).

200. Lambert, C. & Kochevar, I. Electron Transfer Quenching of the Rose Bengal Triplet State. *Photochemistry and Photobiology* **66,** 15–25 (1997).

201. Schoolaert, E. *et al.* Blend electrospinning of dye-functionalized chitosan and poly(e-caprolactone): towards biocompatible pH-sensors. *Journal of Materials Chemistry B* **4,** 4507 (2016).

202. Horwitz, E. *et al.* A lead-selective extraction chromatographic resin and its application to the isolation of lead from geological samples. *Analytica Chimica Acta* **292,** 263–273 (1994).

203. Horwitz, E. & Bloomquist, C. The preparation, preformance and factors affecting band spreading of high efficiency extraction chromatographic columns for actinide separations. *J. Inorg. Nucl* **34,** 3851–3871 (1972).

204. Lamberts, J., Schumacher, D. & Neckers, D. Novel Rose Bengal Derivatives: Synthesis and Quantum Yield Studies. *J. Am. Chem* **106,** 5879–5883 (1984).

205. Chen, X., Ji, M., Fisher, D. & Wai, C. Ionizable Calixarene-Crown Ethers with High Selectivity for Radium over Light Alkaline Earth Metal Ions. *Inorganic Chemistry* **38,** 5449–5452 (1999).

206. Shannon, R. Revised Effective Ionic Radii and Systematic Studies of Interatomic Distances in Halides and Chalcogenides. *Acta Crystallographica* **A32,** 751–767 (1976).

207. Takeda, Y. *et al.* Solvent extraction of alkali metal (Li-Cs) picrates with 18-crown-6 into various diluents. Elucidation of fundamental equilibria which govern the extraction-ability and-selectivity. *Analytical Sciences* **14,** 215–223 (1998).

208. Hancock, R., Siddons, C., Oscarson, K. & Reibenspies, J. The structure of the 11-coordinate barium complex of the pendant-donor macrocycle 1,4,7,10-tetrakis (carbamoylmethyl) -1,4, 7, 10-tetraazacyclododecane: an analysis of the coordination numbers of barium(II) in its complexes. *Inorganica Chimica Acta* **357,** 723–727 (2004).

209. Morgenstern, A. *et al.* Computer-Assisted Design of Macrocyclic Chelators for Actinium-225 Radiotherapeutics. *Inorganic Chemistry* **60,** 623–632 (2021).

210. Gao, Y., Groverb, P. & Schreckenbach, G. Stabilization of hydrated Ac^{III} cation: the role of superatom states in actinium-water bonding. *Chem. Sci.* **12,** 2655–2666 (2021).

211. Stein, B. *et al.* Advancing Chelation Chemistry for Actinium and Other +3 f-Elements, Am, Cm, and La. *J. Am. Chem. Soc.* **141,** 19404–19414 (2019).

212. Kirby, H. & Salutsky, M. *The Radiochemistry of Radium* (Subcommittee on Radiochemistry National Academy of Science – National Reseach Council, Washington, DC, 1964).

213. Deblonde, G., Ricano, A. & Abergel, R. Ultra-selective ligand-driven separation of strategic actinides. *Nature Communications* **10,** 2438 (2019).

214. Dietz, M., Chiarizia, R., Horwitz, E., Bartsch, R. & Talanov, V. Effect of Crown Ethers on the Ion-Exchange Behavior of Alkaline Earth Metals. Toward Improved Ion-Exchange Methods for the Separation and Preconcentration of Radium. *Anal. Chem.* **69,** 3028–3037 (1997).

Appendix A

Mass Spectrometry Data for Ore Processing

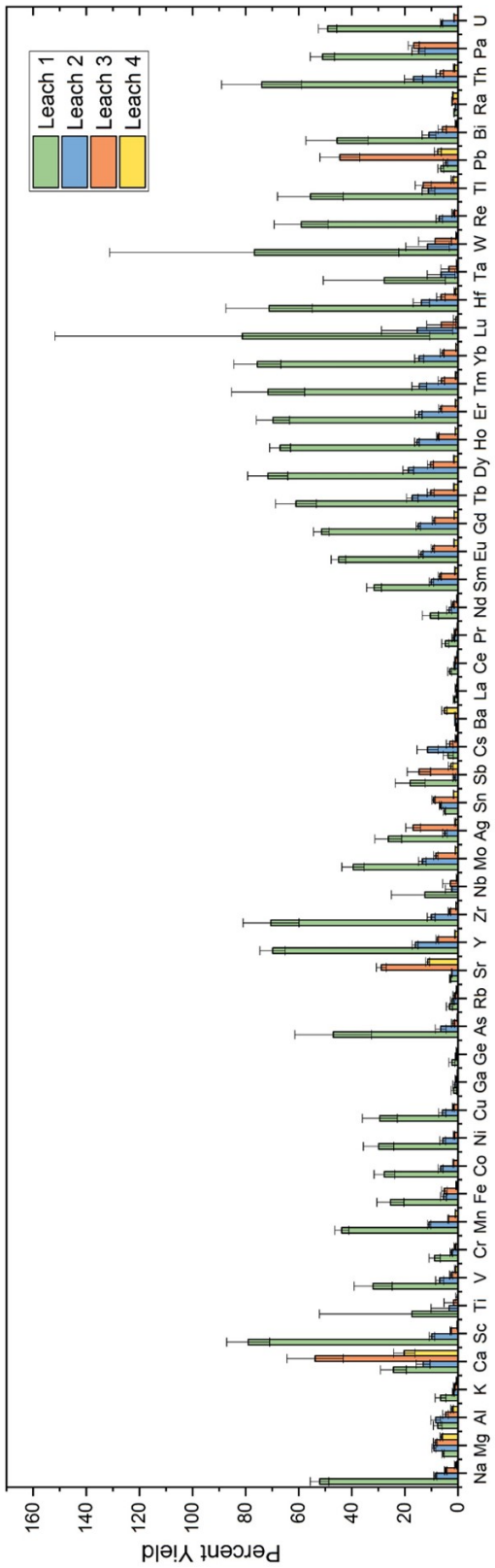

Figure A.1: Full mass spectroscopy data for leaching yields. Note that data for protactinium and radium is from gamma-ray spectrometry of ^{231}Pa and ^{226}Ra as discussed in Chapter 2. For simplified figure in text (Fig. 2.12) elements have been categorized as alkali metals (Na, K, Rb, Cs), alkaline earth metals (Mg, Ca, Sr, Ba), early transition metals (Sc, Ti, V, Cr, Mn, Y, Zr, Nb, Mo, Hf, Ta, W, Re), late transition metals (Fe, Co, Ni, Cu, Ag), lanthanides (La-Lu), and post transition metals (Al, Ga, Ge, As, Sn, Sb, Tl, Pb, Bi); for each group the average leaching yield was calculated.

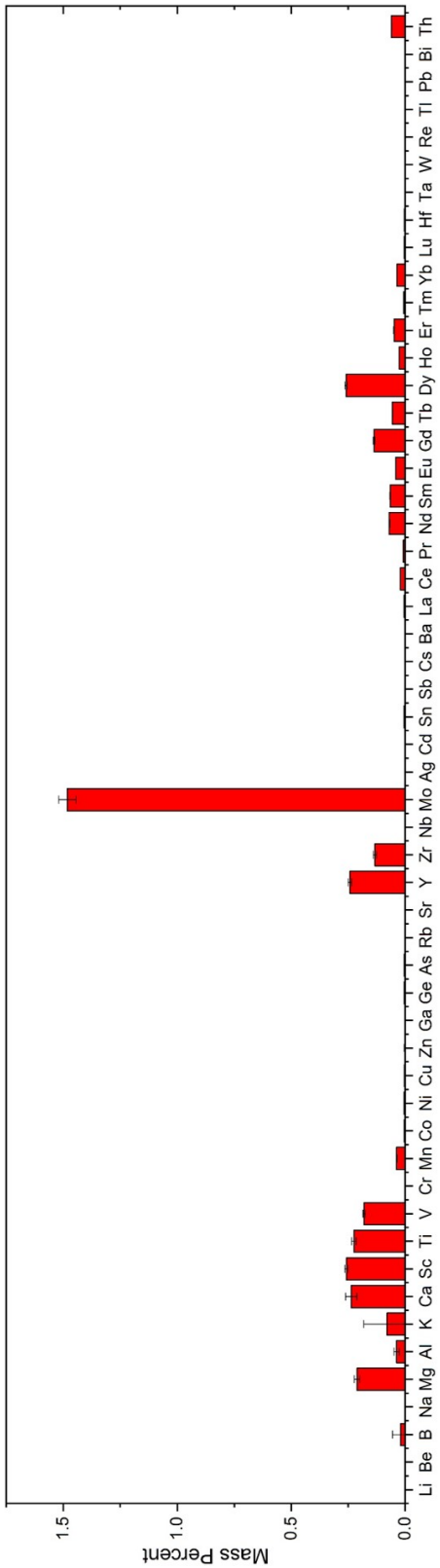

Figure A.2: Full mass spectrometry data for the back-extraction solution in 1 M HF; balance is iron (27.3 $\pm$ 0.71%) and uranium (68.6 $\pm$ 1.4%). For simplified figure in text (Fig. 2.13) elements have been categorized as alkali metals (Li, Na, K, Rb, Cs), alkaline earth metals (Be, Mg, Ca, Sr, Ba), early transition metals (Sc, Ti, V, Cr, Mn, Y, Zr, Nb, Mo, Hf, Ta, W, Re), late transition metals (Co, Ni, Cu, Zn, Ag, Cd), lanthanides (La-Lu) and post transition metals (B, Al, Ga, Ge, As, Sn, Sb, Tl, Pb, Bi); for each group the total mass percent was calculated.

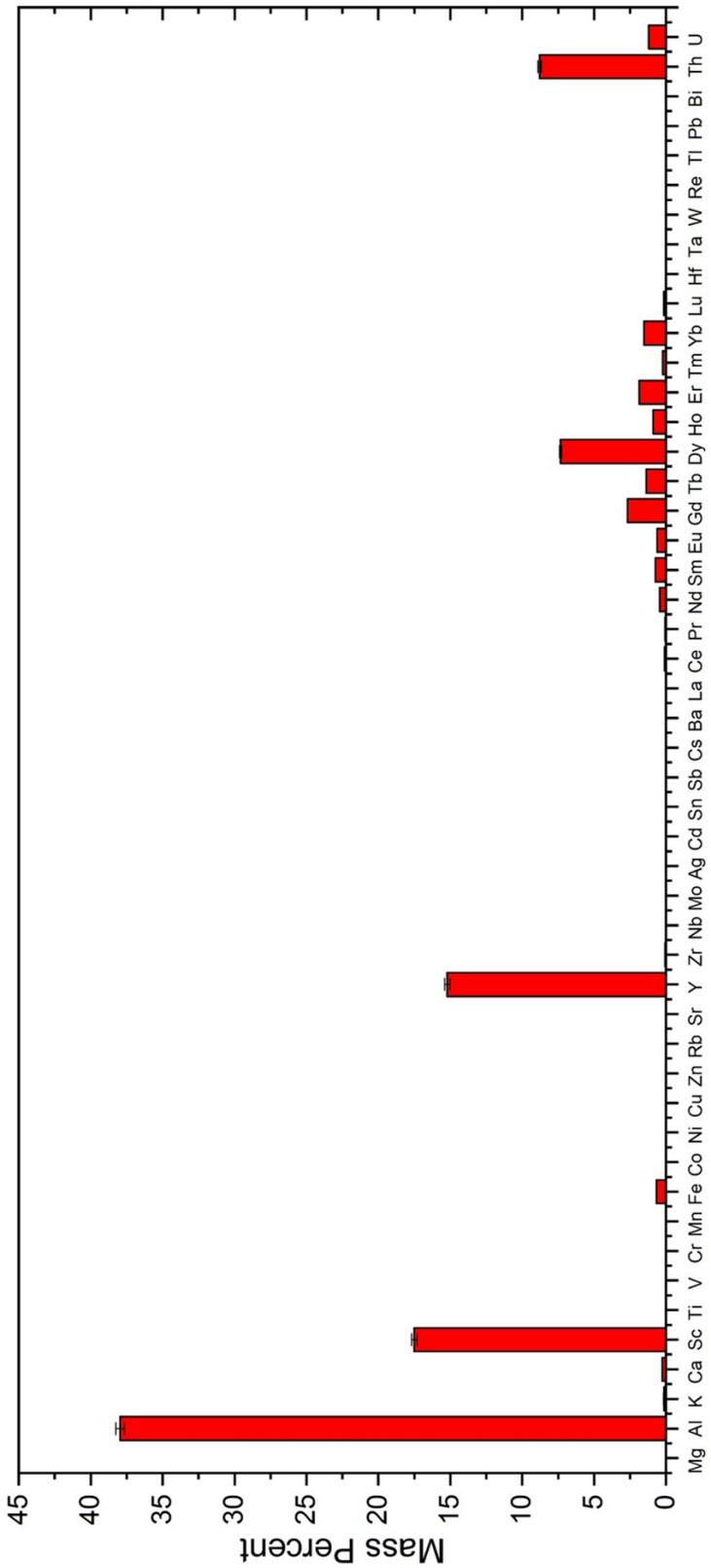

Figure A.3: Full mass spectrometry data for hydroxide precipitate dissolved in conc. HNO_3 acid. For simplified figure in text (Fig. 2.15) elements have been categorized as alkali metals (K, Rb, Cs), alkaline earth metals (Mg, Ca, Sr, Ba), early transition metals (Ti, V, Cr, Mn, Zr, Nb, Mo, Hf, Ta, W, Re), late transition metals (Co, Ni, Cu, Zn, Ag, Cd), lanthanides (La-Lu) and post transition metals (Al, Sn, Sb, Tl, Pb, Bi); for each group the total mass percent was calculated. Sodium not included.

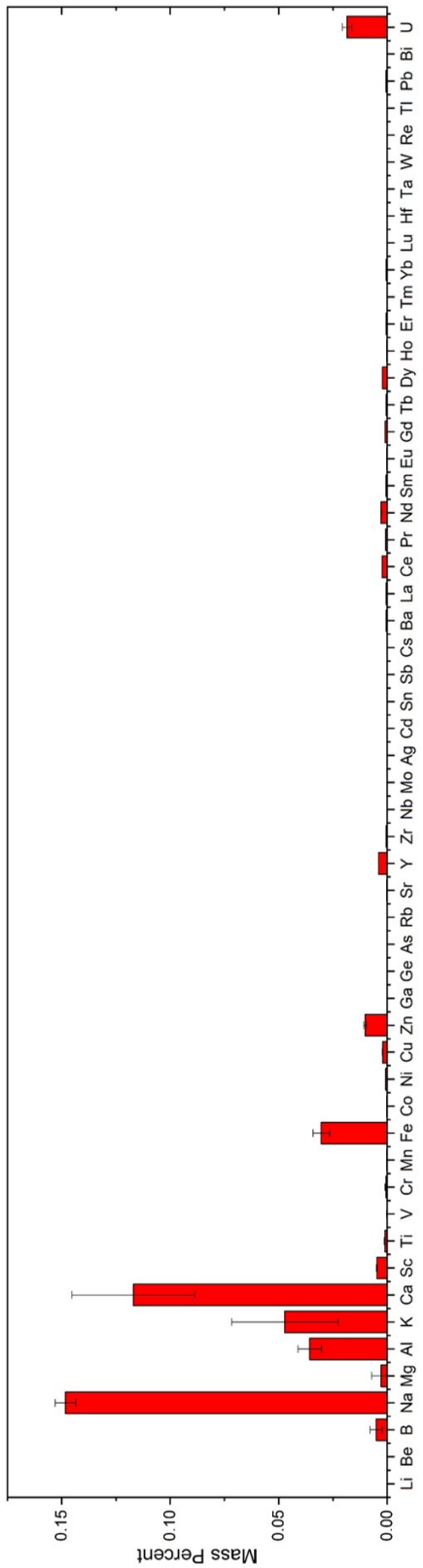

Figure A.4: Full mass spectrometry data for final product in conc. HNO_3 acid; balance is thorium (99.5 ± 1.2 wt. %). For simplified figure in text (Fig. 2.17) elements have been categorized as alkali metals (Li, Na, K, Rb, Cs), alkaline earth metals (Be, Mg, Ca, Sr, Ba), early transition metals (Sc, Ti, V, Cr, Mn, Y, Zr, Nb, Mo, Hf, Ta, W, Re), late transition metals (Fe, Co, Ni, Cu, Zn, Ag, Cd), lanthanides (La-Lu) and post transition metals (B, Al, Ga, Ge, As, Sn, Sb, Tl, Pb, Bi); for each group the total mass percent was calculated.

Appendix B

Fitting of Chromatographic Peaks

Theoretically chromatographic peaks should fit a Gaussian curve, however, in practice numerous different peak functions are used to describe chromatographic peaks as experimental peaks vary widely in shape [164, 165]. In this work, a few particularly symmetric chromatographic peaks fit a Gaussian function, but generally peaks are generally fitted with bi-Gaussian or Giddings functions, both of which are commonly used for chromatographic peak fitting and allow for asymmetrical peak shapes [164]. Some peaks with different shapes required other functions and for these cases the Gram-Charlier Series and Extreme Value function, both of which can also applied to chromatographic peak fitting [164, 165], were used as well. The relevant equations [165] for these functions are listed below, and all fitting was done using the program Origin 2018 (OriginLab).

In all equations, *h, w, z* are adjustable parameters.

1. Gaussian

$$y = h \exp\left[-\frac{(x-z)^2}{2w^2}\right] \tag{B.1}$$

2. Bi-Gaussian:
   For $x < z$

$$y = h \exp\left[-\frac{(x-z)^2}{2w_1^2}\right] \tag{B.2}$$

   For $x \geq z$

$$y = h \exp\left[-\frac{(x-z)^2}{2w_2^2}\right] \tag{B.3}$$

3. Giddings:

$$y = \frac{h}{w}\sqrt{\frac{z}{x}}\left[\exp\left(-\frac{x+z}{w}\right)\right] I_1\left(\frac{2\sqrt{zx}}{w}\right) \tag{B.4}$$

   Where I_1 is a modified Bessel Function [165].

4. Extreme Value:

$$y = h \exp\left[-\exp\left(-\frac{x-z}{w}\right) - \frac{x-z}{w} + 1\right] \tag{B.5}$$

5. Simplified Gram-Charlier Series [165]:

$$y = \frac{h}{w\sqrt{2\pi}} \exp\left(-\frac{(x-z)^2}{2w^2}\right)\left[1 + \left|\sum_{i=3}^{4} \frac{a_i}{i!} H_i(k)\right|\right] \tag{B.6}$$

Where

$$k = \frac{x-z}{w} \tag{B.7}$$

$$H_3 = k^3 - 3k \tag{B.8}$$

$$H_4 = k^4 - 6k^3 + 3 \tag{B.9}$$

Appendix C

Supplementary Information for Cross Section Measurement Experiments

Table C.1: X-ray and gamma-ray energies of relevant protactinium isotopes. Data from Ref. [14] unless otherwise noted.

Isotope	**Half-Life**	**Gamma-ray Energies and Intensities**	**X-ray Energies Intensities**
^{213}Bi	45.59 min	440.45 keV (25.94%)	n/a
^{221}Fr	4.801 min	218.0 keV (11.44%)	n/a
^{228}Pa*	22 ± 1 hours	129.065 keV (4.26%) 338.320 keV (7.6%) 409.462 keV (9.3%) 911.204 keV (23.0%)	89.957 keV (25.7%) 93.350 keV (41.9%) 104.819 keV (5.10%) 105.604 keV (9.8%) 108.583 keV (3.73%) 108.955 keV (1.30%)
^{229}Pa	1.50 ± 0.05 days	119.0 keV (0.129%)	89.957 keV (18.2%) 93.35 keV (29.3%) 104.819 keV (3.63%) 105.604 keV (6.92%) 108.582 (2.65%)
^{230}Pa	17.4 ± 0.5 days	120.90 keV (0.358%) 440.78 keV (0.099%) 443.74 keV (5.8%) 918.50 keV (8.3%) 951.88 keV (29.6%)	89.957 keV (18.4%) 93.35 keV (29.8%) 104.819 keV (3.7%) 105.604 keV (7.0%) 108.582 keV (2.69%)
^{232}Pa	1.31 ± 0.02 days	105.4 keV (1.46%) 109.0 (2.49%) 139.2 keV (0.54%) 150.059 keV (10.4%) 387.884 keV (6.55%) 581.398 keV (6.18%) 819.187 keV (7.34%) 866.760 (7.34%) 969.315 keV (42.3%)	94.654 keV (1.01%) 98.434 keV (1.62%) 110.421 (0.202%) 111.298 keV (0.383%) 114.445 keV (0.149%)
^{233}Pa	26.975 ± 0.0013 days	86.595 keV (1.95%) 300.129 keV (6.63%) 311.904 keV (38.5%) 340.476 keV (4.45%)	94.654 keV (10.56%) 98.434 keV (16.9%) 110.421 keV (2.12%) 111.298 keV (4.01%) 114.445 (1.55%)

* Data from Ref. [174] as it was not available from Ref. [14].

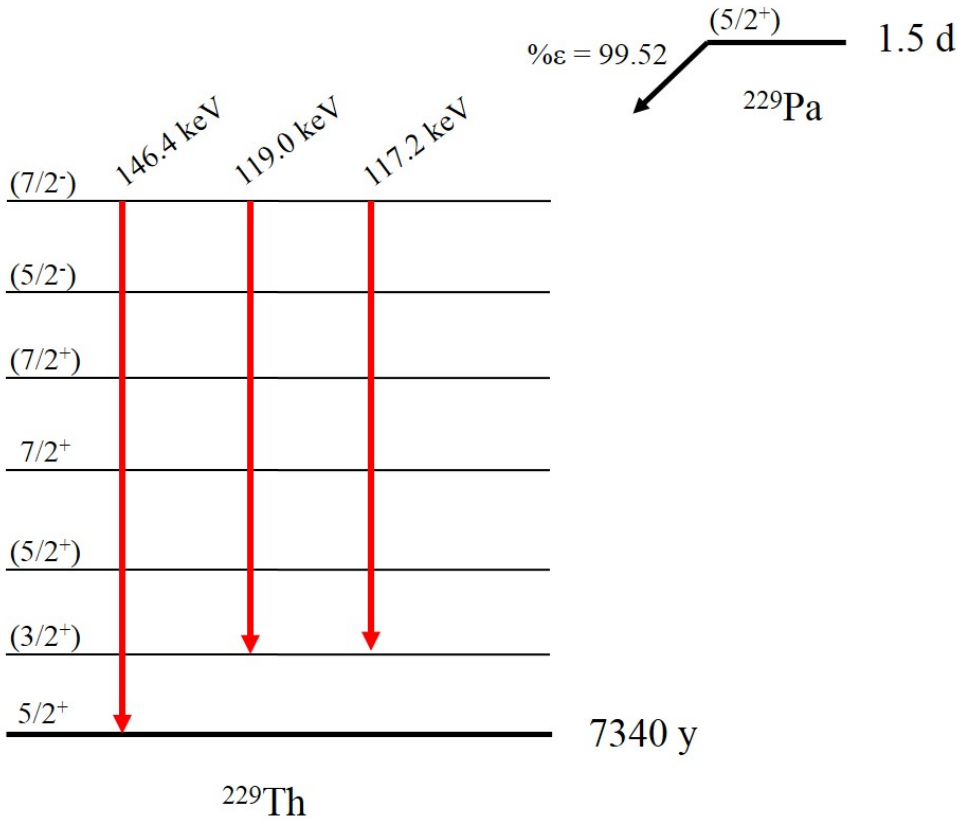

Figure C.1: Simplified decay scheme of ^{229}Pa electron capture decay to ^{229}Th, emphasizing major gamma-ray emissions. Energy level spacing not to scale. Data from Ref. [172].

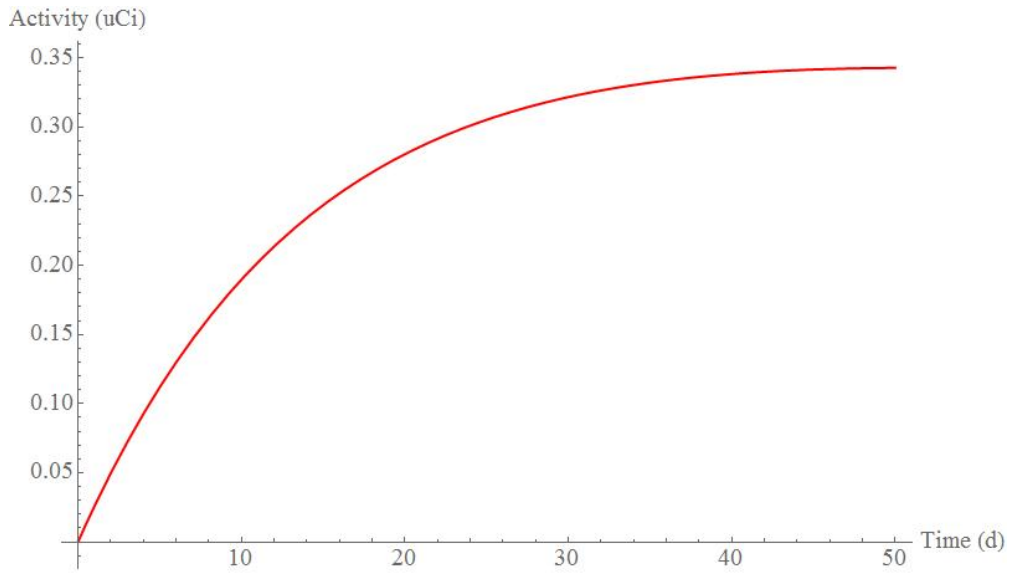

(a) Plot of the Bateman equations for the in-growth of ^{225}Ac (red) into 80 μCi ^{229}Pa.

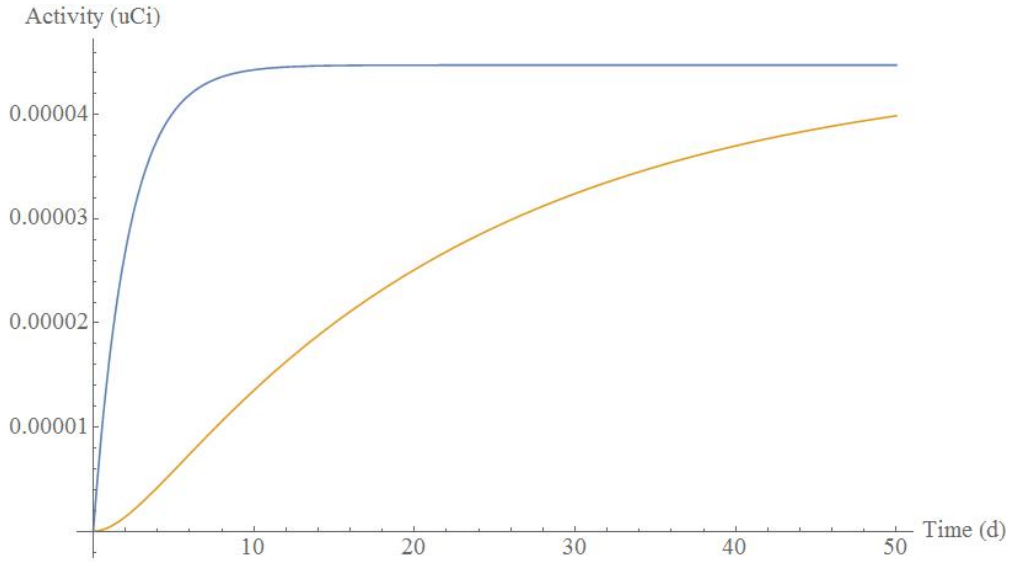

(b) Plot of the Bateman equations for the in-growth of ^{229}Th (blue) and ^{225}Ra (orange) into 80 μCi ^{229}Pa.

Figure C.2: Acitivty curves based on the Bateman equations for the in-growth of ^{229}Pa daughters.